

**AMINO ACID FUNCTIONALIZED NANODIAMONDS AS
GENE DELIVERY VECTORS:
SYNTHESIS, PHYSICOCHEMICAL CHARACTERIZATION
AND CELLULAR INTERACTION STUDIES**

The thesis is submitted to the
College of Graduate Studies and Research
in Partial Fulfillment of the Requirements for the
Degree of Masters of Science in the
College of Pharmacy and Nutrition
University of Saskatchewan
Saskatoon, Saskatchewan
Canada

Saniya Shiraz Alwani

9/13/2015

Permission to use

In presenting this thesis in partial fulfillment of the requirements for a Masters in Science degree from the University of Saskatchewan, I agree that the Libraries of this University may make it freely available for inspection. I further agree that permission for copying of this thesis in any manner, in whole or in part, for scholarly purposes may be granted by the professor who supervised my thesis work or, in their absence, by the Head of the Department or the Dean of the College in which my thesis work was done. It is understood that any copying or publication or use of this thesis or parts thereof for financial gain shall not be allowed without my written permission. It is also understood that due recognition shall be given to me and to the University of Saskatchewan in any scholarly use which may be made of any material in this thesis.

Requests for permission to copy or to make other uses of materials in this thesis in whole or part should be addressed to:

Dean

College of Pharmacy & Nutrition

University of Saskatchewan

Saskatoon, Saskatchewan S7N 2Z4

Canada

OR

Dean

College of Graduate Studies and Research

University of Saskatchewan

107 Administration Place

Saskatoon, Saskatchewan S7N 5A2

Canada

Abstract

Nanodiamonds (NDs) are the most biocompatible member of the carbon nanofamily which are widely researched for diagnostic and therapeutic applications. Unlike other carbon nanomaterials, the surface of NDs is innately reactive, hence capable of conjugating various chemical moieties for targeted actions. This work focuses on utilizing the surface reactivity of NDs for gene therapeutics and addressing the challenges associated with its application in the biological environment. Pristine carboxylated NDs were functionalized with basic amino acids (lysine and lysyl-histidine) through covalent conjugation via a three carbon chain linker. Amino acid functionalized NDs were characterized by infrared spectroscopy, thermogravimetry and size and zeta potential measurements. Lysine conjugation was evident through a marked change in the zeta potential of ND dispersion from negative to a high positive value (-54.6 mV to +26.3 mV). The thermogram of lysine functionalized NDs (Lys-NDs) revealed a significant weight loss from 150°C to 700°C confirming the functionalization through loss of amino acid conjugates from the surface and total loading was calculated as 1.97 mmols/g. Lys-NDs also showed optimum binding with pDNA and siRNA at weight ratios of 1:1 and 1:20 (pDNA/siRNA:ND), respectively. Functionalization of NDs with lysine contributed to limiting aggregation and enhancing the colloidal stability of ND dispersions in biological milieu. The aqueous dispersion of lys-NDs showed minimum sedimentation and remained stable over a period of 25 days. Average sizes under 100 nm and zeta potentials higher than +20 mV indicate a preservation of the cationic surface throughout the testing period. Moreover, size distributions and zeta potentials changed significantly upon incubation of lys-NDs with blood serum suggesting an interaction with biomolecules, mainly proteins and a possible formation of a protein corona.

Cellular internalization of bare lys-NDs and their diamplexes (i.e. complexes of NDs with nucleic acids) was assessed through scanning transmission X-ray microscopy and flow cytometry. Functional efficiency of lysine NDs was determined by flow cytometry monitoring the GFP knockdown through anti-GFP siRNA delivery. Results reveal a promising GFP knockdown of ~17% upon treating the cells with NDs/siRNA diamplexes at a ratio of 20:1. Subsequent analyses regarding the effect of NDs to prevent cellular proliferation and to cause cellular apoptosis confirmed that they are innately biocompatible at a wide range of concentrations. Unlike lysine NDs, lysyl-histidine functionalization was limited and the surface

loading of this conjugate on NDs was very low. Therefore, they were unable to bind pDNA and siRNA even at high weight ratios and hence demand design modifications.

Overall this work demonstrates a novel approach of functionalizing NDs with basic amino acids capable of enhancing colloidal stability and delivering of therapeutic genes into mammalian cells. It represents an important step in the development of safe and efficient gene therapy for inherited and acquired diseases.

Acknowledgement

First and the foremost I would like to thank GOD for everything

I would like to extend sincere gratitude to my supervisor, Dr. Ildiko Badea for believing in me and giving me an opportunity to be the part of her research group at University of Saskatchewan. I thank her wholeheartedly for the invaluable guidance, support and encouragement throughout my project. I am also grateful to the College of Pharmacy and Nutrition and the College of Graduate Studies and Research at University of Saskatchewan for supporting my graduate studies. I duly recognize the Natural Sciences and Engineering Research Council of Canada (NSERC) for funding this project. I thank Tosoh Corporation, USA, for the kind donation of the YTZ® grinding media used in these studies. I sincerely appreciate Dr. Ronald. E. Verrall and Dr. Jackson M Chitanda for their advices and guidance regarding all aspects of my project mainly the chemical synthesis. Special thanks to my committee members Dr. Anas El-Aneed and Dr. Jackson M Chitanda for providing me valued advices and support through their professional knowledge and expertise. I also greatly appreciate the technical assistance offered by Dr. Ferenc Borondics for infrared spectroscopy and Dr. Chitra Karunakaran for scanning transmission x-ray microscopy. Heartiest thanks to Deborah Michel for the extraordinary support and valued guidance throughout my work. I would like to extend my sincere thanks to all my colleagues and friends Randeep Kaur, Jagbir Singh, Waleed Mohammed-Saeid, Masoomah Poorghorban, Joshua Buse, McDonald Donkuru, Hanan Elsayed, Mona Hamada and Istvan Hajdu for their wonderful company and friendly help.

Last but most importantly, I want to thank wholeheartedly my family for their love, support and guidance. I pay greatest thanks to my father (Shiraz Alwani), my mother (Rozmin Alwani), my brother (Sumair Alwani) and my sister (Sumaira Alwani) for their affection and continual financial and moral support. I am especially thankful to my husband (Syed Jamshed Wasi) for his uncountable love, support and encouragement.

Dedication

I would like to dedicate my thesis

- *To my father, Shiraz Alwani and my mother, Rozmin Shiraz Alwani whose love, trust and care were of great support during my studies.*
- *To my husband, Syed Jamshed Wasi without whom nothing would have been possible.*

Table of Contents

Permission to use	i
Abstract.....	ii
Acknowledgement	iv
Dedication.....	v
Table of Contents.....	vi
List of Figures.....	xi
List of Tables	xvi
List of Schemes	xvi
List of Abbreviations	xviii
Introduction	1
1 Introduction to Carbon Nanomaterials as Nano-Delivery Devices	3
1.1 Introduction	3
1.2 Structure and properties of important carbon nanomaterials: fullerenes, carbon nanotubes and nanodiamonds	4
1.3 Carbon nanomaterials as drug delivery devices	7
1.4 Carbon nanomaterials as gene delivery devices	11
1.5 Comparative biocompatibility profiles of carbon nanomaterials	14
1.6 Conclusion	14
2 Nanodiamonds as Novel Nanomaterials for Therapeutics: Structure, Production, Properties and Biomedical Applications	15
2.1 Authors' Contribution.....	15
2.2 Abstract.....	16
2.3 Introduction	16
2.4 Production of NDs	17
2.5 Core structure, surface chemistry and chemical composition of NDs	17
2.5.1 Defects in ND structure.....	18
2.6 Properties of NDs crucial for biomedical applications.....	19
2.6.1 Toughness.....	19

2.6.2	Inertness	20
2.6.3	Large surface area and high adsorption potential.....	20
2.6.4	Photoluminescence of NDs	20
2.6.5	Aggregation.....	21
2.7	Dispersion stability of NDs - a challenge for biomedical application.....	23
2.7.1	Theories related to ND aggregation	23
2.7.2	Methods to mitigate aggregation and produce stable ND dispersion.....	25
2.8	Biomedical applications of NDs.....	34
2.8.1	Biodistribution and cellular uptake of NDs –mechanisms, challenges and controlling factors	34
2.8.2	Biocompatibility and biological affinity	39
2.8.3	Application of NDs in bioimaging and research technologies.....	40
2.8.4	Applications of NDs in therapeutics	40
2.9	Conclusion.....	42
3	<i>Hypothesis and Research Objectives</i>	44
3.1	Hypotheses.....	44
3.2	Research Objectives	44
4	<i>Lysine and Lysyl-Histidine Functionalized Nanodiamonds: Synthesis and Physicochemical Characterizations</i>	46
4.1	Author’s Contributions	46
4.2	Abstract.....	47
4.3	Introduction	47
4.4	Materials and methods.....	48
4.4.1	Materials.....	48
4.4.2	Functionalization of NDs	48
4.4.3	Physicochemical Characterization of fNDs	56
4.4.4	Binding of fNDs to nucleic acids	58
4.5	Result and discussion.....	58
4.5.1	Synthesis of fNDs.....	58
4.5.2	Infrared Spectroscopy (IR).....	67

4.5.3	Thermogravimetric Analysis (TGA).....	69
4.5.4	Particle size distribution of NDs	71
4.5.5	Zeta potential of NDs	73
4.5.6	Binding of fNDs with pDNA and siRNA	74
4.6	Conclusion	75
5	<i>Lysine and Lysyl-Histidine Functionalized Nanodiamonds: Development of Stable Colloidal Dispersion for in vitro Cellular Uptake Studies and siRNA Delivery Application</i>	76
5.1	Authors' contributions	76
5.2	Abstract.....	78
5.3	Introduction	79
5.4	Results and Discussion	81
5.4.1	Dispersion stability of lysine NDs in formulations	81
5.4.2	Interaction of lys-NDs with biological growth medium	83
5.4.3	Cellular Internalization of lys-NDs	87
5.4.4	Cellular Internalization of lys-NDs as diamoplexes	93
5.5	Conclusion	97
5.6	Methodology.....	97
5.6.1	Materials.....	97
5.6.2	Preparation of primary ND dispersions.....	98
5.6.3	Selection of the most compatible dispersion medium.....	98
5.6.4	Particle size and zeta potential measurements	98
5.6.5	Interaction of lys-NDs with serum proteins	99
5.6.6	Cell Culture	100
5.6.7	Scanning Transmission X-Ray Microscopy (STXM).....	100
5.6.8	Flow cytometry for lys-NDs	100
5.6.9	Laser scanning confocal microscopy	101
5.6.10	Flow cytometry for lys-ND/siRNA diamoplexes.....	101
5.6.11	Statistical Analysis	102
5.7	Acknowledgments	102
5.8	Disclosure	103

5.9.	Supplementary Information	103
6	<i>Lysine Functionalized Nanodiamonds as Gene Carriers: Efficacy for In Vitro Cellular Delivery and Expression of Small Interfering RNA and in vitro Toxicity Analysis</i>	110
6.1	Author's Contributions	110
6.2	Abstract	111
6.3	Introduction	111
6.4	Materials and Methods	112
6.4.1	Materials	112
6.4.2	Primary NDs dispersion	113
6.4.3	Flow cytometry analysis for GFP knockdown	113
6.4.4	MTT assay for Cellular Proliferation	113
6.4.5	Annexin V Assay for Cellular Toxicity	114
6.5	Results	115
6.5.1	Flow cytometry analysis for GFP knockdown	115
6.5.2	MTT assay for cellular proliferation	119
6.5.3	Annexin V Assay for Cellular Toxicity	121
6.6	Conclusion	124
7	<i>Conclusive Discussion</i>	125
7.1	Phase 1	125
7.2	Phase 2	127
7.3	Phase 3	128
8	<i>Future Directions</i>	131
8.1	Mechanistic studies for identifying endocytotic pathways and subcellular localization 131	
8.2	Design modifications to optimize the formation of lysyl-histidine NDs.....	132
9	<i>Conclusion</i>	136
10	<i>Appendices</i>	137
10.1	Excerpts of Chapter 2: Nanodiamonds as Novel Materials for Therapeutics	137
10.1.1	Production of Nanodiamonds (Section 2.4)	137
10.1.2	Fluorescence imaging (Section 2.8.3.1)	139

10.1.3	Combined Fluorescence and Magnetic Imaging (Section 2.8.3.2)	141
10.1.4	Scattering imaging (Section 2.8.3.3).....	142
10.1.5	Nanodiamonds for Small Molecule Delivery (Section 2.8.4.1).....	142
10.1.6	Nanodiamonds for Protein Delivery (Section 2.8.4.2).....	145
10.2	Use of Scanning Transmission X-ray Microscopy for Characterizing Nano-Delivery Devices	147
10.2.1	STXM for characterizing hard nano-delivery systems	148
11	<i>Bibliography</i>	154
12	<i>Permissions to Reproduce Figures</i>	191

List of Figures

Figure 1.1 Classification of carbon nanostructures.....	3
Figure 1.2 Structures of carbon nanomaterials: Nanotubes (A) nanodiamonds (B) and fullerene (C).....	5
Figure 1.3 Loading of drugs and other active molecules on the surface (A) and in the hollow cavity (B) of single walled carbon nanotube.....	9
Figure 1.4 (A) Encapsulation of gadolinium molecules in C92 fullerene cage and (B) The molecular surgery” approach for encapsulating chemical moieties in fullerene caging.....	10
Figure 1.5 Barriers to successful in vivo delivery of nucleic acids using non-viral vectors	12
Figure 2.1 (A) Schematic representation of ND synthesis in a detonation chamber. (B) High-resolution transmission electron microscopic image of detonation nanodiamonds (NDs).	138
Figure 2.2 Structure of a single ND particle exhibiting a layered morphology	17
Figure 2.3 (A) Bright-field STEM picture of a DND cluster held in contact by adhesion of a single ND grain. (B) When the contact area was irradiated by a 100 times brighter stationary electron beam, creating heat energy, the cluster was cut off within a minute.	22
Figure 2.4 Example of reactions for inter-particle covalent bonding in nanodiamond agglomerates.....	23
Figure 2.5 Schematic illustration of possible networks of NDs.....	24
Figure 2.6 A simplified model of core aggregate showing NDs and graphitic soot.	25
Figure 2.7 Bead assisted deaggregation of NDs under bath sonication	26
Figure 2.8 Parameters that could improve stirred media milling	27
Figure 2.9 Modes for pre-treatment of ND surface.....	30

Figure 2.10 Wet chemistry and gas phase treatments for ND functionalization.....	31
Figure 2.11 Electrostatic interaction and hydrogen bonding (salt bridges) between primary amine of lysine residue and phosphate oxygen of DNA.....	34
Figure 2.12 Uptake of micro and nanoparticles.	37
Figure 2.13 Left panel: Bright-field image of a HeLa cell after uptake of 35-nm fluorescent NDs. Most of the internalized NDs are seen to distribute in the cytoplasm. Right panel: Epifluorescence image of a single HeLa cell after the ND uptake.	140
Figure 2.14 A schematic diagram representing the binding of detonation nanodiamonds with (A) small molecules (B) proteins (C) plasmid DNA and (D) siRNA.....	41
Figure 4.1 ¹ H NMR spectra for N'- (N α ,N ϵ -bis-boc-lysyl)-N''-fmoc-diaminopropane at 500 mHz	60
Figure 4.2 ¹ H NMR spectra of N'(N α ,N ϵ -Bis-Boc-Lysyl)-N''-Diaminopropane at 500 mHz	60
Figure 4.3 ¹ H NMR of N'-(N α -(N α -Nim-bis-boc histidine) N ϵ - boc-lysyl)-N''-cbz-diaminopropane at 500 mHz	61
Figure 4.4 MS spectra of N'-(N α -(N α -Nim-bis-boc histidine) N ϵ - boc-lysyl)-N''-cbz-diaminopropane.....	62
Figure 4.5 MS/MS spectra for fragmentation of N'-(N α -(N α -Nim-bis-boc histidine) N ϵ - boc-lysyl)-N''-cbz-diaminopropane (C ₃₈ H ₅₉ N ₇ O ₁₀)	64
Figure 4.6 ¹ H NMR spectra of N'-(N α -(N α -Nim-bis-boc histidine) N ϵ - boc-lysyl)-N''-diaminopropane at 500 mHz	65
Figure 4.7 MS spectra of N'-(N α -(N α -Nim-bis-boc histidine) N ϵ - boc-lysyl)-N''-diaminopropane.....	66

Figure 4.8 MS/MS spectra of N’-(Nα-(Nα-Nim-bis-boc histidine) Nε- boc-lysyl)-N’’-diaminopropane (C ₃₀ H ₅₄ N ₇ O ₈).....	67
Figure 4.9 Infra-red spectra of pNDs, rNDs, lysine-NDs, lysyl-histidine-NDs and AA conjugate (N’-(Nα-(Nα-Nim-bis-boc histidine) Nε- boc-lysyl)-N’’-diaminopropane).....	69
Figure 4.10 Thermograms of pNDs, rNDs, lys-NDs and lysyl-histidine NDs	70
Figure 4.11 Size distribution curves for pNDs (blue), rNDs (red), lysine NDs (green) and lysyl histidine NDs (purple).....	72
Figure 4.12 Comparison of zeta potentials of NDs before and after functionalization.....	73
Figure 4.13 Binding of lysine-NDs and lysyl-histidine NDs with pDNA	74
Figure 4.14 Binding of lysine-NDs and lysyl-histidine NDs with SiRNA	75
Figure 5.1 Dispersion of lys-NDs in different media.....	83
Figure 5.2 Interaction of lys-NDs with serum free DMEM and with FBS.....	85
Figure 5.3 SXTM images and spectra for lys-ND internalization.	89
Figure 5.4 Flow cytometry histograms showing concentration dependent uptake of lys-NDs through forward and side scattering.....	91
Figure 5.5 Laser scanning confocal microscopic images of the live cell treated with lys-NDs for 24 hours.....	92
Figure 5.6 Laser scanning confocal microscopic images of four consecutive sections from the middle towards the bottom of the cell treated with lys-NDs.....	93
Figure 5.7 Percent fluorescence shift in flow cytometry for cells treated with lys-NDs/COOH-FNDs alone (blue) & diamoplexes of lys-ND or COOH-FNDs with FITC labelled siRNA (40:1) (red) compared to untreated cells (green) in the wavelength range of FITC (emission maximum 525 nm).	95

Figure 5.8 Fraction of fluorescence shift from FITC labelled siRNA when administered directly or as diamplexes with lys-NDs at a ratio of 40:1 (in presence and absence of serum proteins).	96
Figure 6.1 Flow cytometry outputs showing the distribution of untreated cells (A) and siRNA treated cells (B to G) in high, mid, low and no GFP regions.	118
Figure 6.2 Quantitative percent GFP knockdown calculated through flow cytometry outputs	118
Figure 6.3 MTT assay for cytotoxicity of pNDs (blue), rNDs (red), lysine NDs (green) and lysyl-histidine NDs (purple) in HeLa cells at a concentration ranging from 10 µg/mL to 250 µg/mL	120
Figure 6.4 MTT assay for cytotoxicity of lysine NDs in the presence and absence of serum	121
Figure 6.5 Flow cytometry plots indicating early and late apoptotic cellular distribution based on annexin V vs Propidium Iodide uptake	123
Figure 6.6 Flow cytometry analysis for lys-ND induced apoptosis	124
Figure 9.1 Schematic illustration of histidine mediated endosomal escape.....	133
Figure 9.2 Structural illustration of lysine-lysyl-histidine functionalized NDs.....	135
Figure S 5.1 Overlay of flow cytometry spectra and graphical comparison for percent fluorescence shift for untreated (black), Naked siRNA (orange), lys-ND alone (green), lys-ND/SiRNA (20:1) diamoplex (purple), lys-NDs/siRNA (40:1) diamoplex (pink) and lys-NDs/siRNA (50:1) diamoplexes (blue) treated cells.....	105
Figure S 5.2 Overlay of flow cytometry spectra for percent fluorescence shift for untreated (green), lys-NDs alone (blue) & lys-ND/FITC labelled siRNA treated cells (40:1) (red) in absence of serum.	105

Figure S 5.3 Overlay of flow cytometry spectra for percent fluorescence shift for untreated (green), lys-NDs alone (blue) & lys-ND/FITC labelled siRNA treated cells (40:1) (red) in the presence of serum..... 106

Figure S 5.4 Overlay of flow cytometry spectra for percent fluorescence shift for untreated (green), lys-NDs alone (blue) & lys-ND/FITC labelled siRNA treated cells (40:1) (red) in wavelength range of FITC..... 106

Figure S 5.5 Overlay of flow cytometry spectra for percent fluorescence shift for untreated (green), lys-NDs alone (blue) & lys-ND/FITC labelled siRNA treated cells (40:1) (red) in wavelength range of COOH-FNDs..... 106

Figure S 5.6 Percent fluorescence shift for untreated (green), COOH-FNDs (blue) & COOH-FNDs/FITC labelled siRNA treated cells (40:1) (red) in wavelength range of COOH-NDs (670 LP filter) 107

Figure S 5.7 Dose dependent cellular uptake of lys-ND particles evidenced as increasing side scattering. Untreated cells (A), cells treated with lys-NDs at concentrations of 25 $\mu\text{g/mL}$ (B), 100 $\mu\text{g/mL}$ (C) and 250 $\mu\text{g/mL}$ (D). 108

Figure S 5.8 Optical images of untreated cells, cells treated with lysine-NDs on silicon nitride windows prepared for STXM analysis..... 109

Figure A2. 1 (A) STXM images at 285.2eV (MWCNT signal enhanced) and 289.0eV (Formvar substrate signal enhanced), and corresponding TEM picture (B) (a) Spectra of arc-discharge MWCNT, MWCNT+CNP powder, and Formvar substrate (b) One pixel spectra taken on the MWCNT and on MWCNT and on the CNP..... 149

Figure A2. 2 STXM of the dodecyl-functionalized WCPP (wet chemical purification procedure-SWCNT (single-walled CNT): (left panels) C 1s reference spectra used to fit the C 1s image sequence in order to derive the associated component maps (right panels)..... 150

Figure A2. 3 Internalization of metallofullerenol by macrophages (in vivo and in vitro). (A) A Gd M-edge NEXAFS spectrum obtained from Gd@C₈₂(OH)₂₂ nanoparticles. (B) Soft X-ray STXM dual energy contrast images of Gd@C₈₂(OH)₂₂ internalized by a primary mouse peritoneal macrophage *in vivo*. (C) Soft X-ray STXM dual energy contrast images of time-dependent uptake of Gd@C₈₂(OH)₂₂ by primary mouse peritoneal macrophages and RAW 264.7 cell line *in vitro*. (D) ICP-MS quantification of time-dependent uptake in macrophages of primary mouse peritoneal macrophages. 152

List of Tables

Table 1.1 Comparison of structural features and surface characteristics of different carbon nanomaterials 6

Table 4.1 Surface Loading of NDs as calculated from respective thermograms 70

Table 4.2 Particle size distribution and polydispesity of pNDs, rNDs, lysine NDs and lysyl-histidine NDs..... 72

Table 5.1 Zeta potentials of lys-NDs in aqueous medium at different time points 83

Table 5.2 Zeta potential of lys-NDs in serum free DMEM and after serum incubation 86

Table S 5.1 Particle size distrivution and PDI for lys-NDs in aqueous medium on days 1, 3, 15 and 25 103

Table S 5.2 Particle size distribution and PDI for lys-NDs in serum DMEM and after serum incubation at different time points. 103

List of Schemes

Scheme 1 Preparation of lysine-NDs in the presence of diaminopropane as a three carbon chain linker..... 49

Scheme 2 Preparation of lysyl-histidine-NDs in the presence of diaminopropane as three carbon chain linker 50

Scheme 3 Probable fragmentation pattern of N ^γ -(N _α -(N _α -N _{im} -bis-boc histidine) N _ε - boc-lysyl)-N ^γ '-cbz-diaminopropane (C ₃₈ H ₅₉ N ₇ O ₁₀).....	63
Scheme 4 Probable fragmentation pattern of N ^γ -(N _α -(N _α -N _{im} -bis-boc histidine) N _ε - boc-lysyl)-N ^γ '-diaminopropane (C ₃₀ H ₅₄ N ₇ O ₈).....	66
Scheme 5 Design modification to synthesize lysyl-histidine functionalization	134

List of Abbreviations

(N-V)	Nitrogen vacancy
¹H NMR	Proton Nuclear Magnetic Resonance
4-OHT	Hydroxytamoxifen
AAs	Amino acids
ANOVA	Analysis of Variance
ATP	Adenosine triphosphate
Boc	Di-tert-butyl oxycarbonyl
Cbz	Carboxybenzyl
CDCl₃	Deuterated chloroform
CNTs	Carbon nanotubes
COOH-FNDs	Carboxylated fluorescent nanodiamonds
COOH-NDs	Carboxylic acid–functionalized nanodiamonds
Cyt c	Cytochrome c
DCM	Dichloromethane
DIPEA	Diisopropylethylamine
DMEM	Dulbecco’s Modified Eagle Medium
DMF	Dimethylformamide
DMSO	Dimethyl sulfoxide

DOX	Doxorubicin
D-PBS	Phosphate buffered saline with calcium and magnesium and w/o phenol red
EDTA	Ethylene diamine tetra acetic acid
FA	Folic acid
FACS	Fluorescence Activated Cell Sorting
FBS	Fetal bovine serum
FITC	Fluorescein isothiocyanate
Fmoc	Fluorenylmethyloxycarbonyl
FNDs	Fluorescent NDs
fNDs	Functionalized Nanodiamonds
Gd	Gadolinium
GFP	Green fluorescent protein
GO	Graphene oxide
HATU	N,N,N',N'-tetramethyl-O-(7-azabenzotriazol-1-yl)uroniumhexafluorophosphate
HCl	Hydrochloric acid
HeLa Cells	Human cervical cancer cells
HRTEM	High resolution transmission electron microscopy
IL-6	Interleukin-6

INOS	Inducible nitric oxide synthase
iP	Iso-electric points
IR	Infrared
KBr	Potassium bromide
Linker	1,3-diaminopropane
LMW-PEI	Low molecular weight polyethylene glycol
Lys-NDs	Lysine functionalized nanodiamonds
Lysyl-histidine-NDs	Lysyl-histidine functionalized nanodiamonds
MALDI	Matrix assisted laser desorption/ionization
MALDI-MS	MALDI mass spectrometry
MC	Methylcellulose
MDA	Malondialdehyde
MRI	Magnetic resonance imaging
MTT	3-(4,5-Dimethylthiazol-2-Yl)-2,5-Diphenyltetrazolium Bromide
MWCNT	Multi walled carbon nanotube
NAD	Nicotinamide adenine dinucleotide
ND	Nanodiamond
ND-DOX	ND-doxorubicin

ND-Tf	ND-transferrin
NEXAFS	Near-edge X-ray absorption spectroscopy
Nm	Nanometer
NPs	Nanoparticles
PBS	Phosphate buffer saline
Pd/C	Palladium on carbon
PDI	Polydispersity index
pDNA	Plasmid deoxyribonucleic acid
PEG	Polyethylene glycol
PEI	Polyethyleneimine
PI	Propidium iodide
PLLA	Poly(l-lactic acid)
Pmoles	Pico moles
PND	Photoluminescent ND
pNDs	Pristine nanodiamonds
PS	phosphotidylseriene
QDs	Quantum dots
rNDs	Reoxidized nanodiamonds
ROS	Reactive oxygen species

SDS	Sodium dodecyl sulphate
SiRNA	Small interfering ribonucleic acid
STXM	Scanning transmission X-Ray microscopy
SWCNT	Single walled carbon nanotube
TAE	Tris-acetate ethyldiaminetetraacetic acid buffer
TEA	Triethylammonium groups
TEM	Transmission X-ray Microscopy
TGA	Thermogravimetric analysis
TH	Thionine
TNF- α	Tumor necrosis factor alpha
T_{protein}	Thickness of the protein adsorption layer
YTZ	Yttrium stabilized zirconia
ZS	Zetasizer

Introduction

Targeted medicine is a novel therapeutic concept which has dramatically shifted the treatment approaches for many life threatening and chronic human pathologies. It aims at delivering the therapeutic agent directly to the site of action to ensure maximum efficacy and minimum toxicity. A wide array of research is undertaken using this approach for the treatment of various cancers ¹, ² and devastating infections. ^{3, 4} Two major approaches for targeted medicine include the delivery of biotechnological drugs like genetic materials and antibodies or conventional drug molecules to a specific area in the body. The mechanism of action and toxicity profile of drugs change significantly upon targeted delivery, as it offers the advantage of limited dosing and reduced drug related adverse reactions.

Genetic modifications using deoxyribonucleic acid (DNA), small interfering ribonucleic acid (siRNA) and antibody mediated approaches in particular hold a significant importance in clinical science. It mainly emerged through the research advancements regarding human genomics and molecular medicine. Comprehensively, gene therapy is an approach to target the disease at its most basic molecular level by relying on the cellular transfer of therapeutic genes in the diseased individual. In comparison to conventional pharmacological therapies which target mainly the disease management, gene therapy has a potential to offer a complete one-time cure of the molecular aberration related to the disease. ⁵

Both of the above mentioned therapies offer advantages but require competitive delivery vehicles which can effectively bind, protect, carry and deliver the drug or the gene to its site of action. In particular, the gene delivery vectors should be capable of protecting the genetic material from serum nucleases during circulation ⁶ and lysosomal degradation upon cellular entry. Viral vectors such as adenoviruses and retroviruses perform this function well ⁷ but with complications, mainly the immunogenic toxicity. ⁸ This has encouraged the need of developing non-viral alternatives which could provide the same benefit with limited toxicity. Although non-viral vectors have lower transfection efficiency in comparison to viruses, their relative safety and easy scale-up procedures are the major advantages that have driven the development of several types of nanoparticles (NPs). Continued optimization is underway for many of these NPs to maximize their transfection efficiencies.

Carbon nano family holds a significant standing both as drug delivery and non-viral gene delivery vectors.^{9, 10} Among them diamond NPs; also called nanodiamonds (NDs) are the most biocompatible member of the carbon nanofamily that are widely researched for diagnostic and therapeutic applications. Unlike other carbon nanomaterials, the surface of NDs is innately reactive and contains diverse combinations of functional groups. Homogenizing these surface functionalities allows the conjugation of various chemical moieties to target specific actions. To date, NDs are conjugated to a range of inorganic and organic, natural or synthetic functional groups both through physical adsorption and chemical immobilization.^{11, 12, 13, 14, 15} Due to this surface reactivity it provides a favourable system to induce a positively charged surface to electrostatically bind and deliver the therapeutic genes in mammalian cells.

In light of the above mentioned knowledge, the aim of my research was to develop a competitive ND based gene carrier through surface functionalizations. To achieve this purpose I covalently functionalized the NDs with basic amino acids (AAs) to induce a cationic surface. This thesis provides a brief comparison between various carbon nanomaterials as delivery vehicles in therapeutics, detailed insight regarding the biomedical applications of NDs and novel analyses regarding synthesis, physicochemical characterization and cellular interactions of AA functionalized NDs.

1 Introduction to Carbon Nanomaterials as Nano-Delivery Devices

1.1 Introduction

Carbon nanomaterials have gained significant attention in biomedicine due to their enhanced stability and surface properties. This family basically include diamond, nanotubes and fullerenes which derive from several types of primary prototype nanostructures. They are classified based on the hybridization of carbon atoms and their characteristic sizes. ¹⁶ Figure 1.1 classify the important carbon nanoforms and also illustrate their inter-relationships. These materials allow variety of covalent and non-covalent surface functionalizations, and hence can be tailored to specific applications. This chapter will provide a comparison between widely researched carbon nanomaterials in terms of structure, surface properties and biological interactions. It will also elucidate a brief description regarding delivery applications of these nanomaterials in therapeutics.

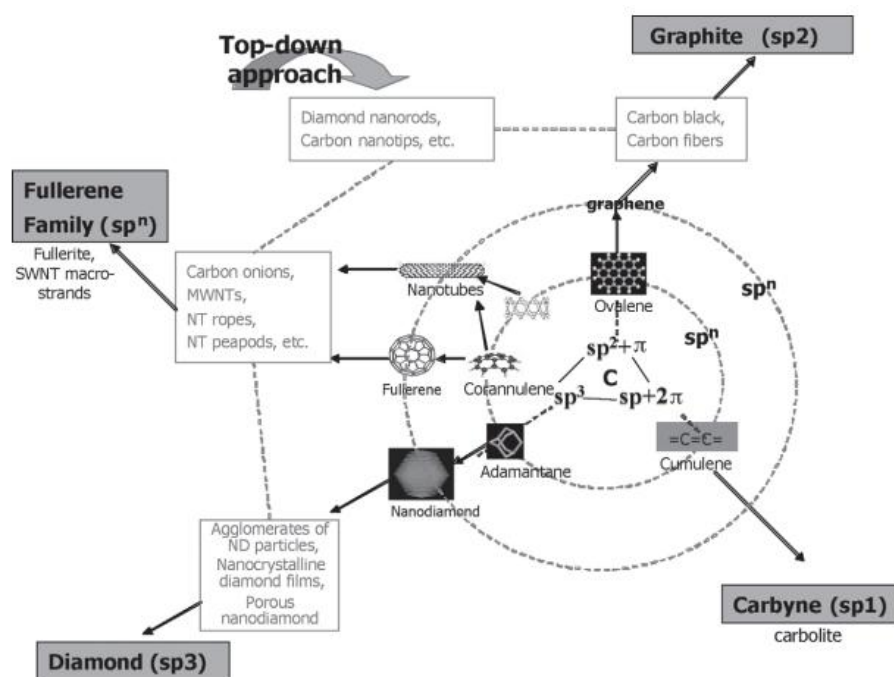
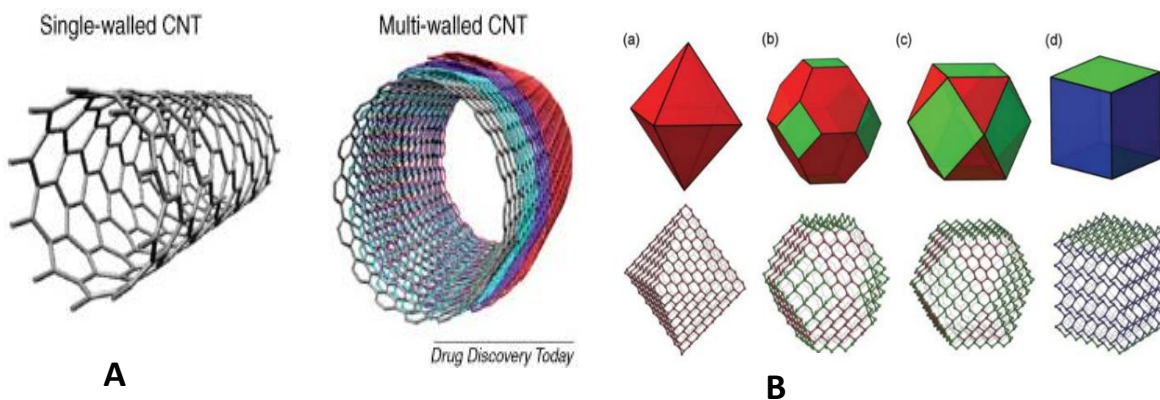


Figure 1.1 Classification of carbon nanostructures. Reprinted with permission from ¹⁶ Copyright © 2002 Taylor & Francis (The mark ‘ sp^n ’ indicates intermediate carbon forms with a non-integer degree of carbon bond hybridization)

1.2 Structure and properties of important carbon nanomaterials: fullerenes, carbon nanotubes and nanodiamonds

The structure of all important carbon nanomaterials including fullerenes, carbon nanotubes (CNTs) and nanodiamonds (NDs) consists of carbon atoms arranged in different configurations (Figure 1.2). A CNT is a tube-like sp^2 hybridized nano-structure having a hollow core (Figure 1.2A). The number of layers defines whether it is a single walled (SWCNTs) or multi walled (MWCNTs) structure (Figure 1.2A).¹⁷ These tubes typically range from sub-nanometers to about 100 nm in size depending upon the number of rings in the structure. The neighbouring tube walls have weak Van der Waals forces, which tend to cause aggregation upon dispersion in the medium.¹⁷ CNTs have an unreactive surface¹⁸ and require chemical modifications to induce functionalizations. Pre-oxidation of the surfaces produce carboxylic and hydroxyl groups which can then be used for covalent coupling of different functional molecules. Although covalent modifications are possible on CNTs, this mode disturbs the structural homogeneity of the tubes and reduces their mechanical stability.¹⁹ Therefore, physical adsorption of desired functionalities still remains the major mode of CNT functionalization. Other important carbon nanomaterials which are considered primitive species for most of the modern forms of carbon based NPs are fullerenes. The most common form of fullerene is the C_{60} molecule (Figure 1.2C) which has 60 carbon atoms arranged as 12 pentagonal and 20 hexagonal conformations. Having a closed-cage morphology, they are considered the most symmetrical structures in the carbon nanofamily.²⁰ Like CNTs, the carbon atoms in fullerene molecules are also sp^2 hybridized. The overall reactivity of the surface is very high due to the electron deficient alkene structure which tends to react readily with electron rich molecules. Unlike other carbon nanomaterials, they can be solubilized in organic solvents like benzene, toluene and chloroform.²⁰



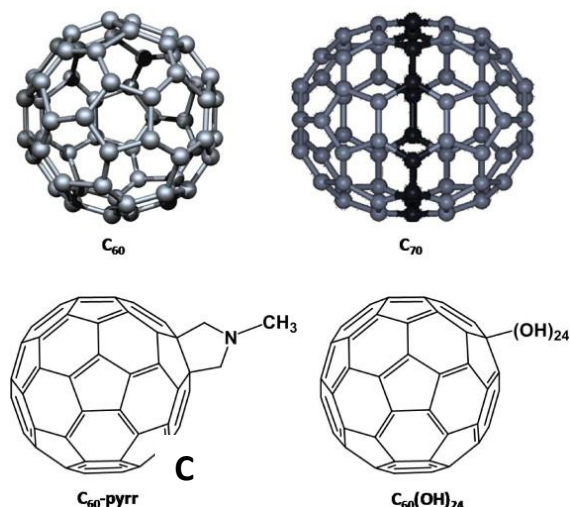


Figure 1.2 Structures of carbon nanomaterials: Nanotubes (A), nanodiamonds (B) and fullerene (C). (A) Shows the molecular structure of single walled and multiwalled carbon nanotubes. Reprinted with permission from ²¹ Copyright © 2010 Elsevier Ltd. (B) shows schematic representations of un-relaxed (initial) structures cleaved from a diamond lattice, showing examples of the (a) octahedral, (b) truncated octahedral, (c) cuboctahedral, and (d) cuboid shapes. Reprinted with permission from ²² Copyright © 2007, Royal Society of Chemistry (C) shows C₆₀ and C₇₀ fullerene structures along with common covalent modifications of C₆₀ molecule (C₆₀-pyridine and C₆₀(OH)₂₄). Reprinted with permission from ²³ Copyright © 2015 Elsevier B.V.

In contrast to above mentioned carbon nanomaterials, NDs possess sp³ hybridized diamond core surrounded by a graphitic shell having sp² hybridized carbon atoms. The sp³ hybridization of the core provides ultrastability to their structure. Diamond nanocrystals can exist in multiple shapes and configurations, which arise due to different arrangements of the facets in the structure. Figure 1.2 B shows few most basic configurations of lattice arrangements in NDs: (a) octahedral (b) truncated octahedral (c) cuboctahedral (d) cuboid shapes. ²² Innately, these structures also possess large number of functional groups which are covalently bonded to the ND particle. ^{24, 25} Unlike other carbon nanomaterials the surface is already reactive and do not require any induction of functional groups to conjugate other chemical species. Functionalization of NDs only demands homogenization of these reactive groups to confer predictable loading of functionally active molecules. Another interesting structural feature that makes NDs superior to other carbon nanomaterials is the presence of colored centres which are point defects in their structure

commonly known as nitrogen vacancies (N-V)⁰ and (N-V)⁻.²⁶ They absorb light at wavelengths of visible, infrared or ultraviolet spectral region,²⁶ and emit bright fluorescence at 550-800 nm.²⁷ Fluorescent nitrogen vacancies in ND core are formed during synthesis and can be further enhanced later, which opens numerous arenas of theranostic applications. Table 1.1 provides a comparison of structural features and surface characteristics of different carbon nanomaterials.

Table 1.1 Comparison of structural features and surface characteristics of different carbon nanomaterials

Carbon nanomaterial	Structure	Surface Properties
Fullerenes	It is a combination of several pentagonal and hexagonal rings of carbon atoms forming a closed cage structure. ²⁰	Surface is highly reactive due to the electron deficient structure. ²⁰ It tends to react readily with electron rich molecules. ²⁰
Carbon nanotubes (multi-walled and single-walled)	SWCTs are circular hollow sheets of graphenes having planer-hexagonal arrangement of carbon atoms distributed in a honeycomb like lattice, while MWCTs are combination of several concentric SWCTs with different diameters. ²⁸	Seamless arrangement of hexagonal rings without any dangling bonds renders the surface to be unreactive innately. ¹⁸ Pre-oxidation is required by various techniques to <i>induce</i> functional groups referred as reactive opening in the structure. ¹⁸
Nanodiamonds	It contains sp ³ hybridized diamond core surrounded by a graphitic shell having sp ² hybridized carbon atoms. ²⁴	Surface contains large number of functional groups which are covalently bonded to the ND particle. NDs only demands homogenization of these

		reactive groups on the surface before functionalization.
--	--	--

1.3 Carbon nanomaterials as drug delivery devices

Carbon nanomaterials can be widely functionalized on the surface to function as delivery devices in therapeutics. CNTs are the most widely researched member of the carbon nanofamily for these applications; however NDs have also recently gained much attention in this area of therapeutic research. NDs offer many advantages over other carbon nanomaterials, which include innately reactive surface, ultrastable diamond core and presence of coloured centres in the diamond core. These characteristics also aid in their application in theranostics through multiple covalent and non-covalent functionalizations. Chapter 2 provides an elaborative discussion regarding the properties and applications of NDs in diagnosis and therapeutics. This section mainly focuses on providing a comparative summary regarding the application of different carbon nanomaterials for drug delivery.

CNTs are functionalized on the external walls to impart favourable aqueous solubility^{29, 30} and binding to therapeutic molecules.⁹ Biological molecules can be attached to CNTs either by wrapping around the surface through functional groups or can be loaded inside the hollow core.³¹ Attachment of the functionalities along the surface is widely accepted and can be done through non covalent hydrophobic or Vander Waals interactions or through covalent binding of biocompatible groups on the surface. Non covalent interactions preserve the aromatic structure of the tubes but are not suitable for targeted delivery applications due to low stability in the biological media.³²

CNTs have applications mainly in cancer therapeutics. Covalent conjugation of drugs on the surface is more preferred due to longer stability profile in the complex biological environment. An example of such an application is the delivery of anticancer drugs like paclitaxel. When CNTs were employed as a delivery vehicle for paclitaxel, a common plant alkaloid used for cancer treatment, it was attached covalently to the surface through a double functionalization approach.

³³ In this approach the surface of CNTs was non-covalently functionalized with amine containing

polymers and paclitaxel was modified into carboxy-paclitaxel. Functionalization was achieved by secondary covalent interaction through amide bonds between the polymer amines on CNT surface and carboxyl groups attached to paclitaxel.³³ This approach to deliver paclitaxel reduced the required dose to achieve tumor suppression due to around 10 fold higher tumour uptake of the drug. On the other hand, successful paclitaxel delivery into the tumour and subsequent tumour suppression is also achieved through NDs.³⁴ However unlike CNTs; conjugation of the drug on NDs did not require any secondary functionalization and was done through direct covalent bonding on reoxidized NDs having carboxylate functional groups on the surface.³⁴

Therapeutic molecules have also been attached to carbon nanomaterials by non-covalent hydrophobic or electrostatic adsorption. SWCNTs have been attached to doxorubicin through pi-pi bonding and hydrophobic interactions between the aromatic rings of doxorubicin and external carbon walls of SWCNTs.³⁵ Another approach to increase surface loading of non-covalently bound anticancer drugs on CNTs involves primary functionalization of the external walls with surfactants followed by secondary complexation of the desired drug through surface bound surfactants. In this approach polyethylene glycol (PEG) with selective terminal functionalities is used to facilitate electrostatic interactions.³² Like CNTs, NDs also allow non-covalent loading of drugs onto its surface.³⁶ All of the studies concluded that carbon carriers facilitated higher uptake of anticancer drug in the cells and reduced cancer cell proliferation.

Although both CNTs and NDs have equal standing as vehicles in drug delivery research, physical adsorption of drugs on ND surface can be more convenient and straight forward.³⁶ Moreover, there are certain advantages presented by each member of the carbon nanofamily:

- NDs have an advantage over CNTs: Complexation and release of the drug from ND surface is pH sensitive, with highest complexation observed at basic pH.^{36, 37, 38} This is due to the presence of ionisable groups (e.g. -COOH, -CONH, -OH, -NH₂, -SH) on the surface, due to which NDs possess a combinational pKa. Changes in pH with respect to pKa can cause variations in the electrostatic charge states of the surface functional groups which in turn facilitate interactions with drug molecules.³⁸ When the pH turns acidic, the conjugated drug becomes protonated and thus release from ND surface.³⁶ This phenomenon is promising to confine the release of anticancer drugs at the acidic tumour site and also facilitate their uptake by cancerous cells which have a lower pH (5.8) than normal cells (pH 7.00-8.06).³⁹

- CNTs have an advantage over NDs: Unlike NDs which allow drug loading only on the surface, CNTs can facilitate drug wrapping around the surface and drug filling in the hollow core (Figure 1.3).^{31, 40} This type of loading can allow gradual and sustained drug release and also protects the therapeutic molecules from biological environment.

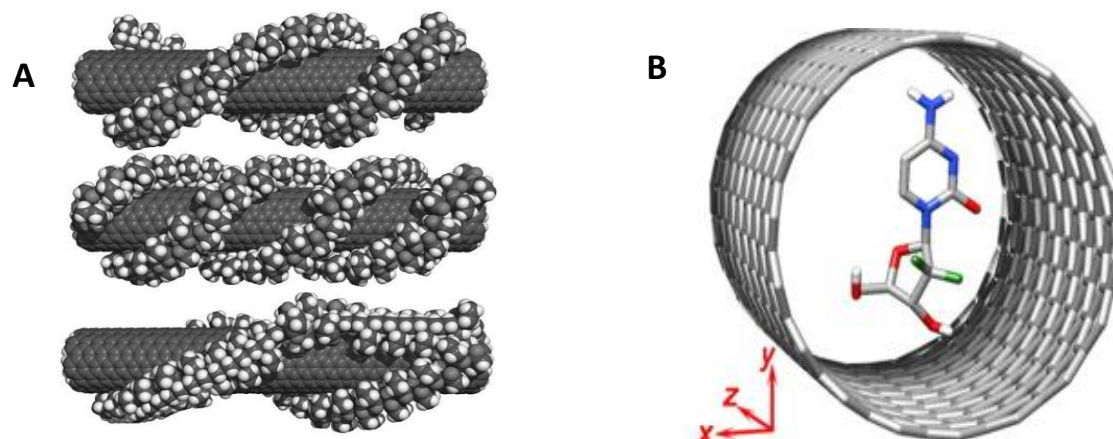


Figure 1.3 Loading of drugs and other active molecules on the surface (A) and in the hollow cavity (B) of single walled carbon nanotube. (A) Shows possible arrangements of the polymer wrapping around the nanotubes. Top image corresponds to a double helix, the middle scheme is a triple helix, whereas the bottom arrangement shows switch backs, which allow multiple parallel wrapping strands to come from the same polymer chain owing to the backbone bond rotations. Reprinted with permission from⁴¹ Copyright © 2001 Elsevier Science B.V. (B) shows the structure of the single-walled carbon nanotube (SWCNT) complexed with the gemcitabine drug. Reprinted with permission from³¹ Copyright © 2010 Elsevier Inc.

In addition to CNTs and NDs, fullerenes another member of the carbon nano-group also have interesting applications in drug delivery. Recently, amphiphilic fullerenes were designed to aid in the delivery of hydrophobic drugs like paclitaxel.⁴² Amphiphilic fullerenes are functionalized in way that facilitates self-assembling like lipids into either a hydrophilic vesicle with an empty cage or a solid nanostructure with a hydrophobic interior.^{42, 43} Water insoluble drugs like paclitaxel can be packed inside the hydrophobic pockets and the hydrophilic surface can facilitate optimum delivery without the use of irritating non-aqueous solvents. Fullerene-mediated anticancer drug delivery is also shown to deliver comparable amounts of drug (paclitaxel) at

tumour site compared to the commercially available nanoparticle albumin-bound form of paclitaxel (Abraxane).⁴² Another common fullerene type is the metallofullerenes which encapsulate metallic ions inside the hollow cage, mostly researched for bioimaging (Figure 1.4A). A classic example of its utilization is the development of gadolinium-encapsulated metallofullerene as contrast agents to enhance MRI quality. Fullerene caging protects the gadolinium against degradation allowing longer residence times.^{44, 45, 46} Recently, a novel technique called ‘molecular surgery’ was introduced to encapsulate drugs and metals in the fullerene cage.^{47, 48} In this approach, a hole is introduced in the sphere through chemical reactions like radical-oxidation and cycloadditions and the desired chemical is inserted in the cavity. Followed by encapsulation, high temperatures are used to reseal the orifice (Figure 1.4B).

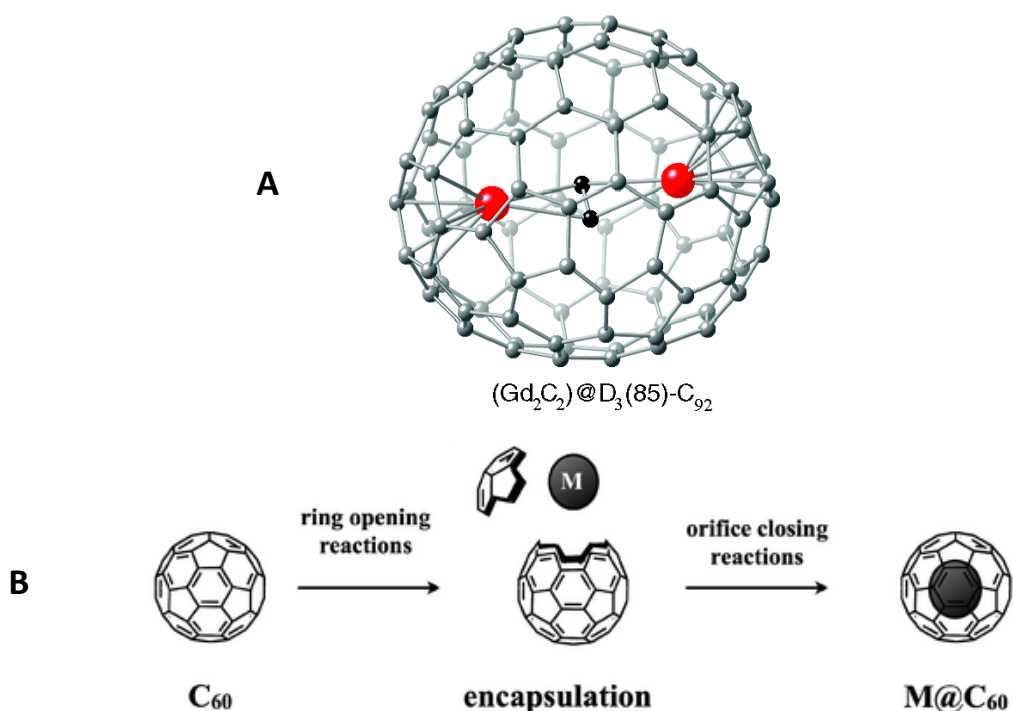


Figure 1.4 (A) Encapsulation of gadolinium molecules in C₉₂ fullerene cage and (B) The ‘molecular surgery’ approach for encapsulating chemical moieties in fullerene caging. (A) is reprinted with permission from⁴⁹ Copyright © 2008, American Chemical Society (B) shows hole generation by provoking σ and π bond scission, insertion of the guest molecule, and reconstruction of the fullerene structure. Reprinted from⁴⁸ Copyright © 2011, Royal Society of Chemistry.

1.4 Carbon nanomaterials as gene delivery devices

Unlike small molecules, biomolecules like proteins and genetic materials cannot internalize the cells due to their anionic nature. In order for a nucleic acid to reach the target cells with full functional capacity and successfully transfect the host cell population, it requires to overcome five major barriers^{50, 51, 51, 52} (Figure 1.5):

- Extracellular degradation by exonucleases during circulation.⁵¹ It makes the delivery of naked nucleic acids through blood circulation almost impractical. Moreover, cationic carrier systems rapidly interact with serum proteins resulting in recognition and elimination by reticuloendothelial system (RES).⁵¹
- Entry into the cells through anionic cell membrane.⁵² Cationic carriers wrap the nucleic acids to bypass the cell membrane, however the positivity of the surface required to facilitate this phenomenon may also cause cellular damage.⁵³
- Endosomal entrapment and subsequent lysosomal degradation is the third and most critical barrier for nucleic acid delivery. Highly acidic nature of late endosomes (pH ~4) triggers their fusion with lysosomes that subsequently cause enzymatic degradation of therapeutic genes.^{54, 55}

A wide array of mechanisms is studied to target the release of nucleic acid-carrier complexes from the lysosomes:

1. Destabilization of the membrane through ion pairing between cationic carrier lipids and anionic lipids of endosomes⁵⁶
 2. Proton sponge effects through molecules with low pKa (like polyethylenimine or histidine) causing endosomal swelling and lysis⁵⁷
 3. Membrane destabilizing proteins that convert to hydrophobic membrane-active forms in acidic medium^{58, 59} to cause endosomal lysis
 4. Hydrophobic modifications of cationic polymeric vectors to cause endosomal lysis⁶⁰
 5. pH sensitive degradable vector that consume hydrogen and degrades in endosome. The hydrogen consumption ultimately increases the osmotic pressure and lyse the endosomal membrane.⁶¹
- Inability of the vector to release the nucleic acid due to excessive strength of binding.^{62, 63} It is encountered as a hurdle after escape of the gene-carrier complexes from lysosomes. It is shown to be another rate limiting step for gene transfection.

- The final barrier for gene transfection is their delivery across nuclear membrane.^{64, 65} In ideal cases, the gene at this stage is free from the carrier and fully functional. Nuclear delivery can occur either via nuclear membrane breakdown or through nuclear pore complexes, both of which pose different challenges to bypass the therapeutic genes.⁶⁵ However, this challenge is only associated for the transfection of pDNA which require nuclear entry and integration in human genome to produce effects. Conversely, RNA interference machinery is present in the cytoplasm and therefore nuclear delivery of siRNA is not required and the above phenomenon does not pose any challenges for its therapeutic action.

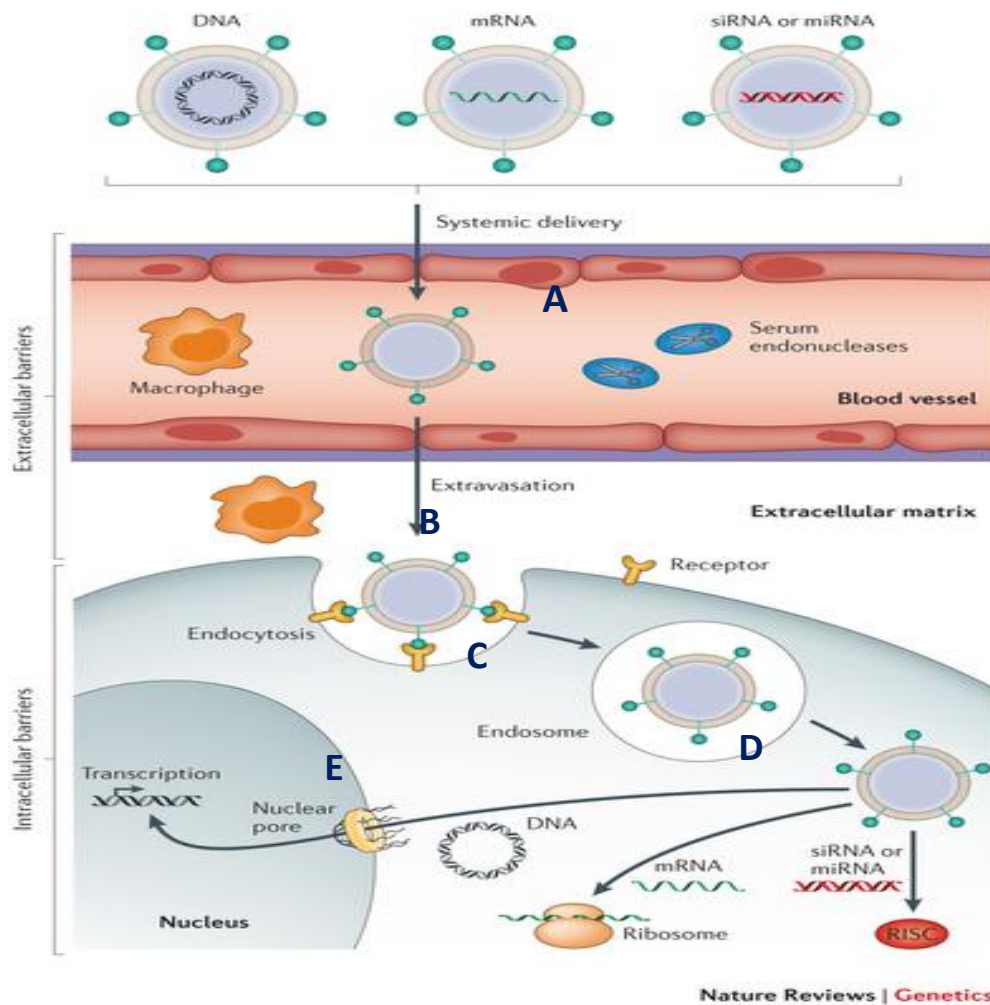


Figure 1.5 Barriers to successful in vivo delivery of nucleic acids using non-viral vectors: (A) Degradation during circulation; (B) Cellular entry through anionic cell membrane; (C) Endosomal entrapment and subsequent lysosomal degradation; (D) Inability of the vector to release the nucleic acid due to excessive strength of binding; (E) DNA delivery across

nuclear membrane. Reprinted with permission from ⁶⁶ Copyright © 2014, Rights Managed by Nature Publishing Group.

Carbon nanomaterials have shown tremendous progress to overcome these barriers and serve as delivery vehicles for biomolecules. Several types of surface functionalizations on carbon NPs creates a possibility to bind and deliver therapeutic genes in the cells. The common approach towards utilizing them as gene carriers is the creation of a cationic surface that can electrostatically bind the nucleic acids. It can be obtained through various covalent and non-covalent functionalizations on the surface of carbon nanoparticles. Among some widely researched cationic molecules used for such functionalizations include peptides like poly-L-lysine,⁶⁷ synthetic ammonium derivatives⁶⁸ and polymers.⁶⁹

Although the cationic surface of functionalized carbon nanomaterials facilitate binding and intracellular delivery of genes, this interaction is required to be optimally controlled. As mentioned earlier, strong interactions between the carrier and the nucleic acid may hinder the release of the gene in the cytoplasm, thereby reducing the transfection efficiency of the system. A modern approach to counter the excessive strength of binding is the incorporation of reducible disulfide bonds on the surface of the carrier.⁵⁰ Disulfide linkages are stable in the extracellular environment, but protonates in the reductive intracellular glutathione rich environment. The cytoplasm of the cells contain 1000 fold higher concentration of glutathione, which favours the cleavage of disulfide bonds causing selective gene release from reducible carriers. Disulfide modifications in the carrier-gene complexes are done through cationic lipids, peptides like poly-L-Lysine, polymers like polyethylenimine, thiol reactive polymers and disulfide modified genetic materials.⁵⁰ Recently, this strategy was applied on CNTs to optimally control their electrostatic interactions with nucleic acids. SWCNTs were decorated by a linker (Sulfosuccinimidyl 6-(3'-[2-pyridyldithio]-propionamido) hexanoate) which conjugated thiolated siRNA through disulphide linkage.⁷⁰ Successful silencing of CXCR4 mRNA was obtained which is promising to knock down the principle receptor CXCR4 responsible for HIV viral entry in human T cells.⁷⁰ Amine functionalized SWCNTs were also decorated with disulphide bonds which interact with thiol derivatives of biomolecules. This functionlization has been successful in transporting, releasing and expressing DNA oligonucleotides better than the conventional transfecting agent

lipofectamine.¹⁰ Detailed review of various functionalizations on ND surface for gene delivery is discussed in chapter 2.

1.5 Comparative biocompatibility profiles of carbon nanomaterials

Due to numerous biological applications of carbon nanomaterials, it is important to understand the biocompatibility of these systems at cellular, organ and organism levels. Toxicity of carbon based NPs is dependent upon mass, purity, surface functional groups, overall surface charge and particle size.⁷¹

To date, NDs are considered the most biocompatible member of the carbon nanofamily. When the toxicity of ND was compared with other members of the carbon nanofamily, i.e., carbon black, multi-walled carbon nanotubes and single walled carbon nanotubes, in neuroblastoma cells and macrophages, it was revealed that the degree of cytotoxicity occurs in following order: single-walled nanotube > multi-walled nanotube > carbon black > ND.⁷¹ In another study, NDs were found to be more inert towards cellular proliferation as compared to CNTs which reduced the cell viability significantly up to 60% at similar concentrations and under same experimental conditions.⁷²

The principal reason toward unpredictable and rudimentary understanding of the biological effects of CNTs is that they exist in different morphologies. By functionalization, these nanomaterials could be rendered as safe and effective as delivery vehicles.^{73, 74, 75} However, details regarding effects of these functionalizations are beyond the scope of this chapter. Comparative biocompatibility of NDs and factors affecting their biological interaction are further discussed in chapter 2.

1.6 Conclusion

Carbon nanomaterials have enormous potentials as delivery vectors in nanomedicine; since they can be tailored according to the application through surface modifications. The comparative analysis provided above also builds an understanding that NDs being the novel members of carbon nano family has a potential to provide promising avenues for safer gene therapy by combining two key parameters: acceptable delivery efficiency and optimum biocompatibility.

2 Nanodiamonds as Novel Nanomaterials for Therapeutics: Structure, Production, Properties and Biomedical Applications

Saniya Alwani and Ildiko Badea

Drug Discovery and Development Research Group, College of Pharmacy and Nutrition,
University of Saskatchewan, Saskatoon, Saskatchewan, Canada

2.1 Authors' Contribution

Saniya Alwani:

- Written and edited the book chapter in its entirety

Ildiko Badea:

- Supervised the entire work
- Assisted in the revision and editing of the text in the book chapter

Note:

The thesis only includes the information that is relevant to work presented in the thesis. Remaining chapter is presented in Appendix 10.1. The information not presented in the thesis is indicated under the respective subheadings.

2.2 Abstract

Nanodiamonds (NDs) being the most biocompatible member of the carbon nanofamily is widely researched for diagnostic and therapeutic applications. Unlike other carbon nanomaterials, the surface of NDs is innately reactive and contains diverse combinations of functional groups. Homogenizing the surface through oxidation or reduction allows conjugation of various chemical moieties to target specific actions. To date NDs are bonded to a range of inorganic and organic, natural or synthetic functional groups both through physical adsorption and chemical immobilization. Functionalization of NDs also provides a chemical means to counter NDs aggregation, which is considered as a major challenge toward its biomedical applications. Physical approaches are also broadly studied to produce well-dispersed stable ND dispersions. NDs are also investigated extensively for its interaction with biological system at cellular and organism levels. They are distributed in the body but are trafficked significantly through various protective mechanisms similar to other nanoparticles. However, significant biocompatibility and affinity for diverse range of biomolecules and therapeutic agents still make them attractive for nanomedicine especially as biomarkers and delivery vehicles. This chapter provides a detailed outlook regarding the structure, composition and properties of NDs. Challenges associated with its utilization and recent approaches to counter them are also elaborated. Diverse array of diagnostic and therapeutic applications of ND based systems are presented.

2.3 Introduction

Carbon is the one of the most abundant element in earth's crust which is known to exist in all life forms. Diamond is considered the hardest allotrope of carbon possessing a tightly packed interpenetrating cubic lattice structure. Extremely high bond energy between two carbon atoms (83kcal/mol) and the directionality of tetrahedral bonds ⁷⁶ account for the ultra-stable nature of the diamond core.

Diamond nanoparticles, also called nanodiamonds (NDs) are carbon nanomaterials which exhibit unique biological, thermal, mechanical and optoelectronic properties. They possess high surface areas and tunable surface structures. Due to their inherent properties, NDs are widely utilized in electronics ⁷⁷, medicine ⁷⁸ and advanced research technologies. ^{79, 80, 81}

2.4 Production of NDs

This portion of the chapter is presented in Appendix 10.1.

2.5 Core structure, surface chemistry and chemical composition of NDs

A single detonation ND is composed of a 4-5 nm diamond particle having sp^3 hybridized carbons atoms surrounded by an amorphous and graphitic sp^2 hybridized carbon layer bearing large number functional groups on the surface,²⁴ as represented in Figure 2.2.

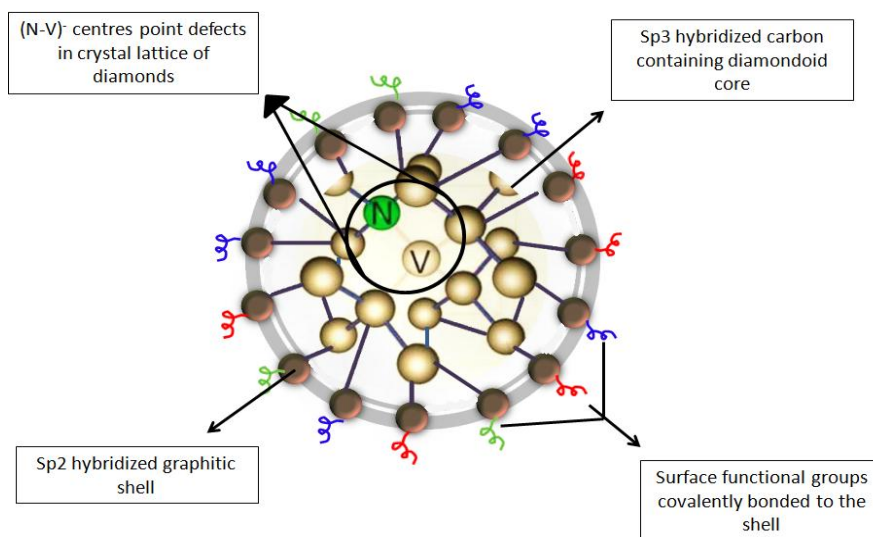


Figure 2.1 Structure of a single ND particle exhibiting a layered morphology

Chemical composition of NDs is well elucidated. They consist of carbon to an extent of 80-88%, and this carbon predominantly forms diamond phase. Along with carbon, NDs also contain oxygen (10% or more), hydrogen (0.5-1.5%), nitrogen (2-3%), and an incombustible residue (0.5-8.0%) by weight.⁷⁷ Recent elemental analysis reports 90% of carbon, 3% of oxygen and 0.8% of hydrogen contents in ND.⁸² The difference in oxygen and hydrogen contents can be attributed to water; since absolute removal of sorbed water is not possible.^{82, 83} A single particle consist of a crystalline diamond core, surrounded by an amorphous shell (coat) comprised of functional groups. These groups are covalently bonded to ND particle and determine the chemical state of its surface.²⁵ The diamond core consists of sp^3 hybridized carbons where all four carbons are bonded via sigma bonds with other carbon atoms and forms a tetrahedral symmetry.⁸⁴ ND shell consists of sp^2 hybridized carbons in which central carbon is attached to

three more adjacent carbons via sigma bonds and has a cloud of delocalized pi-electrons. This sp^2 hybridized carbons arrange in two dimensional planar hexagonal graphite layers⁸⁴ and contain functional groups. These functional groups may include hydroxyl, carbonyl, ether or anhydride. Nitrogen containing groups like amine, amide, cyano or nitro groups might also appear, however evidence suggests that most of the nitrogen is accumulated in the core.⁸⁵ Minute quantities of sulfone, methyl or methylene groups may also be present on the ND surface.²⁴ Apart from functional groups, sorbed water may also be present in the pores between NDs resulting from aggregation.²⁴ The absence of free electrons in the structure accounts for its inert nature.⁸⁴ Spectroscopic and scattering analysis of detonation NDs reveal a core size distribution that peaks at 5 nm.^{86, 87} However clear signals of diamond core are not clearly detectable even after vibrant cleaning, due to extensive layering of non-diamond amorphous carbon appearing as various functional moieties like C-C, C=C, C-H, C-O and C=O.⁸⁷ High temperature high pressure synthesis of NDs greatly reduces this graphite contamination and the diamond peaks in spectroscopic analysis are more discernable.^{87, 88}

2.5.1 Defects in ND structure

Detonation NDs are considered to have a faulty and a defective structure. Experimental analysis using high resolution transmission electron microscopy reveals that the core of ND particle consists of regularly arranged carbon atoms, but may possess few structural aberrations.⁸⁹ A common structural defect in natural and synthetic ND is multiple twinning in which two individual crystals share same crystal lattice symmetry.^{90, 87} Twins once formed; act as preferential sites for impurities and defects.⁹¹ This process may also increase fragility of NDs.⁸⁷ Nitrogen impurity is the most common point defect that may exist in the diamond structure as a result of detonation (Figure 2.2). It consists of a nearest-neighbor pair of nitrogen atom, which substitutes for carbon atom and forms a vacancy in the diamond lattice.⁹¹ The nitrogen vacancy (N-V) centres are responsible for photoluminescence properties of NDs and exploited for medical imaging purposes.

Conclusively, NDs appear to have spherical morphology having a well-defined diamond cage in the core. The structure of the surface varies with synthetic and post synthetic conditions.⁹⁰ This unique structure of ND provides many advantages over other carbon nanomaterials which usually feature a chemically inert bare graphitic surface like in the case of graphenes or carbon nanotubes

or structure-less mixture of different forms of carbon (amorphous or disordered carbon) with less controllable and less accessible external surface.⁹²

2.6 Properties of NDs crucial for biomedical applications

NDs have attracted significant attention in numerous applications due to their innate physical and chemical properties. In particular, detonation NDs have the propensity to form a porous cluster structure in solution, therefore many molecules can be adsorbed on its surface. This phenomenon is exploited for developing novel technologies in nanomedicine like a smart drug complex providing attractive features such as sustained release and targeting. Moreover, they also allow chemical modification of the surface which opens avenues for designing smart hi-tech tools.

The following are some key properties of NDs making them attractive for electronic, mechanical and medicinal research.

2.6.1 Toughness

NDs possess many properties of bulk diamond, among which is the extra ordinary hardness and rigidity,⁹³ suggesting that NDs are highly resistant to deformation under corrosive environments. This property attracts extensive interest in utilizing NDs for designing biological implants.⁹⁴ Implantable delivery systems require optimum hardness characteristics to ensure tunable release rates of the incorporated therapeutic molecule.⁹⁵ NDs due to their rigid structure introduce these properties and can develop biocompatible and mechanically durable implants for localized delivery.

NDs are also investigated for engineering nanocomposites for bone tissue engineering.⁹⁶ Substitution of the composite with NDs resulted in an increase in Young's modulus (200%) and overall hardness (800%) of the system. It was also shown to have least negative impact on osteoblastic proliferation even at high concentrations of 100 $\mu\text{g/mL}$ *in vitro*. Additionally, the proliferation of osteoblasts was also maintained upon direct interaction with the scaffolds containing up to 10% of ND complexes. Osteoblastic activity is critical component of a healthy bone mineralization and to reduce bone resorption.^{97, 98} This opened new avenues to utilize NDs for making up bone scaffolds.⁹⁶

2.6.2 Inertness

This property is particularly useful for biomedical application of NDs, where the particle must have intrinsic ability to protect its integrity in case of any impact from the surrounding environment. ND shows this chemical inertness to a large extent and is capable to maintain its inherent structure and properties in the presence of corrosive biological environment containing acids, bases, enzymes and many other chemicals. A study conducted by Yuan et al revealed that the diameter of NDs remained unchanged even after residing for several days in various organs, highlighting their resistance towards biotransformation and degradation following digestion.⁹⁹

2.6.3 Large surface area and high adsorption potential

Another important feature that makes NDs an interesting tool for biomedicine and engineering is the high surface area to volume ratio that allows a large amount of active moieties to be loaded onto its surface. For therapeutic applications, NDs can be functionalized with various chemical groups to allow adsorption and delivery of therapeutic small molecules and biomolecules. Using this property as a tool, many concepts have been generated to utilize NDs as delivery agents for nanomedicine.^{100, 101, 102} The large surface area of NDs also facilitates their utilization in specialized areas such as an intestinal adsorbent for removing toxic metabolites of protein and non-protein origin like drugs, xenobiotics, radionuclides, metals and exotoxins out of the body.^{103, 104}

NDs retain the functional properties of the adsorbed materials and hence can also be used as analytical tools for extraction and purification of proteins from natural origin and recombinant technologies.¹⁰⁴

2.6.4 Photoluminescence of NDs

NDs are optically transparent and are capable of producing luminescence from coloured centres. These colored centres are point defects in their structure commonly known as nitrogen vacancies (N-V)⁰ and (N-V)⁻ (Figure 2.2). They absorb light at wavelengths of visible, infrared or ultraviolet spectral region,²⁶ and emit bright fluorescence at 550-800 nm.²⁷ Fluorescent nitrogen vacancies in ND core are formed during synthesis, and can be further enhanced by altering the diamond properties through high energy ion beam irradiations and subsequent thermal annealing.

105

In relationship to NDs, fluorescence is often used interchangeably with photoluminescence to define spectroscopic properties of NDs. Photoluminescence is a broader term encompassing both fluorescence and phosphorescence properties of spectroscopically active molecules.¹⁰⁶ Photoluminescence of NDs is dependent on the particle size and excitation laser intensity.¹⁰⁷ For smaller particles (5-50 nm) the spectra show structure-less bands in an emission range of 550-700 nm and for larger particles (100- 500 nm) structured emission bands in 580-720 nm range are observed.¹⁰⁷ Changes in the spectral patterns of NDs with particle size are correlated with the differences in structure and features contributing towards photoluminescence. For smaller particles, the surface is well-defined and hence the natural defects created on the surface are the major contributor towards photoluminescence. Additionally, surface carbons in three-fold coordinated state (i.e. sp^2 hybridization) and the dangling bonds created with surface carbons of adjacent NDs in the cluster also contribute towards emission. The intrinsic diamond core defects are postulated to contribute for structure-less region in the spectra.¹⁰⁷ Unlike small NDs, larger diamond particles do not have a well-defined surface due to aggregation; hence the vacancy centres in the diamond core and the heterogeneity in the diamond phase resulting during synthesis or post synthetic treatment are competing origins of photoluminescence.¹⁰⁷

Stable photoluminescence, lack of photobleaching and numerous opportunities of functionalization render the NDs an attractive probe for bioimaging. However, some limitations, such as low intensity of fluorescence, remain¹⁰⁸ requiring further optimization before its commercial use in diagnosis.

2.6.5 Aggregation

Small sized (5 to 10 nm) NDs possess a tendency to form aggregates of tens to hundreds of nanometers to minimize their surface free energy.¹⁰⁹ Multiple NDs can adhere together forming stable core aggregates. Adhesion between two detonation NDs can be strong enough to hold a large cluster of NDs, as depicted in Figure 2.3. Continuous application of mechanical or vibrational energy through methods such as heating or milling can overcome these adhesive forces leading to disaggregation of ND particles.⁸⁷

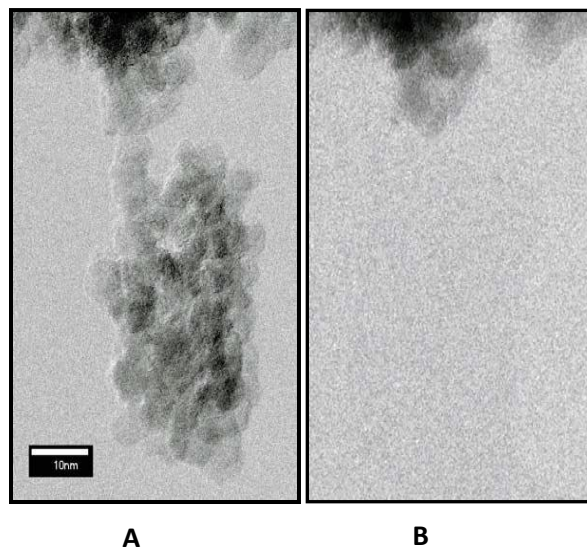


Figure 2.2 (A) Bright-field STEM picture of a DND cluster held in contact by adhesion of a single ND grain. (B) When the contact area was irradiated by a 100 times brighter stationary electron beam, creating heat energy, the cluster was cut off within a minute. (scale bar 10 nm) Reprinted with permission from ³⁰ “Copyright (2008) IOP Publishing”

Aggregation could be an advantageous property to a certain extent as the size of the aggregate majorly controls their cellular uptake in biological system. There is always an optimum particle size which facilitates controlled cellular uptake through a phenomenon called wrapping effect, a process by which the cell membrane encloses the NP for internalization. Very small particle size (5-10nm) results in minimal receptor-ligand interaction which is insufficient to stimulate the cell membrane to wrap around the particle.¹¹⁰ Aggregation of primary NDs sized 2 to 8 nm to 20-30 nm particle size range is favourable for cellular uptake. It could lead to enhanced interactions with receptors on the cell surface¹¹¹, undergoing receptor mediated endocytosis. Aggregation up to a certain degree will result in low surface energy, contributing to the increased stability of the system.

However, there is a narrow range where aggregation results in favourable responses. Large aggregates of 100-200 nm might result in formulation challenges and biological incompatibilities.

¹¹² These issues are discussed in the next chapter.

2.7 Dispersion stability of NDs - a challenge for biomedical application

Formation and maintenance of well-dispersed NP formulation in biologically relevant media is a critical parameter for controlled therapeutic response. Propensity of NDs to aggregate in tight structures of 100 to 200 nm⁸⁵ is a major formulation challenge associated with their biological application, such as incompatibilities. Therefore, this issue is of great interest to researchers utilizing addressed NDs as imaging and therapeutic tools.

2.7.1 Theories related to ND aggregation

Several theories have been formulated to explain ND aggregation. These theories summarize the mechanisms promoting aggregation and the factors affecting these mechanisms.

2.7.1.1 Aggregation mediated through surface functional groups

Unlike other carbon nanomaterials, NDs possess a functionalized surface as a result of the detonation process. The functional groups present on detonation NDs facilitate aggregation through van der Waals interactions or hydrogen bonding between adjacent ND crystals.^{16, 113, 114} The Vander Waals forces are inversely proportional to the particle size of NDs. The typical proportionality of attractive forces to ND size is found to be $1/r^6$, where 'r' represents the radius of particle. For NDs having size less than 10 nm, surface groups may react together forming covalent bonds (Figure 2.4) and yields aggregated crystal- like ordered structures.^{115, 116}

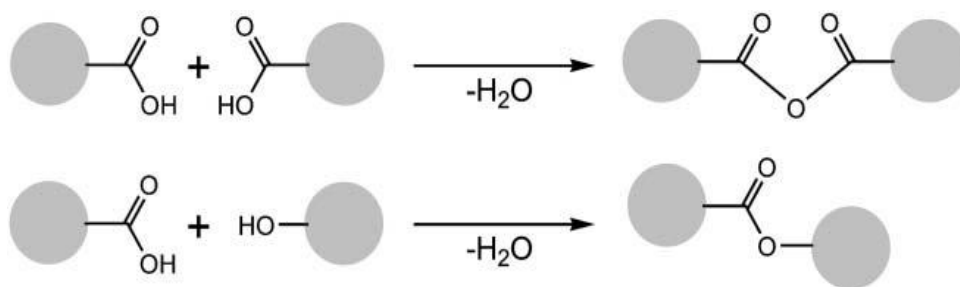


Figure 2.3 Example of reactions for inter-particle covalent bonding in nanodiamond agglomerates. Reprinted with permission from ¹¹⁶ “Copyright (2006) Royal Society of Chemistry”

2.7.1.2 Aggregation mediated through ND facets

This theory suggests self-assembly through electrostatic interactions between different facets of NDs.^{117 118 119} Individual ND particles exhibit anisotropic facet variations i.e. it consists of two distinct facets. These include facets with a net positive charge and facets with either neutral or net negative charge depending upon the degree of graphitization.²² This polyhedral and multi-polar structure of NDs can possibly attract each other and form aggregates. The type of interaction involving neutral facets as primary participants in aggregation of NDs is characterized as ‘coherent interfacial Coulombic interactions’, while all other alternating configurations resulting from random interactions are termed as ‘incoherent interfacial Coulombic interactions’.¹¹⁸ A variety of different one or two dimensional self-assembled networks and supra-structures are possible through these interactions as depicted in Figure 2.5.

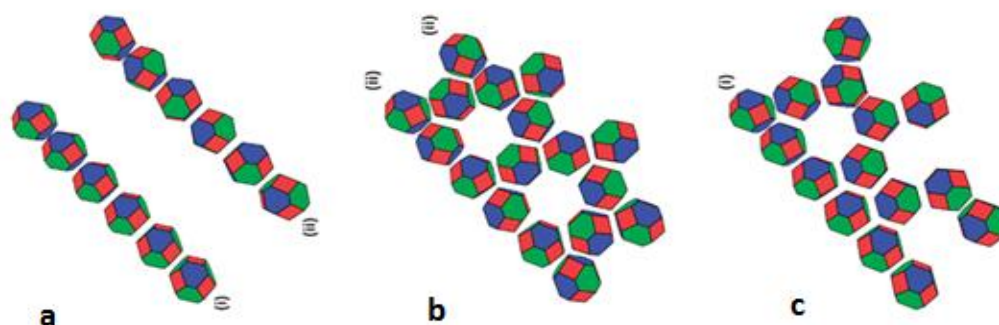


Figure 2.4 Schematic illustration of possible networks of NDs. (a) one-dimensional orientation (b) & (c) two-dimensional orientation based on (111)–(111) and (100)–(111) interaction configurations. (100) represents facets with a net positive charge and (111) represents facets with either neutral or net negative charge. Reprinted with permission from¹¹⁷ “Copyright (2008) Royal Society of Chemistry”

2.7.1.3 Aggregation mediated through graphitic soot

This is the most widely addressed theory of ND aggregation. It suggests that the major cause of aggregation is the graphitic soot formed as a result of the detonation process around the NDs. There are three sets of major events that occur during the deposition of carbon atoms from the detonation mixture, which explains the mechanisms and the factors affecting the formation of core aggregates⁸⁵:

- a. Excess carbon resulting from detonation is subjected to high temperature and high pressure conditions inside the chamber leading to their arrangement as a diamond lattice. This process is very fast leading to the *growth of several diamond nuclei* with uniform morphology.
- b. Alteration in the temperature and pressure conditions stops further growth of ND crystals. At this point the remaining carbons arrange themselves as a stable graphite layer over diamond crystals. Studies report two types of graphite arrangements including ribbon structures¹²⁰ and spherical graphitic shells¹²¹. Graphitic ribbons are formed due to the carbon redistribution process which arrange carbons in haphazard and crumpled fashion (turbostratic structure).¹²⁰ On the other hand, spherical shells result from diamond-to-graphite phase transition.¹²¹ Apart from carbon rearrangement as graphitic layers, this stage of synthesis also creates soot embryos which are spiral sub-NPs composed of several hundred sp^2 carbon atoms.¹²²
- c. The final event that results in formation of a core aggregate involves coagulation of the soot embryos. These embryos continue to generate sphere-shaped but faulty NPs. When they reach an optimum diameter of 10 to 20 nm they begin to coagulate themselves into aggregate structures. These aggregate structures are commonly called soot areas. They may contain soot embryos along with graphitic shells or graphitic ribbon like structures. The aggregation of an irregular graphitic shell around the particle forms a core aggregate of NDs (Figure 2.6).⁸⁵

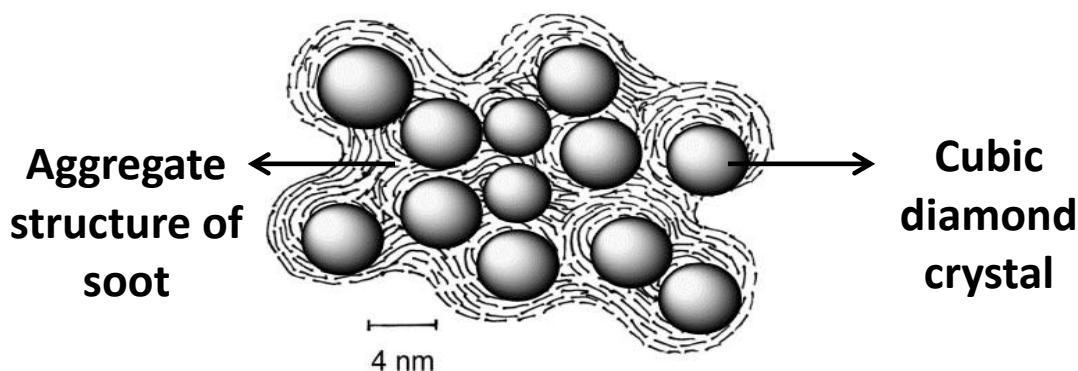


Figure 2.5 A simplified model of core aggregate sowing NDs and graphitic soot. Reprinted with permission from⁸⁵ “Copyright (2005) Elsevier

2.7.2 Methods to mitigate aggregation and produce stable ND dispersion

There are varieties of methods targeting disintegration of the NDs from their core aggregate structures. They are either physical or chemical or a combination methods, selected based on the future applications of the NDs. Physical approaches tend to counter ND aggregation mediated

through graphitic layering, while chemical methods target the surface through various functionalizations to reduce electrostatic attraction and hydrogen bonding between individual particles.

2.7.2.1 Physical methods: stirred media milling and dry-media assisted attrition milling

Physical methods to deaggregate ND colloidal dispersions are widely employed during biomedical researches due to the ease of procedure. Stirred media milling, also called wet grinding is a traditional method to disintegrate NDs. It involves preparing of ND slurries and adding suitable grinding media¹²³. Conventionally, yttrium stabilized zirconia (YTZ) beads, which are available in variable sizes ranging from micrometres to millimetres are used as the grinding media.¹²³ When the ND dispersion containing zirconia beads is subjected to a degree of ultrasonication, the beads hit the graphitic soot and on the diamond core. These collisions induce high energy impact and shear forces¹²⁴, ultimately causing the aggregation to break. In this process bath sonication additionally creates shock waves¹²⁴ adding to the effect of zirconia beads to produce high intensity impact (Figure 2.7).

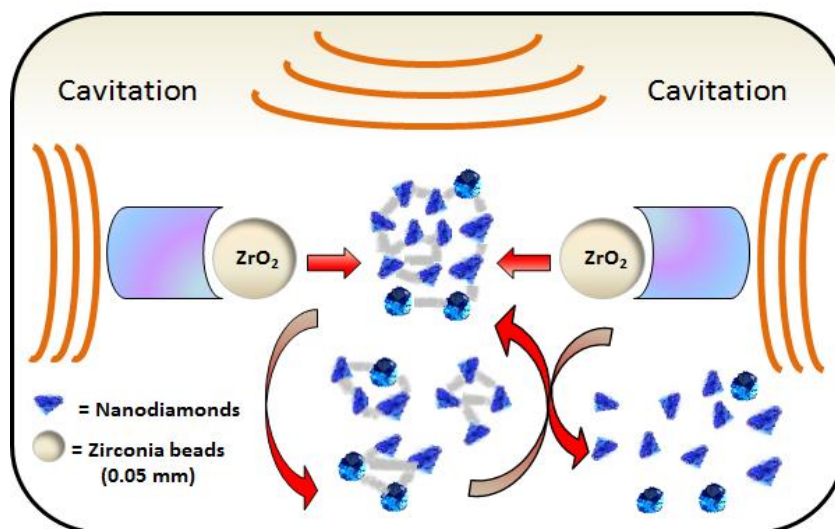


Figure 2.6 Bead assisted deaggregation of NDs under bath sonication

The zirconia beads are softer than the ND core; therefore the impact with the diamond core leads to their erosion during milling.^{82, 125} These eroded zirconia particles are difficult to remove and yield a measurable quantity (0.2%) of contamination in the dispersion.⁸² Certain comprehensive modifications (Figure 2.8) in the parameters of this technique are found effective in reducing this

contamination. Osawa et al. elucidated that the milling conditions should be adjusted to mild levels, so that the bead only hits the susceptible deformed areas of the core aggregates, that is the graphitic soot, and not with the diamond particles. Reducing the milling agitation, milling duration and particle size of the beads to $\sim 30 \mu\text{m}$ can reduce the susceptibility of bead destruction. Additionally, the broken beads can be removed by centrifugation, adsorption onto activated charcoal, or diffusion through an osmotic membrane¹²⁵. Modification of the dispersion media is also recommended to control contamination. Solvents such as ethanol are preferred over water to avoid re-aggregation at the end of the milling process.¹²⁵ The aqueous medium shows better grinding properties and produces finer ND particles as compared to organic medium however, it is shown to induce re-aggregation unlike the organic dispersion medium.¹²⁶ Moreover, water is a biocompatible solvent for medical applications. These strategies are summarized in Figure 2.8.

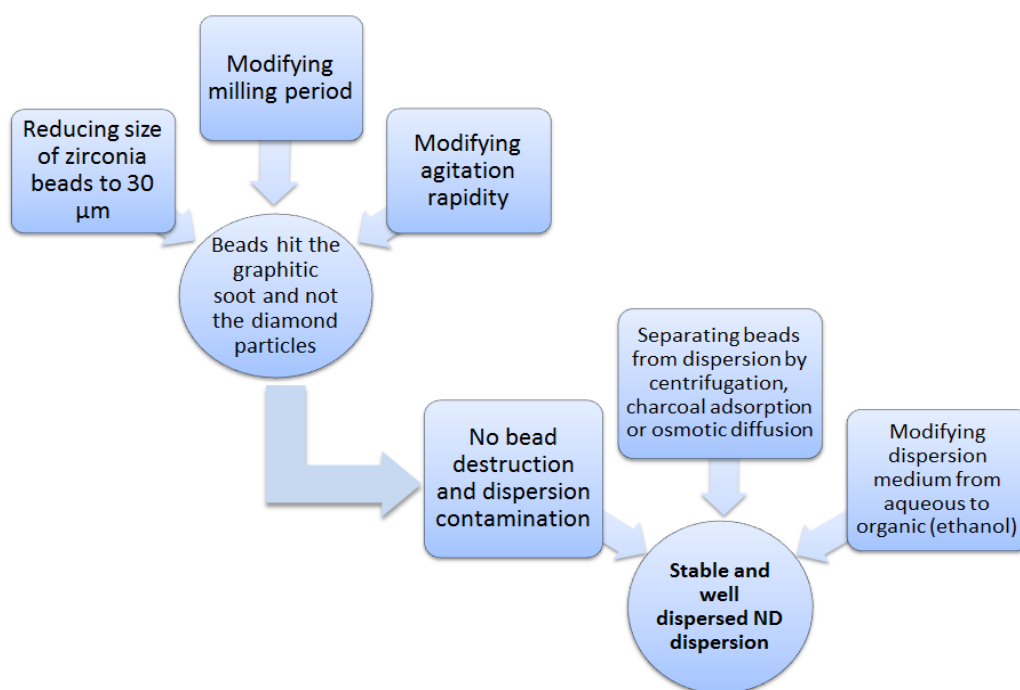


Figure 2.7 Parameters that could improve stirred media milling

Dry-media assisted attrition milling is also a noteworthy approach to formulate stable ND dispersion. In this process, water soluble nontoxic and non-contaminating crystalline materials like sodium chloride or sucrose are used. These crystals can be later removed by rinsing the NDs

with water, hence reduces the susceptibility of contamination unlike ceramic beads. The process is capable to produce NDs of <10 nm, that is close to the primary particle size.¹²⁷

2.7.2.2 Chemical methods: surface functionalization of NDs

Unlike other carbon nanomaterials, the surface of NDs is not inert, therefore opens several avenues for functional group modification and conjugation. Conjugation of various organic or inorganic molecules on the surface of NDs can control aggregation and simultaneously impart specific properties for biological applications.

Surface functionalization to control ND aggregation involves induction of surface homogeneity by modifying variety of functional group (hydroxyl, carbonyl, ether or anhydride) already present on the surface of detonation NDs to facilitate electrostatic repulsion by inducing uniform distribution of similar functional groups. NDs are also functionalized to confer chemical affinity to therapeutic molecules. For example several approaches are kept forward to synthesize a cationic surface for biomolecular conjugation.^{128, 69} Recently, ND functionalization is also focused to target the therapeutic system for enhanced site specific activity¹²⁹, reduced toxicity and limited wastage through processes like opsonisation.¹³⁰ Functionalization of NDs with various chemical moieties to confer specified biomedical application will be discussed later.

The chemical functionalization is a multistep process. First, the surface of the NDs needs to be prepared, and then the actual conjugation of the functional moieties takes place.

2.7.2.2.1 Pre-treatment of NDs before functionalization

All types of ND functionalization begin with pre-treatment to homogenize the surface functionalities. This step is aimed at converting a heterogeneous surface to contain, as much as possible, a single type of functionality. It ensures a similar conjugation behavior of the entire ND surface during functionalization (Figure 2.9). The pre-treatment process can control aggregation mainly by facilitating electrostatic repulsion between similar functional groups on the surface.¹³¹

132 133

Most often, the pre-treatment step involves oxidation (Figure 2.9a). This step removes all impurities like carbon soot and metal ions from the ND surface. Among some complex functional groups involved in oxidation include chromenes (C₉H₈O), pyrones (C₅H₄O₂), phenols and epoxides that are mainly at the edges of graphite surfaces.⁸² Difference in the oxidative agents

may result in variable functional group distribution on the surface after oxidation. For example combination of nitric acid and sulphuric acid may result in carboxylate (COO^-) rich surface^{134, 135}, while the combination of potassium permanganate and sulphuric acid mainly result in SO_3^- or O^- derivatives of phenol.⁸² Oxidation with strong mineral acids causes conversion of many chemical species into carboxylic functional groups which imparts hydrophilicity to NDs.¹³⁶ Oxidation of NDs can also be done by various other methods which include oxidation in air or utilizing other oxidizing agents.¹³⁷

Air oxidation is a much simple and inexpensive approach for disaggregation of NDs.^{131 138} It utilizes either non processed air¹³⁸ or air with enriched oxygen or ozone,¹³¹ and does not require any toxic substances or specific catalyst. It is particularly important to produce NDs with enhanced nitrogen vacancies for biological imaging. It involves a subsequent oxidation step in a tube furnace at controlled temperature of 600 °C for specific time of 30 minutes using air as the medium. Depending on the temperature of air oxidation, different materials are removed from the diamond surface. NDs of 8 nm with stable optical characteristics can be obtained by this technique.¹³⁸ Air oxidation also allows to selectively remove sp^2 -bonded carbon from ND providing control over sp^2/sp^3 carbon ratio on the surface.¹³⁹

Multi-step oxidation including combinations of more than one technique is also considered effective to counter aggregation.¹³³ One of such techniques includes graphitization – oxidation method.¹⁴⁰ It begins with conventional treatment of graphitic soot with strong mineral acids and also involves a subsequent step of re-graphitization in which NDs are heat treated in nitrogen at 1000 °C for an hour resulting in complete blackness of ND particulates. Graphitization is then followed by re-oxidation in which the sample is treated in air at 450 °C for several hours. The black colour of the product starts to fade and eventually disappears indicating that the thin graphite layer has been completely removed, yielding purified NDs. The NDs are then dispersed in water by ultrasonics. This process produces particles of less than 50 nm in size which indicates disaggregation of the NDs core aggregates.¹⁴⁰ However, in most cases oxidized ND presents an overall negative surface charge.

Another mode of pre-treating ND surface is reduction (Figure 2.9b), which is aimed at converting most of the functionalities into hydrogen or hydroxyl groups. Therefore, reduction of NDs can

create either positive surface through hydrogenation or negative surface through hydroxylation of ND surfaces.¹³⁷

Choice of the pre-treatment method is very crucial to control the overall functionalization process. Oxidation or reduction of NDs is selected based on the terminal functional groups required on the surface. For example, carboxylate functionality serves as a typical ligand for covalent conjugation of amine containing chemicals like amino acids (AAs) or proteins.^{134, 141} This conjugation is mediated through the formation of an amide bond (R-CO-NH-R). Therefore, in order to functionalize NDs with biomolecules, oxidation is the best suited approach for pre-treating the surface. On the contrary, certain molecules require hydroxylated surface for conjugation. A typical example is the biotinylation of NDs, before which the surface is reduced through borane forming hydroxyl groups. The hydroxylated surface is then covalently conjugated to biotin through silane linker (3-aminopropyl trimethoxysilane).¹⁴²

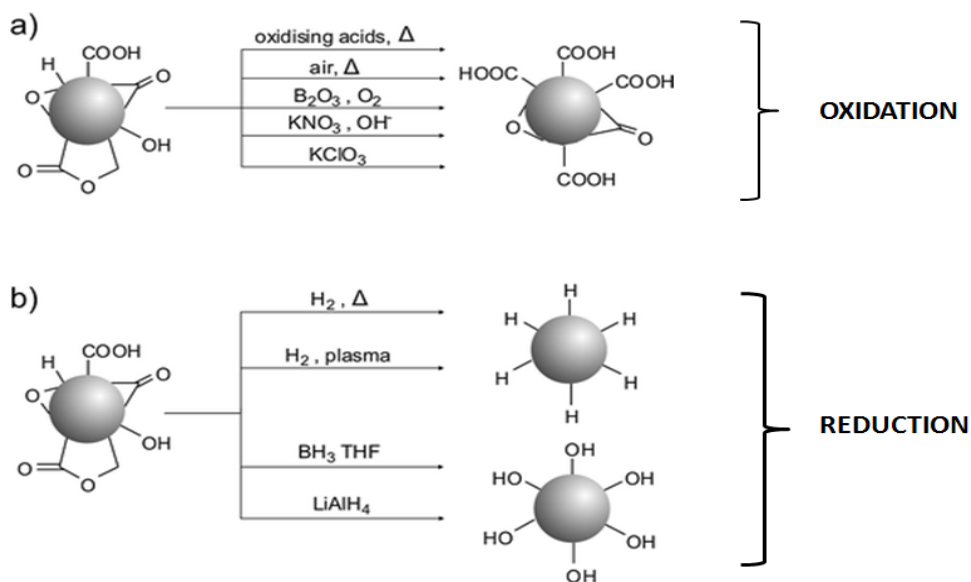


Figure 2.8 Modes for pre-treatment of ND surface. Reprinted with permission from¹³⁷ “Copyright (2008) Royal Society of Chemistry”

2.7.2.2.2 Functionalization chemistry

Surface functionalization occurs after the pre-treatment step ensures homogeneity of the ND surface. It utilizes three different types of surface chemistries: wet chemistry, gas phase methods or atmospheric plasma treatments (Figure 2.10, blue shaded) Different approaches to

functionalize NDs may result in variations in the binding energies and electrostatic features of the surface. ¹⁴³ Due to high surface to volume ratio of detonation NDs, extensive functional group conjugation is possible.

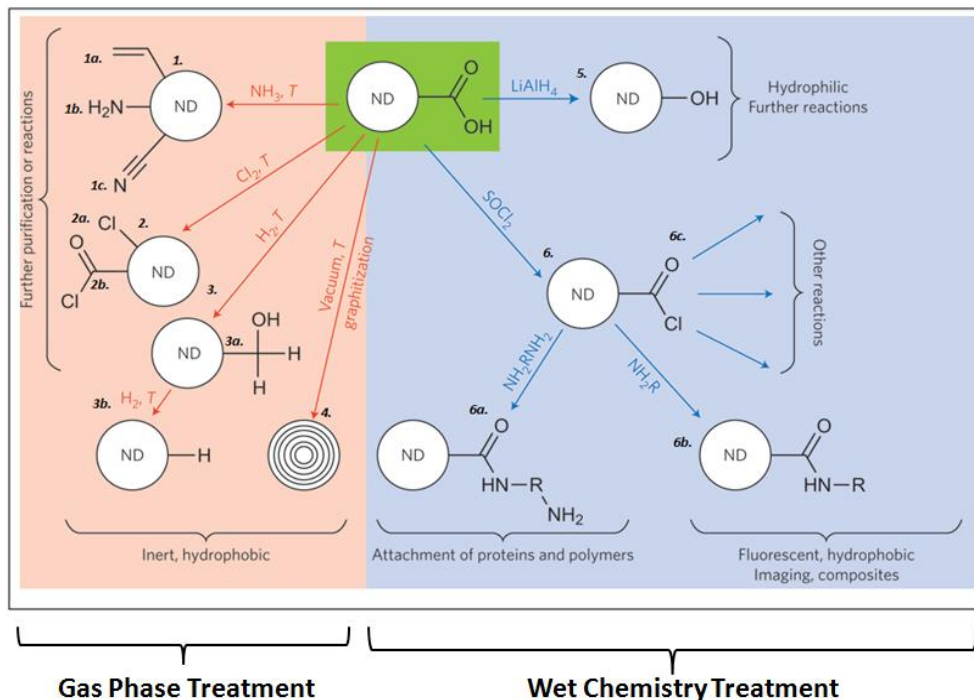


Figure 2.9 Wet chemistry and gas phase treatments for ND functionalization. Reprinted with permission from ⁹³ “Copyright (2011) Nature Publishing Group”

Wet chemistry treatment makes use of suitable solvent systems to introduce functional groups of interest. Depending upon the nature of functional groups to be attached on the surface oxidized carboxylated NDs or reduced hydroxylated NDs can be used. ¹³⁶ For example, carboxylate functionalized NDs can be reacted with thionyl chloride to form highly reactive acyl chloride functionalities which can be further attached to amine containing chemical moieties. ⁹³ The NDs treated by this pathway can be used to conjugate AAs or proteins on their surface. ⁹³ Wet chemistry treatments maintain the crystal characteristics of diamond core even at the size of 5 nm. ¹³⁶

Use of novel concepts has significantly advanced wet chemistry approaches of ND functionalization. A relatively new approach for modifying the surface utilizes a process called atom transfers radical polymerization. ^{128, 144} This process utilizes compounds called radical initiators (benzoyl peroxides, hydroxyethyl-2-bromoisobutyrate or 2, 2, 2-trichloroethanol) which

are attached covalently to oxidized NDs through esterification. Chemical groups are then introduced in the system which polymerize and arrange as brush arrays on the surface. This process can create hydrophilic or hydrophobic surface depending upon the nature of the polymer and hence provide better control over surface reactivity.¹⁴⁴ The radical polymerization phenomenon is also employed to develop a simple approach for introducing polar and non-polar functionalities on graphitized ND surface.¹¹ It begins with surface graphitization and then introduction of these graphitized NDs in a mixture containing monomers of hydrophilic compounds in aqueous medium and hydrophobic compounds in organic medium. Exposing the reactive NDs to polar and non-polar groups at the same time resulted in a combined hydrophilic/hydrophobic surface without undergoing multi-step complex procedures.¹¹

Another approach for surface functionalization involves the treatment of NDs in gas or a vapour reactive medium (Figure 2.10, pink shaded side).¹⁴⁵ This approach is efficient to purify a very low dimensional fraction of the powder having narrow particle size distribution. It facilitates greater penetration into the inter particle spaces than strong acid or salts in liquid phase.¹⁴⁵ The gas phases used can include hydrogen, ammonia, carbon tetrachloride or argon. NDs treated with ammonia yield carbonyl, amine or cyano groups on the ND surface, while treatment with chlorine results in the formation of chloro-NDs or acyl-chloride functionalized NDs. Acyl chloride, in particular, is extremely reactive, since chlorine is readily replaced by the upcoming functional group like alcohol, phenols or amines.¹⁴⁶ Therefore, this mode is particularly important for biomolecular conjugation, where acyl-chloride is reacted with amine containing moieties to facilitate amide bond formation similar to the natural peptides. High temperature gas treatments with hydrogen produce alcohol functionalized NDs or hydrogenated NDs. A complete removal of all functional groups on ND surface might result from thermal treatments of NDs in argon, nitrogen or vacuum medium, which gives rise to graphitic carbon nano onions. Both, hydrogenated NDs and carbon nano onions are inert and hydrophobic in nature.⁹³

Gas phase treatments are conducted in quartz reactors, in which NDs are treated with flowing gas or vapours at high temperatures ranging from 400 °C to 1100 °C and atmospheric pressures for durations ranging from 30 minutes to 5 hours.¹⁴⁵ Gaseous functionalization can result in hydrophilic or hydrophobic and acidic or basic ND terminations.¹⁴⁵

All these functionalization methods lead to the improvement of the dispersibility of the NDs. In addition, the homogeneous surface can serve as a template for binding molecules acting as a carrier, discussed in Chapter 5.

2.7.2.3 Grafting biomolecules on NDs

Introducing protonable biomolecules, including AAs, peptides and proteins on ND surface is a novel approach for functionalization. This is mainly targeted for controlled release of small drug molecules and targeted delivery of biomolecules such as peptides, proteins, RNA and DNA. Functionalization of NDs with biologically active molecules is achieved through non-covalent adsorption or covalent immobilization at the surface. Classic example of non-covalent biomolecular functionalization is presented by decorating the surface with poly-L-lysine, a polypeptide that can bind and isolate DNA oligonucleotides during mass spectrometric analysis.¹⁴⁷ Poly-L-lysine functionalized NDs are also employed to synthesize fluorescent NDs for possible application in human stem cell research.¹⁴⁸ Recently, a more complex system consisting of polyols like glycerol and polypeptides chained with basic AAs (glycine, arginine, lysine and histidine) are also used to functionalize NDs for gene delivery.¹⁴⁹ Similarly, NDs are also adsorbed with specific enzymes like lysozyme for antibacterial activities.¹⁵⁰ These systems are extensively characterized over time for stability, biological interactions and efficacy.^{151 152}

Another approach for grafting biomolecules on the surface involves covalent conjugation that permanently immobilizes the molecules of interest on the surface and creates a controlled and relatively stable functionalized system.¹⁴ Lysozyme, an antibacterial enzyme was covalently attached to the pre-treated carboxylated ND surface.¹⁵⁰ Covalent conjugation did not compromise the antibacterial activity of the lysozyme. The fully functional capacity of the system was ensured up to 10 hours at room temperature and up to weeks if stored at 5 °C following covalent conjugation of the enzyme.¹⁵⁰ NDs modified through biotinylation are also shown to covalently bind coenzymes (vitamins) like biotin.¹⁴

A relatively new concept highlights the use of simpler biomolecules like AAs through covalent immobilization.¹³⁴ This approach creates a primary amine rich ND surface, which facilitate electrostatic interaction with genetic materials (DNA or RNA) to utilize NDs as gene delivery vectors. The concept of grafting AAs on the NP surface arises from the process of natural DNA wrapping in eukaryotic cells. The nuclei of all eukaryotic cells consist of histone proteins which

are alkaline in nature.^{153, 154} These histone proteins are rich in lysine and arginine AAs.¹⁵⁵ The DNA wraps around histone proteins which condense and package the DNA to form nucleosomes.¹⁵⁵ There are many types of interactions between histone proteins and DNA during nucleosome formation.¹⁵⁶ Among these interactions one of the major interactions is the formation of salt bridges between side chains of basic AAs (especially lysine and arginine) of histone proteins and phosphate oxygen of DNA. The salt bridges are the combination of electrostatic interactions and hydrogen bonding between the positively charged amines and the negatively charged phosphate oxygen (Figure 2.11). This natural process is replicated artificially by functionalizing NDs with basic AAs covalently¹³⁴ or non-covalently¹⁵⁷ to induce similar interactions with anionic nucleic acids forming diamplex (complex of diamond NP with DNA or RNA). Moreover, basic AAs also impart water solubility to the complex for stability in hydrophilic environment of the cell.¹⁵⁶

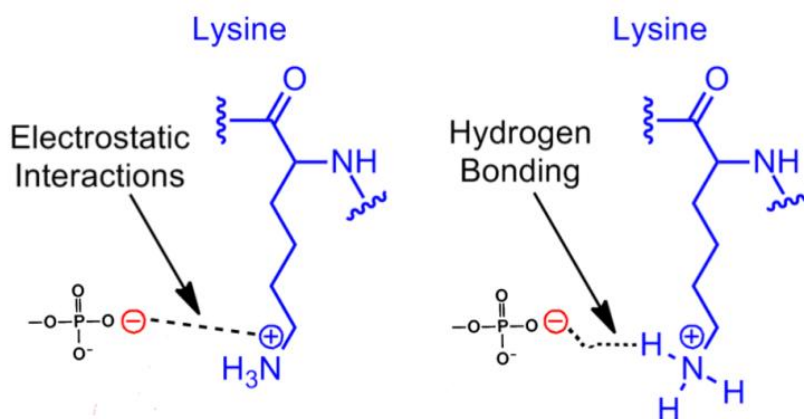


Figure 2.10 Electrostatic interaction and hydrogen bonding (salt bridges) between primary amine of lysine residue and phosphate oxygen of DNA

2.8 Biomedical applications of NDs

2.8.1 Biodistribution and cellular uptake of NDs –mechanisms, challenges and controlling factors

The route of administration into the body is one of the factors that influence the design decisions regarding biomedical devices and delivery systems. The functionalization of the NDs is also governed by the route of administration. After systemic administration, NDs like all other NPs are distributed in the body through blood circulation. The particle size and the shape, surface functionalities and the overall charge in dispersing medium play a critical role in defining their

distribution in the body.¹⁵⁸ NPs less than 5 nm are rapidly cleared, mainly through renal mechanisms and also through extravasations, which promote the discharge of fluids into extravascular spaces and subsequent removal of materials through lymphatics.^{159 160 161} On the other hand, as the particle size increases from nanometers to micrometers, new challenges appear which mainly include NP accumulation in the metabolic organs like liver, spleen and bone marrow.¹⁶² The metabolism of NDs can be stimulated through a process called opsonisation that is associated with non-specific protein adsorption on the surface.^{76, 159, 163, 164} It causes recognition and uptake of NDs by circulating macrophages followed by degradation and excretion, a process called mononuclear phagocytosis (Figure 2.12a). The risk of elimination of the NDs through this process is reduced by functionalizing the surface with polyethylene glycol (PEG). Pegylated NDs reduce opsonisation and phagocytosis, thus increase the chance for tissue accumulation.^{130 165} Another removal pathway which presents a major challenge for ND survival in the body is associated with mechanical filtration through sinusoids in the spleen and Kupffer cells in the liver. These systems are powerful machinery that removes the NDs through reticuloocyte-endothelial system.¹⁶⁶ This process is also stimulated by nonspecific protein adsorption on ND surface.

In addition to general biodistribution, mechanisms and factors involved in cellular uptake is also an extensively studied area to evaluate biological interactions of NDs. Properties mainly the particle size, shape and surface characteristics influence the cellular uptake processes.¹⁵⁸ Difference in the particle size defines the mechanism involved in its internalization and in turn the microenvironment experienced by them intracellularly. Most NPs are internalized in the cells through endocytosis mainly pinocytosis, a process to internalize fluids and molecules within small vesicles formed by the cell membrane folding (Figure 2.12b to e).^{167, 168, 169} Pinocytosis of NPs can occur through different mechanisms mainly dictated through their particle size. However, not all cell types are equipped with the necessary machinery to allow the entire spectrum of endocytotic processes.¹⁷⁰ The major pathway associated with carbon NPs is clathrin-mediated endocytosis.^{171, 172, 173} It is a form of receptor mediated endocytosis, which naturally functions for cellular uptake of proteins such as lipoprotein and transferrin.^{169 174 175} It is also involved in cell and serum homeostasis by regulating membrane electrolytic pumps, for example voltage gated calcium channels.¹⁷⁵ This endocytotic process forms coated pits having transmembranous and cytosolic proteins mainly clathrin (Figure 2.12d). They detach from the

membrane and form a vesicle in the cytoplasm of the cell. The assembly of these vesicles is controlled by another set of proteins called assembly proteins.¹⁷⁵ Another mechanism elucidated for ND uptake is macropinocytosis,^{176, 177} which is responsible to internalize larger particles of 1 μ m.¹⁵⁸ It involves actin-driven membrane protrusion to enclose NDs in aggregated forms (Figure 2.12b). Macropinocytosis seems similar to phagocytosis, however rather than zippering around the engulfed particle in latter it causes the protrusions to collapse and fuse again to the plasma membrane

Investigations regarding ND uptake provide evidence for both macropinocytosis (Figure 2.12b) and clathrin-mediated endocytosis (Figure 2.12d), however latter is more commonly observed.¹⁴⁸¹⁷³¹⁷⁸ Clathrin-mediated endocytosis is mediated through intact microfilament architecture as observed for poly-L-lysine coated NDs.¹⁴⁸ The same mechanism was observed in both healthy and cancerous cells, which indicates that the uptake process is not cell-type specific. However, recent investigation suggests that the uptake is approximately 30% higher in cancerous cells compared to healthy cells at the longest time interval (480 seconds)¹⁷⁸, presumably due to structural, genetic and phenotypic alterations. A study also reveals that slightly larger particles, of 100 nm follow a combination of both mechanisms for cellular uptake.¹⁷⁶ This is due aggregation of NDs resulting in non-uniform particle size distribution that may stimulate a combination of pathways, each specific for a particle size range. NDs ranging from 46-150 nm are found to be internalized via clathrin mediated endocytosis; however aggregated NDs of 1 μ m in size can be internalized via macropinocytosis.¹⁷⁷

The kinetics and extent of ND cellular uptake like all other NPs can be controlled by two parameters: thermodynamic driving force for membrane wrapping (determined by particle size) and diffusion kinetics of the receptors responsible for NP interaction.¹⁷⁹ Thermodynamic driving force for wrapping creates the required free energy for NP internalization while the diffusion kinetics of receptors corresponds to the availability of receptors to initiate receptor mediated endocytosis.¹⁷⁹ Research indicates that the optimal particle size for wrapping and receptor interaction is 55 nm.¹⁸⁰ Smaller NPs do not have enough energy for membrane wrapping and therefore cannot undergo endocytosis. For bigger NPs (>50 nm) more time will be consumed for membrane wrapping and hence will have reduced cellular uptake.¹⁸⁰

NPs conjugated to more sophisticated targeting moieties adopt a different pathway for cellular uptake as compared to the NPs without these molecules.¹²⁹ They follow caveolin-dependent endocytosis, which result in the formation of flask-shaped invaginations of the plasma membrane (Figure 2.12c).¹⁷⁵ Endothelial cells that lack the machinery for caveolin-mediated endocytosis are unable to bind and uptake serum proteins,¹⁸¹ and therefore this pathway can facilitate uptake of protein coated NPs.¹⁸² Unlike other receptor mediated endocytotic pathways, caveolin pits can also encapsulate larger amounts and sizes of NPs. A single caveolin mediated membrane invagination was found to accommodate three 20 nm and two 40 nm and one 100 nm polymeric NPs.¹⁸² This highlights that ND aggregates may be internalized in the cells through this mode as well. However limited studies are available to date to support this mechanism for cellular uptake of NDs.

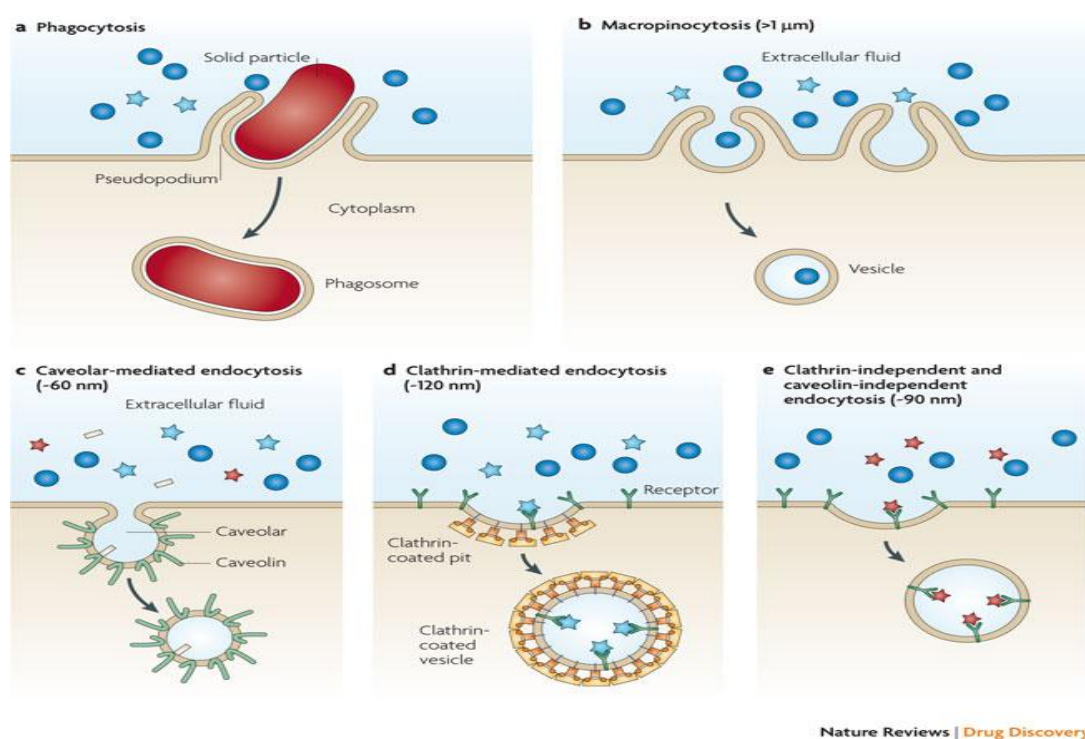


Figure 2.11 Uptake of micro and nanoparticles. Internalization of large particles is facilitated by phagocytosis (a). Nonspecific internalization of smaller particles (>1 μm) can occur through macropinocytosis (b). Smaller nanoparticles can be internalized through several pathways, including caveolar-mediated endocytosis (c), clathrin-mediated endocytosis (d) and clathrin-independent and caveolin-independent endocytosis (e).

Nanoparticles are represented by blue circles (> 1 μm), blue stars (about 120 nm), red stars (about 90 nm) and yellow rods (about 60 nm). Reprinted with permission from ¹⁵⁸ “Copyright (2010) Nature Publishing Group”

Another interesting phenomenon that affects cellular uptake kinetics is the interaction of NDs with serum proteins. It is extensively researched to learn about the in vivo utilization of ND complexes. NDs have a reactive surface and hence are capable of adsorbing proteins forming a layer called protein corona. ^{183, 184, 185} Several studies indicate that adsorbed proteins down regulate the cellular uptake of NPs and also lead to aggregation. ^{148, 183, 184, 185} Serum proteins can adsorb rapidly on NP surface leading to an increase in the overall particle size ¹⁸⁶ as well as flip the surface charge into high negative values inherent to the protein itself. ¹⁸⁶ This process can compromise the electrostatic interactions of cationic NPs with cell membrane and hence affects cellular uptake and toxicity profiles. Protein coronas are formed on all NPs irrespective of their surface charges; ¹⁸⁷ however the composition of the layer might vary with positivity or negativity of the surface. In general, adsorption of proteins on NP surface is a dynamic process, such that the identities of adsorbed proteins may change over time but the total amount remains roughly constant. ¹⁸⁸ There are certain conflicting evidences that suggest that serum proteins mainly albumin enhance cellular uptake of carbon nanomaterials. ¹⁸⁹ Therefore, understanding the behaviour of NDs in native biological environment is a prerequisite for their therapeutic evaluation.

After cellular internalization ND based delivery systems face many challenges intracellularly. One of such challenges is the entrapment of NDs in endosomes following internalization. ¹⁹⁰ The endosome is an acidic organelle due to the presence of digestive enzymes, and therefore endosomal entrapment especially affects gene transfection and delivery of acid-labile small molecules. ^{191 192} Disruption of the endosomal membrane through proton sponge effect is one way to protect NDs from endosomal degradation. ¹⁹³ It is mediated by chemical groups with high buffering capacity and propensity to swell upon protonation. Protonation causes influx of H^+ ions causing membrane to rupture. ¹⁹⁴ These groups may include pH sensitive molecules like histidine which can be covalently attached to ND surface ¹⁹⁵ to reduce endosomal trapping. Another study also suggests that diverting the uptake process in favour of macropinocytosis also increase the potential of gene (siRNA) transfection. ¹⁷⁷ This diversion is observed to depend on size and well

as the shape of NDs. In aggregated NDs weak electrostatic interactions may change the spherical shape of the particle. This may result in variations in the surface area acquired during membrane adhesion, which may ultimately change the mechanism of uptake.¹⁷⁷ Overall, size, surface properties, interactions with biomolecules, serum proteins, cell membranes and cellular organelles are all factors that contribute to the biological effect and toxicity of the NDs.

2.8.2 Biocompatibility and biological affinity

Biocompatible nature is a major pre-requisite for all therapeutic and diagnostic aids used in biomedicine. NDs certainly provide well-established evidence of limited toxicity at cellular and organ levels, demonstrating the highest biocompatibility among the members of the nanocarbon family.⁷¹

When the toxicity of ND was compared with other carbon nanomaterials including carbon black, multi-walled carbon nanotubes and single walled carbon nanotubes, the degree of cytotoxicity occurred in following order: single-walled nanotube>multi-walled nanotube>carbon black>ND.⁷¹ NDs do not induce any mitochondrial membrane damage and preserving high cell viability.⁷¹ Unlike other carbon nanomaterials, they do not fragment DNA³⁷ or alter gene and protein expression profiles of living cells at a wide range of concentrations and particle sizes.⁷² Regardless of the terminal functional moieties, NDs show no over expression of genes like interleukin-6, tumor necrosis factor alpha, and inducible nitric oxide synthase, hence are expected to show absence of inflammatory responses upon administration.³⁷

These properties are particularly advantageous to develop ND based delivery vectors. Serum proteins are also shown to play a significant role in influencing the biocompatibility of NDs.¹⁹⁶ In vitro studies reveal that the cell culture medium containing serum proteins enhance the biocompatibility of oxidized carboxylated NDs even at high doses. This builds an evidence for ND safety in protein rich biological system. The adsorbed serum proteins are not only protective but are also shown to increase hydrophilicity and stability of ND dispersion.¹⁹⁶

In vivo biocompatibility of NDs is also addressed. The most important organ system considered for its effects is the respiratory system, since powdered detonation NDs may cause environmental pollution.¹⁹⁷ NDs are considered non-toxic to the respiratory system as did not show any oxidative damage to lung tissues upon long term residence.¹⁹⁷ They are shown to be excreted out

of the body mainly through lymphatic tissue or directly through cough. ¹⁹⁷ NDs also maintain their biocompatibility after prolonged exposures through oral ¹⁹⁸ or subcutaneous ¹⁰⁴ routes.

2.8.3 Application of NDs in bioimaging and research technologies

Artificial induction and enhancement of fluorescing centres have gained much attention over years to utilize NDs as biological probes. ^{199, 200}

2.8.3.1 Fluorescence imaging

This portion of the text is presented in Appendix 10.1

2.8.3.2 Combined fluorescence and magnetic imaging

This portion of the text is presented in Appendix 10.1

2.8.3.3 Scattering imaging

This portion of the text is presented in Appendix 10.1

2.8.4 Applications of NDs in therapeutics

Due to continuous advancements in the knowledge of disease conditions at molecular levels, many traditional therapies are now under constant optimizations to treat these diseases at their most basic levels. These novel approaches include targeted and controlled drug delivery, gene therapy and personalized medicine. Targeted drug and gene therapy appears to be the most widely researched approaches especially for various chronic illnesses like cancers. They require efficient and biocompatible carriers. NDs due to their innate biocompatibility and extensive functionalization opportunities can be utilized to protect and deliver new or conventional therapeutic moieties to specific targets in the physiological system (Figure 2.14), rendering ND technologies highly desirable for biomolecular and drug delivery applications.

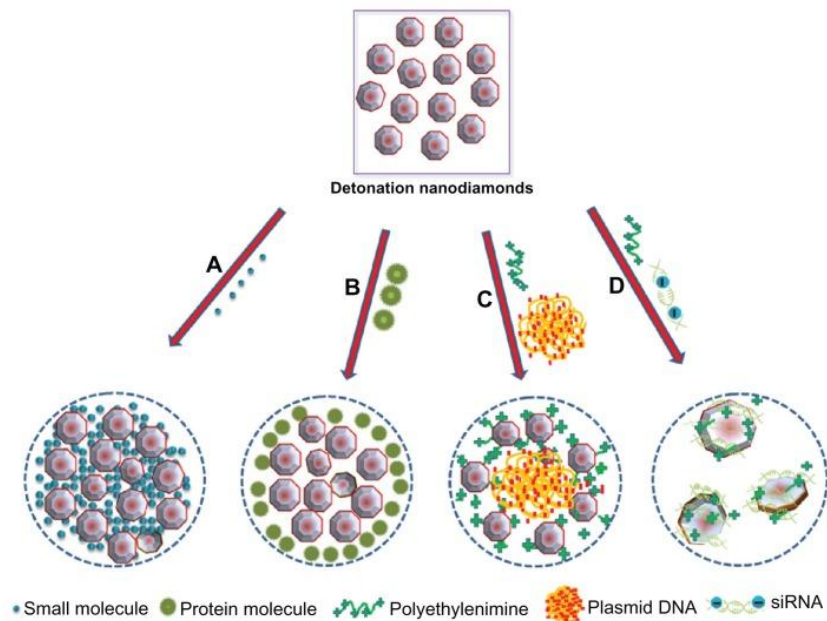


Figure 2.12 A schematic diagram representing the binding of detonation nanodiamonds with (A) small molecules (B) proteins (C) plasmid DNA and (D) siRNA. Reprinted with permission ⁸⁴ from “Copyright (2013) Dove Medical Press”

2.8.4.1 NDs for small molecule delivery

This portion of the text is presented in Appendix 10.1

2.8.4.2 NDs for protein delivery

This portion of the text is presented in Appendix 10.1

2.8.4.3 NDs for the delivery of genetic materials

NDs have attracted great attention as non-viral vectors for gene therapy. For this application NDs must possess a cationic surface to bind and carry genetic materials which are anionic in nature.¹²⁸ Cationic NDs are synthesized through a variety of methods ranging from non-covalent functionalization with polymers like polyethyleneimine (PEI) to covalent conjugation of derived organic moieties like triethylammonium groups.⁶⁸ NDs adsorbed with LMW PEIs produce higher transfection efficiency and reduced toxicity in comparison to polymer used alone.⁶⁹ ND-PEI complex showed a protein expression at four order of magnitude higher compared to naked DNA. Cell viability was sufficiently maintained up to 80% after administration of ND-PEI

complexes at a concentration of 90 µg/mL, thus reduced the innate cytotoxicity of cationic polymers.

Hydroxylated NDs functionalized inorganic molecules like triethylammonium groups also bind and deliver plasmid DNA in the nucleus of cancerous cells, as evidenced qualitatively by the induction of fluorescence. The cells treated with free plasmid DNA did not show any fluorescence, while the cells treated with the plasmids bound to these functionalized NDs showed optimum fluorescence as well as protein expression.⁶⁸

Carboxylated NDs, functionalized covalently with 2-bromoisobutyric acid to¹²⁸ polymerize methacrylates on the surface to function as gene delivery vectors and as biolabels to track intracellular processes.¹²⁸ These functional groups gather on the surface to form a cationic brush like borders which condense DNA into stable NPs.

Cationic brushed NDs efficiently transfect the plasmid DNA and produce a gene expression of 106 -106 RLU/mg of proteins. Different types of methacrylate borders were coated on NDs, all of them producing several folds higher transfection efficiency as compared to naked DNA and DNA complexed to polyethyleneimine.

Functionalizing NDs with protonable biomolecules like AAs¹³⁴ is also a potential approach for gene delivery. Covalent immobilization of basic AAs directly on the oxidized ND surface can form stable diamplexes with DNA and RNA,¹³⁴ and thus are promising as vectors for gene therapy. Peptides like poly-L-lysine can also be coated on NDs to create a positively charged surface.^{147, 148} Such functionalization can also facilitate electrostatic binding with genetic materials, however limited investigations are done to utilize peptide modified NDs for gene delivery.

2.9 Conclusion

Innate biocompatibility at micro and macro levels with biological systems, new methods to overcome aggregation challenges and novel approaches for specific surface functionalization have greatly introduced NDs as encouraging platform for numerous biomedical applications. Continual evaluations are still required to understand the surface changes occurring under various biological conditions with special focus on newly derived synthetic approaches. Also, more research is needed to further elaborate on the cellular interaction of NDs, localization in sub-

organelle levels, biodistribution after *in vivo* delivery and consequences of long term residence in biological system. This information will encourage development of more sophisticated nano-delivery systems with better control and accurate predictions that will improve modern medicine.

3 Hypothesis and Research Objectives

From the previous chapters it is evident that NDs are an emerging class of nanomaterials for biological applications. It provides numerous advantages as delivery vectors; but with a major challenge of achieving stable dosing dispersion due to aggregation. With an aim to overcome this barrier and to further enhance the ND based gene delivery approach, I put forward the hypotheses and research objectives of my study.

3.1 Hypotheses

- *Detonation NDs functionalized with lysine, histidine alone or in combination will facilitate in limiting aggregation leading to the formation of a stable colloidal dispersion.*
- *The amino acid functionalized NDs will form diamplexes capable of delivering therapeutic genes safely into mammalian cells. Additionally, lysyl-histidine functionalized NDs will present a gene delivery vehicle capable of escaping endosomal degradation to increase the transfection efficiency of the system.*

3.2 Research Objectives

- I. To functionalize NDs with amino acid (AA) conjugates.
 - To optimize the covalent attachment process for lysine functionalized NDs.
 - To introduce histidine as a pH sensitive molecule covalently linked with lysine AAs on ND surface to facilitate endosomal escape of the diamplexes.
 - To characterize & evaluate degree of functionalization for lys-NDs & lysyl-histidine-NDs.
- II. To evaluate the physicochemical properties of functionalized NDs (fNDs).
 - To determine the changes in the size and the surface characteristics of NDs after functionalization
 - To analyse the stability of fNDs in various biologically relevant media as a function of time.
 - To select the most suitable medium for the design of fNDs formulations capable of maintaining dispersion stability for *in vitro* experiments.
- III. To evaluate the functional efficiency of AA-fNDs as novel gene delivery vector.
 - To complex fNDs with nucleic acids and to evaluate their binding efficacies with genetic materials

- To perform physical characterization of the resulting diamoplex.
- To monitor the internalization of bare fNDs and diamoplexes in HeLa cells (cervical cancer cells).
- To evaluate the efficiency of the diamoplex to transfect functionally active siRNA within GFP/HeLa cells for expression.
- To evaluate in vitro toxicity of fNDs as gene delivery vector within HeLa cells.

4 Lysine and Lysyl-Histidine Functionalized Nanodiamonds: **Synthesis and Physicochemical Characterizations**

Saniya Alwani, Jackson M Chitanda, Ferenc Borondics, Ildiko Badea

4.1 Author's Contributions

Saniya Alwani

- Conducted the synthesis of lysine NDs in its entirety under the guidance of Dr. Jackson M Chitanda and using the protocol published in:
“Kaur R, Chitanda JM, Michel D, Maley J, Borondics F, Yang P, Verrall RE, Badea I, Lysine functionalized nano diamonds: synthesis, physiochemical characterization and nucleic acid binding studies. *Int J Nanomed* 2012, 7, 3851–3866”
- Developed the method and conducted synthesis of lysyl-histidine NDs in its entirety under the guidance of Dr. Jackson M. Chitanda.
- Performed all physicochemical characterizations reported in the text except thermogravimetry and Infrared spectroscopy.

Dr. Jackson M Chitanda

- Provided guidance and supervision for the synthesis of functionalized NDs.
- Assisted in the interpretation of ¹HNMR results.
- Performed thermogravimetric analysis of functionalized NDs.

Dr. Ferenc Borondics

- Performed infrared spectroscopic analysis of lysine and lysyl-histidine NDs and amino acid conjugates.

Dr. Ildiko Badea

- Supervised the entire work.
- Assisted in the revision and editing of the text in the chapter.

4.2 Abstract

Nanodiamonds present an innately reactive surface with different functional groups to facilitate chemical modification suited for therapeutic application. In this chapter, covalent conjugation of lysine and lysyl-histidine with NDs is presented. It is important to homogenize the functional groups on the surface to confer predictable conjugation of chemical moieties during functionalization. Homogenization of the surface is achieved by pre-treating the NDs either through oxidation or reduction. Suitable synthetic chemical reaction is designed according to the functional groups on the conjugate to achieve functionalization. Since carboxylic acid groups were required on the surface to facilitate amide bond formation with three carbon chain linker (1, 3 diaminopropane), oxidation with strong mineral acids was performed to homogenize the surface during pre-treatment. Lysine and lysyl-histidine amino acid (AA) conjugates with 1, 3 diaminopropane were synthesized separately using peptide chemistry. ¹HNMR and mass spectrometry was used at all steps of the conjugate synthesis to confirm the presence of the desired compound and identify the product impurities. These AA conjugates were then covalently attached to NDs after converting the surface carboxylic acids into acyl chloride groups to increase reactivity. Functionalization of lysine on the surface of NDs was evident through infrared spectroscopy, thermogravimetry, size and zeta potential measurements. However, lysyl-histidine functionalization was limited and the surface loading of this conjugate on NDs was very low. Lys-NDs also showed optimum binding with pDNA and siRNA at minimum ratios of 1:1 and 1:20 (pDNA/siRNA:ND) respectively. Due to the lack of positive surface charges lysyl-histidine NDs were not able to bind pDNA and siRNA even at high weight ratios.

4.3 Introduction

Lysine functionalization of NDs was performed with two aims: 1) to confer surface homogeneity that can minimize aggregation by allowing repulsive forces to dominate in the colloidal dispersion and 2) to induce a primary amine (NH_3^+) onto the surface of ND to electrostatically bind genetic materials for cellular delivery. Histidine was introduced in the system as a pH-sensitive AA to allow endosomal destabilization and the release the gene in the cytosol, avoiding lysosomal degradation. However, optimum surface loading of lysyl-histidine on NDs was not achieved which demand further optimization of synthetic approach used for functionalization.

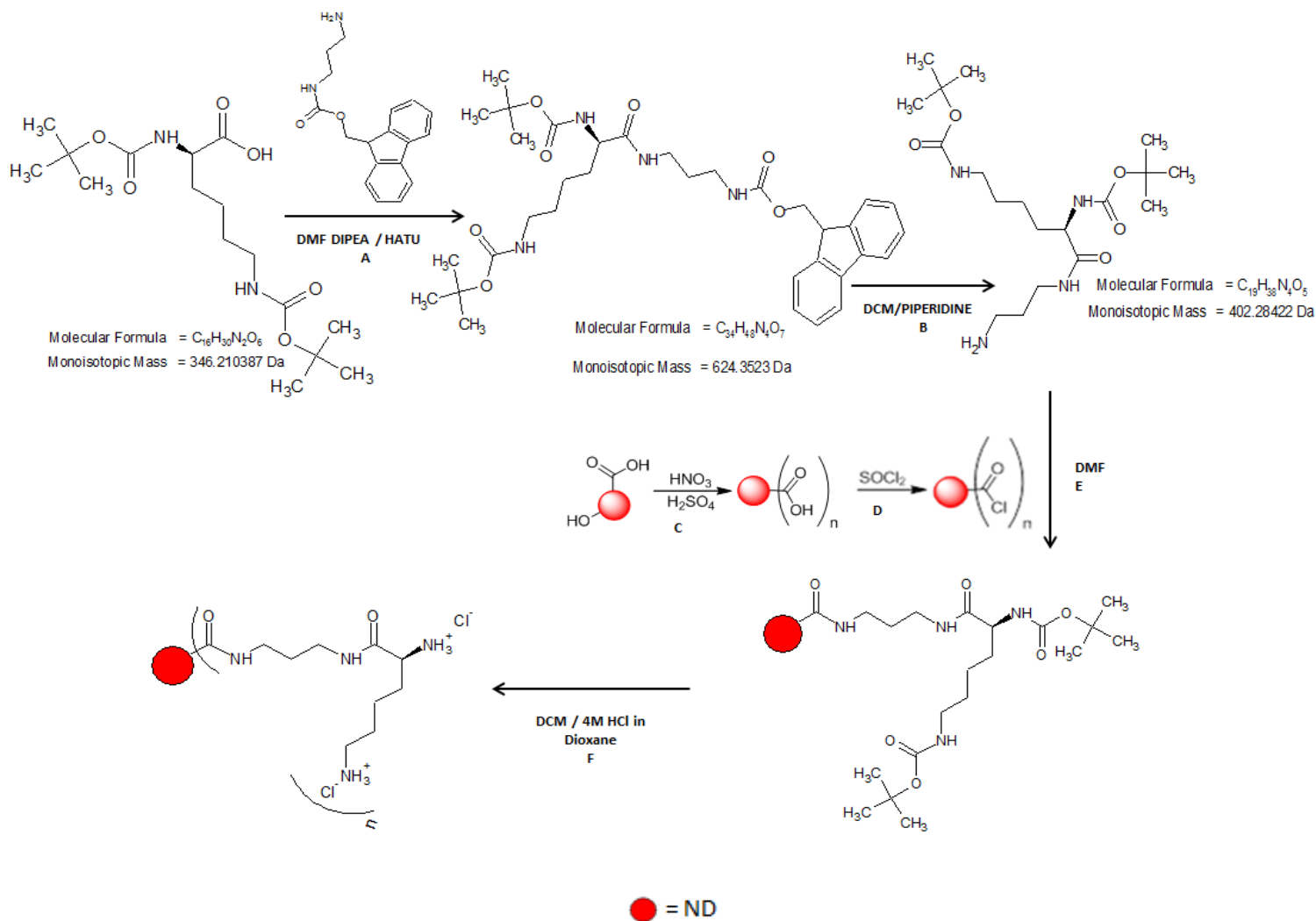
4.4 Materials and methods

4.4.1 Materials

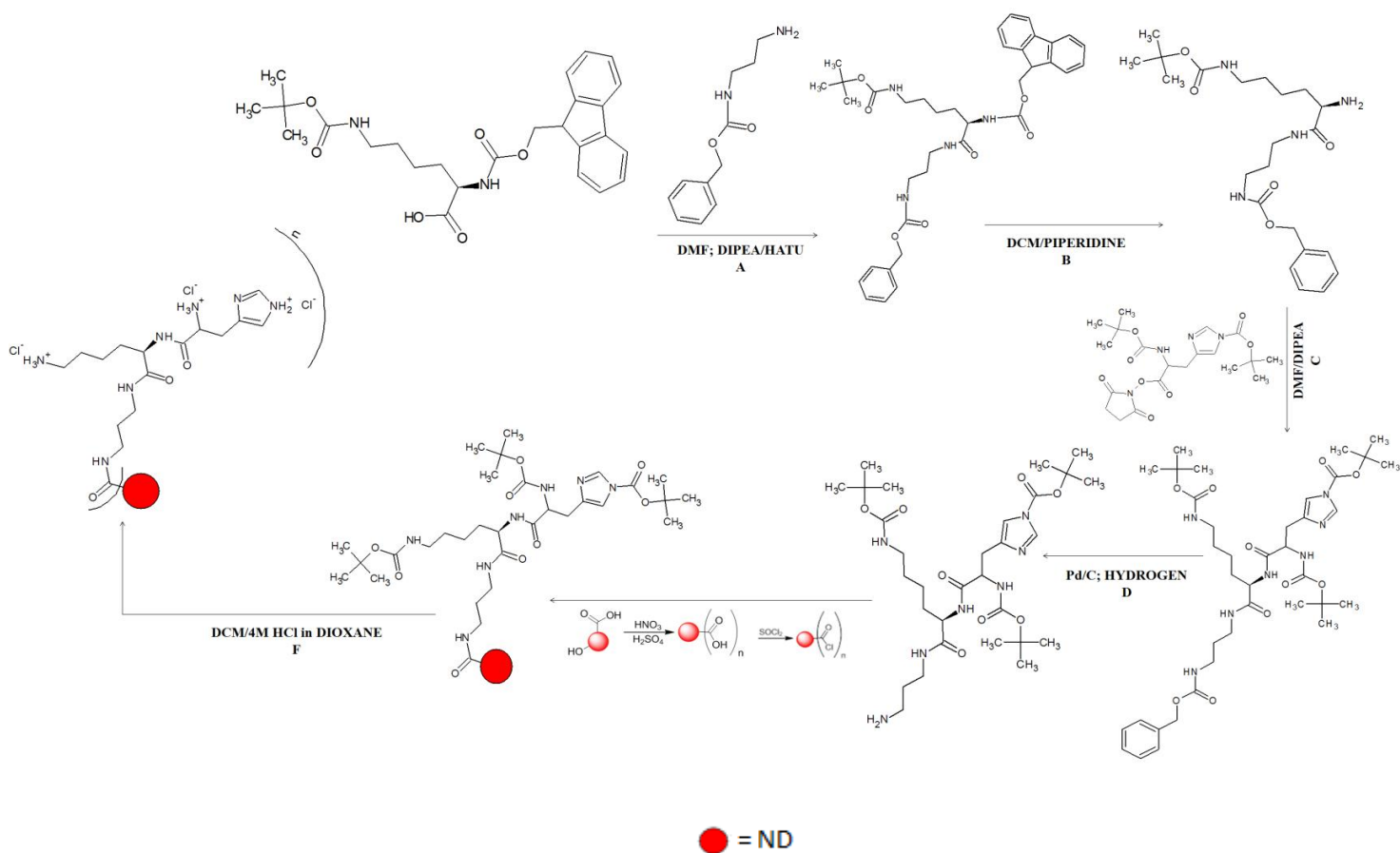
Dry dimethylformamide (DMF), 4 M hydrochloric acid (HCl) (in dioxane) and ethidium bromide solution (~1% in water) were obtained from Sigma-Aldrich (Oakville, ON, Canada). Boc-lysine(boc)-OH, fmoc-NH(CH₂)₃NH₂·HCl, N α -fmoc-N ϵ -boc-L-lysine, Z-1, 3-diaminopropane·HCl, N α ,N \imath m-bis-boc-L-histidine-N-hydroxysuccimideester, diisopropylethylamine (DIPEA), piperidine, and HATU [N,N,N',N'-tetramethyl-O-(7-azabenzotriazol-1-yl)uroniumhexafluorophosphate] were obtained from Chem-Impex International, Inc (Wood Dale, IL). Dichloromethane (DCM) (high-performance liquid chromatography grade) was purchased from Thermo Fisher Scientific (Waltham, MA) and was dried using a solvent purification system (MBraun Incorporated, Stratham, NH). Thionyl chloride was acquired from Alfa Aesar (Ward Hill, MA). Molecular porous cellulose membrane (MWCO: 6000-8000) was obtained from Spectra/Por®.

4.4.2 Functionalization of NDs

Standard Schlenk technique was used to maintain all the reaction steps under inert nitrogen environment. Ultrasonication was applied in certain steps using a bath sonicator to maintain dispersion and improve the reaction possibilities on the surface of individual nanosized particles. Scheme 1 and 2 describes the schematic illustration for synthesis of lysine and lysyl-histidine NDs



Scheme 1 Preparation of lysine-NDs in the presence of diaminopropane as a three carbon chain linker: **(A) Synthesis of N'- (N $_{\alpha}$,N $_{\epsilon}$ -bis-boc-lysyl)-N''-fmoc-diaminopropane; (B) Fmoc deprotection from N' (N $_{\alpha}$,N $_{\epsilon}$ -bis-boc-lysyl)-N''-fmoc-diaminopropane; (C) Reoxidation of pNDs (D) Acid chlorination of rNDs (E) Attaching fmoc deprotected N'(N $_{\alpha}$,N $_{\epsilon}$ -bis-boc-lysyl)-N''-diaminopropane to acyl chloride fNDs (F) Boc deprotection from lysine-NDs**



Scheme 2 Preparation of lysyl-histidine-NDs in the presence of diaminopropane as three carbon chain linker:

(A) Synthesis of N'-(N_α-fmoc- N_ε- boc-lysyl)-N''-cbz-diaminopropane; (B) Fmoc deprotection from N'-(N_α-fmoc- N_ε- boc-lysyl)-N''-cbz-diaminopropane; (C) Attachment of N_α-N_{im}-bis-boc histidine to fmoc deprotected N'-(N_α- N_ε- boc-lysyl)-N''-cbz-diaminopropane; (D) Cbz deprotection from N'-(N_α-(N_α-N_{im}-bis-boc histidine) N_ε- boc-lysyl)-N''-cbz-diaminopropane; (E) Attaching Cbz deprotected N'-(N_α-(N_α-N_{im}-bis-boc histidine) N_ε- boc-lysyl)-N''-diaminopropane to acyl chloride fNDs; (F) Boc deprotection from lysyl-histidine-NDs

4.4.2.1 Reoxidation of NDs

Pristine NDs (pNDs) (150 mg) were added in a dry Schlenk flask with YTZ grinding media (200 mg). A mixture of concentrated H₂SO₄ and HNO₃ (3:1 v/v) was added in the reaction flask in a volume sufficient to cover the pNDs. The reaction mixture was ultrasonicated at 25 kHz (without

heating) for 12 hours followed by overnight reflux under inert nitrogen environment using oil bath. To ensure the completion of the reaction, the mixture was again ultrasonicated for one hour and was finally refluxed for two hours.

In order to remove the unreacted acid content from the reoxidized NDs (rNDs), dialysis was performed using cellulose membrane (cut off MWCO: 6-8,000), deionized Millipore water (pH ~7) as external bath and diluting the reaction mixture up to 5% with deionized water. The dialysis was continued until the pH of the reaction mixture and the external bath was no more acidic and came close to the pH of deionized water. The process of dialysis was terminated upon obtaining an equilibrium between internal and external dialysis environments.

4.4.2.2 Acid chlorination of rNDs

Reoxidized NDs (rNDs) (150 mg) were added in a dry Schlenk flask maintained under nitrogen atmosphere along with YTZ grinding media (200 mg). Thionyl chloride (10 mL) was added in the reaction flask. Thionyl chloride itself acted as a solvent. The reaction mixture was ultrasonicated at 25 kHz without heating for 4 hours. Ultrasonication was followed by refluxing of the reaction mixture for 18 hours using an oil bath. During reflux the temperature of the oil bath was maintained at 100 °C. To ensure the completion of the reaction, the mixture was resonicated for 2 hours and refluxed for 3 hours.

An excess of thionyl chloride was pumped off using high vacuum pump/ Schlenk line technique. Exposure to moisture or air was avoided at all times during and after the reaction to maintain the stability of acyl chloride functional groups.

4.4.2.3 Preparation of functional moieties: Lysine

4.4.2.3.1 Step 1: Synthesis of N'- (N_α, N_ε-Bis-Boc-Lysyl)-N''-fmoc-diaminopropane (conjugation of lysine with the linker)

N_α, N_ε-bis-boc-lysine-OH (8.661 mmoles) was dissolved in dry DMF (10 mL) in Schlenk flask maintained under nitrogen atmosphere. This dissolution was followed by addition of HATU and DIPEA. HATU was added at a mole ratio of 1:1.25 (lysine: HATU) while DIPEA was added in mole ratio of 1:1.7 (HATU: DIPEA). The mixture was stirred for 15 minutes, after which fmoc-1, 3-diaminopropane hydrochloride was added in the reaction mixture in mole ratio of 1:1.15

(Lysine: linker). Dry DMF (15 mL) was added to ensure complete dissolution of all the starting materials. The reaction was kept under constant stirring for 20 hours after which DMF was removed under high vacuum from the reaction mixture by rota vapour. The solid was then dissolved in DCM (100 mL) and extracted using saturated aqueous solution of sodium bicarbonate (3x 100 mL). The purified organic phase obtained as a result of extraction was dried by the addition of sodium sulphate, followed by vacuum filtration to remove the hydrated sodium sulphate from the organic phase. DCM was removed under high vacuum and the obtained solid was washed with excess ether. The precipitates obtained as a result of ether washing were filtered under vacuum and subjected to solvent evaporation under vacuum to produce the desired compound which appeared as light yellow powder.

The percentage yield of N'- (N_α, N_ε-bis-boc-lysyl)-N''-fmoc-diaminopropane was 79 %.

4.4.2.3.2 Step 2: Fmoc deprotection from N' (N_α, N_ε-bis-boc-lysyl)-N''-fmoc-diaminopropane

The removal of fmoc protecting group of N' (N_α,N_ε-bis-boc-lysyl)-N''-fmoc-diaminopropane (5.773 mmoles) was done by dissolving it in 50% dry DCM/piperidine (v/v, 12 mL) mixture under nitrogen atmosphere in the Schlenk flask. The reaction was kept overnight. The precipitates observed in the reaction mixture at the end of the reaction were filtered and dried DCM was removed under high vacuum. Excess quantity of hexanes was added to the dry compound and allowed to stand for 15 minutes. The hexane-soluble portion was decanted to separate hexane-insoluble precipitates of the desired compound. The precipitates were washed with fresh portion of hexane (3x100 mL) and filtered to obtain purified desired compound. The clean precipitate was subjected to solvent evaporation to obtain dry compound.

The percentage yield of fmoc deprotected N' (N_α, N_ε-bis-boc-lysyl)-N''-diaminopropane was 48.1%.

4.4.2.4 Preparation of functional moieties: Lysyl-histidine

4.4.2.4.1 Step 1: Synthesis of N[']-(N_α-fmoc- N_ε- boc-lysyl)-N^{''}-cbz-diaminopropane (conjugation of lysine with the linker)

N_α-fmoc- N_ε- boc-lysyl (8.661 mmoles) was dissolved in 15 mL of dry DMF, followed by the addition of HATU (10.82 mmoles) and DIPEA (17.97 mmoles) maintained under nitrogen atmosphere in the Schlenk flask. The reaction mixture was stirred for 15 minutes.

Cbz-diaminopropane (9.925 mmoles) was dissolved in 10 mL of dry DMF and DIPEA (10.92 mmoles) was added into it. The solution of cbz-diaminopropane was added to the reaction mixture. The reaction was kept under constant stirring overnight. After completion of the reaction, DMF was removed under vacuum and a solid white compound was dissolved in 100 mL of DCM. Vortexing was done to ensure complete dissolution. The compound was extracted using a saturated solution of sodium bicarbonate (3x 100 mL), dried with sodium sulphate and filtered under vacuum. The obtained purified organic phase was subjected to solvent evaporation under vacuum. The solid compound was redissolved in a minimum amount of DCM and washed with excess ether. The precipitates obtained as a result of ether washing were filtered and dried under vacuum to produce desired compound which appeared as white powder.

The percentage yield of N[']-(N_α-fmoc- N_ε- boc-lysyl)-N^{''}-cbz-diaminopropane was 71 %

4.4.2.4.2 Step 2: Fmoc deprotection of N[']-(N_α-fmoc- N_ε- boc-lysyl)-N^{''}-cbz-diaminopropane:

N[']-(N_α-fmoc- N_ε- boc-lysyl)-N^{''}-cbz-diaminopropane (6.1173 mmoles) was dissolved in 50% dry DCM (10 mL) and 50% piperidine (10 mL) under nitrogen atmosphere in the Schlenk flask. The reaction was monitored for completion by TLC. The reaction was completed in two hours. After completion, excess acetone was added to the reaction mixture. Upon standing, white crystalline precipitate of piperidine by-product was formed in the mixture which was filtered under vacuum. Solvent evaporation was performed to obtain dry compound. The compound was redissolved in minimum amount of DCM and washed with excess hexane. The hexane insoluble portion was separated and subjected to solvent evaporation producing yellowish oil as the desired compound.

The percentage yield of fmoc deprotected N[']-(N_α-N_ε-boc-lysyl)-N^{''}-cbz-diaminopropane was 77.7%

4.4.2.4.3 Step 3: Attachment of N_α-N_{im}-bis-boc histidine to fmoc deprotected N[']-(N_α-N_ε-boc-lysyl)-N^{''}-cbz-diaminopropane

N_α-N_{im}-bis-boc histidine (2.35 mmoles) was dissolved in 15 mL of dry DMF, followed by addition of DIPEA (4.86 mmoles) under the nitrogen atmosphere maintained in the Schlenk flask. HATU was not added since histidine was already in the form of an activated ester. Fmoc deprotected N[']-(N_α-N_ε-boc-lysyl)-N^{''}-cbz-diaminopropane (2.35 mmoles) was dissolved in 10 mL of dry DMF and the solution was added to the reaction mixture. The reaction was kept under constant stirring overnight. After completion, DMF was removed under vacuum and the compound was dissolved in 100 mL of DCM followed by extraction using saturated sodium bicarbonate (3x100 mL) and 10% sodium chloride (1x100 mL). The organic phase was dried using sodium sulphate and filtered under vacuum. Purified organic phase was subjected to solvent evaporation to obtain dark yellow oil as the desired compound.

The percentage yield of N[']-(N_α-(N_α-N_{im}-bis-boc histidine) N_ε-boc-lysyl)-N^{''}-cbz-diaminopropane was 73.9%

4.4.2.4.4 Step 4: Cbz deprotection from N[']-(N_α-(N_α-N_{im}-bis-boc-histidine) N_ε-boc-lysyl)-N^{''}-cbz-diaminopropane

A catalytic amount of palladium on carbon (Pd/C) approx. 50% was suspended in 10 mL of methanol under nitrogen environment in the Schlenk flask. N[']-(N_α-(N_α-N_{im}-bis-boc histidine) N_ε-boc-lysyl)-N^{''}-cbz-diaminopropane (1.7443 mmoles) was dissolved in 10 mL of methanol and the solution was added in the reaction mixture. A hydrogen filled balloon was attached to the reaction flask using a syringe connection. Nitrogen supply was stopped to allow hydrogen to flow through the reaction mixture. The reaction was kept under constant stirring overnight. After completion, filtration was performed to remove palladium. Minute quantities of palladium left in the filtrate were removed by refiltration using celite. The clean filtrate was then subjected to solvent evaporation to remove methanol under vacuum and white crystalline powder of the desired compound was obtained.

The percentage yield of Cbz deprotected N'-(N_{α} -(N_{α} - N_{im} -bis-boc histidine) N_{ϵ} -boc-lysyl)-N''-diaminopropane was 99%

4.4.2.5 Conjugation of AA functional moieties with NDs

Acid chloride NDs (150 mg) were suspended in dry DMF (10 mL) under nitrogen atmosphere maintained in the Schlenk flask.

Fmoc deprotected N' (N_{α} , N_{ϵ} -bis-boc-lysyl)-N''-diaminopropane (0.772 mmoles) was dissolved in dry DMF (5 mL) and air was purged from the solution by bubbling nitrogen through it. The solution was added to the reaction mixture under nitrogen. The reaction mixture was sonicated at 25 kHz for 4 hours and refluxed using oil bath for 20 hours. The temperature was maintained at 100 °C. After completion, the mixture was again sonicated under same conditions for 2 hours followed by reflux for 3 hours. DMF was removed under vacuum and the lys-NDs were suspended in methanol for dialysis to remove unattached starting material and by-product impurities using cellulose membrane and 90% ethanol as the bath. The ethanol bath was changed at regular intervals until all the starting material and by-product impurities were eliminated.

Cbz deprotected N'-(N_{α} -(N_{α} - N_{im} -bis-boc histidine) N_{ϵ} - boc-lysyl)-N''-diaminopropane (0.468 mmoles) was attached to another set of acyl chloride fNDs (150 mg) by the same procedure to prepare lysyl-histidine-NDs.

4.4.2.6 Boc Deprotection from N' (N_{α} , N_{ϵ} -bis-boc-lysyl)-N''-diaminopropane fNDs and N'-(N_{α} -(N_{α} - N_{im} -bis-boc histidine) N_{ϵ} - boc-lysyl)-N''-diaminopropane fNDs:

N' (N_{α} , N_{ϵ} -bis-boc-lysyl)-N''-diaminopropane fNDs and N'-(N_{α} -(N_{α} - N_{im} -bis-boc histidine) N_{ϵ} -boc-lysyl)-N''-diaminopropane fNDs were subjected to solvent evaporation to remove methanol. The dry fNDs were suspended in 10 mL of DCM in the separate Schlenk flasks maintained under nitrogen environment and 10 eq. 4 M HCl (in dioxane) was added into each. The reaction mixtures were stirred for 90 minutes and the solvent was pumped off after completion. They were then subjected to freeze drying for 3 days to obtain boc deprotected lys-NDs and lysyl-histidine-NDs.

4.4.3 Physicochemical Characterization of fNDs

4.4.3.1 Nuclear Magnetic Resonance and Mass spectrometric characterization

Proton Nuclear Magnetic Resonance ($^1\text{HNMR}$) spectra were recorded for fmoc deprotected $\text{N}'(\text{N}_\alpha, \text{N}_\epsilon\text{-bis-boc-lysyl})\text{-N}''$ -diaminopropane and cbz deprotected $\text{N}'\text{-}(\text{N}_\alpha\text{-}(\text{N}_\alpha\text{-N}_{\text{im}}\text{-bis-boc histidine)} \text{N}_\epsilon\text{- boc-lysyl})\text{-N}''$ -diaminopropane before attaching these AA residues to acyl NDs. Chemical shifts for $^1\text{HNMR}$ are reported in ppm in reference to the residual ^1H resonances of deuterated chloroform (CDCl_3) (δ 7.26) which was used as the solvent.

A mass spectrum was obtained for Cbz deprotected $\text{N}'\text{-}(\text{N}_\alpha\text{-}(\text{N}_\alpha\text{-N}_{\text{im}}\text{-bis-boc histidine)} \text{N}_\epsilon\text{- boc-lysyl})\text{-N}''$ diaminopropane to confirm the HNMR result using the QSTAR ® XL MS/MS system with electrospray ionization source.

$^1\text{HNMR}$ was also done after all subsequent steps of the synthesis to confirm the formation and purity of the resulting compounds.

4.4.3.2 Infrared Spectroscopy

Infrared spectra were recorded at Canadian Light Source (CLS) for pNDs, rNDs, lys-NDs, lysyl-histidine-NDs and cbz deprotected $\text{N}'\text{-}(\text{N}_\alpha\text{-}(\text{N}_\alpha\text{-N}_{\text{im}}\text{-bis-boc histidine)} \text{N}_\epsilon\text{- boc-lysyl})\text{-N}''$ -diaminopropane using Bruker IFS 66v/S Fourier transform spectrometer in the mid-IR region having a mercury cadmium telluride detector. However, infrared spectra of fmoc deprotected $\text{N}'(\text{N}_\alpha, \text{N}_\epsilon\text{-bis-boc-lysyl})\text{-N}''$ -diaminopropane from the previous batch was used for comparison.¹³⁴ All samples were measured in solid state as homogenous powder dispersions in potassium bromide (KBr) pellets. Absorbance spectra were calculated based on the average of individual interferograms for both the background and the sample measurements. Data analysis was performed with a Bruker OPUS software package (v6.5, Bruker Optics).

4.4.3.3 Thermogravimetric Analysis

Thermogravimetric analysis (TGA) was carried out using TGA Q500 V20.13TGA (TA instruments, DE, USA). Samples (ca. 5-10 mg) were heated in a nitrogen atmosphere from 25°C to 700°C at a heating rate of $10^\circ\text{C}/\text{min}$, and the % weight loss was obtained as a function of the temperature. It was assumed that pNDs primarily have carboxylic acid functional groups on the

surface and upon reoxidation most of the remaining functionalities on the surface of pNDs were also changed to carboxylic acid functional groups. Based on this assumption, surface loading pNDs, rNDs, lys-NDs and lysyl-histidine-NDs were calculated using the following relationship:

$$\text{Surface Loading} = \frac{(\text{Number of moles of lost functional groups})}{(\text{Weight of the total sample} - \text{weight of the lost sample})} \dots\dots\dots (\text{Eq 4.1})$$

4.4.3.4 Size and Zeta Potential Measurements

2 mg/mL dispersion of pNDs, rNDs, lys-NDs and lysyl-histidine-NDs were prepared in purified water (Millipore, Milford, MA). YTZ grinding media was added to all the ND dispersions. The ND dispersions were then subjected to ultrasonication for 4 hours at a frequency of 25 kHz without heating. The ultrasonicated dispersions were then centrifuged at 5200 g for 5 minute to sediment the YTZ grinding media and the aggregated ND particulates. Particle size distributions of aqueous ND dispersions were obtained using Malvern zetasizer Nano ZS instrument (Malvern Instruments Ltd, Malvern, Worcestershire, UK). Solvent properties were as follows: refractive index = 1.330, dielectric constant = 78.5 and viscosity at 25°C = 0.8872 cP. Using CONTIN algorithm, the decay rates as a function of the translational diffusion coefficients of the particles ‘D’ were analysed. The hydrodynamic radius R_H of the particles was then calculated using the Stokes-Einstein equation ($R_H = kT/6\pi\eta D$), where k = Boltzman constant, T is the temperature (25 °C), and η = viscosity of water at 25 °C. The calculated particle size is an estimate based on the hydrodynamic radius of spherical particles having the translational diffusion coefficient equal to the particles in the dispersion. All the size distribution readings were derived from six measurements. Each measurement had a minimum of ten individual runs. The resulting data was reported as volume distribution. The size distribution was plotted as a graph to compare the polydispersity and the average particle size of four ND dispersions.

Zeta potential measurements were performed for pNDs, rNDs, lys-NDs and lysyl-histidine-NDs. These measurements were based on Doppler electrophoresis and phase analysis. All the reported zeta potentials are the average of three measurements. Each measurement had hundred individual runs.

4.4.4 Binding of fNDs to nucleic acids

4.4.4.1 Agarose gel electrophoresis

1% agarose gel was prepared in purified water to determine successful binding of lys-NDs and lysyl-histidine-NDs with pDNA. Complexes of lys-NDs and lysyl-histidine-NDs with pDNA were prepared by dispersing pDNA and NDs in different weight ratios (NDs: pDNA ranging from 1:1 to 1:30) and incubating the dispersions for 30 minutes at room temperature. pDNA without fND dispersion was used as the control. The amount of pDNA in each sample was 500 ng. The samples were loaded in the gel and were subjected to electrophoresis at 100 V for one hour using Bio-Rad PowerPac HC electrophoresis apparatus (Bio-Rad Laboratories, Tnc. Mississauga, ON, Canada). The gel was then imaged using AlphaImager imaging system (Alpha Innotech Corporation, San Leandro, CA) to detect fluorescence.

Binding of lys-NDs and lysyl-histidine NDs to siRNA was also analysed using 2% agarose gel in the same way. 50 μ M negative control siRNA (Ambion Inc.) was used as the stock solution of siRNA and 2 mg/mL stock solutions of lys-NDs and lysyl-histidine-NDs were used. The amount of siRNA in each sample was 500 ng. Complexes of lys-NDs and lysyl-histidine NDs with siRNA were prepared by dispersing SiRNA and NDs in different weight ratios (NDs: siRNA ranging from 1: 10 to 1: 50) and incubating the dispersions for 30 minutes at room temperature. siRNA without fND dispersion was used as the control. Electrophoresis was run for 30 minutes at 50 V and the samples were analysed similar to the pDNA complexes.

4.5 Result and discussion

4.5.1 Synthesis of fNDs

Lysine and lysyl-histidine conjugates with diaminopropane spacer were synthesized and were covalently bonded to NDs. The NDs were pre-functionalized with acyl chloride groups to enhance amide bond formation between the carbonyl group on ND surface and free amine group of diaminopropane acting as a linker.

Completion of reaction of the lysine linked to diaminopropane was evident from the ^1H NMR Spectrum (Figure 4.1). The ^1H NMR spectrum of N'- (N $_{\alpha}$,N $_{\epsilon}$ -bis-boc-lysyl)-N''-fmoc-

diaminopropane was used to confirm the structure: ^1H NMR (500 MHz, deuterated chloroform CDCl_3) δ 7.75 (d, 2H, fluorenyl of fmoc protecting group), 7.60 (d, 2H, fluorenyl of fmoc protecting group), 7.39 (t, 2H, fluorenyl of fmoc protecting group), 7.30 (t, 2H, fluorenyl of fmoc protecting group), 7.26 (s, solvent chloroform), 6.72(s, 1H, NH of amide), 5.47 (s, 1H, NH of amide), 5.23 (s,1H, NH of amide), 4.67 (s, 1H, NH of amide), 4.38 (d, 2H CH_2 of fluorenyl), 4.20 (t,1H, CH of the central ring of fluorenyl in fmoc protecting group), 4.03 (s,1H, fluorenyl ring of fmoc protecting group), 3.47(q, 1H, CH group of lysine bonded to amide linkage between lysine and linker), 3.29 (m, 2H), 3.20 (m, 2H), 3.09 (m, 2H) 1.64-1.9 (m, 4H) and 1.43 (s,18H boc protecting group). However in the ^1H NMR spectra the peaks in the range of 1.39 to 1.49 integrates for 24H which may be the combination of a singlet peak of tertiary butyl groups $(\text{CH}_3)_6$ of boc and CH_2 groups of lysine. The methylene groups of lysine may be at 1.37 integrating for 2H and at 1.46-1.49 integrating for 2H for the remaining CH_2 group. The ^1H NMR spectra for N'' - (N_α , N_ϵ -bis-boc-lysyl)- N'' -fmoc-diaminopropane integrates for 49H, which is relevantly consistent with the compound structure having 48H. Therefore it is evident that the compound is intact. The four NH peaks appearing within the range of 4 to 7 indicates four different amide linkages, that are two amide linkages on lysine with boc protecting groups, one amide linkage between lysine and the linker and one amide linkage between the linker and fmoc protecting group. Before attaching the AA conjugate to acyl chloride functionalized NDs, the fmoc protecting group attached to the linker (1, 3- diaminopropane) was removed. The ^1H NMR of N'' - (N_α , N_ϵ -bis-boc-lysyl)- N'' -diaminopropane (Figure 4.2) shows absence of peaks in aromatic region, indicating removal of fmoc from the linker.

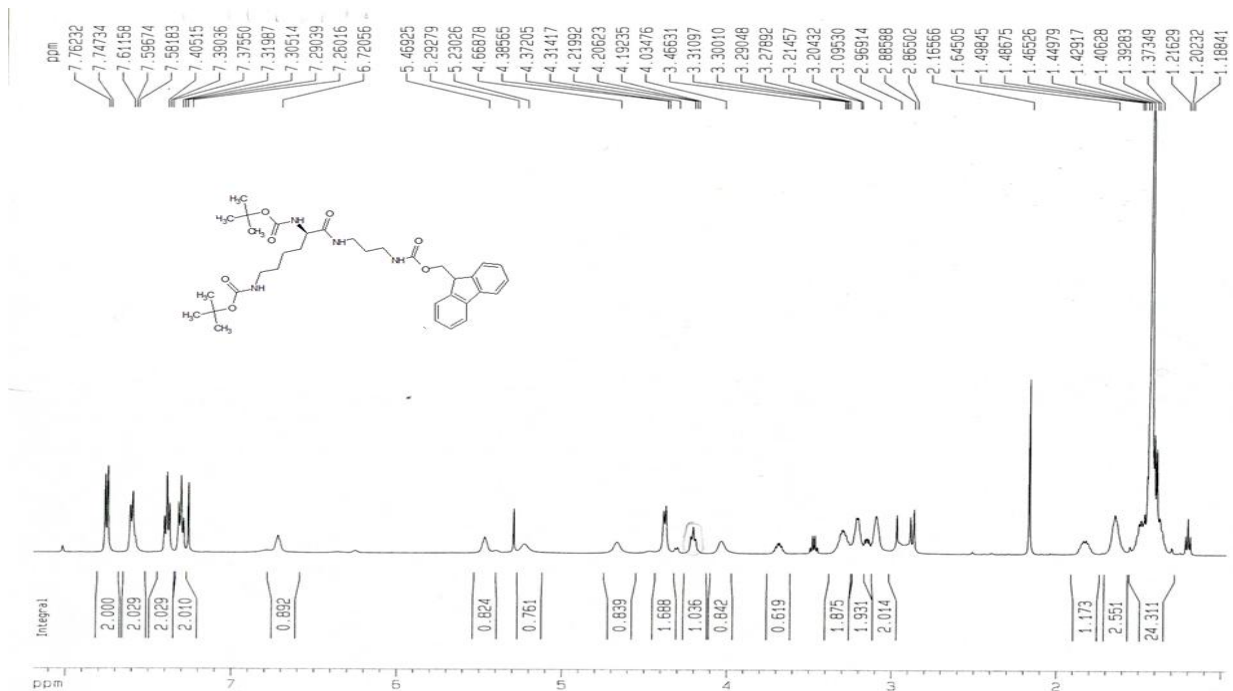


Figure 4.1 ^1H NMR spectra for $\text{N}'\text{-(N}_\alpha, \text{N}_\epsilon\text{-bis-boc-lysyl)-N''\text{-fmoc-diaminopropane}$ at 500 mHz

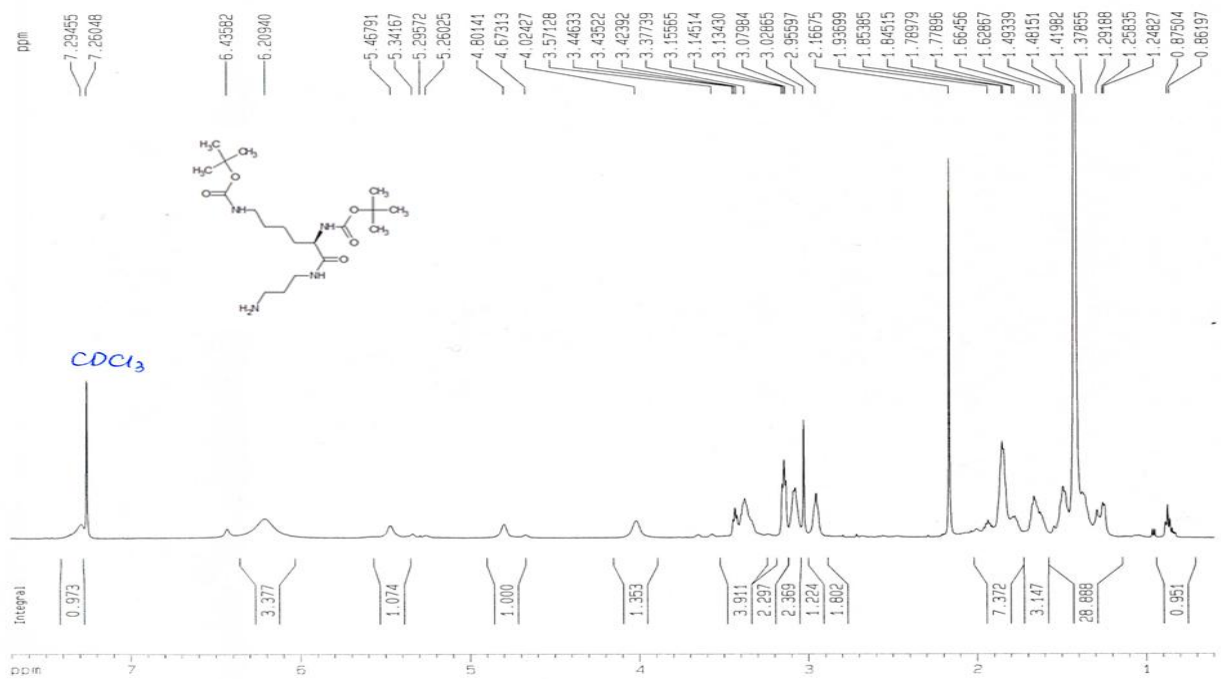


Figure 4.2 ^1H NMR spectra of $\text{N}'\text{(N}_\alpha, \text{N}_\epsilon\text{-Bis-Boc-Lysyl)-N''\text{-Diaminopropane}$ at 500 mHz

Synthesis of lysyl-histidine linked to diaminopropane was also analysed by using ^1H NMR (Figure 4.3). The spectrum showed the presence of the compound; however it integrated for more protons than expected in the aliphatic region as well as the aromatic region, suggesting an impurity of the starting material. Therefore to confirm the presence of compound mass spectrometry analysis was performed. Lysyl-histidine linked with diaminopropane was identified through the mass spectrum (Figure 4.4) and MS/MS spectrum (Figure 4.5) of $\text{N}'\text{-(N}_\alpha\text{-(N}_\alpha\text{-N}_{\text{im}}\text{-bis-boc histidine) N}_\epsilon\text{- boc-lysyl)-N''-cbz-diaminopropane}$ ($\text{C}_{38}\text{H}_{59}\text{N}_7\text{O}_{10}$). Electrospray ionization mass spectrometry mass-to-charge ratio calculated for $\text{C}_{38}\text{H}_{59}\text{N}_7\text{O}_{10}$: 773.43 [M] and 774.43 [M+H] $^+$, found 774.57 [M+H] $^+$. The compound was also confirmed by its distinct fragmentation pattern obtained in the MS/MS spectra. The fragmentation spectrum indicates subsequent loss of boc protecting groups as indicated in Scheme 3. $\text{C}_{33}\text{H}_{52}\text{N}_7\text{O}_8$: 674.40 [M+H] $^+$ indicates loss of boc from imidazole ring of histidine AA, $\text{C}_{28}\text{H}_{44}\text{N}_7\text{O}_6$: 574.32 [M+H] $^+$ indicates subsequent loss of boc from terminal amine of lysine AA and $\text{C}_{23}\text{H}_{36}\text{N}_7\text{O}_4$: 474.24 [M+H] $^+$ indicates subsequent loss of boc from histidine AA (Figure 4.5).

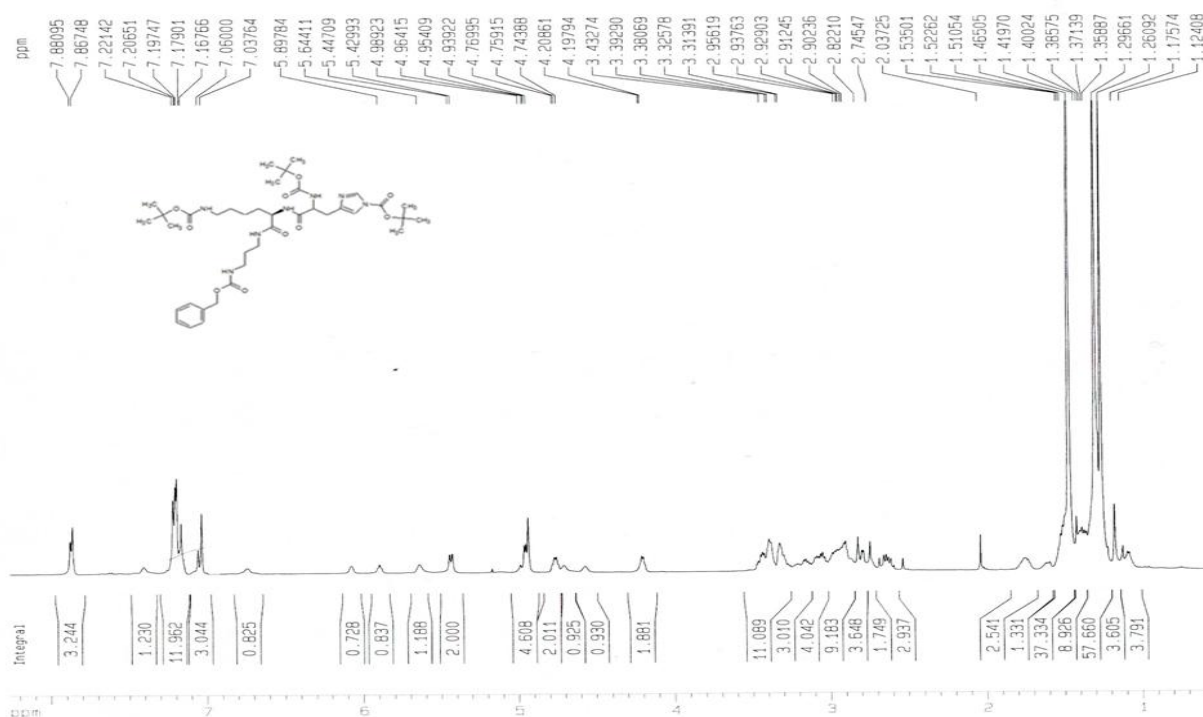


Figure 4.3 ^1H NMR of $\text{N}'\text{-(N}_\alpha\text{-(N}_\alpha\text{-N}_{\text{im}}\text{-bis-boc histidine) N}_\epsilon\text{- boc-lysyl)-N''-cbz-diaminopropane}$ at 500 MHz

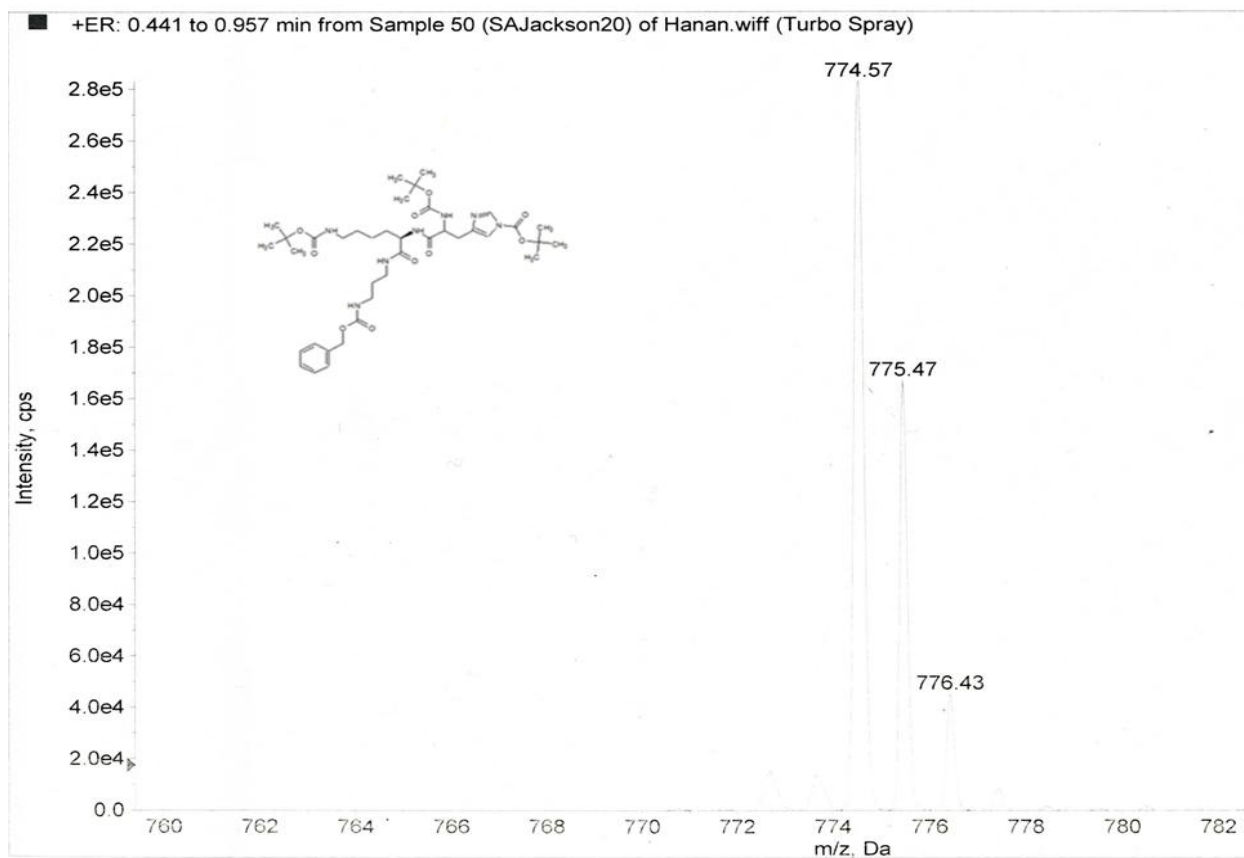
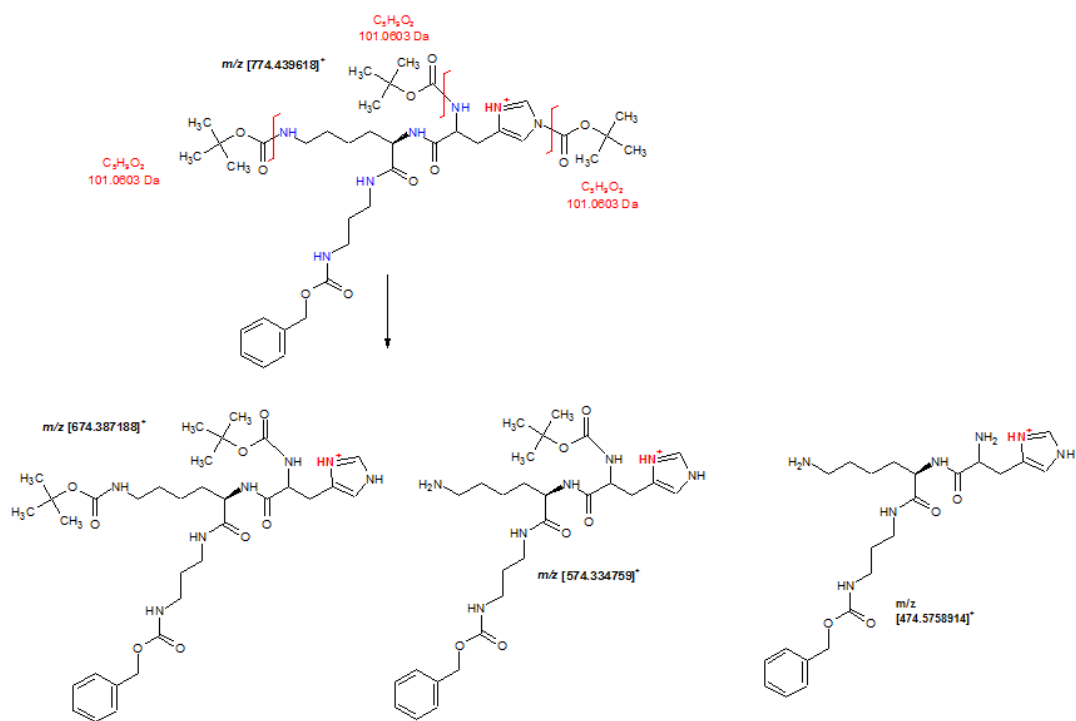


Figure 4.4 MS spectra of N'- $(N_{\alpha}$ - $(N_{\alpha}$ -Nim-bis-boc histidine) N_{ϵ} - boc-lysyl)-N''-cbz-diaminopropane



Scheme 3 Probable fragmentation pattern of N'-(N $_{\alpha}$ -(N $_{\alpha}$ -N $_{im}$ -bis-boc histidine) N $_{\epsilon}$ - boc-lysyl)-N''-cbz-diaminopropane (C₃₈H₅₉N₇O₁₀)

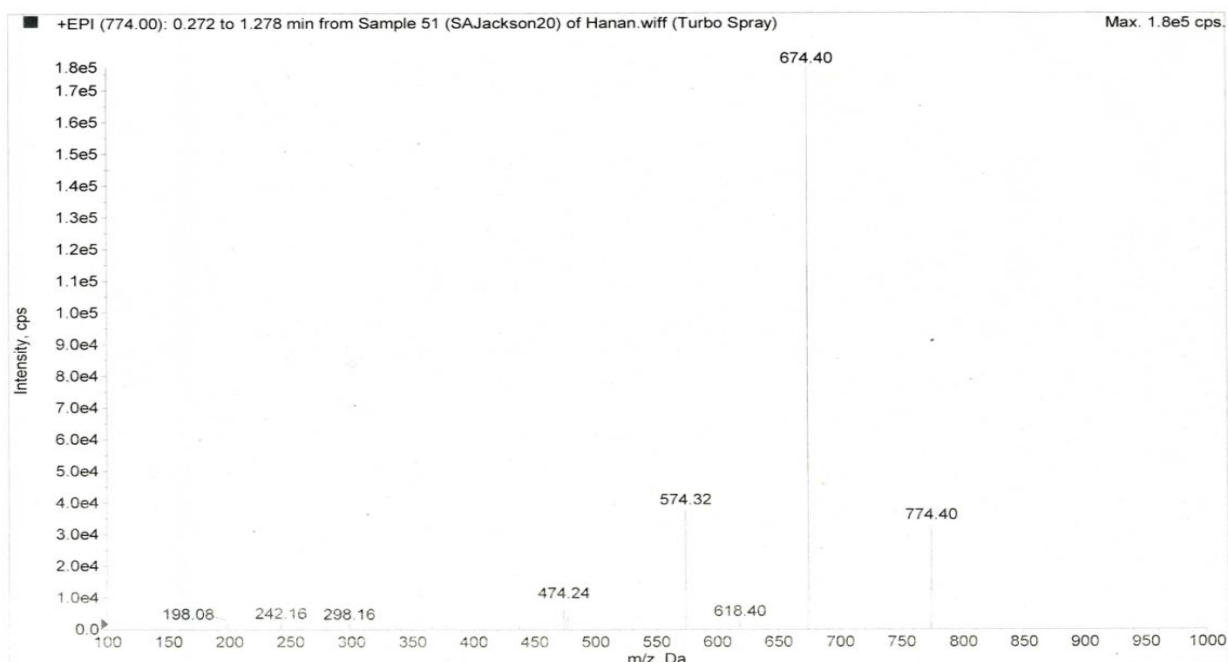


Figure 4.5 MS/MS spectra for fragmentation of N'-(N $_{\alpha}$ -(N $_{\alpha}$ -N $_{im}$ -bis-boc histidine) N $_{\epsilon}$ - boc-lysyl)-N''-cbz-diaminopropane (C $_{38}$ H $_{59}$ N $_7$ O $_{10}$)

Before attachment of the AA conjugate to acyl chloride functionalized NDs the carboxybenzyl (Cbz) protecting group attached to the linker (1, 3-diaminopropane) was removed. The ^1H NMR spectrum of N'-(N $_{\alpha}$ -(N $_{\alpha}$ -N $_{im}$ -bis-boc histidine) N $_{\epsilon}$ - boc-lysyl)-N''-diaminopropane (Figure 4.6) shows absence of cbz peaks in the aromatic region indicating deprotection. N'-(N $_{\alpha}$, N $_{\epsilon}$ -bis-boc-lysyl)-N''-fmoc-diaminopropane ^1H NMR (500 MHz, deuterated chloroform CDCl $_3$) δ 7.26 (s, solvent chloroform), 8.01 (d, 1H, imidazole ring of histidine), 7.20 (d, 1H, imidazole ring of histidine). The aliphatic region consist of three boc peaks at around 1.59, 1.42 and 1.41 indicating the presence of intact compound. However, the aliphatic region of the spectrum shows excess number of proton depicting the presence of a possible impurity. Therefore to confirm presence of the compound mass spectrometric analysis was performed. The mass spectrum of N'-(N $_{\alpha}$ -(N $_{\alpha}$ -N $_{im}$ -bis-boc histidine) N $_{\epsilon}$ - boc-lysyl)-N''-diaminopropane (C $_{30}$ H $_{54}$ N $_7$ O $_8$) (Figure 4.7) and MS/MS spectrum (Figure 4.8) showing particular fragmentation of the compound is an indication of deprotection. Electrospray ionization mass spectrometry mass-to-charge ratio calculated for C $_{30}$ H $_{54}$ N $_7$ O $_8$: 639.395 [M] and 640.395 [M+H] $^+$, found 640.41 [M+H] $^+$. The compound was also confirmed by its distinct fragmentation pattern obtained in the MS/MS spectra. The fragmentation spectrum indicates subsequent loss of boc protecting groups as indicated in

Scheme 4. $C_{25}H_{46}N_7O_6$: 540.40 $[M+H]^+$ indicates loss of boc from imidazole ring of histidine AA, $C_{20}H_{38}N_7O_4$: 440.48 $[M+H]^+$ indicates subsequent loss of boc from terminal amine of lysine AA and $C_{15}H_{30}N_7O_2$: 340.72 $[M+H]^+$ indicates subsequent loss of boc from histidine AA (Figure 4.8).

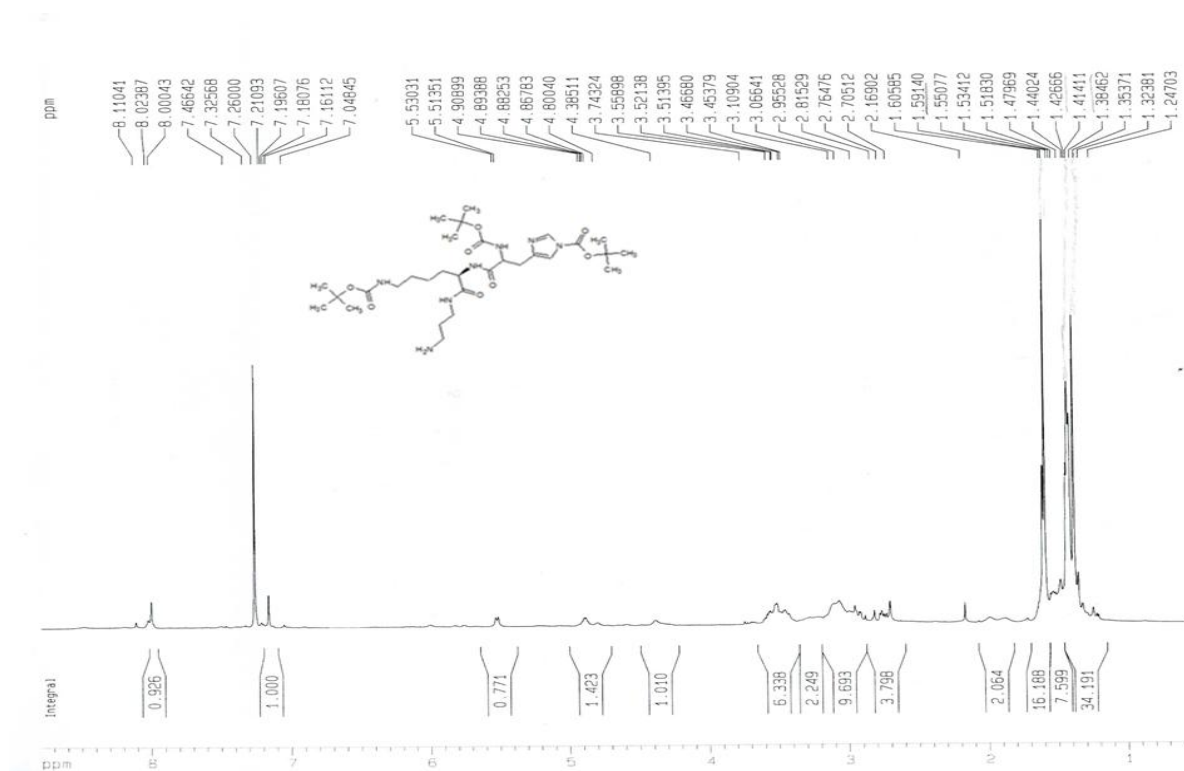


Figure 4.6 1H NMR spectra of $N'-(N_\alpha-(N_\alpha-N_{im}\text{-bis-boc histidine}) N_\epsilon\text{-boc-lysyl})-N''\text{-diaminopropane}$ at 500 MHz

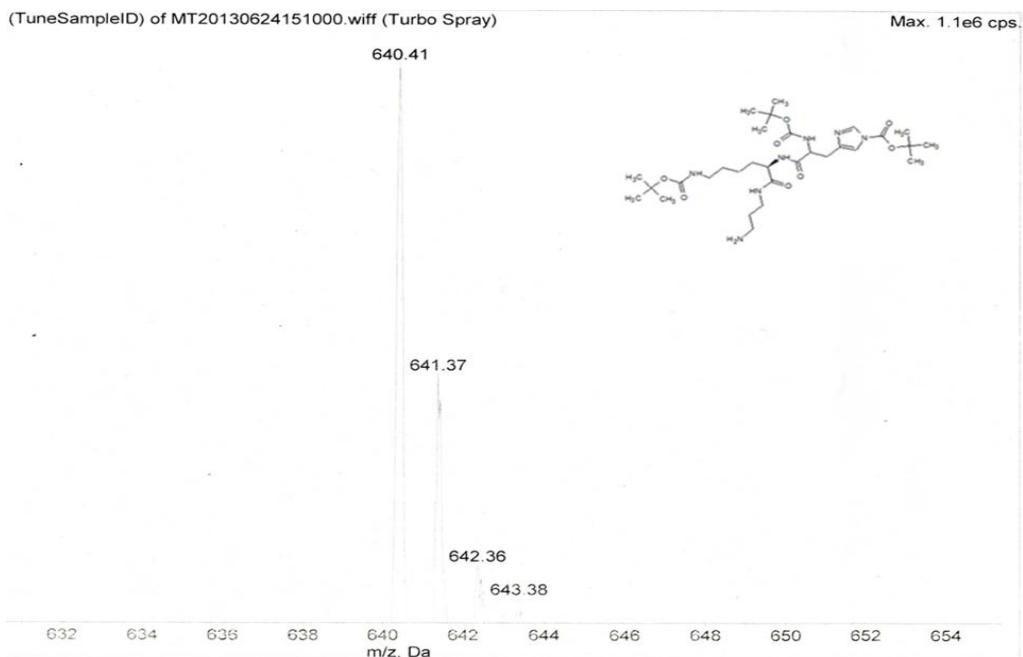
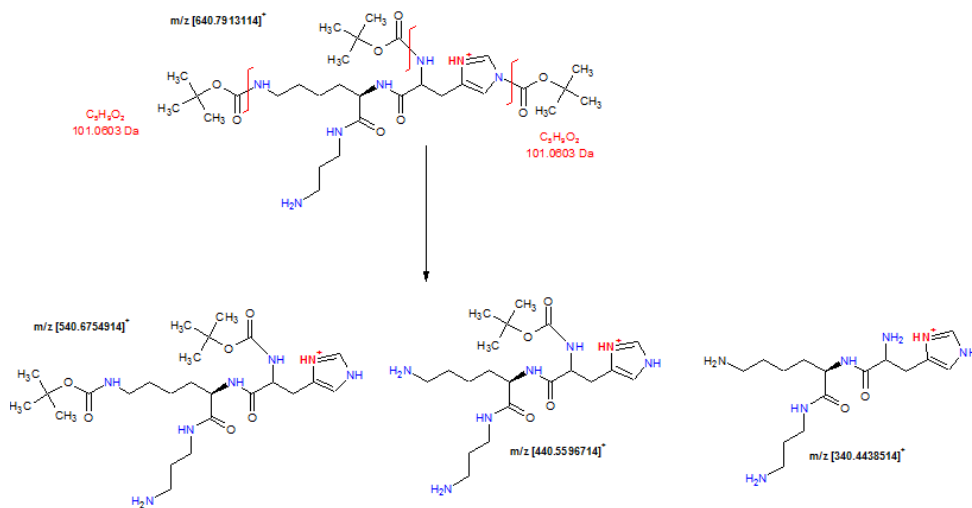


Figure 4.7 MS spectra of N'-(N $_{\alpha}$ -(N $_{\alpha}$ -N $_{im}$ -bis-boc histidine) N $_{\epsilon}$ - boc-lysyl)-N''-diaminopropane



Scheme 4 Probable fragmentation pattern of N'-(N $_{\alpha}$ -(N $_{\alpha}$ -N $_{im}$ -bis-boc histidine) N $_{\epsilon}$ - boc-lysyl)-N''-diaminopropane (C₃₀H₅₄N₇O₈)

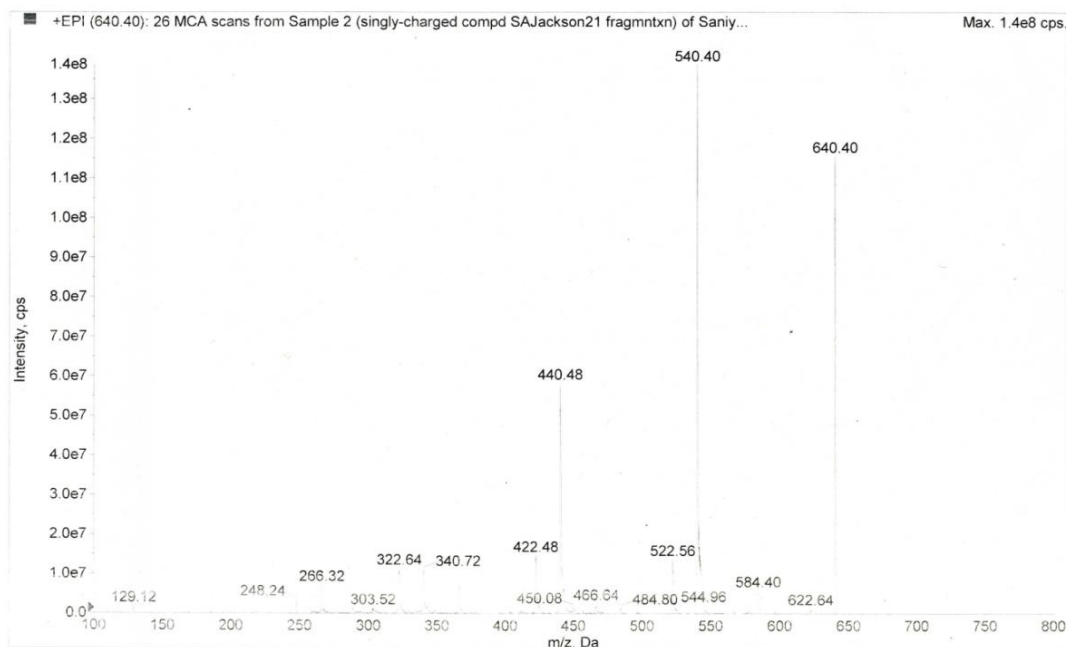


Figure 4.8 MS/MS spectra of N'-(N $_{\alpha}$ -(N $_{\alpha}$ -N $_{im}$ -bis-boc histidine) N $_{\epsilon}$ - boc-lysyl)-N''-diaminopropane (C $_{30}$ H $_{54}$ N $_7$ O $_8$)

4.5.2 Infrared Spectroscopy (IR)

Lysine and lysyl-histidine functionalization of NDs was confirmed by performing IR of pNDs, rNDs, lys-NDs, lysyl-histidine-NDs and N'-(N $_{\alpha}$ -(N $_{\alpha}$ -N $_{im}$ -bis-boc histidine) N $_{\epsilon}$ -boc-lysyl)-N''-diaminopropane (Figure 4.9). NDs possess a fingerprint region in the range of 1000 cm $^{-1}$ to 1500 cm $^{-1}$ where they show a combination of many overlapping peaks.⁹³ The FTIR spectra of all the NDs showed distinct peaks at ~ 1130 cm $^{-1}$ and ~ 1260 cm $^{-1}$ which are the characteristic peaks of diamond.²⁰¹ These peaks represent C-O (stretch) due to vibrations of ether like groups.¹³⁴ This ether like linkages might arise due to inter-particle interaction between carboxylic acids or hydroxyl groups on the surface of NDs.¹³⁴ The peak at ~1650 cm $^{-1}$ which is consistent in the IR spectra of all NDs and the AA conjugate corresponds to C=O (stretch) of amide bond and carboxylate in fNDs and non-functionalized pNDs and rNDs respectively. Carboxylate functionality is expected to be compromised after functionalization due to the formation of an amide linkage between the carbonyl on NDs and amines on the linker. Unlike rNDs, fNDs do not show the broad peak at ~3400 cm $^{-1}$ corresponding to O-H (stretch) of carboxylate functionality further confirming the functionalization. The absence of a sharp O-H (stretch) peak in pNDs indicates the completion of reoxidation process where most of the functionalities are

converted to carboxylic acid. The presence of peaks for N-H (stretch) at $\sim 3000\text{ cm}^{-1}$ and N-H (bend) at $\sim 1490\text{ cm}^{-1}$ in the spectra of AA conjugate, lysine NDs and lysyl-histidine NDs indicates the presence of amide linkages. These peaks are absent for pNDs and rNDs, thereby suggesting successful functionalization.

Primary amines are identified by two N-H (stretch) bands in the region of ~ 3000 to 3500 cm^{-1} : one due to symmetric stretching, the other due to asymmetric stretching. Presence of another pronounced peak of N-H (stretch) at $\sim 3090\text{ cm}^{-1}$ in lys-NDs IR spectra indicates the presence of more primary amines as compared to lysyl-histidine-NDs in which one primary amine is lost due to histidine attachment. Therefore, the IR spectrum for lysyl-histidine NDs shows a very weak signal for another N-H (stretch) in this region. The presence of a peak for C-N (stretch) at $\sim 1080\text{ cm}^{-1}$ in the spectra for lys-NDs and lysyl-histidine-NDs further confirms the presence of amines on their surface. These peaks are absent in pNDs and rNDs, therefore they indicate successful functionalization. Peaks for H-C-H (stretch) at $\sim 2900\text{ cm}^{-1}$ and H-C-H (bend) at $\sim 1400\text{ cm}^{-1}$ in the spectra of AA conjugates, lys-NDs and lysyl-histidine-ND indicates the presence of aliphatic CH_2 groups of AA on the ND surface.

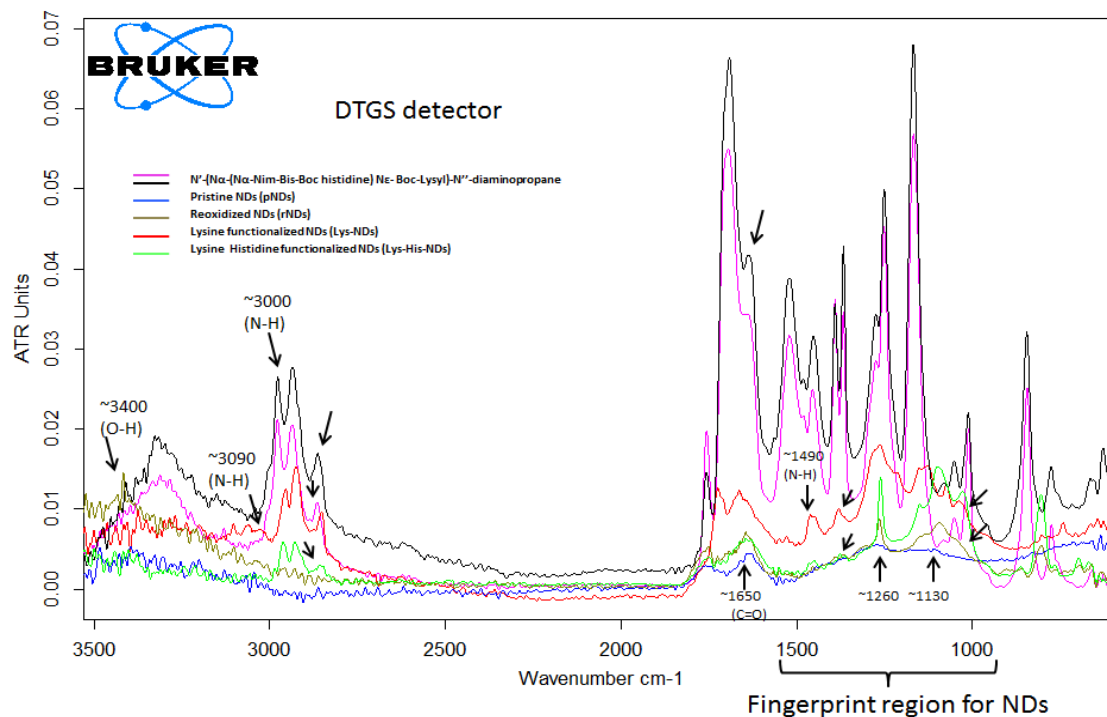


Figure 4.9 Infra-red spectra of pNDs, rNDs, lysine-NDs, lysyl-histidine-NDs and AA conjugate (N'-(N_α-(N_α-N_{im}-bis-boc histidine) N_ε- boc-lysyl)-N''-diaminopropane) Infrared spectra for N' (N_α,N_ε-bis-boc-lysyl)-N''-diaminopropane was referenced from ¹³⁴ and hence not shown above.

4.5.3 Thermogravimetric Analysis (TGA)

Surface functionalization of NDs is also shown by TGA (Figure 4.10). The thermograms of pNDs and rNDs did not show considerable weight loss in the range of 100-500°C depicting lack of functional groups which may be labile in the specific temperature range. It is reported that CO₂ yielding complexes like carboxylic acids, anhydrides and lactones start to decompose at 500 K (227 °C) with maximum desorption occurring at 600 K (327 °C) and 900 K (627 °C).^{202,203} The thermogram of rNDs shows an increased weight loss in this range as compared to pNDs which illustrates more abundance of COOH groups on ND surface as a result of reoxidation. Thermograms of lys-NDs and lysyl-histidine-NDs show a sharp weight loss from 150 °C to 700 °C illustrating the loss of AA functional groups which is an evidence of surface functionalization. It should be noted that weight loss for fNDs is reported at high temperatures (200 °C to 700 °C) which indicates covalent nature of surface functionalization.¹⁴²

Surface loading of functional groups onto the NDs was calculated from the respective thermograms (Table 4.1). The surface loading of carboxylic acid (COOH) groups on pNDs and rNDs was estimated to be 1.0 and 1.74 mmols/g respectively, while the surface loading of lysine AA conjugated with 1, 3-diaminopropane on lys-NDs was higher being 1.97 mmols/g. However surface loading of lysine and histidine AA conjugated with 1, 3-diaminopropane on lysyl-histidine-NDs was estimated to be only 0.55 mmols/g. The surface loading for rNDs is significantly higher as compared to pNDs, which indicates that reoxidation step was successful in increasing the number of COOH groups onto the NDs surface. Moreover, the surface loading of COOH groups on rNDs is very close to the surface loading of lysine conjugate functionalities on lys-NDs, which indicates that the process of functionalization was capable of converting most of the COOH groups on the rND surface. The low surface loading for lysyl-histidine-NDs may be explained by the large surface area covered by this AA conjugate that may create steric hindrance for adjacent COOH groups to be functionalized. Alteration in the spacer length or the design sequence for attaching histidine moiety can possibly counter the steric hindrance

allowing complete surface functionalization. This design modification is further discussed later in the thesis.

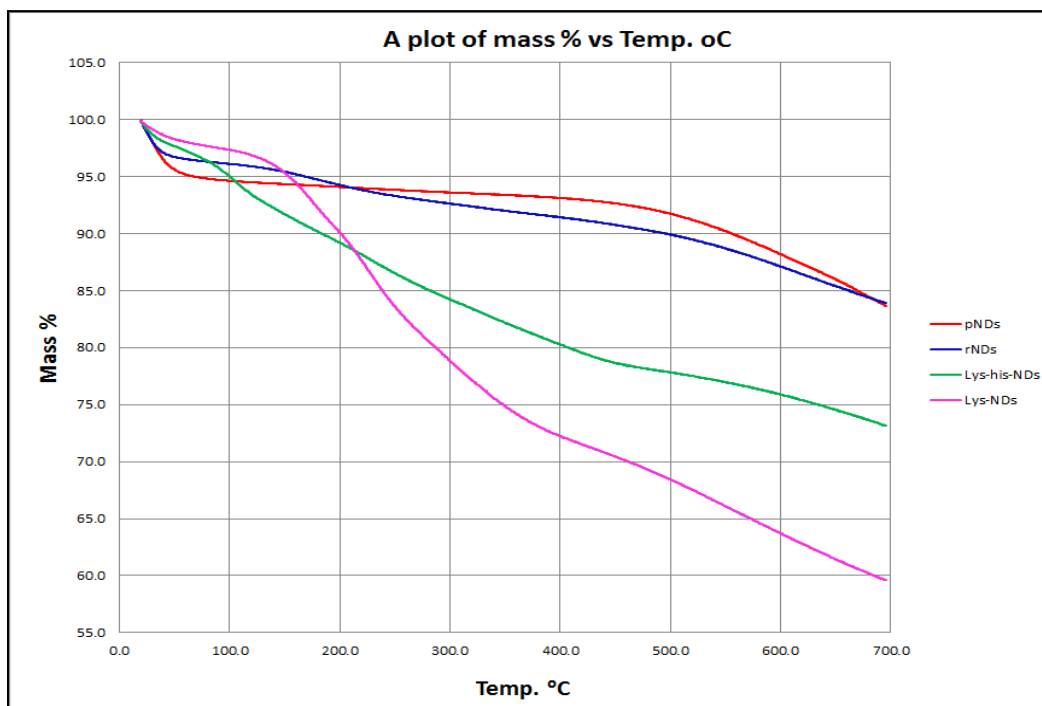


Figure 4.10 Thermograms of pNDs, rNDs, lys-NDs and lysyl-histidine NDs

Thermogram of lysine NDs shows the highest % weight loss followed by lysyl-histidine NDs, rNDs and pNDs

Type of NDs	Surface Loading (mmols/g)
pNDs	1.0
rNDs	1.74
lys-NDs	1.97
lysyl-his NDs	0.55

Table 4.1 Surface Loading of NDs as calculated from respective thermograms

Weight loss below 115 °C is excluded considering it due to water loss from the samples

4.5.4 Particle size distribution of NDs

Size of the NP system is an important characteristic in gene delivery as the kinetics of cellular uptake and saturation concentration varies with NP size.²⁰⁴ NP size is also crucial to enhance therapeutic effects and to control toxicity.²⁰⁵ Moreover, polydispersity of NP system affects their behaviour inside the cell and therefore has to be critically controlled. NP gene delivery systems should have uniform sized particle dispersion in order to obtain a predictable response.²⁰⁴ NPs within 2-100 nm size range can alter signaling processes essential for basic cell function.²⁰⁶ Therefore, particle size and polydispersity were measured for all functionalized NDs. The pristine NDs (pNDs) exhibit wide size distribution, with two major peaks obtained at 68.55 (30%) and 15 nm (14%) (Figure 4.11). The polydispersity index is high (0.244) (Table 4.2). This may be explained due to non-uniformity of functional groups present on the surface of pNDS. Reoxidized NDs (rNDs) show considerable reduction in size variability. The process of re-oxidation creates uniform sized NDs majority centered around 79 nm (Figure 4.11); due to the conversion of majority of functionalities on NDs surface to COOH. However, the rNDs system also contains aggregated NDs in 106-190nm size range (Table 4.2). Lys-NDs show a sharp peak at 50.8 nm (Figure 4.11), depicting that lysine functionalization was able to create highly uniform ND dispersions having most of the particles possessing a desirable size of approximately 50 nm.¹⁷⁹ Lys-NDs system show minimum amount of aggregated particles in 106-190 nm size range (Table 4.2). On the contrary, lysyl-histidine-NDs were found to form a polydispersed system (0.419) (Table 4.2) with wider particle size distribution centered in the range of 615-955 nm (Figure 4.11). This may be a result of uneven functionalization.

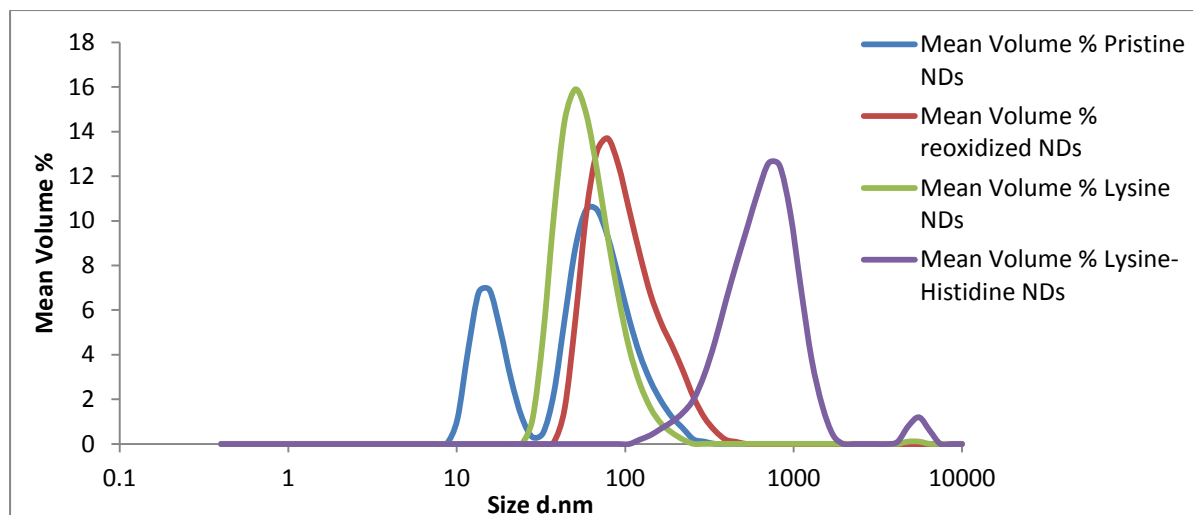


Figure 4.11 Size distribution curves for pNDs (blue), rNDs (red), lysine NDs (green) and lysyl histidine NDs (purple)

Each size distribution curve is measured by dynamic light scattering and is derived from three measurements with 10 individual runs

Type of NDs	Particle Size range (nm)	Mean volume %	Polydispersity Index (PDI)
pNDs	10-24	28%	0.244
	38-91	54.5%	
	106-190	15.5%	
rNDs	44-51	7 %	0.145
	59-91	50%	
	106-190	35.5%	
Lys-NDs	33-91	89 %	0.142
	106-190	10%	
Lysyl-his NDs	295-531	32%	0.419
	615-955	47 %	
	1106-1484	13%	

Table 4.2 Particle size distribution and polydispersity of pNDs, rNDs, lysine NDs and lysyl-histidine NDs

Each size distribution data indicates mean of three measurements with 10 individual runs

4.5.5 Zeta potential of NDs

Charges possessed by a particle also play a vital role in NP-cell interaction.²⁰⁴ It has been reported that cationic particles can bind to negatively charged cell membrane,²⁰⁷ and can easily translocate across the cell membrane. Moreover, cationic NPs are used as primary gene delivery systems, since they possess positive ionic groups to bind with the negatively charged genetic material. Therefore, zeta potentials were measured for all four types of NDs to obtain a comprehensive view of surface charges. pNDs and rNDs showed a highly negative zeta potential of -54.6 mV and -32.2 mV, respectively, while lysyl-NDs show a positive zeta potential of +26.3 mV (Figure 4.12). The positive zeta potential of lys-NDs indicates the dominance of positively charged amine groups on the surface which in turn may lead to high binding capacity with genetic material and higher interaction with negatively charged cell membrane. Lysyl-histidine-NDs also showed a positive zeta potential of +2.65 mV (Figure 4.12) indicating that fewer positively charged amine groups are present on the surface compared to lysyl-NDs.

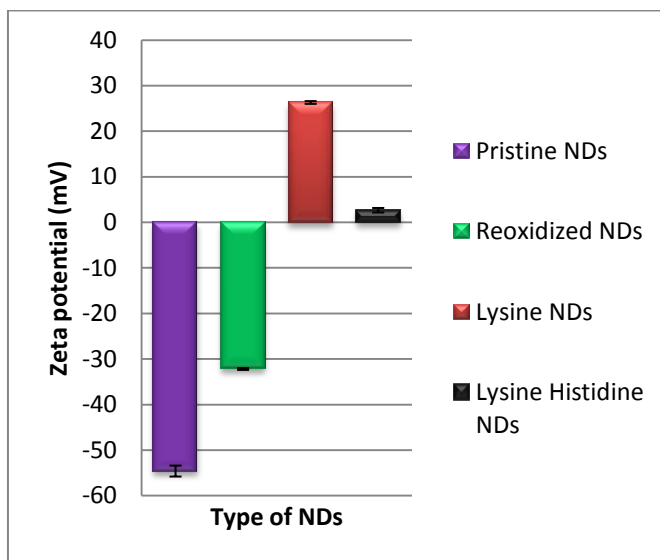


Figure 4.12 Comparison of zeta potentials of NDs before and after functionalization

Each value represents the mean \pm standard deviation of three measurements with 100 individual runs

4.5.6 Binding of fNDs with pDNA and siRNA

In order to act as an efficient nucleic acid delivery vehicle, lys-NDs and lysyl-histidine-NDs should be capable of binding the genetic material to a degree that enables the transfer of nucleic acid inside the cell and release them near the cell nucleus.²⁰⁸ To analyse the nucleic acid binding capacity of fNDs, gel electrophoresis was performed for fNDs: pDNA complexes (Figure 4.13) and fNDs : siRNA (Figure 4.14) complexes. Results for fNDS: pDNA show a visible band for naked pDNA. Lys-NDs: pDNA complexes ranging from ratio 1:1 to 1:30 show no visible band for pDNA, which indicates that lys-NDs are capable of binding to pDNA and prevent migration, even at minimum ratio of 1:1. However, the lysyl-histidine-NDs: pDNA complexes ranging from 1:1 to 1:30 show a visible band for pDNA, which indicate that lysyl-histidine-NDs are not capable to bind the pDNA even in high ratios. This can be explained due to low positive surface charge of lysyl-histidine NDs as explained earlier.

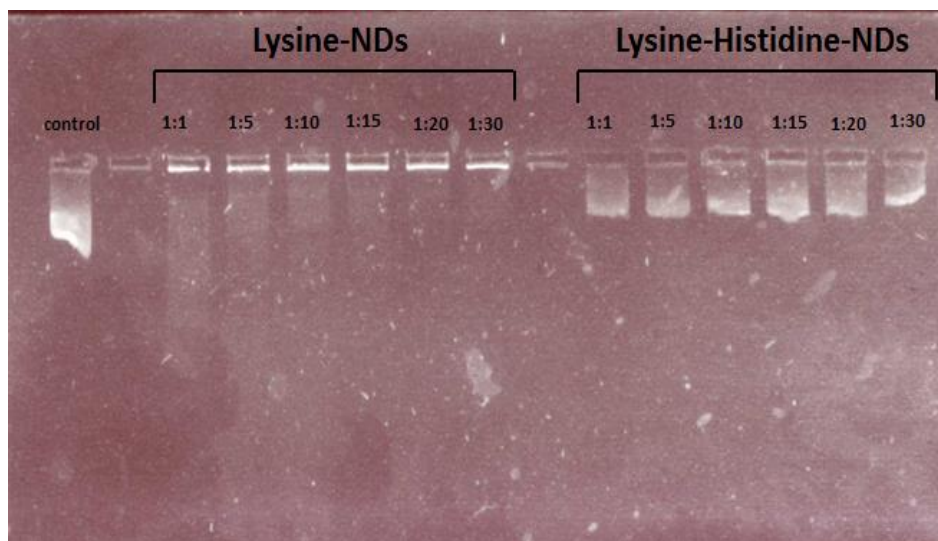


Figure 4.13 Binding of lysine-NDs and lysyl-histidine NDs with pDNA

Result of agarose gel electrophoresis for lysine NDs/lysyl histidine NDs-plasmid DNA with increasing weight ratios of fNDs to pDNA

Results for fNDS: siRNA show a visible band for naked siRNA. Lys-NDs: siRNA complexes show a light band at 1:10 ratio, which indicates a weak binding of lys-NDs with SiRNA at this ratio. However, lys-NDs: siRNA complexes ranging from ratio 1:20 to 1:50 show no visible band for siRNA, which indicates that lys-NDs are capable of binding to siRNA completely at a weight

ratio of minimum 1:20. The lysyl-histidine-NDs: siRNA complexes ranging from 1:10 to 1:50 behaved similarly to lysyl-histidine-NDs: DNA complexes, showing a visible band for siRNA, which indicate that lysyl-histidine-NDs are not capable to bind siRNA even in high ratios. This can be explained due to low positive surface charge of lysyl-histidine NDs as explained earlier.

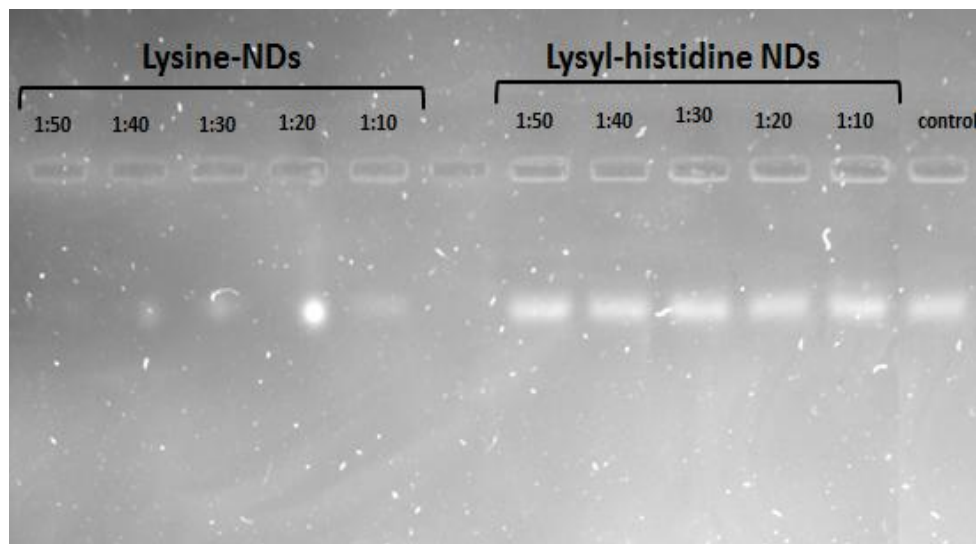


Figure 4.14 Binding of lysine-NDs and lysyl-histidine NDs with SiRNA

Result of agarose gel electrophoresis for lysine NDs/lysyl histidine NDs-small interfering RNA with increasing weight ratios of fNDs to siRNA

4.6 Conclusion

NDs were successfully functionalized with lysine with a high surface loading capable of creating a cationic surface. Lysine functionalization was also able to limit aggregation and produced uniform sized ND particulates to generate stable dispersion in aqueous medium. However, lysyl-histidine functionalization was limited and very low surface loading was obtained. An altered synthetic approach is designed to synthesize lysyl-histidine NDs with an aim to limit steric hindrance and increase the surface loading of this AA conjugate. Details of this approach are summarized under the heading of conclusions and future directions.

5 Lysine and Lysyl-Histidine Functionalized Nanodiamonds: Development of Stable Colloidal Dispersion for in vitro Cellular Uptake Studies and siRNA Delivery Application

Saniya Alwani¹, Randeep Kaur¹, Deborah Michel¹, Jackson M Chitanda², Ronald E Verrall³, Chithra Karunakaran⁴ and Ildiko Badea¹

¹Drug Design and Discovery Research Group, College of Pharmacy and Nutrition, University of Saskatchewan, ²Department of Chemical & Biological Engineering, University of Saskatchewan, ³Department of Chemistry, University of Saskatchewan, ⁴Canadian Light Source, Saskatoon, SK, Canada

5.1 Authors' contributions

Saniya Alwani:

- Written and edited the research article in its entirety.
- Conducted all the assays reported in the article except laser confocal scanning microscopy (part 5.4.3.3 and 5.6.9).

Randeep Kaur:

- Performed and interpreted laser confocal scanning microscopy (part 5.4.3.3 and 5.6.9) for internalization of bare lysine functionalized NDs.

Deborah Michel:

- Assisted all flow cytometry assays (part 5.4.3.3, 5.4.4, 5.6.8 and 5.6.10).

Jackson M Chitanda:

- Assisted in the synthesis and characterization of lysine functionalized NDs.

Ronald E. Verrall:

- Assisted in the synthesis and characterization of lysine functionalized NDs.
- Assisted in the revision and editing of the text in the research article.

Chithra Karunakaran:

- Assisted in the performance of scanning transmission X-ray microscopy at Canadian Light Source (part 5.4.3.1 and 5.6.7).

Ildiko Badea:

- Supervised the entire work.
- Assisted in the revision and editing of the text in the research article.

Note:

*The Manuscript is accepted for publication in **International Journal of Nanomedicine***

5.2 Abstract

Purpose: Nanodiamonds (NDs) are emerging as an attractive tool for gene therapeutics. To reach their full potential for biological application, NDs should maintain their colloidal stability in biological milieu. This study describes the behavior of lysine-functionalized ND (lys-ND) in different dispersion conditions with an aim to limit aggregation and improve the colloidal stability of ND-gene complexes called diamoplexes. Furthermore, cellular and macromolecular interactions of lys-NDs are also analysed *in vitro* to establish understanding of ND mediated gene transfer in cells.

Methods: Lys-NDs were synthesized earlier through covalent conjugation of lysine AA to carboxylated NDs surface generated through re-oxidation in strong oxidizing acids. Here, dispersions of lys-NDs were prepared in various media and the degree of sedimentation was monitored for 72 hours. Particle size distributions and zeta potential measurements were performed for a period of 25 days to characterize the physicochemical stability of lys-NDs in the medium. The interaction profile of lys-NDs with fetal bovine serum (FBS) showed formation of a protein corona which was evaluated by size and charge distribution measurements. Uptake of lys-NDs in cervical cancer cells was analyzed by scanning transmission X-ray microscopy, flow cytometry and confocal microscopy. Cellular uptake of diamoplexes (complex of lys-NDs with small interfering RNA) was also analyzed using flow cytometry.

Results: Aqueous dispersion of lys-NDs showed minimum sedimentation and remained stable over a period of 25 days. Size distributions showed good stability, remaining under 100 nm throughout the testing period. A positive zeta potential of over +20 mV indicated a preservation of surface charges. Size distribution and zeta potential changed for lys-NDs after incubation with blood serum suggesting an interaction with biomolecules, mainly proteins and a possible formation of a protein corona. Cellular internalization of lys-NDs was confirmed by various techniques such as confocal microscopy, soft x-ray spectroscopy and flow cytometry.

Conclusion: This study establishes that dispersion of lys-NDs in aqueous medium maintains long-term stability, and also provides an understanding that lysine functionalization enables NDs to interact effectively with the biological system to be used for RNAi therapeutics.

Keywords: colloidal stability, particle size, zeta potential, protein corona, diamoplex, microscopy, flow cytometry

5.3 Introduction

Diamond nanoparticles, also called nanodiamonds (NDs) exhibit unique thermal, mechanical and optoelectronic properties. In recent years much attention has focused towards utilizing NDs for biomedical applications. The key feature that makes their utilization so attractive in therapeutics is their innate biocompatible nature at cellular^{71,72} and organ levels.¹⁹⁷ NDs are the most biocompatible member of the carbon nano family⁷¹ and show no structural damage, such as fragmentation of the genetic materials,³⁷ and thus can act as efficient gene carriers. Despite several favourable characteristics, the major challenge associated with utilizing NDs for biological applications is the high degree of aggregation, which leads to the formation of extremely tight structures of 100 to 200 nm in size.²⁰⁹ Unlike other carbon nanomaterials, NDs possess a functionalized surface as a result of its synthesis method. The functional groups present on detonation NDs can facilitate aggregation through Van der Waals interactions or hydrogen bonding between adjacent ND crystals.^{210, 211, 16} However, the major cause of aggregation is the graphitic soot formed around the NDs as a result of the detonation process which creates core aggregates.⁸⁵ These aggregates give rise to several complications in terms of formulation, colloidal stability and cellular uptake. Several physical methods, such as micro bead, sugar or salt assisted stirred media milling have employed to limit aggregation and to produce stable, well-dispersed ND formulations.^{123, 127}

To control aggregation and ensure long term stability of ND dispersions, chemical modification of the surface can be utilized.^{212, 140, 138} Rational functionalization of ND surfaces with different moieties to serve multiple purposes is a relatively new approach. For example, functional groups can be grafted to simultaneously counter aggregation and facilitate binding with small chemical molecules or biomolecules with a purpose to serve as drug, protein and gene carriers.^{212, 134, 213}

Utilizing NDs and other carbon nanomaterials for gene delivery is of high interest nowadays due to the advantages of DNA or siRNA based therapeutics targeted towards malignant forms of cancer and viral infections like HIV.^{214, 215, 216} In order to synthesize ND based gene carriers, the aim is to generate a cationic surface which can electrostatically interact with anionic genetic materials.^{128, 217} Such examples are non-covalent functionalization with polymers like polyethyleneimine (PEI)⁶⁹ and covalent conjugation of derived organic moieties like triethylammonium groups.⁶⁸ Introducing protonable biomolecules, including amino acids (AAs),

peptides and proteins on the ND surface is a novel approach for functionalization. Its first application was centered on a physical adsorption, such as coating the ND surface with poly-L-lysine, a polypeptide frequently used as carrier for genetic materials.¹⁴⁷ The coating occurs through non-covalent adsorption of chemicals on the nanoparticle surface through electrostatic interactions and van der Waals forces. It is easy to achieve but may lead to desorption and competitive displacement of active moieties in complex biological environment, thus compromising the long-term stability of the system.²¹⁸ To overcome this deficiency, covalent conjugation could permanently immobilize the molecules of interest on the surface and create a controlled and relatively stable functionalized system.¹⁴² We demonstrated for the first time that covalent immobilization of basic AAs mainly lysine directly on the ND surface can form diamplexes with DNA and siRNA and can be used for gene delivery purposes.¹³⁴ Lysine functionalization imparts a primary amine rich cationic surface that is capable of binding anionic genetic material and proteins. This concept is modeled on the natural DNA wrapping in the eukaryotic cells by histone proteins, rich in lysine and arginine AAs forming salt bridges.¹⁵⁶ Positive charges on the surface can also aid in cellular uptake through electrostatic interaction with the acidic residues on the mammalian cell membrane. Surface functionalization of NDs with lysine AA conjugates is evident through various complimentary techniques reported in our previous publication.¹³⁴

Previously, we reported that lysine functionalization induced homogeneity of the surface limiting aggregation of NDs in aqueous environment for a short period of time.¹³⁴ Here, we expand the stability assessment of lysine-functionalized NDs (lys-NDs) in biologically relevant media to an extended time period of 25 days. Moreover, the interaction of lys-NDs with serum proteins was also investigated.

Interaction of (nanoparticles) NPs with physiological proteins is an extensive area of research, since their random adsorption on NP surfaces can alter formulation properties and carrier stability profiles.^{185, 219, 220} A protein adsorption layer (protein corona) can rapidly evolve as a result of nanoparticle interacting with biological fluids and is a critical issue as it can affect the fate of NPs.^{221, 222, 183, 184} Several studies have shown that formation of a protein corona hinders cellular uptake of the gene delivery NPs, leading to diminished biological activity.^{183, 223} However, recently it has been observed that serum can serve as a dispersant for carbon nanomaterials,

without compromising the cellular uptake.²²⁴ For example, serum albumin can facilitate cellular uptake of carbon nanotubes in white blood cells.¹⁸⁹ Therefore, understanding the effect of a protein corona on cellular uptake of lys-NDs is a prerequisite for their therapeutic evaluation.

Lastly, cellular uptake of lys-NDs and the diamoplexes was also investigated in the study. NDs, like many other carbon nanomaterials, commonly follow an energy-dependent clathrin mediated endocytosis pathway for internalization in mammalian cells.^{148, 173} However, the pathway and extent for ND uptake may vary depending on the particle size and surface coatings.¹⁷⁷ Cellular uptake of lys-NDs and the siRNA conjugated diamoplexes was assessed by a variety of techniques, including confocal microscopy, scanning transmission x-ray microscopy (STXM) and flow cytometry.

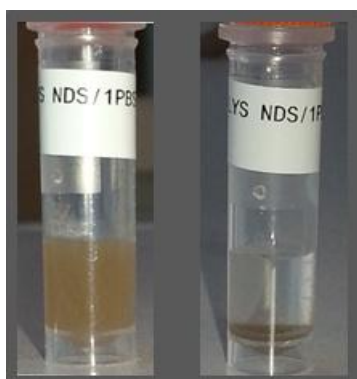
5.4 Results and Discussion

5.4.1 Dispersion stability of lysine NDs in formulations

The choice of a dispersion medium is critical in attempting to define optimum physicochemical characteristics of and biological responses to the NPs. Therefore, a series of biologically relevant media were evaluated for preparing lys-NDs dispersions. The dispersions in phosphate buffer saline (PBS) showed extensive sedimentation within 3 days (Figure 5.1A). Lys-NDs in 0.5% methylcellulose gel aggregated slightly, observed by visual monitoring for 3 days (Figure 5.1B), whereas aqueous dispersion of lys-NDs showed minimum sedimentation over a period of 25 days (Figure 5.1C). PBS promotes ND aggregation due to its high ionic strength which disturbs the charge distribution on the ND surface. This ultimately causes destabilization which is mediated through random van der Waals interactions.^{225, 226} Methylcellulose is an amphiphilic molecule which is commonly employed in stabilizing hydrophobic carbon nanomaterials, especially uncharged carbon nanotubes (CNTs).²²⁷ However, in the case of cationic NPs it can reduce the positive charge density of the surface by masking the functional groups through adsorption.²²⁸ This phenomenon can ultimately lead to flocculation and reduce colloidal stability of the lys-NDs. It could also hamper the binding efficacy with genetic materials and hinder the formation of diamoplexes.

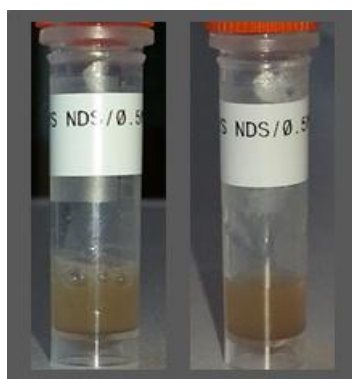
Lys-NDs remained well dispersed in water showing minimum sedimentation over 25 days, thus the stability of aqueous ND dispersion was further analysed using particle size distribution and

zeta potential measurements. The distributions remained relatively mono-modal (Figure 5.1D) throughout the period of analysis and hence average particle sizes were calculated. The average particle size of the fresh ND dispersion (day 1) was 51 ± 16 nm (PDI: 0.142) (Figure 5.1D) with 89% of the particles in the optimal size range of 33-91 nm (Supplementary Information: Table 5S.1). Subsequently, the size increased slightly to 79 ± 10 nm on day 3 to 91 ± 13 and 91 ± 12 nm by days 15 and 25, respectively. The zeta potential remained relatively stable being $+26.3\pm 0.3$ mV on day 1, $+21.2\pm 0.4$ mV on day 3, $+31.3\pm 0.6$ mV on day 15 and $+29.6\pm 0.4$ mV on day 25 (Table 5.1). The stability is due to the fact that the aqueous medium does not compromise the positive charges on lys-NDs, thus electrostatic repulsion between homogenous adjacent surfaces is maintained and the formation of core aggregates is hindered.



Day 1 Day 3

(A) Lys-NDs in PBS



Day 1 Day 3

(B) Lys-NDs in methylcellulose



Day 1 Day 3 Day 15 Day 25

(C) Lys-NDs in Water

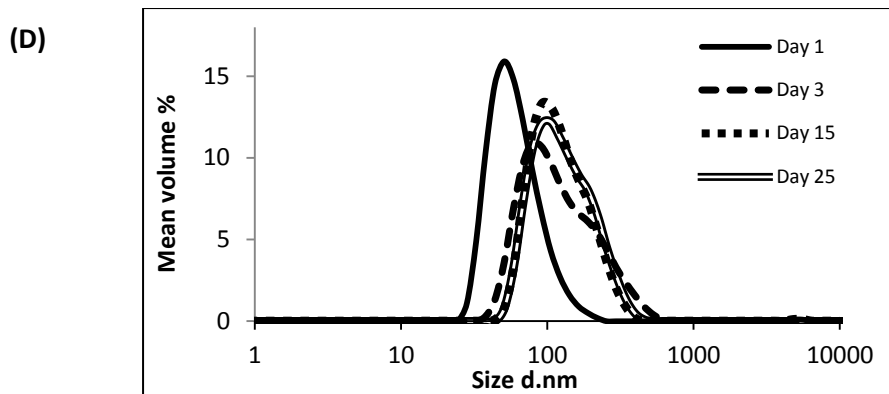


Figure 5.1 Dispersion of lys-NDs in different media. Dispersions of (A) Lys-NDs in phosphate buffered saline (PBS) (B) Lys-NDs in methylcellulose gel and (C) Lys-NDs in aqueous medium at different time points showing maximum aggregation of ND particles in PBS upon 3 days of standing and minimum aggregation of ND particles in aqueous medium over 25 days; (D) Size distribution curves for lys-NDs in aqueous medium on day 1, day 3, day 15 and day 25. Each curve is derived from an average of 6 distributions with 10 individual scans

Aqueous dispersion of lys-NDs	
Time point	Zeta Potential (mV)
Day 1	+26.3 ± 0.3
Day 3	+21.2 ± 0.4
Day 15	+31.3 ± 0.6
Day 25	+29.6 ± 0.4

Table 5.1 Zeta potentials of lys-NDs in aqueous medium at different time points

*Each zeta potential measurement indicates mean of six measurements with 100 individual runs.

5.4.2 Interaction of lys-NDs with biological growth medium

Additional to the inherent properties of NPs, physicochemical changes mediated through the biological growth medium can also modulate the transfection efficiency.^{229, 230} Therefore, we investigated the behavior of NPs in biologically relevant media used for *in vitro* transfection

(mainly, cell culture medium and protein rich serum). Stability analysis of lys-NDs was performed in both serum free and supplemented DMEM to understand this behavior.

Lys-NDs in serum free DMEM exhibited poor dispersibility and showed visible sedimentation within 24 hours after sonication (Figure 5.2A). Particle size distribution also revealed a high degree of aggregation with the majority of ND particles having a diameter of 500 ± 10 nm (Figure 5.2B) (Supplementary Information, Table 5S.2). A zeta potential of -2.2 ± 2.6 mV (Table 5.2) indicated that the positively charged surface of lys-NDs was also compromised. Since the systems were highly aggregated within 24 hours, analyses at further time points were not performed. We postulate that lys-NDs become unstable in DMEM due to high ionic strength of the growth medium, which promotes the flocculation of the colloidal system.^{111, 231, 232} Macromolecules and electrolytes in growth media show random electrostatic interactions with the functional groups on the ND surface, thus concealing the positive charges of primary amines responsible for repulsion of individual particles, similar to the effect of PBS. Ultimately, inter-particle interaction is enhanced resulting in increased level of aggregation and particle sedimentation, due to the screening effect of counter ions.²³¹

Interaction of lys-NDs with serum proteins was also investigated in fetal bovine serum (FBS) to assess the formation of a protein adsorption layer on ND. The Lys-ND/protein interaction was analyzed by observing the change in particle size and zeta potential as a function of incubation time with FBS. Upon visual inspection, the lys-NDs showed no visible sedimentation up to 3 days (Figure 5.2C) indicating good dispersibility. However, lys-NDs exhibited an approximately 5 fold increase in diameter immediately after protein adsorption with size distributions ranging from 150 to 500 nm (Figure 5.2D) (Supplementary Table 5S.2) compared to lys-NDs in water (range of 33-91 nm) or the serum alone (range of 4-11 nm) (Figure 5.2D), which remained fairly constant for 3 days. The disappearance of the lys-ND and serum peaks indicates dynamic association of serum proteins with cationic ND surface. In nanoparticulate systems, an increase in diameter after protein adsorption can vary greatly depending upon the size of adsorbing proteins^{233, 234} and the surface-to-volume ratio of the particles,²³⁵ as observed for systems reported herein. Adsorption of the serum proteins was confirmed by the change in zeta potential of the ND system from +26.3 mV to -12.4 mV (Table 5.2) suggesting the formation of an anionic protein

corona. Due to positively charged surface of lys-NDs, there is an increased possibility for adsorption of proteins with low iso-electric points (<5.5) such as albumin.²³⁵

Protein adsorption is a two edged process. It can change the biological identity of NPs affecting its cellular uptake and distribution,¹⁸³ but also can be beneficial for limiting nanoparticle mediated cellular toxicity and conferring target specificity.²³⁵ In the present study, the ability of lys-NDs to adsorb proteins can be utilized in the future for improving the cellular uptake and targeting by allowing the formation of a selective protein corona, like apolipoproteins, which have been employed to enhance cellular uptake of NPs.^{235, 236}

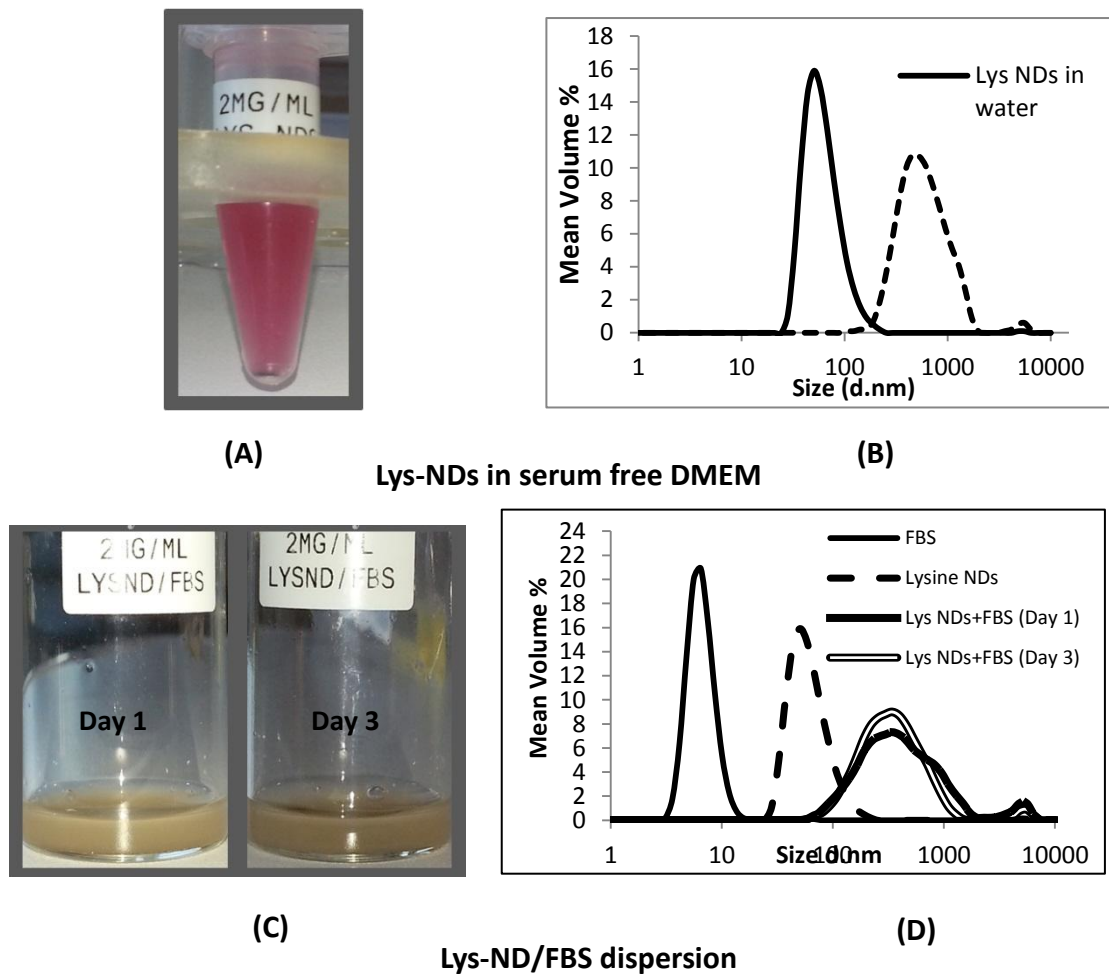


Figure 5.2 Interaction of lys-NDs with serum free DMEM and with FBS. Dispersions of (A) Lys-NDs in serum free DMEM showing sedimentation within 24 hours due to reduced dispersibility (B) Size distribution curve for lys-NDs in serum free DMEM compared to the

aqueous dispersion. (YTZ grinding media was added at 1:1 ratio in the DMEM dispersion) (C) Lys-NDs/FBS dispersion at different time points showing no sedimentation up to 3 days suggesting uniform dispersibility over time; (D) Size distribution curves for lys-NDs after serum incubation: FBS alone, lys-NDs alone, lys-ND/FBS on day 1 and lys-NDs/FBS on day

2. Each curve is derived from an average of 6 distributions with 10 individual scans

Time Point	Zeta Potential (mV)*
Lys-NDs in serum free DMEM	
Day 1	-2.2 ± 2.6
Lys-NDs after incubation with FBS	
FBS alone (Day 1)	-8.0 ± 0.8
Lys-NDs alone (Day 1)	+26.3 ± 0.3
Lys-NDs/ FBS (Day 1)	-12.4 ± 0.1
Lys-NDs/ FBS (Day 3)	0.3 ± 2.1

Table 5.2 Zeta potential of lys-NDs in serum free DMEM and after serum incubation

*Each zeta potential measurement indicates mean of six measurements with 100 individual runs.

To measure the extent of protein adsorption, the thickness of the protein adsorption layer (T_{protein}) was calculated. This calculation was based on the assumption that formation of a protein corona around NDs resembles a classical ligand binding model, and thus follows the law of mass action.²³⁷ Accordingly, the affinity of protein for NDs can be defined by the dissociation constant (K_D), corresponding to the concentration at which half of the NDs are saturated with proteins at equilibrium.²³⁷ T_{protein} with FBS was 157 nm immediately after incubation of lys-NDs with serum, which correlates with multiple layers of proteins and other biomolecules on the ND surface. A negligible decrease in the thickness of the adsorption layer to 155 nm and significant increase in zeta potential towards positive value of 0.3 ± 2.1 mV (Table 5.2) in three days indicates the occurrence of a continuous adsorption and desorption of proteins (Vroman effect).¹⁸⁸ These results suggest that the identities of adsorbed proteins may change over time but the total amount remains roughly constant. Neutral zeta potential after 3 days can also be the result of electrostatic interactions between protein coated and bare lys-ND particles resulting in the formation of coagulated masses with reduced electrophoretic mobility.²³⁸ While the particle size

increased significantly in the presence of serum, the lack of sedimentation in the 3 days of the testing period renders these dispersions pharmaceutically acceptable.

5.4.3 Cellular Internalization of lys-NDs

Cellular uptake of lys-NDs was studied by using three complimentary techniques providing a combination of spectroscopic, microscopic and light scattering principles. Soft X-rays offered microscopic imaging with detailed spectral sensitivity, by allowing microspectroscopy to record the cellular spectra from identified spots on the image. Further indication of ND internalization in the cells was obtained using flow cytometry which utilized light scattering patterns to differentiate the cells before and after ND uptake. Finally, laser confocal scanning microscopy was used to confirm the presence of lys-NDs in the cells by utilizing their innate fluorescence property.

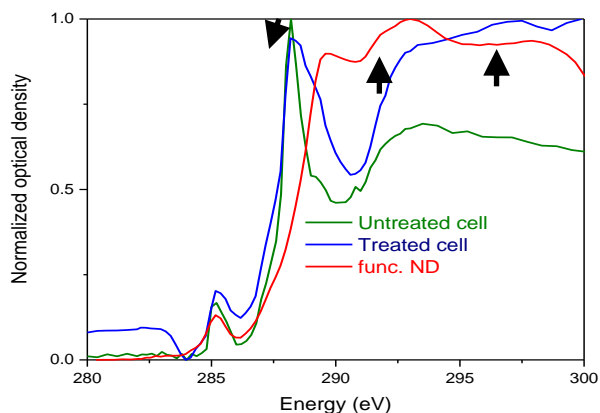
5.4.3.1 Scanning Transmission X-ray Microscopy

In order to identify NDs in a biological environment a unique spectrum, different from cellular macromolecules (mainly proteins and lipids) is sought. Soft X-ray spectroscopy of the cells incubated with lys-NDs was carried out by scanning transmission X-ray microscopy (STXM). This technique provides many advantages over conventional techniques used for characterizing NPs and investigating their cellular interaction. It allows high resolution imaging which enables evaluation of interactions on the level of individual particles.^{239, 240, 241} Most importantly, it can be applied to fully hydrated biological materials, which allows functional analysis of molecular mechanisms in a living cell under native biological conditions.²⁴² Soft X-rays also provide spatial resolution of around 50 nm²⁴³ and spectral resolution on the order of 100 MeV,^{244, 245} that can differentiate between classes of biomolecules and can identify NPs as therapeutic carriers in cells and tissues.²⁴⁰

The spectrum of lys-NDs (red) (Figure 5.3A) recorded as a reference, shows identifiable peaks at 288.2 eV, 292.5 eV and 297.5 eV, indicated by arrows, which are absent in the spectrum of intracellular proteins (green) (Figure 5.3A) obtained from the untreated cells. For detailed evaluation, untreated cells and lys-ND treated cells were scanned separately through STXM at wide range of photon energies. Spectra from the identifiable regions in the cells were recorded (Figures 5.3B and E). In untreated cells (Figure 5.3C), the green spectrum showed absorption at

peaks 285 and 287.5 eV and hence was assigned to proteins.²⁴⁵ The red spectrum also indicated absorption peaks at the same x-ray energies but with relatively lower intensities, and therefore was assigned to proteins from the cellular growth media (DMEM) surrounding the cell. The blue spectrum can be assigned to nucleus-and near-nucleus-derived mixture of macromolecules.

The lys-ND treated cells (Figure 5.3F), scanned at the same x-ray energy also indicate absorption spectra of non-protein macromolecules (blue), intracellular (green) and growth medium-derived proteins (red). However, the red spectrum exhibit weak features of absorption at 288.2, 292.5 and 297.5 eV corresponding to the specific lys-ND signals as indicated by black arrows separately in Figure 5.3A. Clear lys-ND signals are masked and appeared weak due to the interference of the overlapped intracellular and growth medium derived proteins on lys-ND surface. Unlike for untreated cells (Figure 5.3D), color composite image of lys-ND treated cells indicate localization of NDs (red) overlapped with proteins mostly around cellular edges and cytoplasm, with some being in close proximity to the nucleus (Figure 5.3G), indicated by arrows. While these 2D images in STXM show the cellular uptake of lys-NDs, future work is planned to use the high resolution capability of STXM (30 nm) combined with 3D imaging for a more precise localization of the lys-ND particles within the cells.



(A)

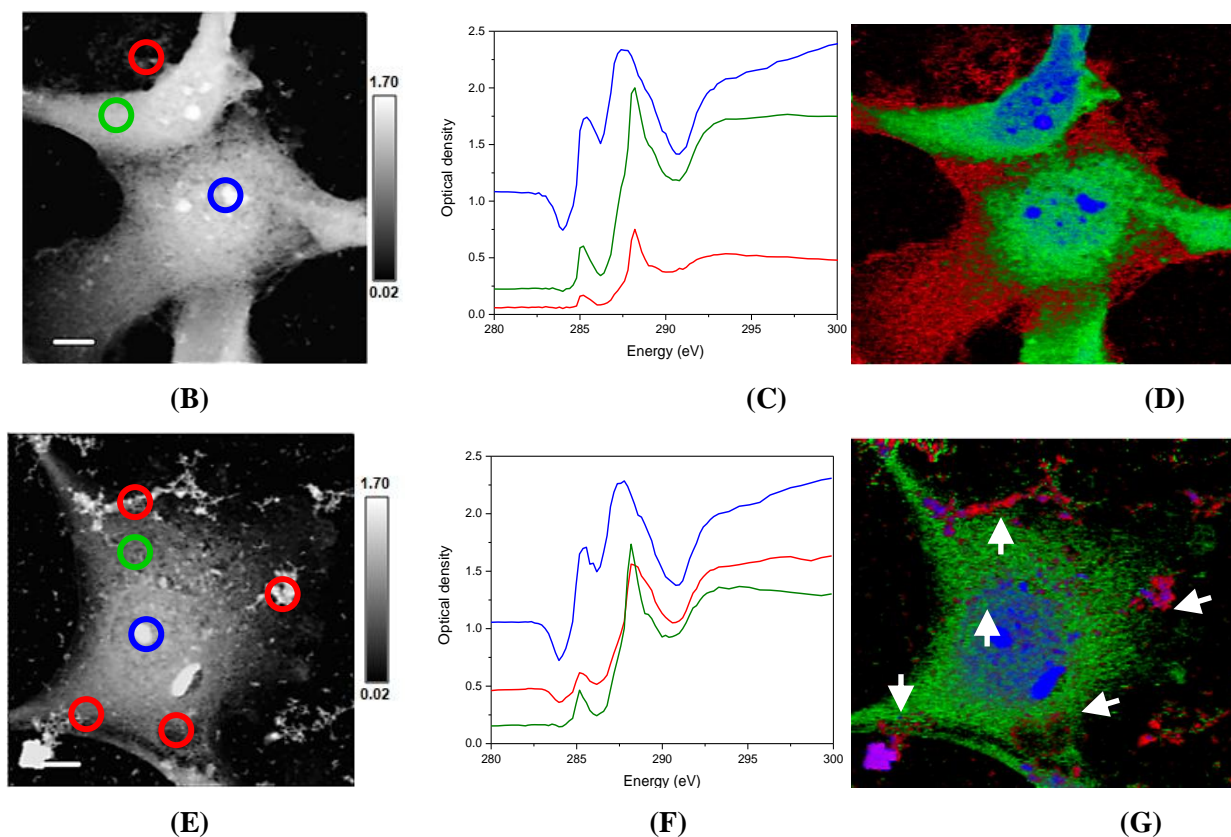


Figure 5.3 SXTM images and spectra for lys-ND internalization. (A) Comparison of intracellular protein spectra of lys-ND treated cells (blue) and untreated cells (green) with the reference spectrum of lys-NDs (red). The arrows indicate the ND derived features in the treated cells in comparison with the reference lys-ND spectrum. STXM image of (B) untreated cells and (E) lys-ND treated cells taken as an average of stack images from 280-295 eV along with their absorption spectra (untreated cells (C) and lys-ND treated cells (F)). Images (D) and (G) indicate color composite maps of macromolecular and ND distribution in untreated and lys-ND treated cells respectively.

5.4.3.2 Flow Cytometry

Flow cytometry was used to assess the molecular and morphological changes in the cells when treated with lys-NDs. Changes in forward and side scattering patterns were recorded to encounter the internalization of lys-NDs in cells. Side scattering, i.e. the light scattering measured at 90° angle, increases with an increase in granularity and internal complexity of the cell, thus the uptake of NPs can be detected by monitoring this scattering intensity.²⁴⁶ A dose dependent increase was observed in side scattering resulting after administration of lys-NDs to the cells

(Figure 5.4). The untreated cells exhibit the least side scattering (Figure 5.4A) and showed a tightly condensed population (Supplementary Figure 5S.7A). However, after treatment with lys-ND, the cell populations became increasingly dispersed (Supplementary Figure 5S.7B to 5S.7D) and exhibited an increase in side scattering with concentration ranging from 25 $\mu\text{g/mL}$ to 250 $\mu\text{g/mL}$ (Figure 5.4A). This dose dependent increase in side scattering can be correlated with an increase in the internal complexity and light scattering moieties inside the cells.²⁴⁶ NDs are efficient light scattering moieties, since they possess high refractive index ($n= 2.42$) owing to their diamond core.^{247, 248} Due to the high refractive index, the elastically scattered light from a ND particle is estimated to be 300-fold brighter than a same sized cell organelle.²⁴⁸ In addition to increased light scattering, there can be an increased activation of lysosomes for trapping the internalized ND particles,²⁴⁹ which also contributes toward side scattering.²⁵⁰

While there is a change in the side scattering, the forward scattering (indicative of the size of the cell) remained unchanged before and after the treatment (Figure 5.4B), suggesting that the NDs are internalized into the cells and not adhered to the surface. Forward scattering of light based on refraction is directly proportional to the cell size and surface area, thus a larger surface area is associated with more forward scattering.²⁵¹ We inferred that if NPs are adhered to the surface of the cell it would increase the overall surface area and can contribute towards the refraction of light. However, the cells treated with all concentrations of NDs show similar refraction patterns to the untreated cells (Figure 5.4B). There were no significant positive shifts in forward scattering which indicate absence of surface adhered ND particles. Although this finding cannot be attributed to an absolute absence of surface adhesion, it indicates that there is no significant surface localization of NDs. The combination of the above two parameters corresponds to a dose dependent cellular uptake of lys-NDs.

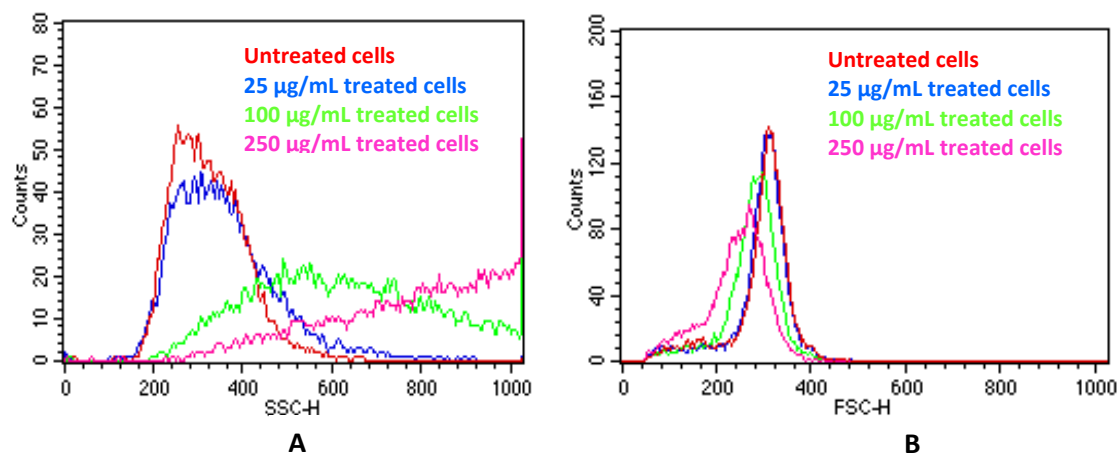


Figure 5.4 Flow cytometry histograms showing concentration dependent uptake of lys-NDs through forward and side scattering. Histograms indicating side scattering (A) of untreated cells (red) and lys-ND treated cells at concentrations of 25 µg/mL (blue), 100 µg/mL (green) and 250 µg/mL (pink) showed a significant dose dependent increase. Histograms indicating forward scattering (B) of untreated cells (red) and lys-ND treated cells at concentrations of 25 µg/mL (blue), 100 µg/mL (green) and 250 µg/mL (pink) shows no significant difference. The horizontal axis represents side scattering (A) and forward scattering (B) signal value in channel numbers and the vertical axis represents the number of events per channel. Events observed are lined into a channel of its corresponding signal value. Brighter the signals displayed in the channel, higher would be the rightward shift.

5.4.3.3 Laser Confocal Scanning Microscopy

To further confirm the cellular uptake of lys-NDs, laser scanning confocal microscopy was carried out. The fluorescence (Figure 5.5A), brightfield (Figure 5.5B) and overlay of brightfield and fluorescence (Figure 5.5C) images of the top, middle and bottom z-positions (corresponding to the 44th, 22nd and 1st section, respectively) of a lys-ND treated cell are shown. An overlay of brightfield and fluorescence images of the middle slice of lys-ND treated live cells revealed internalization of a few ND particles, as marked by the red circle (Figure 5.5C, middle). These particles appear to be localized near the nucleus of the cell. However the fluorescence of these particles in the middle z-section was not distinctly identified due to the interference originating from cellular auto-fluorescence. Upon longer exposure time, the auto-fluorescence of the cells was quenched and the fluorescence (Figure 5.6A) and brightfield images (Figure 5.6B) of four consecutive slices when overlaid revealed more distinct ND fluorescence emission (Figure 5.6C).

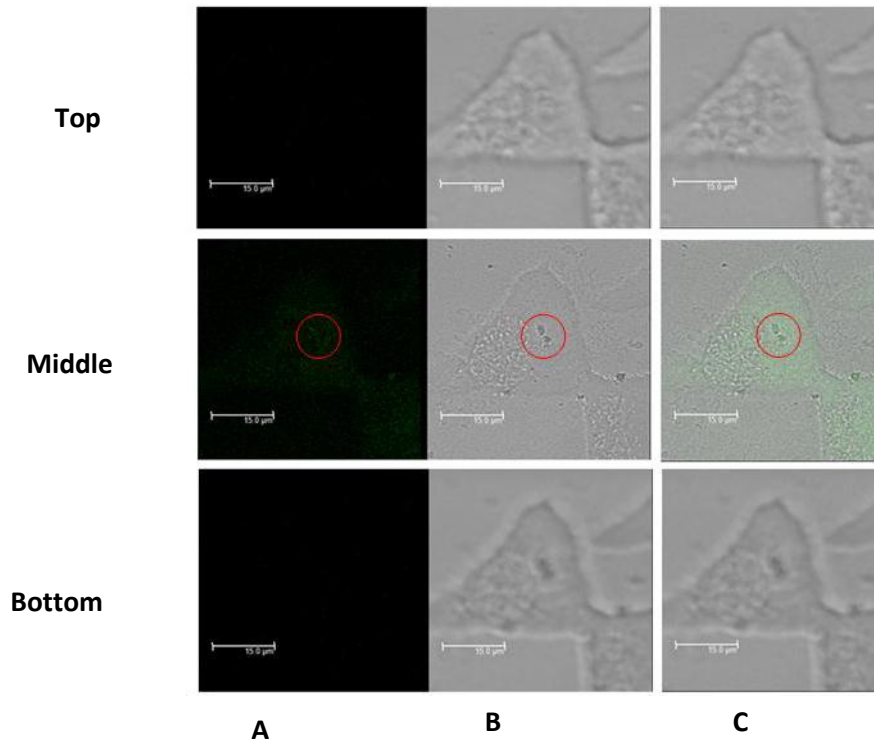


Figure 5.5 Laser scanning confocal microscopic images of the live cell treated with lys-NDs for 24 hours. From left to right- (A) fluorescence images, (B) bright field images and (C) overlay of fluorescence and bright field images. Excitation was performed using a 476 nm wavelength laser source and emission was collected from 492 to 677 nm wavelengths. A total of 44 slices were imaged with 0.38 μm intervals.

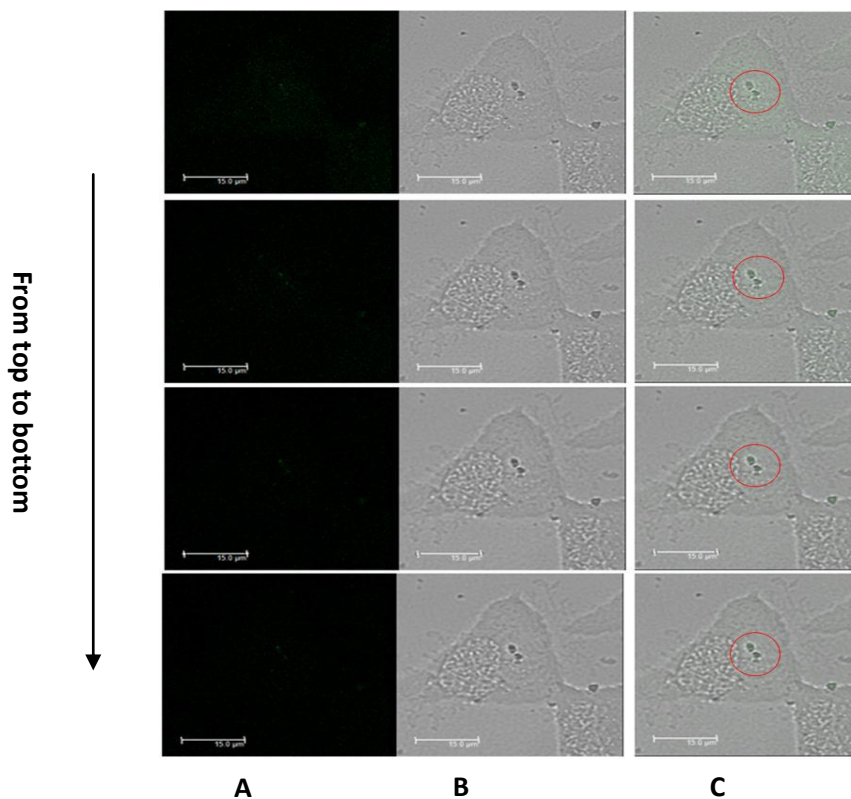


Figure 5.6 Laser scanning confocal microscopic images of four consecutive sections from the middle towards the bottom of the cell treated with lys-NDs. From left to right; (A) fluorescence images, (B) bright field images and (C) overlay of fluorescence and bright field images. From top to bottom; sections 21, 20, 19 and 18 (intervals of 0.38 μm). Excitation was performed using 476 nm wavelength laser source and emission was collected from 492 to 677 nm wavelengths.

5.4.4 Cellular Internalization of lys-NDs as diamplexes

Previously, we reported that lys-NDs can bind to siRNA.¹³⁴ This fact was implemented to enhance the investigation of lys-NDs suitability for gene delivery as described here. Although detonation NDs show a slight innate fluorescence as observed during the confocal microscopy, but this fluorescence is not sufficiently intense for detection during flow cytometry. Therefore, lys-NDs were complexed with FITC labelled siRNA to provide an intense fluorescence for probing these diamplexes inside the cells. After treating the cells with these diamplexes, the presence of FITC fluorescence from siRNA was correlated with cellular association of lys-NDs/siRNA diamplexes.

Cells treated with diamoplexes prepared from lys-NDs dispersed in serum free DMEM showed no positive shift for FITC fluorescence (Supplementary Figure 5S.1), attributed to the poor binding of lys-NDs with siRNA secondary to their unstable charge distribution in DMEM. Cells treated with diamoplexes prepared from aqueous dispersion of lys- NDs showed a statistically significant positive shift in FITC fluorescence of $14 \pm 2.1\%$ compared to the untreated cells ($5 \pm 0.2\%$) (Figure 5.7) (Supplementary Figure 5S.2). The positive fluorescence shift indicates successful internalization of the labelled siRNA. Addition of serum to the formulation enhanced the FITC fluorescence shift to $20 \pm 2.3\%$ (Figure 5.7) (Supplementary Figure 5S.3). This increase in fluorescence is an indicative that protein corona facilitates the cellular uptake of diamoplexes.

In order to confirm that primary amine-rich cationic surfaces created through functionalization of NDs facilitates electrostatic binding with negatively charged siRNA; diamoplexes were also prepared with carboxylated red fluorescent nanodiamonds (COOH-FNDs). Here, the NDs used were additionally treated to induce brighter fluorescence capable of detection in flow cytometry. The cells treated with these diamoplexes showed no significant positive shift for FITC fluorescence (Figure 5.7) (Supplementary Figure 5S.4) revealing that the COOH-FNDs are unable to carry nucleic acids inside the cells due to the negative surface charge. However, interestingly they show cellular internalization independent of siRNA carriage, as observed through the positive shift obtained for the treated cells in the wavelength region exclusive to the fluorescence of NDs (550-800 nm). (Supplementary Figure 5S.5 and 5S.6).

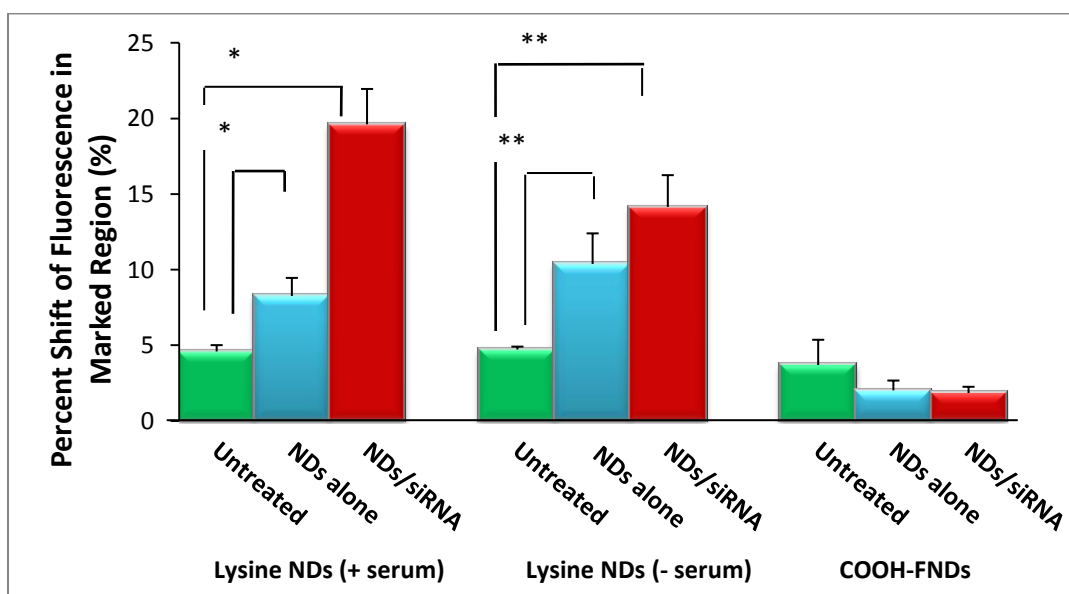


Figure 5.7 Percent fluorescence shift in flow cytometry for cells treated with lys-NDs/COOH-FNDs alone (blue) & diamoplexes of lys-ND or COOH-FNDs with FITC labelled siRNA (40:1) (red) compared to untreated cells (green) in the wavelength range of FITC (emission maximum 525 nm). The three treatment groups are: 1) lysine-ND in the presence of serum 2) lysine-ND in the absence of serum and 3) COOH-FNDs. Each group further comprise of treatments with ND alone, diamoplexes and their subsequent controls. Each bar represents mean \pm S.D. of three measurements.

*One way ANOVA; Tukeys post hoc for multiple comparison; $p < 0.05$ & **Kruskal Wallis ANOVA; Mann Whitney U test for comparison; $p < 0.05$

The efficacy of each siRNA delivery method was quantitatively analyzed by comparing the fraction of fluorescence shift caused exclusively due to siRNA independent of the weak interference from ND fluorescence. The fraction of FITC fluorescence is considered directly proportional to the amount of labelled siRNA delivered to the cells. Only 0.15 fraction of siRNA fluorescence was observed when the cells were treated with 75 pmoles of naked siRNA. The fraction of siRNA fluorescence increased significantly, to 2.7 folds (0.4 ± 0.01) (Figure 5.8) when the same amount of siRNA was delivered in conjugation with lys-NDs at a ratio of 40:1. This illustrates the ability of the lys-NDs to perform intracellular delivery of nucleic acids.

Moreover, the fraction of siRNA fluorescence was 1.8 times (0.7 ± 0.05) greater in the presence of serum (Figure 5.8) compared to the serum-free environment, which might indicate that proteins can protect the integrity of diamoplexes and facilitate their cellular uptake.

Despite previous reports indicating an inhibitory effect of serum on cellular uptake of nanoparticle-gene complexes,^{252, 253} we observed that serum proteins can cause increased cellular uptake of diamoplexes. Protein adsorption on NP surface can alter the particle size and the overall surface charge of the system. Therefore, the serum-induced increase in cellular uptake of diamoplexes can be attributed to multiple factors. Lys-NDs have a cationic surface due to the presence of primary amines, which may result in favourable interaction with the negatively charged albumin, the main component of the serum. This interaction could impede the electrostatic interaction between lys-NDs in the diamoplexes and the phospholipids of the cell membrane. Therefore, the change in surface charge does not explain the increase in cellular uptake.

It was also determined that the size of the diamoplexes increased significantly due to protein adsorption. The adsorbed proteins increased the hydrodynamic radius of the NPs. There are previous studies indicating that protein adsorption increases the overall cellular uptake of hard NPs like polystyrene.²⁵⁴ It is speculated that the serum-induced increase in the particle size of diamoplexes can switch the most prominent clathrin mediated endocytosis of NDs to claveoli mediated endocytosis,²⁵⁵ which is responsible for the uptake of complexes sized around 500 nm or above.^{256, 257} Moreover albumin, the main component of FBS, can also facilitate cellular uptake of diamoplexes.^{258, 259} Upon incorporation it can act as a ligand that binds to the albumin-binding protein on the claveolar plasma membrane to induce more affinity for claveoli or lipid raft mediated endocytosis of diamoplexes.^{182, 260, 261} Moreover, the bio-reactivity of the surface due to the adsorption of physiologically active proteins like albumin on the surface can also serve to facilitate specific receptor mediated endocytosis. Unfolding of the adsorbed proteins resulting in a specific conformation can induce differential binding to target receptors on the cell surface.^{262, 263} Although the optimum size for cellular uptake is defined to be 20-40 nm,¹⁸² the altered endocytic pathway might facilitate cellular association of larger sized protein-coated diamoplexes by altered pathways, thus increasing the intracellular amount of FITC labelled siRNA. Detailed mechanistic analysis will be conducted to understand this altered cellular uptake behavior of diamoplexes.

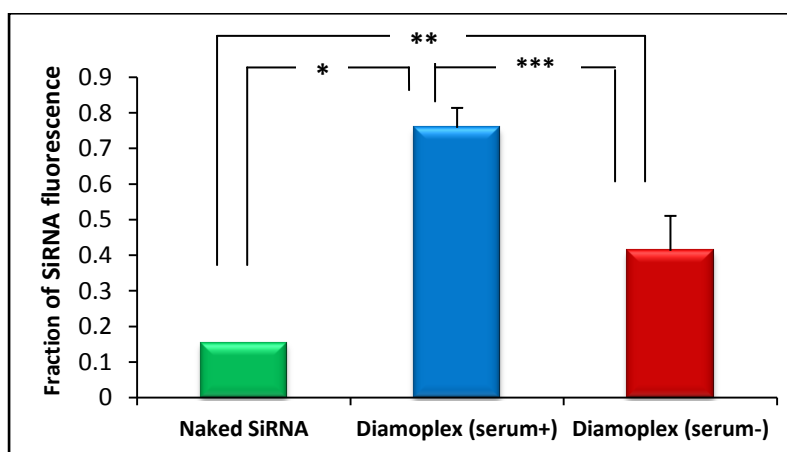


Figure 5.8 Fraction of fluorescence shift from FITC labelled siRNA when administered directly or as diamoplexes with lys-NDs at a ratio of 40:1 (in presence and absence of serum proteins). Each bar (except naked SiRNA) represents mean \pm S.D. of three measurements.

ANOVA (p-value \leq 0.05), Tukey's post hoc multiple comparisons (*p-value $<$ 0.001, **p-value=0.007, *p-value=0.002)**

5.5 Conclusion

In this study, we demonstrated that aqueous dispersion of lys-NDs exhibit excellent dispersibility and preservation of their physicochemical properties for at least 25 days. Unlike in aqueous medium, the stability of lys-NDs is significantly compromised in physiological growth media, which in turn diminishes their siRNA binding capacity and cellular uptake. Lys-NDs interact with serum to form a protein shell around the core. This protein corona stabilizes ND/siRNA complexes and facilitates the process of cellular uptake. The increased cellular uptake in the presence of serum proteins is a promising finding, rendering the lys-ND diamplexes amenable for parenteral administration for gene therapy. Successful cellular uptake of lys-NDs, alone, and as stable complexes with siRNA encourages further investigations to evaluate their transfection efficiency and biocompatibility as gene carriers for RNAi therapeutics.

5.6 Methodology

5.6.1 Materials

Pharmaceutical-grade (ND98) carboxylic acid-functionalized NDs with an average particle size of 5 nm were purchased from Dynalene Inc. (Whitehall, PA). Lysine functionalized NDs (lys-NDs) were synthesized in house following the procedure previously described.¹³⁴ Carboxylated fluorescent NDs (COOH-FNDs) were obtained from Adamas Nanotechnologies (Raleigh, NC). Tosoh Corporation (Grove City, OH) graciously provided YTZ® (Yttrium Stabilized Zirconia) grinding media (0.05 mm). Methylcellulose USP (4000 mPa.s) was obtained from Medisca (Richmond, BC). 0.5% Methylcellulose gel was prepared in deionized distilled water obtained from a Milli-Q Integral Water Purification System, EMD Millipore (Billerica, MA). HyClone® HyPure Molecular Biology Grade Water, HyClone™ 1x Phosphate Buffered Saline (1xPBS) and HyClone™ Dulbecco's Modified Eagle's medium (DMEM)/High; glucose with L-glutamine and sodium pyruvate was obtained from ThermoFisher Scientific (Waltham, MA). Fetal bovine serum (FBS) was acquired from Gibco (ON, Canada). HeLa cells (human cervical cancer cells) were obtained from American Type Culture Collection (VA, United States). Trypsin and

antibiotics were obtained from Sigma Aldrich (ON, Canada). Anti-GFP siRNA was purchased from Ambion (ON, Canada). Fluorescein isothiocyanate (FITC) conjugated control siRNA was purchased from Santa Cruz Biotechnology Inc (CA, United States). Cell culture flasks and plates, centrifuge tubes and cell strainer tubes were purchased from Falcon BD (ON, Canada).

5.6.2 Preparation of primary ND dispersions

Primary dispersions of lys-NDs were prepared in purified deionized water, PBS, 0.5% methylcellulose gel and serum free DMEM separately. Primary dispersion of COOH-FNDs was prepared in purified deionized water. All dispersions were prepared at a concentration of 2 mg/mL. YTZ grinding media was added in all dispersions at a ratio of 1:1. All primary dispersions were subjected to ultrasonication for 4 hours at a frequency of 25 kHz without heating. The ultrasonicated dispersions were then centrifuged at 5200 g for 5 minute to sediment the YTZ grinding media and the aggregated ND particulates. The resulting dispersions were used in the subsequent experiments.

5.6.3 Selection of the most compatible dispersion medium

In order to select the best medium to disperse lys-NDs for subsequent physicochemical analysis and cellular experiments, primary dispersions of lys-NDs in purified deionized water, PBS and 0.5% methylcellulose solution and serum free DMEM were allowed to stand for 72 hours at room temperature without any additional ultrasonication and centrifugation. Images were obtained at 24 and 72 hours to compare the degree of sedimentation for lys-NDs in different media.

5.6.4 Particle size and zeta potential measurements

Particle size distribution and zeta potential measurements were performed over a period of 25 days by using Malvern Zetasizer Nano ZS instrument (Malvern Instruments Ltd, Worcestershire, UK). Values for water properties used for measurement were as follows: refractive index = 1.330, dielectric constant = 78.5 and viscosity at 25°C = 0.8872 cP. Solvent properties were changed for DMEM as hydrodynamic viscosity $\eta = 3$ cP, refractive index = 1.345²⁶⁴ and dielectric constant = 80.

Particle size was measured as a function of the light scattered by individual diamond particles at an angle of $\theta = 173^\circ$, which allowed the calculation of translational diffusion coefficients ‘D’ of particles by applying the CONTIN algorithm. The hydrodynamic radius R_H of lys-NDs was then calculated using the Stokes-Einstein equation ($R_H = kT/6\pi\eta D$), where k = Boltzman constant, T is the temperature (298K), and η is the viscosity of water at 25°C. All size distributions were derived from 6 measurements with 10 individual scans. Particle size distributions for all time points were plotted as mean volume % to compare the degree of aggregation that occurred over the period of analysis. Polydispersity indices (PDI) were also calculated by cumulant fitting. Zeta potential measurements were based on Laser Doppler Electrophoresis and values reported are an average of 6 measurements with 100 individual scans.

5.6.5 Interaction of lys-NDs with serum proteins

Aqueous dispersion of lys-NDs at a concentration of 2 mg/ 500 μ L concentration was prepared as mentioned above. After ultrasonication and centrifugation, 500 μ L of FBS dispersion was added and allowed to stand at room temperature for 45 minutes to allow the formation of protein adsorption layer around the ND particles. The dispersion of lys-ND/FBS was then lyophilized for 3 days to obtain complete desiccation. The powder obtained was then dispersed in purified water by gentle shaking at a final concentration of 2 mg/mL. Aggregation of the dispersion was monitored visually at 24 and 72 hours. Changes in particle size and electrokinetic charge distribution resulting from interaction of lys-NDs with FBS were analysed similarly as above over a period of 3 days. Zeta potentials were recorded as a function of time to monitor the formation and stipulate the stability of the protein corona. The average particle diameter obtained from volume weighted size distributions was used to calculate the approximate thickness of the protein adsorption layer (T_{protein}) by equation 1:

$$T_{\text{protein}} = \frac{\text{diameter of protein coated lysND particle} - \text{diameter of uncoated innate lysND particle}}{2} \dots \text{(Eq 5.1)}$$

Since the lys-ND/FBS system shows polymodal distribution (PDI: 0.265), the Z-average calculated by the instrument’s cumulants technique might cause an overestimation of average particle diameter, even in the presence of minimum core aggregates. In order to minimize the erroneous estimation of T_{protein} , average particle diameter was calculated before and after protein adsorption using the mean volume % obtained by size distribution data.

5.6.6 Cell Culture

Frozen HeLa cells were grown in DMEM (containing L-glutamine and sodium pyruvate) supplemented with 10% (v/v) FBS and 1% (v/v) antibiotic. The cells were incubated at 37 °C and 5% CO₂ and allowed to grow up to 90% confluency. When the cells were confluent, they were sub passaged to allow the growth of healthy population. The sub-passaged cells were then seeded in well plates for subsequent cellular experiments.

5.6.7 Scanning Transmission X-Ray Microscopy (STXM)

Cell samples used to obtain STXM were prepared on silicon nitride windows. Optical images of the cells plated on membranes are shown in supplementary information Figure S5.8. HeLa cells were seeded and treated with lys-NDs at an amount equalizing 40:1 diamoplex ratio, i.e. 41.5 µg/well. The treated cells were resuspended in 2.5 mL of serum supplemented media and added to the silicon nitride windows in a 6 well plate. The cells were incubated for 24 hours at 37 °C and 5% CO₂ again to allow cellular attachment to the silicon nitride (Si₃Ni₄) windows (size 1x1 mm, thickness 100 nm). The membranes were mounted on the STXM sample holder and imaged using STXM at the soft x-ray spectromicroscopy beam line of the Canadian Light Source (CLS) (University of Saskatchewan, Saskatoon, SK, Canada). Both control and lys-ND treated cells were adjusted to the same optical density and scanned at x-ray energies of 280 to 295 eV of C-1 edge and absorbance spectra from different identifiable regions on the sample were collected. Changes in the absorbance spectra obtained from the cells as a result of ND uptake were recorded.

5.6.8 Flow cytometry for lys-NDs

HeLa cells were plated on a 6 well plate at a density of 2×10^5 cells/ well and incubated at 37 °C and 5% CO₂ to allow attachment. Thereafter, the cells were treated with lys-NDs at a concentration of 25 µg/mL, 100 µg/mL and 250 µg/mL. Untreated cells were used as controls. The treatments were terminated after 20 hours followed by washing with 1xPBS three times for 5 minutes each. The cells were then harvested using trypsin and 0.25% EDTA and centrifuged at 95 g and 4 °C for 5 minutes to obtain cell pellets. The individual cell pellets were resuspended in 500 µL of 1xPBS, transferred into 5mL flow cytometer tubes and the amounts of ND particles taken up by the cells were analyzed using BD FACS Calibur™ (BD Biosciences, CA, USA). The

laser beam (488 nm) illuminates cells in the sample stream. It is then scattered by the cells at narrow angles to the axis of the laser beam is called forward scattering (FS) and at about a 90° angle to the axis of the laser beam called side scattering (SC). The intensities of FS and SS are proportional to the size and intracellular complexity, respectively.

5.6.9 Laser scanning confocal microscopy

To evaluate whether lys-NDs can be detected in the cells based upon their intrinsic fluorescence, laser scanning confocal microscopy was performed. HeLa cells seeded at the density of 40,000 cells per well were allowed to adhere to coverslip placed in 12 well plate, for 24 hours. The cell media were replaced with 1 mL of lys-NDs dispersion prepared at a concentration of 50 µg/mL. After 6 hours, FBS was added to the media of the cells at a final concentration of 10% (w/v). The cells were incubated for a total of 24 hours and then washed three times with PBS (5 minutes each). Slides of the live cells were prepared and imaged with a Leica TCS SP5 laser scanning confocal microscope (Leica Microsystems Inc., Bensheim, Germany; WCVL, University of Saskatchewan, Saskatoon, Canada) using a 63X oil immersion objective. The sample excitation was carried out with a 476 nm argon laser source and the emission was collected from 492 to 677 nm. A total of 44 z-sections of cells were imaged, each with a step size of 0.38 µm.

5.6.10 Flow cytometry for lys-ND/siRNA diamoplexes

Flow cytometry was used again to evaluate the cellular association of lys-NDs as diamoplexes by complexing them with FITC labelled control siRNA. HeLa cells were seeded and plated similarly as above. FITC labelled siRNA was complexed with lys-NDs dispersed in aqueous and DMEM at different weight ratios of siRNA to lys-NDs ranging from 1:20 to 1:50 by incubating the dispersion with siRNA for 30 minutes at room temperature. The attached cells were then treated with lys-ND/siRNA diamoplexes diluted in serum supplemented or serum free DMEM. The final concentration of siRNA in each well was 75 pmoles. Untreated cells and lys-NDs treated cells were used as controls. The treatments were terminated after 24 hours followed by washing, harvesting and resuspending as described above. FITC fluorescence was measured using BD FACS Calibur™ (BD Biosciences, CA, USA). Fluorescence from FITC siRNA was recorded using FL1-H band pass filter (530/30 BP) by plotting log of fluorescence intensity versus number of events. Healthy cell population was gated and a total of 10,000 events were recorded in the

gated region per sample. The data was analyzed using BD CellQuest™ Pro software (version 6.0). Relative fluorescence shift (from negative to positive) for diamoplex treated cells were compared to the auto fluorescence of the untreated cells and fluorescence from lys-NDs treated cells through the marker (M1). This marker was applied to quantify the positive shifts resulting from the treatments.

Fraction of FITC siRNA fluorescence was calculated using % fluorescence shifts as follows:

$$\text{Fraction of siRNA fluorescence} = 1 - \left[\frac{(\text{LysND treated cells} - \text{Untreated cells})}{(\text{Diamoplex treated cells} - \text{Untreated cells})} \right] \dots\dots\dots (\text{Eq 5.2})$$

Flow cytometry was also used to analyze cellular association of COOH-FNDs as diamoplexes with FITC siRNA. Fluorescence from COOH-FNDs was recorded using FL3-H long pass filter (670 LP), while fluorescence from FITC labelled siRNA was recorded using FL1-H BP filter.

5.6.11 Statistical Analysis

Flow cytometry results for cellular association of lys-NDs and COOH-FNDs in aqueous medium were expressed as the mean of $n=3 \pm$ S.D. One way ANOVA and Tukey's post hoc multiple comparisons were used for analysis when samples were normally distributed and had homogenous variance. Kruskal Wallis ANOVA and Mann Whitney U test for post hoc comparison were used for analysis when samples were not normally distributed or had non-homogenous variance. The significant differences were considered at $p \leq 0.05$ level of significance (α).

5.7 Acknowledgments

The authors acknowledge the Natural Sciences and Engineering Research Council of Canada (NSERC) and the University of Saskatchewan for funding this project. Saniya Alwani would also like to thank the College of Pharmacy and Nutrition, the College of Graduate Studies and Research at the University of Saskatchewan for supporting her graduate studies. The authors thank Tosoh Corporation, USA, for the kind donation of the YTZ grinding media used in these studies. The scanning transmission X-ray microscopy data described in this paper were collected at the Soft X-Ray Spectromicroscopy beamline of the Canadian Light Source (CLS), which is supported by NSERC, the National Research Council Canada (NRC), the Canadian Institutes of

Health Research (CIHR), the Province of Saskatchewan, Western Economic Diversification Canada, and the University of Saskatchewan.

5.8 Disclosure

The authors report no conflicts of interest in this work.

5.9. Supplementary Information

Table S 5.1 Particle size distribution and PDI for lys-NDs in aqueous medium on days 1, 3, 15 and 25

Aqueous dispersions of lys-NDs			
Time Point (Days)	Particle size range (nm)	Mean volume* (%)	PDI
1	33-91	89 %	0.142
	106-190	10%	
3	33-91	43%	0.180
	106-190	38%	
	220-295	13 %	
15	33-91	37%	0.126
	106-190	51%	
	220-295	11%	
25	33-91	34%	0.130
	106-190	50%	
	220-295	14%	

*Each size distribution data indicates mean of six measurements with 10 individual runs

Table S 5.2 Particle size distribution and PDI for lys-NDs in serum DMEM and after serum incubation at different time points.

Time Point	Particle size range (nm)	Mean volume* (%)	PDI
Lysine NDs in serum free DMEM			
Day 1	106-190	1.3%	0.259
	290-342	14%	
	396-615	42%	
	712-955	23%	
Lysine NDs after incubation with FBS			
FBS alone (Day 1)	4-11	98%	0.592
	14-21	1.2%	
Lys-NDs alone (Day 1)	33-91	89 %	0.142
	106-190	10%	
Lys-NDs/ FBS (Day 1)	59-91	3%	0.265
	106-190	18%	
	220-295	21%	
	342-531	33%	
	615-955	20%	
Lys-NDs/ FBS (Day 3)	59-91	2 %	0.234
	106-190	21%	
	220-295	25%	
	342-531	32%	
	615-955	16%	

*Each size distribution data indicates mean of six measurements with 10 individual runs

Figure S 5.1 Overlay of flow cytometry spectra and graphical comparison for percent fluorescence shift for untreated (black), Naked siRNA (orange), lys-ND alone (green), lys-ND/SiRNA (20:1) diamoplex (purple), lys-NDs/siRNA (40:1) diamoplex (pink) and lys-NDs/siRNA (50:1) diamoplexes (blue) treated cells.

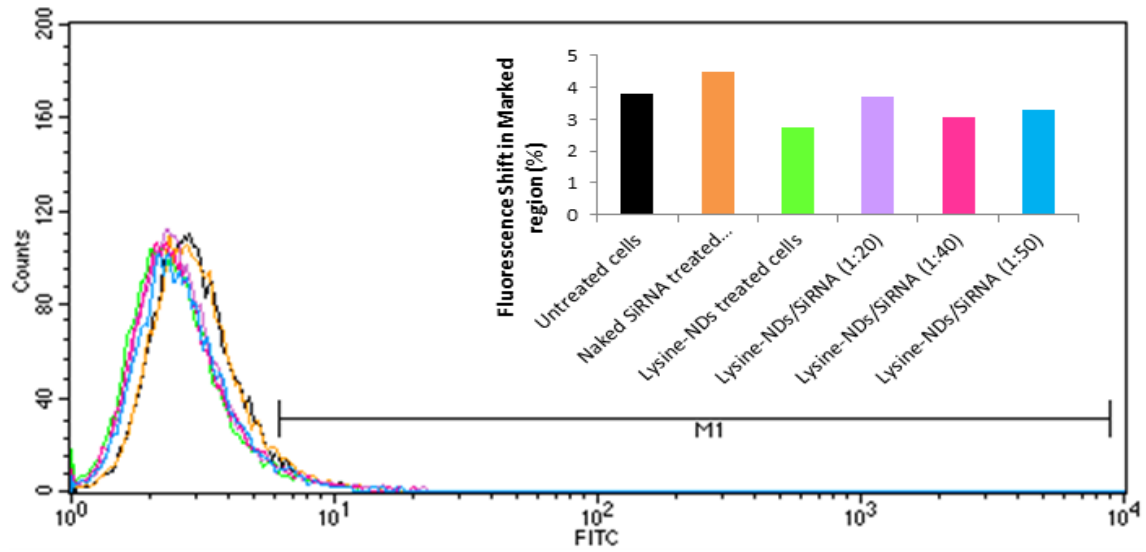


Figure S 5.2 Overlay of flow cytometry spectra for percent fluorescence shift for untreated (green), lys-NDs alone (blue) & lys-ND/FITC labelled siRNA treated cells (40:1) (red) in absence of serum.

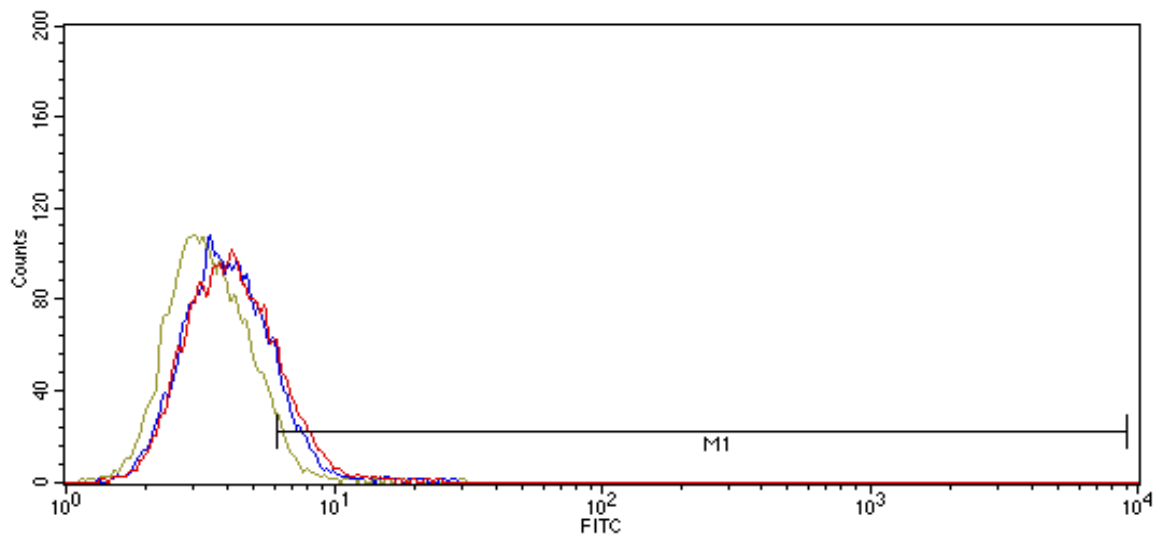


Figure S 5.3 Overlay of flow cytometry spectra for percent fluorescence shift for untreated (green), lys-NDs alone (blue) & lys-ND/FITC labelled siRNA treated cells (40:1) (red) in the presence of serum.

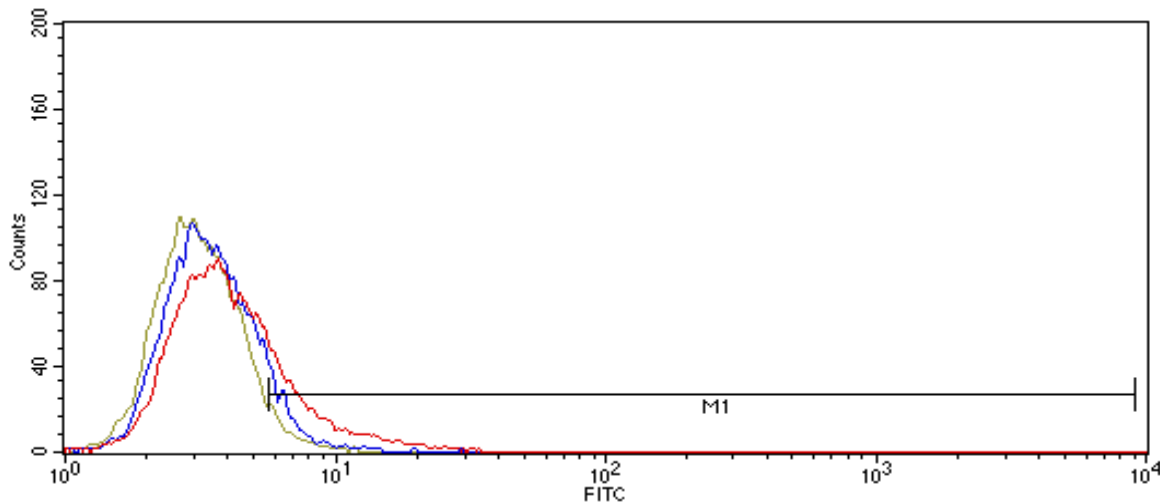


Figure S 5.4 Overlay of flow cytometry spectra for percent fluorescence shift for untreated (green), lys-NDs alone (blue) & lys-ND/FITC labelled siRNA treated cells (40:1) (red) in wavelength range of FITC.

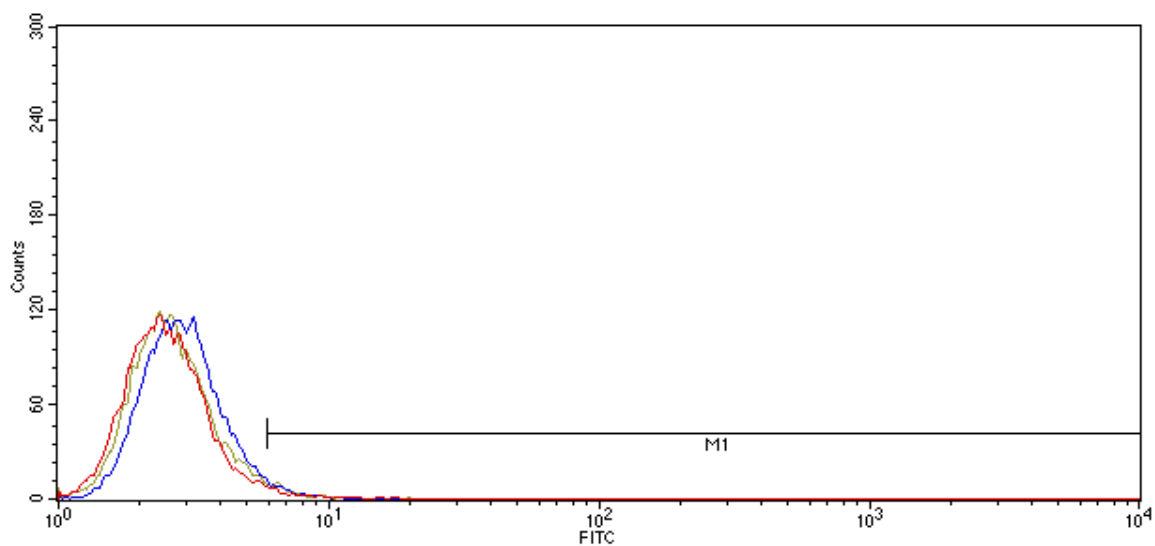


Figure S 5.5. Overlay of flow cytometry spectra for percent fluorescence shift for untreated (green), lys-NDs alone (blue) & lys-ND/FITC labelled siRNA treated cells (40:1) (red) in wavelength range of COOH-FNDs

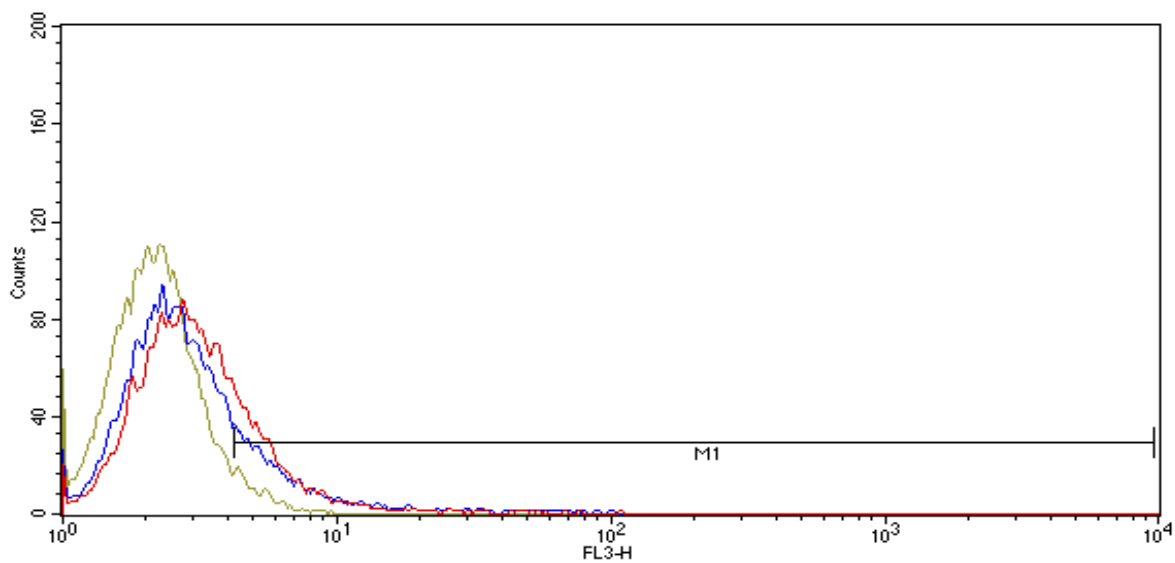


Figure S 5.6 Percent fluorescence shift for untreated (green), COOH-FNDs (blue) & COOH-FNDs/FITC labelled siRNA treated cells (40:1) (red) in wavelength range of COOH-NDs (670 LP filter)

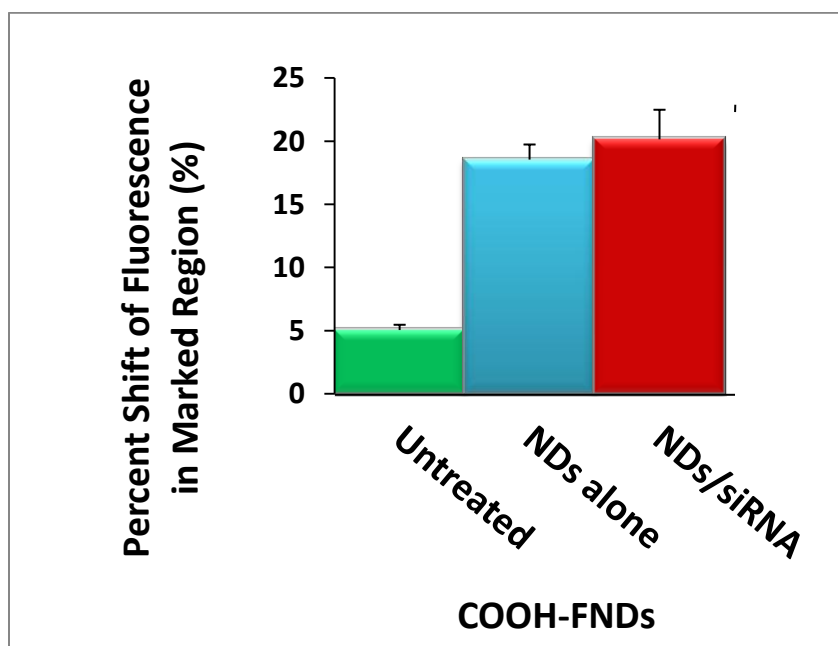


Figure S 5.7 Dose dependent cellular uptake of lys-ND particles evidenced as increasing side scattering. Untreated cells (A), cells treated with lys-NDs at concentrations of 25 $\mu\text{g/mL}$ (B), 100 $\mu\text{g/mL}$ (C) and 250 $\mu\text{g/mL}$ (D).

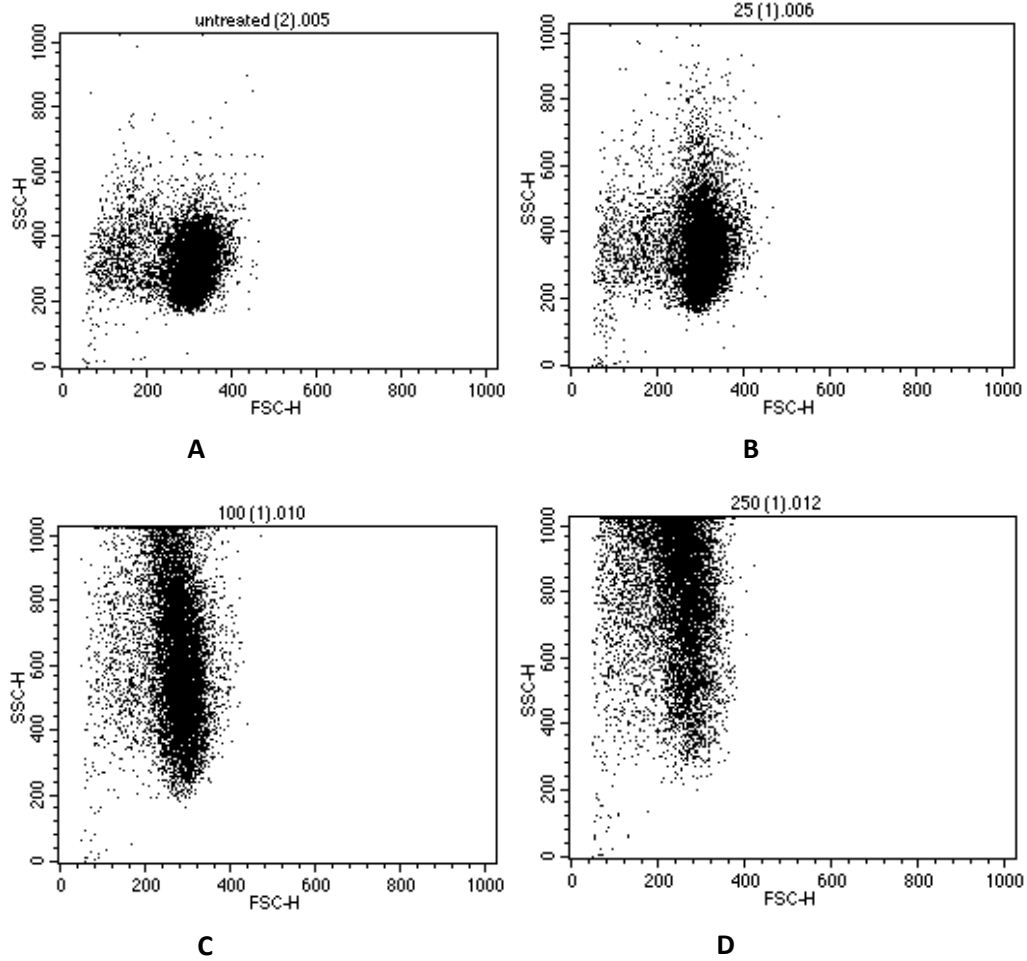
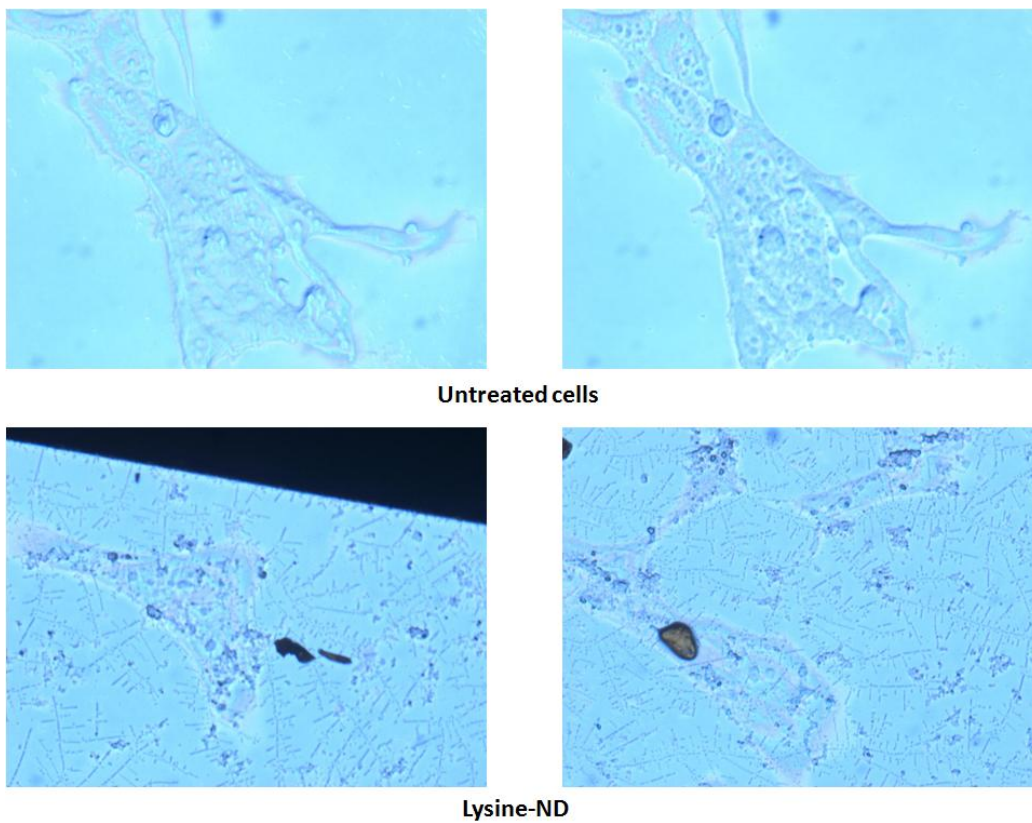


Figure S 5.8 Optical images of untreated cells, cells treated with lysine-NDs on silicon nitride windows prepared for STXM analysis



6 Lysine Functionalized Nanodiamonds as Gene Carriers: Efficacy for In Vitro Cellular Delivery and Expression of Small Interfering RNA and in vitro Toxicity Analysis

Saniya Alwani, Deborah Michel and Ildiko Badea

6.1 Author's Contributions

Saniya Alwani

- Written and edited the text of the chapter in its entirety.
- Developed the method and performed all assays under the guidance of Deborah Michel and Dr. Ildiko Badea.
- Interpreted the results of all assays performed.

Deborah Michel

- Assisted and provided guidance regarding the performance and interpretation of flow cytometry assays.

Ildiko Badea

- Supervised the entire work.
- Assisted in the revision and editing of the text in the chapter.

6.2 Abstract

Lysine functionalization of NDs presents as a novel approach to limit aggregation and to maintain long term stability of these carbon nanomaterials. The cationic surface of lysine functionalized NDs is capable of binding the nucleic acids optimally and hence shows tremendous potential as gene delivery vectors. Determination of optimum stability and cellular uptake of lys-NDs alone and as diamplexes served as a foundation to evaluate the functional efficiency and biocompatibility of this vehicle in the biological system. Flow cytometry analysis aimed at studying the efficacy of lys-NDs to deliver functionally active siRNA revealed promising results for gene delivery and expression. GFP knockdown of ~17% was recorded when the cells were treated with NDs/siRNA diamplexes at a ratio of 20:1. However, this decrease is not significant compared to the lipofectamine control (~44%) and demand further modification of the system to enhance the gene delivery efficiency. Ratios of NDs/siRNA diamplexes lower and higher than 20:1 did not show any reductions in the fluorescence. Subsequent analyses regarding the effect of NDs to prevent cellular proliferation and their effect on cellular death, namely apoptosis confirmed that they are innately biocompatible and amino acid-functionalizations do not compromise their biocompatibility.

6.3 Introduction

Non-viral vectors for gene delivery have gained much attention after the discovery of immunogenicity and oncogenicity of the viral vectors.^{265, 266, 267, 268} Among the variety of different alternatives^{269, 270} carbon nanomaterials also confer several advantages due to stability and several possibilities for functionalizations. Use of carbon nanomaterials including NDs for genetic therapy is discussed in chapter 1.

Cellular internalization of NDs both alone and as diamplexes, as described in earlier chapters, served as a promising basis to identify the system's functional capacity. Therefore, the ability of lys-NDs to deliver functionally active siRNA capable to exert biological effect was tested using GFP knockdown assay. Primary amines as carriers for siRNA have been successfully used previously by other hard nanoparticulate systems. Amine groups are induced on the surface either through artificial synthetic methods like chemical reduction of anionic gold NPs²⁷¹ or through

non-covalent attachment of biomolecular peptide like poly-L-Lysine via secondary modifications on the surface.²⁷² In contrast to these previous attempts, the mode we adopted to introduce primary amines on the surface was to conjugate covalently the natural amino acid (AA) residues on the surface. This renders the system to be more native and compatible to the biological environment, which consist of these AAs in abundance. Covalent conjugation also protects against the loss of functionalized surface characteristics secondary to non-specific macromolecular and electrolytic disturbances in biological media.

Another important parameter requiring investigation was the safety of functionalized NDs. Despite of the fact that several reports indicate the innate biocompatible nature of NDs,^{208, 148, 71} it was crucial to investigate whether AA-functionalization affects this biocompatibility. Therefore, cellular toxicity of lys-NDs and lysyl-histidine NDs was analysed using a standard MTT analysis. It is also important that the materials used as carriers in therapeutics should be completely inert in order to achieve a predictable response of delivered therapeutic moiety. This inertness for lys-NDs as gene carriers was confirmed through Annexin V assay to elucidate carrier induced apoptosis of cells. This chapter provide details of assays performed to evaluate the functional capacity and biocompatibility of functionalized NDs.

6.4 Materials and Methods

6.4.1 Materials

Materials and chemicals used for these experiments were similar as mentioned in chapter 5 with following additions:

Anti GFP siRNA, Silencer® GFP (eGFP) siRNA (50 µM, 5nmoles) was purchased from Ambion, ON, Canada. FITC Annexin V/Dead Cell Apoptosis Kit with FITC annexin V and propidium iodide for flow cytometry was obtained from Invitrogen, NY, USA. Melphalan was purchased in powder form by Sigma-Aldrich ON, Canada. HyClone™ D-PBS (with calcium and magnesium and w/o phenol red) was obtained from ThermoFisher Scientific Waltham, MA. MTT (3-(4,5-Dimethylthiazol-2-yl)-2,5-Diphenyltetrazolium Bromide) was purchased from Invitrogen, NY, USA and was prepared as 5mg/mL solution in PBS. Dimethyl sulfoxide (DMSO) was purchased from ThermoFisher Scientific Waltham, MA. Lipofectamine™ RNAiMAX was also purchased from Invitrogen, NY, USA.

6.4.2 Primary NDs dispersion

Primary dispersions of lys-NDs were prepared in purified deionized water at a concentration of 2 mg/mL. YTZ grinding media was added in all dispersions at a weight ratio of 1:1. The suspension was subjected to ultrasonication for 4 hours at a frequency of 25 kHz without heating. The ultrasonicated dispersions were then centrifuged at 5200 g for 5 minute to sediment the YTZ grinding media and the aggregated ND particles.

6.4.3 Flow cytometry analysis for GFP knockdown

Flow cytometry was used to evaluate the transfection efficiency of lys-NDs/anti-GFP siRNA diamoplexes prepared at ratios 10:1 to 40:1. HeLa/GFP cells were treated with the diamoplexes similarly as described for cellular association assay. Cells treated with lipofactamine/siRNA complexes were used as positive control and untreated cells were used as negative control. The final concentration of anti-GFP siRNA in each well was 75 pmoles and the treatments were terminated after 48 hours. GFP fluorescence was then measured using FL2-H band pass filter (585/42 BP). A total of 13000 events were recorded for each sample. In order to analyse the negative shift in GFP fluorescence, the histograms representing GFP intensity were divided into four regions (no-GFP, low-GFP, mid-GFP and high-GFP). Relative downshift in GFP fluorescence intensity from high to low region (i.e. Percent GFP knockdown) was determined by combining moderate and high GFP quadrants and comparing with untreated cells as follows:

$$\% \text{ GFP knockdown} = \left[1 - \frac{\% \text{ GFP fluorescence in mid and high regions for siRNA treated cells}}{\% \text{ GFP fluorescence in mid and high regions for untreated cells}} \right] \times 100 \dots \text{(Eq 6.1)}$$

6.4.4 MTT assay for Cellular Proliferation

Cytotoxicity of pNDs, rNDs, lysine NDs and lysyl-histidine NDs was evaluated in HeLa cells by MTT (3-(4, 5-Dimethylthiazol-2-Yl)-2,5-Diphenyltetrazolium Bromide) assay. The stock dispersions of NDs were made at a concentration of 1 mg/mL in aqueous medium. The cells were plated in 96 well plate at a density of 5,000 cells per well and incubated at 37° and 5% CO₂ to allow attachment to the plate surface. The cells in different wells were then treated with NDs at concentrations ranging from 10 µg/mL to 250 µg/mL (100 µL volume). After 20 hours, the treatments were terminated and the cells were washed with 1XPBS three times each. 10 µL of MTT stock solution (5mg/mL of MTT in PBS) diluted in 90 µL of serum supplemented media

was added in each well, and the cells were incubated at 37°C/5% CO₂ for one hour. Thereafter, the supernatant was removed, and formazan crystals resulting from the mitochondrial reduction of MTT were extracted using 100 µL of dimethyl sulfoxide (DMSO). The plates were incubated for another 10 minutes to remove air bubbles. The absorbance was read at 550 nm using microplate reader (BioTek® Microplate Synergy HT, VT, U.S.A.). Untreated cells were used as the control. Percent cell viability was calculated using the following formula:

$$\% \text{ cell viability} = \frac{\text{Absorbance}_{\text{treated}}}{\text{Absorbance}_{\text{control}}} \times 100 \dots\dots\dots (\text{Eq 6.2})$$

6.4.5 Annexin V Assay for Cellular Toxicity

The cells were plated in 6 well plates at a density of 1x10⁵ cells per well and incubated at 37° and 5% CO₂ to allow attachment to the plate surface. The cells in different wells were then treated with aqueous lys-NDs dispersions diluted to concentrations of 25 µg/mL, 50 µg/mL, 100 µg/mL and 250 µg/mL using serum supplemented media (2.5 mL volume). Melphalan was used as a positive apoptotic control and the solution was prepared in acidified ethanol at an initial stock concentration of 50 mM. The solution was diluted with acidified ethanol to 3.6 mM. Subsequent dilutions were made using serum supplemented media at final concentrations of 36 µM, 26 µM and 16 µM. The treatments were added in the cells. All the treatments were terminated after 20 hours, and the cells were washed with 1XPBS three times for 5 minutes each. The cells were harvested using trypsin and 0.25% EDTA and centrifuged at 95 g and 4 °C for 5 minutes to obtain cell pellets. The individual cell pellets were resuspended in 500 µL of D-PBS (with calcium and magnesium and w/o phenol red), transferred into 5mL flow cytometer tubes and the cellular apoptosis resulting from the treatments was analyzed using BD FACS Calibur™ (BD Biosciences, CA, USA). 5 µL of Annexin V and 5 µL of PI were added in all cell samples just before the analysis. The cells were analysed using two filters i.e. FL1-BP (530/30) for Annexin V detection and FL2-BP (585/42) for PI detection. Healthy population was gated and 10,000 events were obtained in the gated region. Secondary gating was applied on the graph showing cellular distribution of Annexin V vs Propidium Iodide to distinguish following populations Annexin V⁻/PI⁻ (non-apoptotic), Annexin V⁺/PI⁻ (early apoptotic), Annexin V⁺/PI⁺ (late apoptotic) labelled R1, R2 and R3 respectively. % of events in each quadrant was obtained to compare the treated and untreated cells. Untreated cells stained with Annexin V and PI separately was used for compensation of the filters.

6.5 Results

6.5.1 Flow cytometry analysis for GFP knockdown

RNA interference using small interfering RNA (siRNA) is a powerful tool to suppress abnormal gene expression to treat malignant diseases like cancer.^{273, 274} siRNA is a small fragment of RNA containing 21-23 nucleotides. Upon cellular entry, it binds to RNA interference induced silencing protein complexes and targets specific RNA sequence. Subsequent steps during RNA interference involve unwinding of siRNA duplex and degradation of the complimentary mRNA sequences by endo and exonucleases.^{275, 276} In order to investigate the ability of lys-NDs to function as delivery vehicles, anti-GFP siRNA was complexed to them at different weight ratios to form diamoplexes. The cells treated with lys-ND/anti-GFP siRNA diamoplexes (ratios ranging from 10:1 to 40:1) were compared to the cells treated with anti-GFP siRNA complexed with lipofectamine, as a standard transfecting agent.

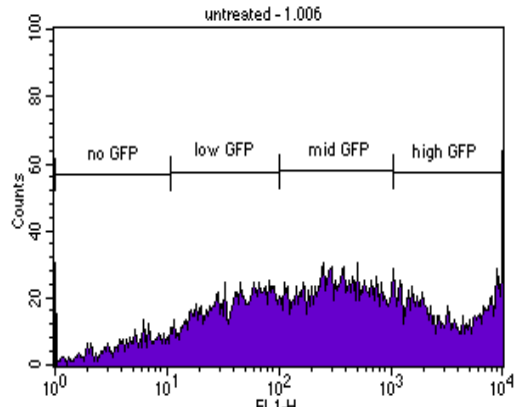
The untreated HeLa/GFP cells show very high fluorescence with ~67% of the population appearing in moderate and high GFP regions (Figure 6.1A). When naked siRNA (i.e. without any delivery vehicle) was introduced in the cells, ~63% of cells exhibit moderate or high GFP fluorescence which shows that this approach do not produce any GFP knockdown (Figure 6.1C). However, when siRNA was delivered by lipofectamine, the cells producing moderate or high intensity GFP fluorescence dropped down significantly to ~37% (Figure 6.1B). In contrasts to the controls, lys-NDs/anti-GFP siRNA diamoplexes showed a promising decrease in cells exhibiting moderate and high fluorescence to ~55% at a ratio of 20:1 (Figure 6.1E). However, there were no reductions in the cellular fluorescence at lys-ND/anti-GFP siRNA ratios 10:1, 30:1 and 40:1 with ~66% (D), 64% (F) and 65% (G) cells in moderate and high GFP regions (Figure 6.1).

Quantitative GFP knockdowns obtained through various treatments were calculated for better representation of the results (Figure 6.2). As expected, lipofectamine showed 44% i.e. the highest reduction in GFP fluorescence. When the same amount of siRNA was delivered without any vehicle, only 5.3% knockdown was obtained. This is due to the anionic nature of siRNA which hinders its cellular internalization through the negatively charged cell membrane. Moreover, it is not practical to deliver naked siRNA *in vivo* as well, since it can be rapidly degraded by exonucleases in the blood circulation. Complex chemical modifications to the nucleotide backbone are required to deliver naked siRNA *in vivo* for therapeutic purposes. These

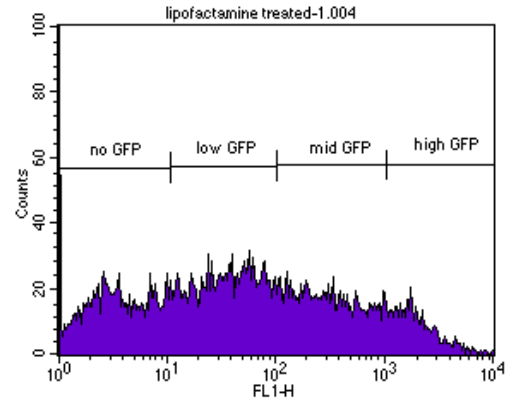
modifications can delay the degradation from minutes to hours but cannot prevent it for longer time periods unlike carrier mediated delivery.²⁷⁷ Moreover, these modifications should be extremely selective to minimize the loss of potency and maintain targeted activity of siRNA.²⁷⁸ In comparison to naked siRNA and lipofectamine mediated siRNA delivery, lys-NDs only showed a promising GFP knockdown of ~17% at a ratio of 20:1. It was shown to be the lowest effective ratio at which lys-NDs were able to bind and retard the movement of siRNA in gel electrophoresis (Chapter 4). Therefore, at a lower ratio of 10:1 no GFP knockdown (~1%) was observed. Additionally, at higher lys-ND/anti-GFP siRNA diamoplexes ratios of 30:1 and 40:1 the intensities of GFP fluorescence remained high and an insignificant knockdown of only ~4% and ~2% was obtained respectively. Progressive decline in siRNA delivery upon increasing the mass ratio of lys-NDs to siRNA can be due to an extensive binding and packing of siRNA, which renders the diamoplex incapable of releasing the nucleic acids in the cells.

Although a notable GFP knockdown was obtained at 20:1 weight ratio, it was not significant compared to the lipofectamine control. Moreover, we were not able to validate this positive effect through successive trials. Non reproducible nature of the transfection demands analysis and modifications to the system to enhance its functional efficiency. The major reason to diminished siRNA activity can be related to the endosomal trafficking and degradation in the cells. For successful gene delivery and expression, it is important for the diamoplexes to escape from the harsh acidic environment of late endosomes and lysosomes.²⁷⁹ This can be achieved by introducing pH sensitive molecules like histidine that can disrupt the endosomal membrane to release the diamoplexes in the cytosol. This was aimed by synthesizing lysyl-histidine NDs, which now requires further modifications for enhanced surface loading. The idea of introducing histidine moiety on ND surface will be further discussed in the last chapter of the thesis under future directions to optimize functionalization.

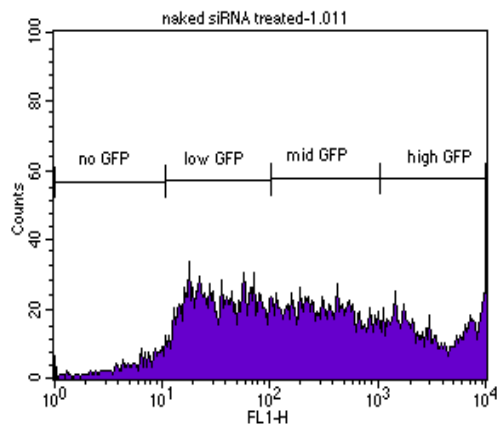
It is also important to keep in mind the highly toxic nature of lipofectamine during the treatment period.²⁸⁰ Morphological changes were observed within one hour of the treatment induction and a significant cell loss was observed at the end of the treatment period. Although the healthy cell population was gated during the analysis and uniform numbers of cells were counted for all samples, substantial changes in the cellular morphology and function due to lipofectamine induced toxicity may contribute towards reducing the GFP fluorescence intensity of these cells.



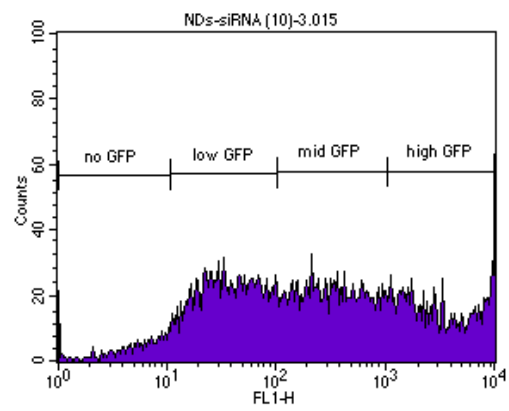
A



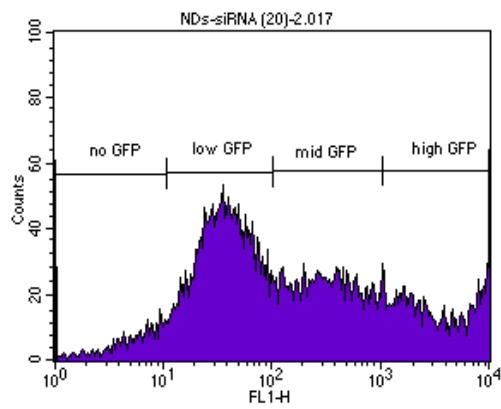
B



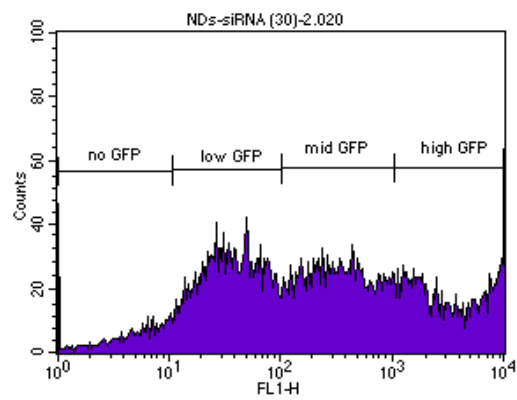
C



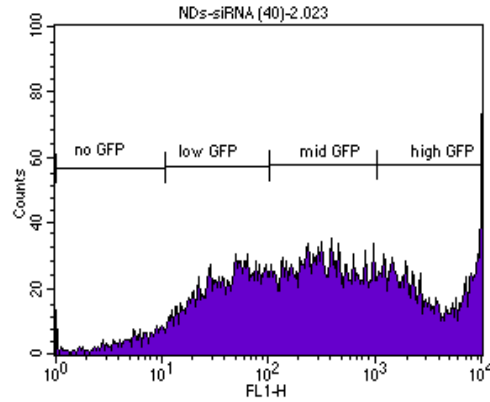
D



E



F



G

Figure 6.1 Flow cytometry outputs showing the distribution of untreated cells (A) and siRNA treated cells (B to G) in high, mid, low and no GFP regions. The figure also shows the negative shift of cellular population from mid and high GFP regions to low and no GFP regions secondary to treatments with anti-GFP siRNA in naked form (C), through lipofectamine (B) and as lys-NDs/siRNA diamoplex ratio of 10:1 (D), 20:1 (E), 30:1 (F) and 40:1 (G). GFP knockdown was only observed for cells treated with lys-NDs/anti-GFP siRNA at a ratio of 20:1, in comparison to the lipofectamine control.

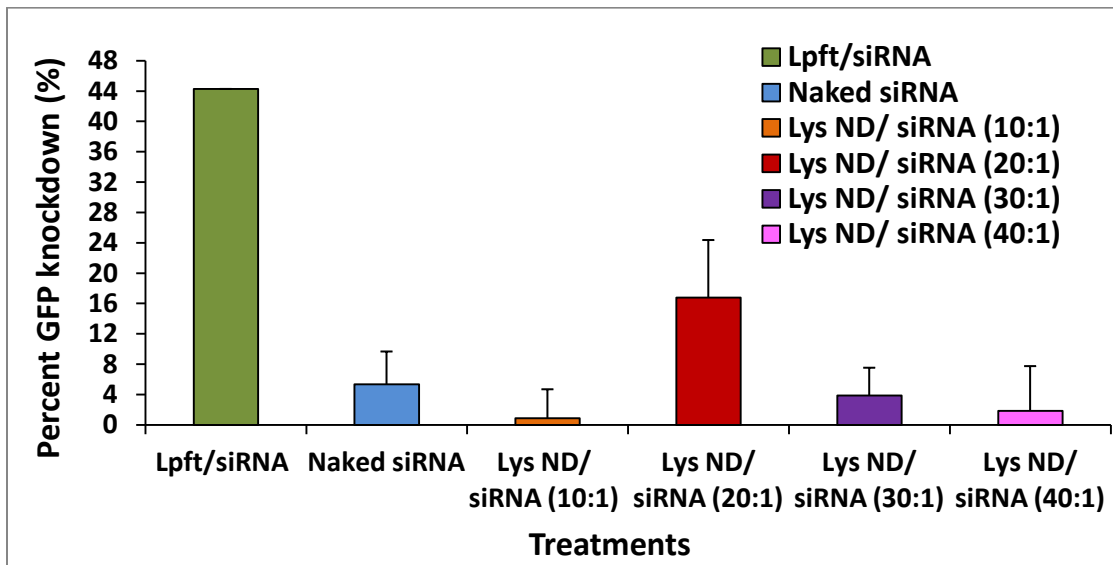


Figure 6.2 Quantitative percent GFP knockdown calculated through flow cytometry outputs for the cells transfected with anti-GFP siRNA as naked (blue), through lipofectamine (green) and as lys-NDs/anti-GFP siRNA diamoplexes at a ratio of 10:1 (orange), 20:1 (red), 30:1 (purple) and 40:1 (pink). The highest percent GFP knockdown of

17% was recorded for the cells treated with diamoplexes at a ratio of 20:1 in comparison to the lipofectamine control (44%). Except lipofectamine, each bar represents the mean \pm S.D. of three measurements.

6.5.2 MTT assay for cellular proliferation

It is crucial that a delivery vehicle should not impose any cytotoxic events upon interaction with the mammalian cells. Therefore, biocompatibility of NDs before and after AA functionalization was monitored at a wide range of concentrations. Results reveal no significant reduction in cell viability for all NDs treated cells compared to the control (Figure 6.3). Kruskal Wallis ANOVA, p value > 0.05) which ultimately indicates their innate biocompatible nature. The mean cellular viability after treatment with pNDs remained in the range of 83-91% (Figure 6.3), while with rNDs was in the range of 78-91% (Figure 6.3) indicating that COOH NDs may harm the cells at high concentrations. Comparatively, mean cellular viability after lys-ND treatment remained in the range of 83-91% (Figure 6.3) indicating that lysine functionalization does not affect the innate biocompatibility of NDs. Lysyl-histidine NDs showed mean cellular viability almost similar to rNDs (79-91%) for concentrations ranging from 10-100 $\mu\text{g}/\text{mL}$ (Figure 6.3). A slight increase to 110% was observed in cell viability at 250 $\mu\text{g}/\text{mL}$ suggestive of an unexpected proliferation. However, further investigations are required to elucidate this effect.

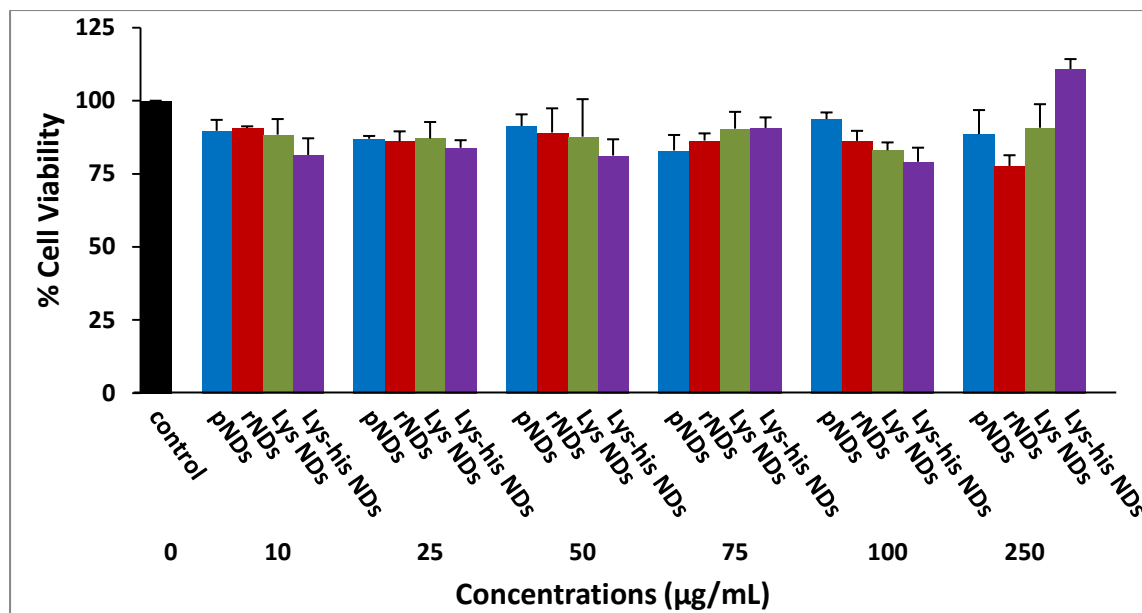


Figure 6.3 MTT assay for cytotoxicity of pNDs (blue), rNDs (red), lysine NDs (green) and lysyl-histidine NDs (purple) in HeLa cells at a concentration ranging from 10 µg/mL to 250 µg/mL (Kruskal Wallis ANOVA, p -value > 0.05)

Biocompatibility of lysine NDs was also evaluated with respect to the presence and absence of serum. The mean cellular viability after treatment with lysine NDs at concentrations ranging from 10 µg/mL to 75 µg/mL in the presence of serum remained in the range of 87-90% (Figure 6.4), while reduced to of 74-83% in the absence of serum (Figure 6.4). Although the decrease observed for the cells treated with lys-NDs in the absence of serum was statistically significant, its clinical relevance cannot be concluded. Additionally, lack of available nutrients required for cell growth and proliferation can also be a contributing factor. Conclusively, it can be said that the presence of serum proteins further protect the cells in the presence of NDs.

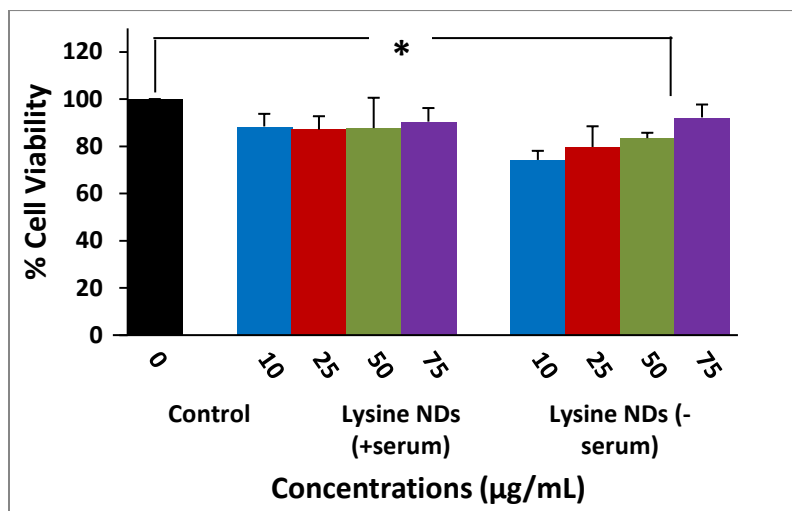


Figure 6.4 MTT assay for cytotoxicity of lysine NDs in the presence and absence of serum at concentration of 10 µg/mL (blue), 25 µg/mL (red), 50 µg/mL (green) and 75 µg/mL (purple). Statistically significant decrease was observed in cell viability after treating the cells with lys-NDs in the absence of serum (One-Way ANOVA, p -value<0.05, *Tukeys’s post hoc analysis, p -value<0.05).

6.5.3 Annexin V Assay for Cellular Toxicity

Apoptosis is a programmed cell death, a phenomenon in which cells induce self-destruction.²⁸¹ It is a widely researched mode of treatment induced by therapeutic genes²⁸², drugs²⁸³ and antibodies²⁸⁴ targeting chronic life threatening dysfunctions. However, carrier induced apoptotic injury is one of the major drawback for a controlled therapy. The carriers should ideally be inert, non-toxic and least reactive, to allow optimal control and prediction of the efficacy for the delivered therapeutic moiety. As indicated through MTT analysis, NDs are innately biocompatible at a wide concentration range irrespective of functionalizations. In order to further confirm this finding, annexin V FITC assay was performed to evaluate lys-ND inertness and safety. Loss of the plasma membrane integrity is the first step in this pathway, which ultimately translocates the phospholipid phosphatidylserine (PS) to the external membrane surface. Annexin V being a calcium dependent phospholipid binding protein binds to the exposed PS and can be used for the detection of early apoptosis after conjugation of a fluorophore. Therefore, early apoptosis is identified as an Annexin V⁺/PI population of cells indicated as R2 in Figure 6.5. Untreated cells exhibit a very tight population in the healthy cells quadrant (R1) and show no

events in the R2 quadrant indicating complete absence of apoptosis (Figure 6.5A). On the other hand, melphalan which is an apoptosis inducing agent used for melanomas ²⁸⁵ shows a distinct apoptotic population, with 10%, 15% and 11% events in R2 quadrant at 16 μ M, 26 μ M and 36 μ M concentrations respectively (Figure 6.5B to D and Figure 6.6). There is a positive correlation between melphalan concentration and apoptotic changes identified as annexin V uptake. However, at a higher concentration of 36 μ M majority of events are shifted towards R3 quadrant i.e. the late apoptosis stage and hence shifts down the population in R2 quadrant. In comparison to melphalan, lys-NDs did not induce apoptosis as observed in Figure 6.5E to H. There is no separate population observed in the R2 quadrant indicating an absence of annexin V uptake. Lys-NDs exhibited 0.53% \pm 0.27, 0.31 \pm 0.08, 0.49 \pm 0.21 and 3.88% \pm 0.61 uptake in annexin V at 25 μ g/mL, 50 μ g/mL, 100 μ g/mL and 250 μ g/mL concentrations respectively (Figure 6.6). Slightly higher counts observed for 250 μ g/mL does not necessarily depict an increase in apoptotic population and can be considered an anomaly related to the high scattering from NDs internalized by the cells. Rather than achieving a separation between the apoptotic and healthy population as in melphalan treated cells, the cellular distribution after lys-NDs treatment shifted upwards as a whole in a tightly compacted fashion. Therefore, it cannot be attributed to an increased apoptosis, but rather related to interference from concentration dependent increase in the side scattering following ND internalization as explained in Figure 5.4.

The number of events observed in the R3 quadrant reveals Annexin V⁺/PI⁺ cellular population. This quadrant captures the cells which are either undergoing end stage apoptosis or dead. PI is a membrane impermeable DNA stain and is taken up by the cells once the membrane integrity is completely compromised and the cell is in the necrotic stage. ²⁸¹ Melphalan treated cells exhibit populations separated from the healthy cells with a concentration dependent increase in dead cells or the cells undergoing late apoptosis being 2.38%, 3.51% and 13.48% at 16 μ M, 26 μ M and 36 μ M concentrations respectively (Figure 6.5B to D). In contrast, the lys-NDs treated cells exhibits an upward shift of a whole tightly connected population, which cannot be a true representative of dead cells, since they show no distinction from the healthy cellular population as described above.

These analyses reveal that lys-NDs do not induce any apoptotic injury or reduce cellular viability at a wide range of concentrations. Moreover, innate biocompatibility of NDs irrespective of functionalizations and serum presence is concluded.

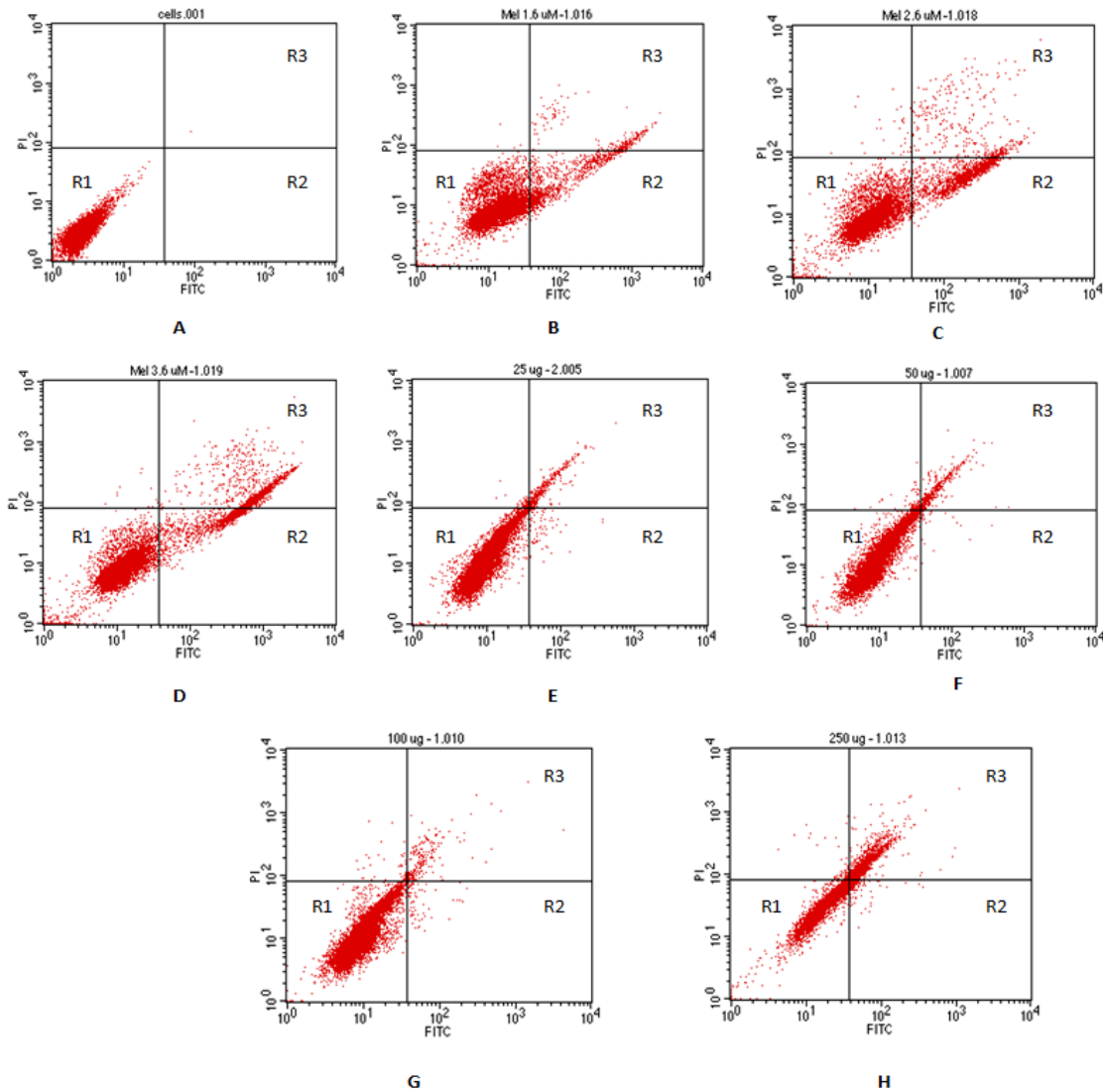


Figure 6.5 Flow cytometry plots indicating early and late apoptotic cellular distribution based on annexin V vs Propidium Iodide uptake for untreated (A), melphalan at 16 μ M (B), 26 μ M (C), 36 μ M (D) and lys-NDs at 25 μ g/mL (E), 50 μ g/mL (F), 100 μ g/mL (G), 250 μ g/mL (H) treated cells. Quadrant R1, R2 and R3 indicate annexin V⁻/PI⁻ (non-apoptotic), annexin V⁺/PI⁻ (early apoptotic), annexin V⁺/PI⁺ (late apoptotic) cell populations.

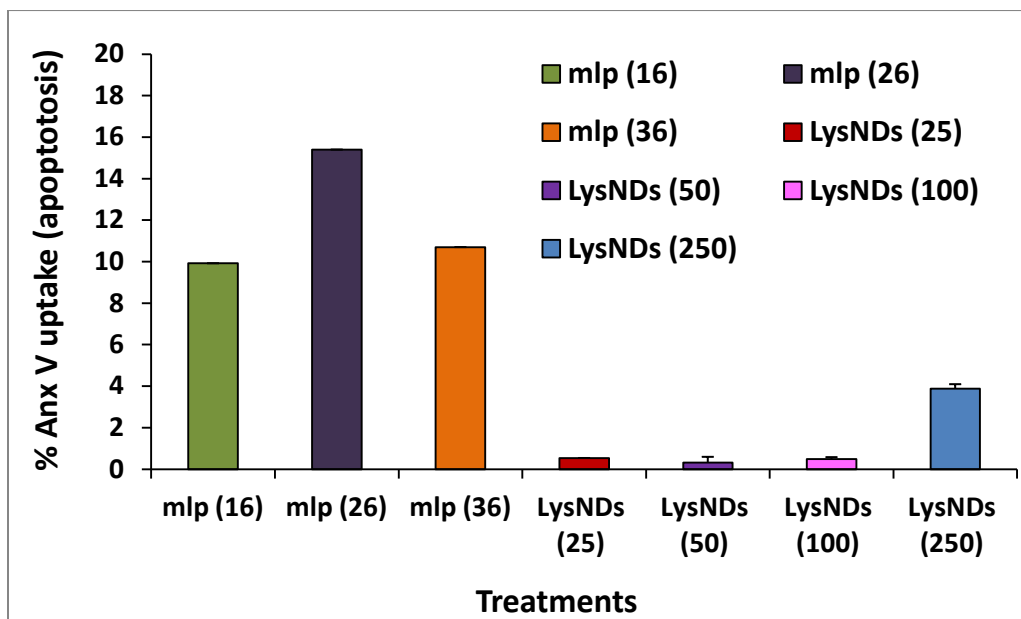


Figure 6.6 Flow cytometry analysis for lys-ND induced apoptosis at 25 $\mu\text{g}/\text{mL}$ (red), 50 $\mu\text{g}/\text{mL}$ (purple), 100 $\mu\text{g}/\text{mL}$ (pink) and 250 $\mu\text{g}/\text{mL}$ (blue) concentration in comparison with melphalan induced apoptosis at 16 μM (grey), 26 μM (brown) and 36 μM (green) concentrations.

6.6 Conclusion

This study provides a basis of hope to further modify AA functionalized NDs in order to increase their efficiency as gene delivery vehicles. A slight success was observed regarding its function as gene carriers, but this was not significant in terms of therapeutics. Possible reasons mainly the endosomal degradation can be targeted by introducing pH sensitive molecules on ND surface as a mode of improving its function in the future trials. However, the study confirmed that NDs remain biocompatible after functionalizations and are inert in the cellular environment. No apoptosis was observed even at very high concentrations of lys-NDs, which laid a benefit to design a system which can ensure predictable response of the therapeutic moiety.

7 Conclusive Discussion

This study has addressed three phases for developing a novel carbon nanomaterial called nanodiamonds (NDs) as gene carriers for RNAi therapeutics. The first phase elucidated the development of amino acid (AA) functionalized NDs as competitive systems capable of optimum binding and delivery of therapeutic genes in mammalian cells. The second phase of the study involved physicochemical characterizations of functionalized NDs and the development of an optimized treatment protocol for *in vitro* applications. The final phase of the study probed multiple aspects regarding the behavior of functionalized NDs in the biological environment including: interactions of the reactive surface with physiological proteins, cellular uptake of bare NDs and the diamoplexes (ND-gene complexes), effect of proteins on the cellular uptake process, assessment of gene delivery efficiency and finally their biocompatibility profiles. This is the first report to our knowledge of AA functionalization of NDs for gene delivery purposes.

The major aspects covered in the individual phases of the study are discussed as follows:

7.1 Phase 1

The first phase was aimed at functionalizing the surface of NDs with basic AAs. This functionalization was performed to achieve two major objectives: 1) to minimize aggregation for formulating a stable colloidal dispersion and 2) to create a cationic surface to electrostatically bind the nucleic acids for cellular delivery. Additionally, histidine was introduced in the system as a pH-sensitive AA for avoiding lysosomal entrapment of diamoplexes in the cells.

Functionalization of NDs through covalent conjugation of lysine and lysyl-histidine on the innately reactive surface comprised of three major steps: homogenizing the surface by pre-treating the NDs through oxidation, increasing the reactivity of the surface functional groups and covalently attaching the AAs to the surface through a three carbon chain spacer (Scheme 1 and 2). The presence of peaks corresponding to carbonyl and amine groups and absence of peak for hydroxyl group in the infrared spectra of functionalized NDs elucidate the formation amide linkage between NDs and amine terminated spacer attached to the AAs (Figure 4.9). Thermograms of NDs after functionalization further confirms the presence of AAs on the surface through a significant weight loss induced upon heat induction (Figure 4.10). This weight loss

corresponds to the breakage of covalent linkages at high temperatures and loss of surface functional groups. Thermogravimetric analysis also reveals that the surface loading of carboxylate functionalities significantly increased after re-oxidation, which later facilitated the formation of lysine terminated ND surface (Table 4.1). Functionalization enhancement after re-oxidation of the surface resulted due to increased possibilities for the formation of amide linkages. It served as a better approach to increase the overall surface loading of the chemical conjugates on NDs in comparison to other modes previously reported in the literature. NDs previously functionalized with long alkyl chains directly on the partially hydroxylated pristine surface produced a surface loading of 0.3-0.4 mmoles/g.²⁸⁶ In contrast to that, the re-oxidized NDs having an almost completely carboxylated surface allowed the surface loading to increase up to 1.97 mmoles/g (Table 4.1). Another example of biomolecular conjugation on NDs is presented through covalent bonding of lysozyme on the surface with a loading capacity of 0.2-0.25mg of lysozyme on 1 mg of NDs.²⁸⁷ Here lysozyme was directly conjugated to the native ND surface after the activation of functional groups. Apparently, an additional re-oxidation process used to synthesize lysine functionalized NDs (lys-NDs) improved the surface loading to 0.61 mg of lysine on 1 mg of NDs.

In order to design NPs for gene delivery, the creation of a cationic surface is the most feasible and commonly employed approach. It is achieved through varieties of covalent and non-covalent surface functionalizations.^{67, 68, 69} Use of native biological molecules for this purpose is rare and is mostly mediated through physical adsorption.⁶⁷ However, soft NPs like Gemini lipids covalently functionalized with amino acid conjugates have shown significant potential as gene carriers due to functionalization stability and optimum binding with nucleic acids.^{288, 289} Keeping in view this commendable efficacy of bio-molecular cationic surface for gene delivery, NDs were functionalized for the first time with lysine and lysyl-histidine AA conjugates.¹³⁴ The positive zeta potential of lys-NDs (Figure 4.12) indicates the dominance of cationic primary amines on the surface capable of binding the anionic genetic materials and also to electrostatically interact with the cell membrane.

Unlike lysine conjugation, lysyl-histidine functionalization on NDs was not successful possibly due the larger surface area of the conjugate; creating a steric hindrance against adjacent COOH groups for functionalization.

7.2 Phase 2

This phase characterized the physicochemical properties of functionalized ND (fNDs) based gene carriers. NDs have tremendous potential as delivery vehicles in nanomedicine; however the strong aggregation tendency complicates their application to a great extent. Stirred media milling is used as a principal physical approach to counter aggregation; however it poses a challenge of bead contamination and long term maintenance of a stable well-dispersed formulation.^{82, 125} Chemical functionalization of the surface capable of reducing non-specific interactions between individual particles can complement the mechanical method of disaggregation to achieve long term stability.²⁸⁶ Functionalization of NDs with long alkyl chains have enhanced their dispersion stability in organic solvents by reducing the particle size to nanometer size range (15 μm to 150 nm).²⁸⁶ Similarly, decorating the surface with fluorine¹⁵ and borane¹⁴ reduced the size of pristine NDs up to 160 and 50 nm respectively. In my work, lysine functionalization created a homogenous cationic surface capable of dominating the repulsive forces between particles to minimize aggregation.

Physicochemical stability testing was performed in various biologically relevant media to evaluate the stability of NDs through this mechanochemical approach. These characterizations were also aimed at developing a treatment protocol for *in vitro* dosing application. Lys-NDs exhibited highest long term stability and uniform particle size distribution in the aqueous medium. Previously, it was reported that lysine functionalization limited aggregation of NDs in the aqueous environment for a short period of time.¹³⁴ Here, the analysis further reveals that lys-NDs are well-dispersed and remain stable in water for an extended time period of 25 days (Figure 5.1). This is due to the fact that water does not compromise the positivity of surface²⁹⁰ and maintain the electrostatic repulsion between adjacent cationic surfaces to hinder core aggregation. In order to achieve the similar long term colloidal stability in the aqueous medium, CNTs another very common gene delivery vector were also physically functionalized with natural and synthetic dispersants.²⁹¹ However, unlike lysine functionalization which is capable of maintaining ND size in the range of 50-90 nm in water (Figure 4.11), these approaches failed to reduce the size of CNTs below 400 nm during an almost same time interval.²⁹¹

In contrast to lys-NDs, lysyl-histidine NDs exhibited poor stability in water, producing a system with a particle size distribution centered in the range of 615-955 nm (Figure 4.11). This resulted

due to an uneven functionalization that failed to maintain the electrostatic repulsion between adjacent ND surfaces.

In addition to optimum physicochemical characteristics of colloidal fNDs dispersion, their suitability as gene carriers was exhibited by their ability to bind the plasmid DNA and small interfering RNA effectively at minimum ratios of 1:1 and 1:20 respectively (Figure 4.13 & 4.14). In contrast to polymer functionalized NDs (polyallylamine hydrochloride) which requires a high mass ratio of 1:70 for complete binding,²¹⁷ lys-NDs are required in very low amounts to form stable diamoplexes. This provides a promising opportunity to reduce the overall ND exposure during *in vivo* treatments. Moreover, the diamoplexes of lys-NDs with siRNA remain intact in the *in vitro* biological environment rendering the system capable for intracellular delivery of the genes.

7.3 Phase 3

This phase of the study provided comprehensive understanding regarding the behavior of fNDs in the biological system and addressed two major aspects: interactions with the physiological media and interactions with the mammalian cells.

Despite of the inherent stability of lys-NDs, physicochemical changes mediated through the biological growth medium can modulate their transfection efficiency. Therefore, it was crucial to identify the most suitable dosing medium to formulate NDs and diamoplexes treatments for cellular experiments. Unlike aqueous formulations which maintained stability of lys-NDs for an extended time, formulations in cell culture medium exhibited poor stability possibly due to high ionic strength of the media promoting flocculation of the colloidal system (Figure 5.2).^{111, 231, 232}

In addition to the cell culture medium, physicochemical characterization and dispersion stability testing were also performed in other biologically relevant media (including water, phosphate buffered saline (PBS) and methylcellulose). The dispersions of lys-NDs in PBS showed extensive sedimentation within 3 days due to the high ionic strength of PBS that disturbed the surface charges and promoted random van der Waals interactions (Figure 5.1).^{225, 226} On the contrary, lys-NDs in 0.5% methylcellulose gel and water showed minimum aggregation during 3 days (Figure 5.1). However, methylcellulose being an amphiphilic molecule can reduce the positive charge density of the surface in the long run through random surface adsorptions.²²⁸ Due to this

fact and the overall dispersion quality of the aqueous ND formulation, water was selected as the choice for the dosing medium.

In addition to the dispersion stability, the ability of fNDs to interact with the macromolecules in the physiological systems can serve as another contributing factor for changes in their innate characteristics. Like all other charged nanoparticles, NDs can also interact with proteins forming a corona that can change the overall surface reactivity.^{261, 184, 220, 188} Due to positively charged surface of lys-NDs, there is an increased possibility for the adsorption of proteins with low isoelectric points (<5.5) such as albumin.²³⁵ Massive increase in the particle diameter and the change of potentials to high negative values occurring immediately after protein adsorption indicated the formation of an anionic protein corona around fNDs (Figure & Table 5.2). Thickness of the protein corona remained constant for 3 days, however the surface characteristics changed drastically indicating the dynamic nature of protein adsorption. This illustrates that the identities of adsorbed proteins may change over time leading to variations in the surface charges; but the total amount of proteins on the surface remains roughly constant. Evaluation of their interaction with physiological proteins can provide useful understanding regarding their behavior in the blood stream.

After the development of best dosing formulation, interactions of lys-NDs with mammalian cells were evaluated. At first, Internalization of bare lys-NDs and diamoplexes (i.e. ND-gene complexes) was observed through a combination of spectroscopic, microscopic and light scattering techniques previously reported in the literature^{217, 292, 293} and through novel techniques such as STXM. Results reveal that lys-NDs internalize the cells in a dose dependent fashion and localize mostly around the cellular edges and the cytoplasm, with some being in close proximity to the nucleus (Figures 5.3-5.6). They are found to significantly overlap with intracellular and growth medium derived proteins. Unlike carboxylated anionic NDs, lys-NDs shows optimum binding and internalization of siRNA in the cells (Figure 5.7). Additionally, the protein corona also contributes towards maintaining the stability and facilitating the cellular uptake of diamoplexes (Figure 5.8). It was shown as a significant increase of 1.8 folds in the fraction of siRNA fluorescence in the presence of serum (Figure 5.8) as compared to the serum-free environment and is speculated to be the result of serum-induced increase in the particle size of diamoplexes which can switch the internalizations pathways to favour the uptake of large

complexes. Increase in the overall particle size of the protein coated diamoplexes can switch the most prominent clathrin mediated endocytosis of NDs to caveoli mediated endocytosis,²⁵⁵ which is responsible for the uptake of complexes sized around 500 nm or above.^{256, 257} Moreover albumin, the main component of FBS can also facilitate towards the alteration of internalization pathway by acting as a ligand that binds to the albumin-binding protein on the caveolar plasma membrane.^{182, 260, 261}

After demonstrating the cellular uptake of lys-NDs alone and the diamoplexes, functional assays were conducted to evaluate its transfection efficiency. Lys-NDs showed a promising GFP knockdown of ~17% at a ratio of 20:1 (Figure 6.1 & 6.2), evidencing binding, delivery and release of functional siRNA in the cells. Unfortunately, this level of transfection is not enough in terms of therapeutics especially when compared to other functionalization approaches like polymer adsorption (polyethyleneimine) which showed a 4 fold higher transfection in contrast to the naked DNA delivery.⁶⁹ The major reason for reduced functional efficiency of lys-ND derived diamoplexes is their endosomal trafficking and subsequent intra-endosomal degradation of the genetic materials. It can be improved through various chemical modifications on the system that will be discussed later in the thesis.

Finally, the biocompatibility of NDs before and after AA functionalization was monitored at a wide range of concentrations. Results reveal no significant reduction in the viability for the cells treated with pristine NDs, re-oxidized NDs, lys-NDs and lysyl-histidine NDs at all concentrations, confirming their innate biocompatibility (Figure 6.3). It was further confirmed by conducting an apoptosis assay to assess the inertness of fNDs. In comparison to a standard apoptosis inducing chemotherapeutic drug ‘melphalan’, the cells treated with lys-NDs did not show any uptake for Annexin V, a phospholipid binding protein that binds to the exposed phosphatidylserine (Figure 6.5 & 6.6). This validates the intact nature of the cell membrane and absence of apoptotic injury through NDs unlike other carbon nanomaterials particularly CNTs.²⁹⁴ Moreover, NDs also do not fragment DNA³⁷ or alter protein expression profiles of the living cells at wide range of concentrations and particle sizes.⁷² Previously reported studies and current biocompatibility analysis confirms that NDs are the most biocompatible members of the carbon nanofamily.

8 Future Directions

Evidences regarding disaggregation, well-maintained stability, optimum cellular uptake, intracellular delivery and expression of siRNA and biocompatibility obtained through this study paved the way for future evaluations and modifications aimed at improving this nanocarrier. The future directions will focus on the following aspects of NDs as delivery vehicles:

8.1 Mechanistic studies for identifying endocytotic pathways and subcellular localization

Most nanocarriers internalize the cells through the process called pinocytosis which internalize fluids and molecules within small vesicles formed by the cell membrane folding. As mentioned earlier, the internalization pathway adopted by nanoparticles (NPs) significantly affects their fate in the cells. Therefore, clear understanding of internalization pathways will provide a unique opportunity to adjust the properties of nanodiamonds (NDs) in order to overcome the cellular barriers for gene expression. However, lack of biocompatible labels for long term tracking of NPs in the cells is a principle obstacle for the study of these pathways in detail. Following strategies will be directed in the future to study this aspect:

- Selective mechanistic inhibition will be performed to determine the most prominent internalization mechanism for functionalized NDs and the diamoplexes. Standard inhibitors of various endocytotic machineries will be used to evaluate the changes in the diamoplex uptake and siRNA expression in the cells. This assay will be performed by using two techniques:
 - Transmission Electron Microscopy (TEM) to show the specific changes occurring in the cell membrane elucidating the uptake pathway (e.g. pseudopods demonstrating macropinocytosis or formation of pits indicating clathrin or caveoli mediated endocytosis).
 - Flow cytometry for quantitative detection of diamoplexes uptake secondary to the selective inhibition of various endocytotic pathways. This assay would utilize the side scattering patterns of the treated cells to correlate the amount of diamoplexes internalized in the cells.
- Upon successful investigation of pathways involved in the uptake of diamoplexes, functional assays for gene expression would be conducted using flow cytometry to evaluate the most

optimum pathway allowing efficient gene release and expression. Knowledge regarding the effect of internalization pathways on the functional efficiency of diamoplexes will serve as a basis for future design modifications in NDs (particularly particle size) to adopt the most optimum internalization route for maximum efficacy.

- Next step would be to investigate the subcellular localization of diamoplexes by using artificially doped fluorescent NDs (FNDs). FNDs can be functionalized on the surface with AA conjugates, since they can be tracked easily through various techniques due to its bright fluorescence. Confocal microscopy with selective organelle labelling will be carried out to create color composite maps illustrating the subcellular distribution of functionalized-FNDs.

8.2 Design modifications to optimize the formation of lysyl-histidine NDs

Histidine is a positively charged polar AA having an imidazole ring which becomes fusogenic at physiological pH. As explained earlier, introduction of histidine as a pH sensitive AA on the ND surface will act as an endosomal destabilizer to cause the release of the genetic materials in the cytosol (Figure 9.1).

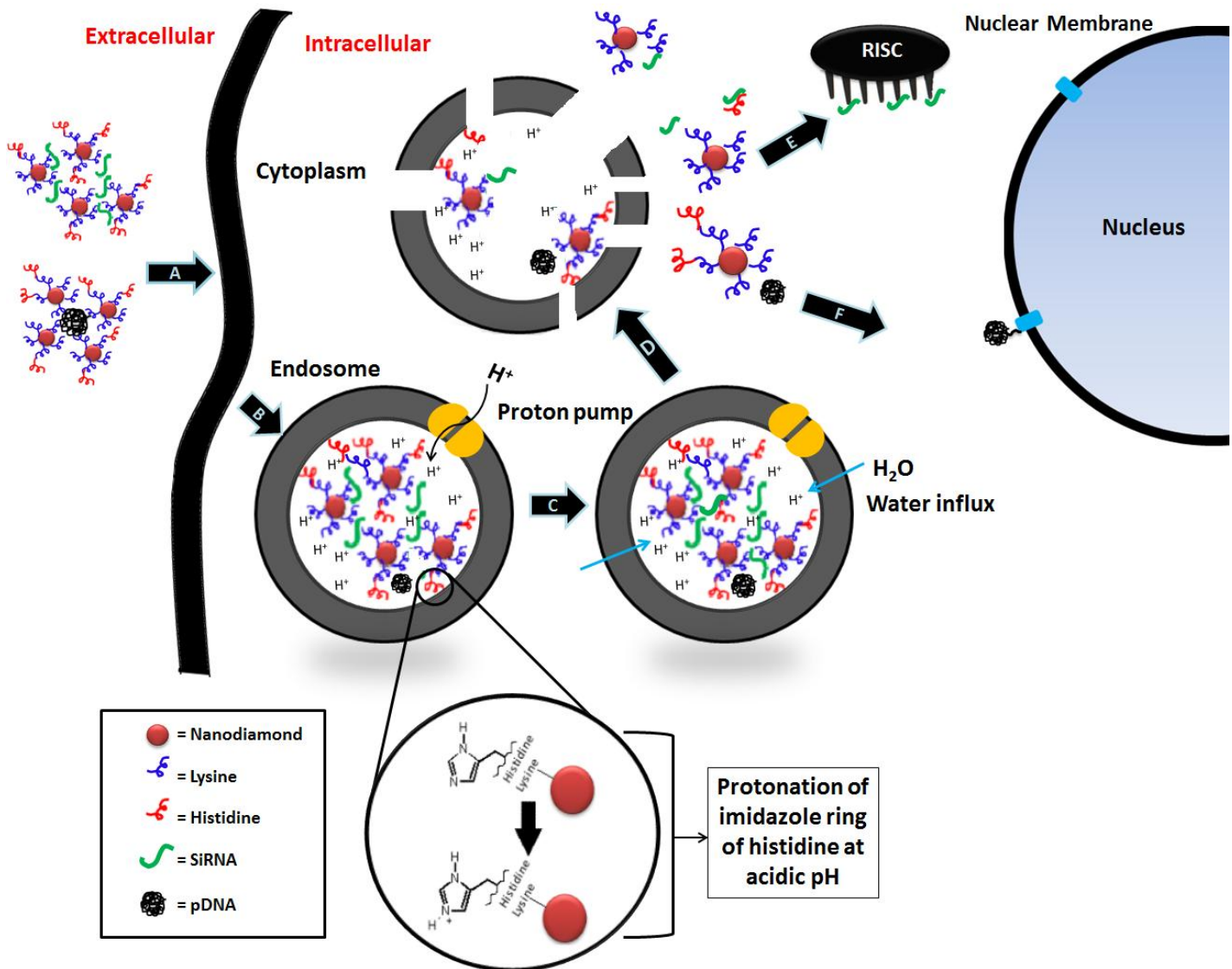
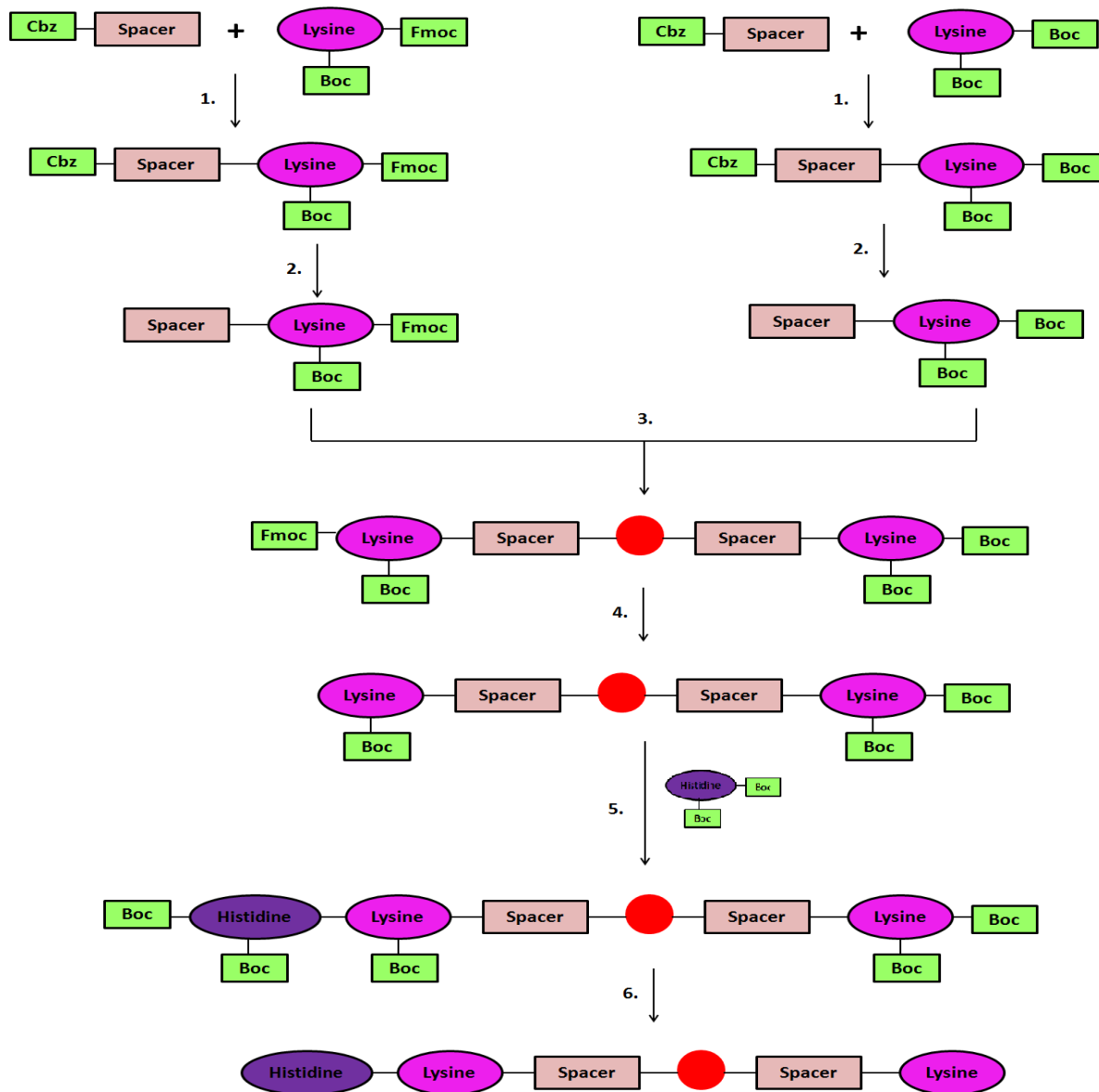


Figure 8.1 Schematic illustration of histidine mediated endosomal escape (A) endocytosis of diamoplex by cell membrane (B) formation of endosome, acidification and subsequent protonation of histidine to become fusogenic (C) disruption of hydrophilic/hydrophobic balance within endosome (D) rupture of endosomal membrane and release of diamoplex in the cytosol (E) Binding and expression of siRNA by RNA-induced silencing complex (RISC) in the cytoplasm (F) Transfer of pDNA to the nucleus for expression by nuclear membrane transport proteins

Design modifications to optimize lysyl-histidine NDs will be directed towards overcoming the steric hindrance posed by the large size of the conjugate impeding complete surface

functionalization. The new strategy to synthesize lysyl-histidine NDs will be influenced by the process of lysine functionalization in lieu of the optimum surface loading achieved for lysine AA conjugate. This process will primarily form lysine functionalized NDs followed by secondary histidine functionalization onto the lysine functionalized ND surface as illustrated in scheme 5.



Scheme 5 Design modification to synthesize lysyl-histidine functionalization. (1) Conjugation of lysine with the spacer to form N'- (N_α,N_ε-bis-boc-lysyl)-N''-cbz-diaminopropane & N'- (N_α-fmoc,N_ε-boc-lysyl)-N''-cbz-diaminopropane conjugates (2) Deprotection of the spacer moiety to form N'- (N_α,N_ε-bis-boc-lysyl)-N''-diaminopropane &

N^ε- (N_α-fmoc,N_ε-boc-lysyl)-N^ε'-diaminopropane (3) **Attachment of N^ε'- (N_α,N_ε-bis-boc-lysyl)-N^ε'-diaminopropane & N^ε'-(N_α-fmoc,N_ε-boc-lysyl)-N^ε'-diaminopropane to acyl chloride functionalized NDs (Cl-C=O) (4) **Removal of fmoc protecting group to form N^ε'- (N_α,N_ε-bis-boc-lysyl)-N^ε'-diaminopropane & N^ε'-(N_α,N_ε-boc-lysyl)-N^ε'-diaminopropane functionalized NDs (5) **Attachment of histidine to fmoc deprotected lysine residue to form N^ε'- (N_α,N_ε-bis-boc-lysyl)-N^ε'-diaminopropane & N^ε'- (N_α-bis-boc-histidine, N_ε-boc-lysyl)-N^ε'-diaminopropane functionalized NDs (6) **Removal of boc protecting groups to form lysine-diaminopropane & lysyl-histidine-diaminopropane functionalized NDs.********

Cbz= Carboxybenzyl; fmoc= Fluorenylmethoxycarbonyl; boc= Di-tert-butyl oxycarbonyl

The following is the proposed structure of lysine-lysyl-histidine functionalized NDs (Figure 9.2)

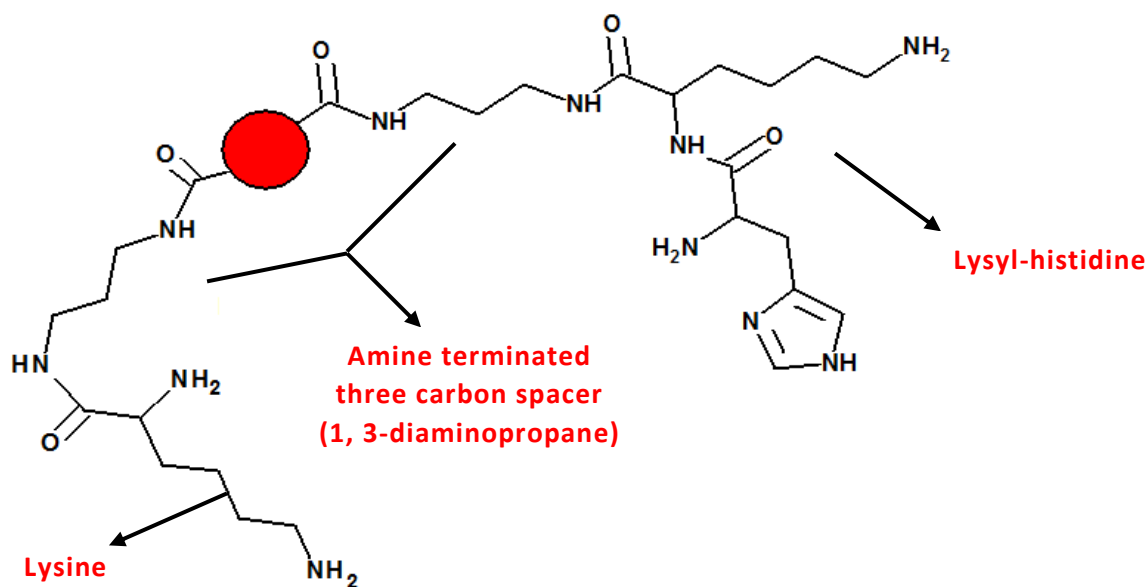


Figure 8.2 Structural illustration of lysine-lysyl-histidine functionalized NDs

9 Conclusion

This study demonstrated for the first time that covalent immobilization of basic amino acids (AAs) mainly lysine directly on the ND surface render their utilization in gene therapeutics by forming stable diamplexes with nucleic acids. This mode of surface transformation also limits aggregation to design a well-dispersed aqueous formulation, which is promising for its stability in the biological milieu. Like all other NPs, AA functionalized NDs also attract proteins and form a corona around its surface. However, this protein corona stabilizes ND-siRNA complexes and facilitates the process of cellular uptake. The increased cellular uptake in the presence of serum proteins is another promising finding, rendering them amenable for parenteral administration for gene therapy. Although not significant in terms of therapeutics, lys-NDs show an encouraging functional efficiency to deliver siRNA in the cells. Major reasons for its weak activity can be targeted in future to improve their functional capacity. The study also elucidate that NDs remain biocompatible after functionalizations and are inert in the cellular environment. No apoptosis was observed even at very high concentrations of lys-NDs, which laid a benefit to design a system which can ensure predictable response of the therapeutic moiety. Future analyses regarding mechanisms of cellular uptake and subcellular localization can reveal further insight regarding possible modifications to optimize the delivery system.

10 Appendices

10.1 Excerpts of Chapter 2: Nanodiamonds as Novel Materials for Therapeutics

10.1.1 Production of Nanodiamonds (Section 2.4)

NDs naturally exist in different levels of universe. Carbonaceous chondrites which are a special type of stony meteorite ²⁹⁵are the major naturally occurring source of NDs sized 2.5 nm. These NDs also contain hydrogen, nitrogen and oxygen impurities. ⁹⁰

NDs are synthetically produced by many different approaches. Each method yields particular sized diamond nanoparticles (NPs), which are suitable for specific applications. Based on the primary particle size, NDs are categorized into nanocrystalline particles (1 to ≥ 150 nm), ultrananocrystalline particles (2 to 10 nm), and diamondoid structures (1 to 2 nm). ^{296, 84}

Ultradispersed diamond NPs (Figure 2.1a) ranging from 2-8 nm are produced by detonation and are widely researched for biomedical applications. ⁹³ In this process NDs are synthesized by detonating a mixture of trinitrotoluene (TNT) and hexogen in a negative oxygen balance to facilitate carbon-carbon interaction (Figure 2.1b). Detonation involves transformation of the explosive material; it requires constant maintenance of optimal thermodynamic conditions. During detonation pressure and temperature is maintained at levels capable of allowing the appearance of free carbon in the product and at the same time also inhibiting diamond to graphite transition due to explosion. ²⁹⁷ The process creates soot containing nano-sized diamond particles which are then isolated and purified. To maximize the yield up to 90 % the soot is subjected to high energy electronic irradiation and heat treatment at 800 °C followed by rapid cooling. Isolation of NDs from the soot is carried out by boiling in acid at high temperature of 3000°C–4000 °C and high pressure of 20–30 GPa for 1 to 2 days. ^{84, 16, 298, 113} Despite of various novel approaches for ND synthesis, detonation NDs holds primary focus to generate NDs for nanomedicine research, majorly as therapeutic delivery vectors. ^{100, 101, 134}

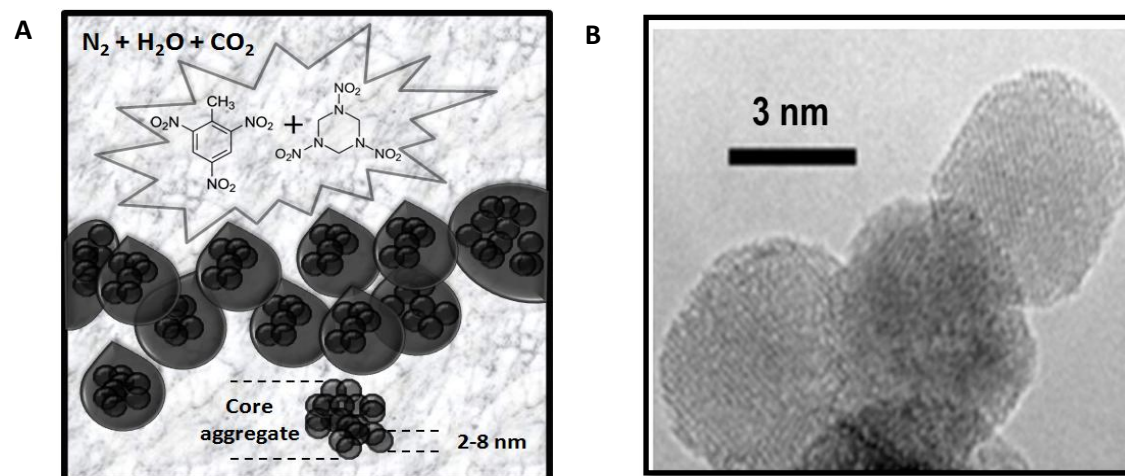


Figure 10.1 (A) Schematic representation of ND synthesis in a detonation chamber. (B) High-resolution transmission electron microscopic image of detonation nanodiamonds (NDs). (A) Explosion of TNT and hexogen in negative oxygen balance created by nitrogen carbon dioxide and water produces soot containing core aggregates of ND particles which are then isolated and purified. (B) Reprinted with permission from ⁸⁴ “Copyright (2013) Dove Medical Press”

Novel techniques for generating NDs synthesis focus primarily on reducing the formation of core aggregates in the synthetic process and producing disaggregated primary diamond NPs. ²⁹⁹ The core aggregates are formed mainly due to sp^2 graphitic carbon contamination present in the soot resulting from detonation. ⁸⁵ Most of these novel techniques involve conversion of graphite into diamond structures by creating optimal conditions of temperature and pressure through different modes. ^{299, 300, 301} One of such high temperature and pressure technique kept forward involves decomposition of graphitic carbon nitride to produce uniform sized, single phased NDs with no graphite contamination. ²⁹⁹ Graphitic carbon nitride treated at 800-900 °C and between 22 to 25 GPa pressure decomposes directly to diamond and nitrogen. ³⁰² Unlike detonation, this approach is centered upon creating high temperature and high pressure conditions during the synthesis phase of NDs. It offers many advantages over detonation. Mainly it produces pure ND crystals with virtually no graphitic contamination; and hence allows their utilization in as-synthesized form with minimal requirement of post synthetic purification. ²⁹⁹

Ultrasonic cavitation is another approach to synthesize NDs based on high pressure high temperature technique. ³⁰⁰ This process involves transition of graphite into diamond in organic

liquid at temperature of 120 °C and atmospheric pressure but in presence of ultrasonic waves. Ultrasonic cavitation acts as super-high pressure shock waves producing necessary combination of temperature and pressure to facilitate this transformation. However, this process produces very low yield of up to 10 %.³⁰⁰

High energy laser irradiation of graphite is an alternate method of producing NDs.^{301, 303} This technique involves irradiating the graphite powder with high energy pulsed laser beam at room temperature and atmospheric pressure. Pulsed laser energy produces high temperature which heats the raw graphite powder, followed by rapid cooling that generates high pressure. Thus high temperature and high pressure combination is created to form nanosized diamond particles of 5 nm with fewer impurities as compared to detonation process.³⁰¹

While these alternative techniques offer high quality NDs, the major source of biomedical applications today remains the detonation NDs particularly due to high yield and convenience for its application at industrial scale.

10.1.2 Fluorescence imaging (Section 2.8.3.1)

Internal structural defects and impurities cause NDs to emit visible fluorescence, which show some advantages compared to the conventional dyes used for fluorescence imaging. Under the same excitation conditions, a single 35nm sized diamond NP is significantly brighter than commonly used dye molecules such as Alexa Fluor 546.¹⁰⁵ In addition to higher fluorescence, NDs also resist photobleaching and fluorescence blinking for longer duration of 5 minutes unlike Alexa Fluor which photobleaches within 10 seconds.¹⁰⁵ Photobleaching is one of the major deficiencies of imaging probes, where the fluorophore undergoes chemical degradation due to the generation of reactive oxygen species (ROS) in biological system as a by-product of fluorescence excitation.³⁰⁴ Fluorescence blinking is the phenomenon showing intermittent light and dark bands upon continuous illumination, common in hard nanomaterials like quantum dots.³⁰⁵ Fluorescence blinking presents as a problem for single-molecule spectroscopy³⁰⁵ due to lack of image consistency. In addition to the above mentioned problems, auto-fluorescence of cellular structures like mitochondria and lysosomes is also a concern in the design of imaging probes.³⁰⁶ It usually arises in the emission wavelength range common to many fluorescent dyes (i.e. 510-560 nm), and therefore creates intense background signals making the detection of the probe increasingly challenging. However, NDs when excited with 532 nm wavelength light, produces

an emission between 650-720 nm thereby reducing the interference of cellular auto-fluorescence.
105

Various approaches have been utilized to induce or enhance the fluorescence centres in NDs. One of such techniques involves irradiation of NDs with helium ions (He^+) at 40 keV followed by thermal annealing at 800°C to create vacancies.¹⁹⁹ Hydrogen ions (H^+) at 3 MeV are also used in place of helium to induce nitrogen vacancy centers in ND core.³⁰⁷ Another way to create nitrogen vacancies is to directly incorporate nitrogen atoms as native nitrogen ^{14}N ³⁰⁸, its isotope ^{15}N ³⁰⁹ or as cyanide (CN^-) ions³¹⁰ directly in the core. To preserve fluorescence from the nitrogen vacancies NDs are encapsulated by bulky groups like phenols, which reduces the non-radioactive decay pathways of colored centres.³¹¹ Fluorescence can also be produced through surface conjugation. For example, NDs can be functionalized with a hydrophobic molecule octadecylamine producing bright blue fluorescence and can be useful for imaging hydrophobic components of the body.³¹²

Opportunities to induce and enhance the fluorescence centres in NDs along with its innate biocompatibility at all levels has attracted their use as cellular biomarkers for tracking natural and therapeutic processes^{176 313 314} Fluorescence of NDs can be clearly detected in the treated cells and allows detailed localization of NDs and the conjugated the therapeutic moiety (Figure 2.13).

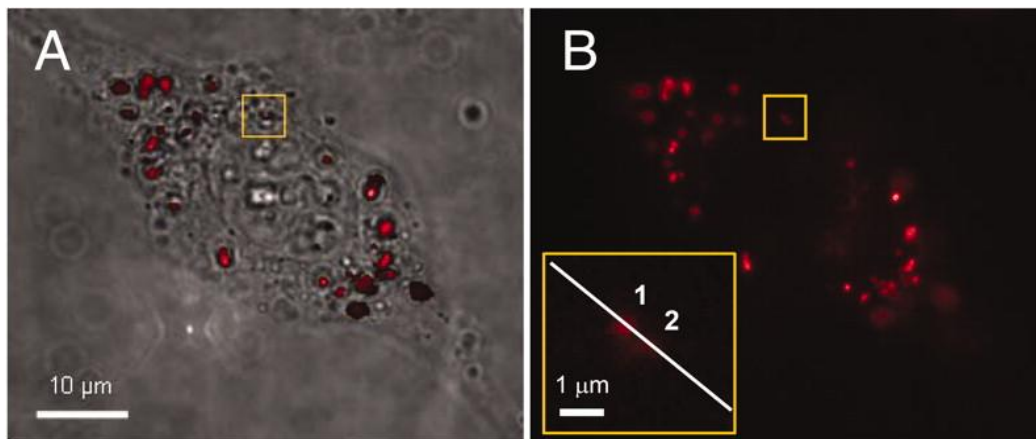


Figure 10.2 Left panel: Bright-field image of a HeLa cell after uptake of 35-nm fluorescent NDs. Most of the internalized NDs are seen to distribute in the cytoplasm. Right panel: Epifluorescence image of a single HeLa cell after the ND uptake. An enlarged view of the fluorescent spots (denoted by “1” and “2”) with diffraction-limited sizes (FWHM \approx 500 nm)

is shown in Inset. The separation between these two particles is $\approx 1 \mu\text{m}$. Reprinted with permission¹⁰⁵ from “Copyright (2007) National Academy of Sciences”

Fluorescent NDs are also employed for targeted bio-imaging to study ligand-receptor binding kinetics. NDs bio-conjugated with transferrin were observed through laser scanning fluorescence microscopy to evidence the over expression of these receptors on cancerous cells.³¹⁵ Here, the NDs act both as a carrier for transferrin and as an imaging tool, hence no additional imaging probe is required to study these interactions. Fluorescent NDs are also considered as candidates of interest for long term cell tracking and sorting using flow cytometry.³¹⁶

More recently, theranostic applications of NDs are examined, which enables their utilization for multiple purposes like delivering therapeutic molecules, imaging biological processes and tracking treatment approaches at the same time. This is particularly done by artificial induction of enhanced fluorescing centers and simultaneously inducing specific surface functionalizations to confer affinity for therapeutic drugs and biomolecules.³¹⁷ A recent example of such an approach is the conjugation of ND with an anti-cancer drug cisplatin both through physical and chemical conjugation. Here, NDs acted as a delivery vehicle for cisplatin and also as a probe for cellular imaging.³¹⁸

In biomedical analyses, the nitrogen vacancy centers in NDs can also be used as a light source for imaging optical microscopic imaging.²⁴⁸ It provides a fluorescence alternative to scattering imaging of cells and can ensure less photo damage.²⁴⁸

10.1.3 Combined Fluorescence and Magnetic Imaging (Section 2.8.3.2)

Magnetism is an additional property of NDs that can impart further advantages for bio imaging. Magnetic NDs can serve as contrast agents in magnetic resonance imaging (MRI),³¹⁹ a commonly diagnostic tool. NDs can provide a safer alternative to traditional gadolinium which is a free solubilised ion and is considered highly toxic especially in renally impaired patients.³²⁰ NDs due to their biocompatibility can alleviate this health concern and serve as MRI reporting marker to elucidate metabolic fate and distribution of nanoparticulate delivery systems.³¹⁹

Alternative to complete replacement of traditional contrast agents, NDs can also be conjugated with these contrast agents for better resolution and localization.⁷⁸ Gadolinium/ND complexes are useful for long term cellular examination and evaluation of disease progression. NDs tend to

attract water molecules to the surface of gadolinium and increase the relaxivity of the contrast agent, resulting in higher resolution imaging compared to traditional gadolinium tracers.⁷⁸

Recent investigations focus on modulation of NDs by magnetic resonance and serve to develop a highly proficient technique called deterministic emitter switch microscopy, which can enable super-resolution imaging particularly useful for nanomedicinal research.³²¹

10.1.4 Scattering imaging (Section 2.8.3.3)

Elastically scattered light from a single 55 nm diamond is 300 folds brighter than that of a single cell organelle of the same size. As compared to the metal based scattering labels like gold and silver, ND also produces a stable image with minimum photo damage.²⁴⁷ Therefore, NDs are investigated to improve optical bioimaging.^{247, 322} NDs also produce a sharp Raman signal and an isolated signature peak at 1332 cm^{-1} , therefore can be detected in the cells through Raman mapping.^{323, 324} A nano-complex prepared by conjugating lysozyme to NDs is shown to provide useful information regarding the interaction of the enzyme with bacterial cells through Raman spectroscopic mapping.¹⁵⁰ In this complex, NDs not only act as carrier for the enzyme, but also serve as a nano-probe to track the biomolecular changes resulting from enzyme delivery.¹⁵⁰

While these techniques are mainly employed on laboratory scale for in vitro processes, there is a growing understanding that they might be expended into clinical applications for medical imaging and diagnosis.

10.1.5 Nanodiamonds for Small Molecule Delivery (Section 2.8.4.1)

Many studies have elucidated the use of NDs as effective drug delivery vehicles due to diverse surface characteristics. Opportunities to modify the surface of NDs according to functional groups of the drug attract their utilization for drug delivery to specific targets. High surface loading, physicochemical stability of the complexes in physiological system and opportunities to target ND complexes towards specific cells encourage the administration of minimal drug quantities to hit the optimum efficacy standards. These properties prevent the toxicity and adverse effects associated with the drug and also limit the drug wastage. NDs are investigated for both, localized and systemic delivery of drugs.

NDs can serve as a potential carrier for systemic drug delivery due to its nano size range, diverse surface area and several possibilities of surface functionalizations as described earlier.⁹⁵ NDs,

like other nanosized carriers can overcome the physiological barriers, reduce systemic exposure times and allow delivery of potent drugs like chemotherapeutic agent to targeted tissues. An apoptosis inducing anti-cancer drug doxorubicin hydrochloride (DOX) was conjugated successfully to NDs.^{325 326} This complex provided slow and sustained dissociation of the drug from the complex with maximum release after 16 hours of administration *in vitro*. This builds a potential to utilize NDs for reducing the dosing frequency and synthesizing controlled drug delivery system. ND-DOX complexes accumulated in the tumour after systemic administration and subsequently the efficacy of DOX increased to four times. Accumulation in kidneys and associated nephrotoxicity was reduced compared to free DOX.³²⁵ However, it was postulated that NDs alone also possess some anti-cancer properties which could add to the effect of the drug and contribute to prolonged life span in tumour induced mice.³²⁵ Elaborative investigations are required to study this effect more clearly. Release of potent drugs from ND complexes can be tightly controlled by producing pH dependent adsorption and desorption.³²⁷ It can be achieved by attaching acid phosphatase, an enzyme responsible for switching the drug on ND surface with other substrates in acidic medium.³²⁷ This study provides a proof of concept for designing nanocarriers for target-specific actions.

NDs complexes also overcome drug efflux processes in chemoresistant tumours.²¹³ The cancerous cells which were treated with ND-DOX complexes retained higher amount of the drug (0.26 µg/mL) compared to free DOX (0.02 µg/mL) after 4 hours of efflux. The overall intensity of DOX action is slightly reduced after complexation, however, these complexes are still able to elicit significant cell death for tumour suppression.²¹³

Polymers like polyethylene glycol (PEG) adsorbed on ND surface can increase the drug loading capacity of NDs.¹⁶⁵ The PEGylated ND complex allowed for a slower drug release producing a peak of drug concentration after 20 hours which remained constant up to 80 hours. This sustained release of drug highlights the potential to design controlled delivery systems particularly for potent drugs. The cell death mechanisms of chemotherapeutic drugs like DOX are preserved after ND conjugation.¹⁶⁵

Another example of utilizing NDs for cancer chemotherapy involves their conjugation with active plant alkaloids like paclitaxel, which have anti-cancer properties.³⁴ This complex is generated by covalent immobilization of the alkaloid on ND after a series of surface treatments.

This complexation mediated a dose dependent cellular uptake of paclitaxel and promoted cell death through mitotic arrest and apoptosis.³⁴ The activity of paclitaxel conjugated to NDs produced similar activity *in vitro* at 50 µg/ml concentration when compared to 50 nM of paclitaxel alone after 24 hours. The ND-paclitaxel complex also significantly reduced the tumour size at an average of 25 mm³.³⁴

NDs are also employed to reduce challenges associated with hydrophobic drug delivery. Administration of drugs with low aqueous solubility always presents a problem to leading to a reduced bioavailability.³²⁸ Low aqueous solubility also creates formulation challenges to prepare these drugs for systemic delivery. Water insoluble drugs can be conjugated with NDs for passage within the hydrophilic body environment to reach its targets. A variety of hydrophobic drugs like purvalanolA, 4- hydroxytamoxifen (4- OHT) and dexamethasone are investigated for delivery as ND complexes.¹⁰⁰ The particle size of these drugs greatly reduced from micrometer to nanometers after complexation with NDs (for example purvalanol changes from 340 µm to 556 nm), indicating greater dispersibility in aqueous medium. The effective surface charge also changed to positive values, presumably because the water molecules have higher affinity to hydrate the charged form of the drugs resulting from complexation compared to the neutral forms.¹⁰⁰

Multi-component ND based system were also designed for systemic delivery by conjugating on the surface diagnostic, therapeutic and targeting chemical species.³¹⁷ One of the examples of a versatile ND construct was synthesized by conjugating NDs with monoclonal antibodies to induce receptor mediated endocytosis in tumour cells and chemotherapeutic drugs like paclitaxel to induce tumour cell death. The drug is attached to the NDs through fluorescently labelled oligonucleotides for intracellular tracking of conjugated therapeutics.³¹⁷

In addition to systemic delivery, NDs are also frequently used to design topical drug delivery systems. An effective topical drug delivery system must possess a structure which is innately biocompatible, inert, allows adjustable release rates and is highly resistant to deformation. Design of multi-layered ND films presents as a successful approach to localize combinations of molecules in a single delivery system.³²⁹ ND films are synthesized using layer-by-layer deposition, in which initially poly-L-lysine is deposited on a plain negatively charged quartz surface. This layer creates a positive surface charge which was then interacted electrostatically

with NDs to form a secondary layer. This assembly creates inter-layer cavities for drug loading, and impart high stability to the system through electrostatic interactions between NDs and the peptide. A multi-layered ND film provide an advantage of high drug loading capacity and controlled release of the drug, and therefore is investigated for topical administration of an anti-inflammatory glucocorticoid called dexamethasone.³²⁹ The multi-layered film continuously eluted the drug in a sustained fashion over 24 hours. The film and inter-layer cavities can be constructed with full control, thus further reduction in drug elution rate can be achieved through incorporating the drug into the inner layers.³²⁹ These films can also be used to simultaneously administer both cationic and anionic drugs without using multiple delivery systems. However, limited studies are available regarding the synthesis of multi-drug delivery NDs systems.

ND microfilms are also synthesized as implants using polymers like parylene C for unidirectional, slow and continuous release of chemotherapeutic drugs for prolong time periods.³³⁰ This system was used to investigate the release of an anti-cancer drug DOX. The rate of drug elution was at least three times higher over the first day for uncovered ND-DOX complexes as compared to the complexes sandwiched between the polymer films. The film created an additional elution control layer, which resulted in constant drug release and prevention of an initial burst release.³³⁰ The incorporation of such potent drugs into this form can reduce the adverse effects associated with sudden rise in drug levels immediately after administration.

10.1.6 Nanodiamonds for Protein Delivery (Section 2.8.4.2)

NDs are also investigated for the delivery of proteins particularly hormones or enzymes. An example of such an application is the development of ND-insulin complexes designed for local delivery of insulin as a growth hormone to heal wounds.¹⁰¹ This system specifically elute insulin in alkaline medium of wounds associated with bacterial infections, thus increase the local concentration of the therapeutic protein. During the investigation, NaOH was used as an alkaline medium while water was used for comparison as a non-alkaline medium. The amount of insulin released by the first day was more than 20 times higher in the alkaline medium compared to water. This pattern also continued similarly on the fifth day with 46% insulin released in alkaline medium in comparison to only 2% drug released in the water. This change in the release of insulin from ND complexes can be correlated with the change occurring in the charge distribution due to pH variations. Insulin in the aqueous medium possesses a net negative charge, which

becomes much stronger upon increasing the alkalinity of the medium. Electrostatic interactions between NDs and insulin are disturbed at this instance causing desorption of the protein. The amounts of the insulin desorbed are directly proportional to the increase in the alkalinity of the medium from pH 9 to pH 11.5. Most importantly, the functional capacity of the protein was not compromised due to this pH switching and desorption.

As an analytical tool cytochrome C was investigated as a potential biomarker to evaluate conformational changes occurring to proteins in solution and on the surface.^{331 332} Conjugated to NDs, cytochrome C could generate an optimized probe for fluorescence and optical microscopy.¹² In addition to proteins, fluorescent peptides such as thiolated peptide are also conjugated to ND surface through connecting groups like maleimide ($\text{H}_2\text{C}_2(\text{CO})_2\text{NH}$) functionality for fluorescence bio-imaging.¹³

NDs are also employed as matrix for matrix-assisted laser desorption ionization (MALDI) mass spectrometry to specifically capture and analyse glycoproteins.³³³ This opens new avenues to utilize NDs for proteomic research.

10.2 Use of Scanning Transmission X-ray Microscopy for Characterizing Nano-Delivery Devices

X-ray absorption spectroscopy has always been a valuable tool for assessing novel nanomedicinal approaches.^{334, 335, 336} The technique has further developed over decades, with particular advancements made in synchrotron dependent X-ray based analysis.^{337, 338} Synchrotron sources offer generation of X-rays with enhanced brightness that allows tremendous improvement in spatial resolution and spectral fingerprints.^{339, 340} Synchrotron based X-ray absorption techniques mediate a diversified combination of spectroscopy and microscopy as spectromicroscopy and microspectroscopy.³⁴¹ The term spectromicroscopy relates to the microscopic imaging combined with detailed spectral sensitivity, which further encompasses microspectroscopy that allows recording spectra from small spots on the image.³⁴¹

Scanning Transmission X-ray Microscopy (STXM) is one of such modern characterization techniques. STXM follows near-edge X-ray absorption spectroscopy (NEXAFS) as its characteristic contrast mechanism, which describes the interaction of soft x-rays with matter at absorption edges.²³⁹ STXM utilizes synchrotron generated soft x-rays of λ ranging from ~ 50 to 100 \AA to cause the ionization of inner shell electrons, and collect fine scale details of the spectrum at each absorption edge.²⁴⁴ These spectral details can be used to deduce the chemical structure of unknown compounds or to locate and quantitate the elements of known features in substrate like cell or tissues. Upon first incidence of x-rays over an absorption edge, the structure associated with electronic excitation to the lowest unoccupied molecular level (π electrons of unsaturated double or triple bonds) is revealed, followed by the structure associated with the transition of electrons to highest unoccupied molecular levels (σ electrons of saturated single bonds).²⁴⁴ Since these transitions greatly depend upon conformation³⁴² and bonding environment,^{343, 344} the NEXAFS spectrums of individual samples can serve as a fingerprint.

Work flow of scanning X-ray microscope is straight forward. It picks up high energy x-rays from the source and produce an intensified focal spot of diameter 50 nm and $3\text{-}10 \text{ }\mu\text{m}$ wide²⁴⁴ on the image. This focal spot is generally created through a Fresnel zone plate which works to maximize the exposure of photons to smallest spot size on the sample.³⁴⁵ The sample is raster-scanned by the transmitted x-ray signals from the focal spot to create an image.^{239, 244} Microspectroscopy can be done by exposing x-ray beam at the spot of interest followed by scanning of photon energy

from the specified spot.²⁴⁴ For biological applications, all X-ray microscopic studies including STXM are usually done using photon energies in the range of K shell absorption edges of oxygen i.e. 543 eV and carbon i.e. 284 eV .³⁴⁶

STXM provides many advantages over conventional techniques used for characterizing nanoparticles (NPs) and investigating their cellular interaction.^{239, 240, 241} Most importantly, it can be applied to fully hydrated biological materials, which allows functional analysis of molecular mechanisms in a living cell under native biological environment.²⁴² Soft X-rays also provide spatial resolution better than 50 nm^{244, 243} and spectral resolution on the order of 100 meV,^{244, 245} that can sufficiently differentiate between classes of biomolecules and can identify NPs as therapeutic carriers in cell and tissues.²⁴⁰ Unlike electron microscopy, soft X-ray based techniques like STXM allows imaging of unsectioned cell with full thickness to produce high contrast images without any stains, exclusively based on intrinsic cellular components.³⁴⁷ Moreover, it also offers an understanding of solvent mediated NP interactions since it greatly depends upon the surrounding environment.³⁴⁸ Unlike confocal laser microscopy, STXM offers the possibility to distinguish between wide variety of individual NPs sized to few tens of nanometers and having different chemical compositions.³⁴⁸

10.2.1 STXM for characterizing hard nano-delivery systems

Challenges associated with the delivery of therapeutic drugs and genes to targeted cells and tissues are greatly addressed by advances made in nanotechnology.^{349, 350, 351, 352, 353} Several NP based delivery systems are designed to target gene therapy, particularly by RNA interference (RNAi) therapeutics as personalized treatments of chronic illnesses.^{354, 355, 356} NPs provide a cohesive system to protect naked genetic materials from endogenous enzymatic degradation and deliver it to the target cells.³⁵⁷ Elaborative physicochemical and biological characterization of NPs is required to ensure the development of safe, reproducible and controllable delivery vectors. Recently, STXM is employed as a potential tool for characterizing hard core NPs like carbon nanomaterials and evaluating their interactions with biological systems.

STXM due to its dependence upon NEFAXS spectroscopy offers good sensitivity to define the structural properties and composition of carbon based materials.³⁵⁸ Single-walled and multi-walled carbon nanotubes (CNTs) are the members of carbon nano family which are utilized as

gene carriers. Several surface functionalization attempts are done on CNTs to induce complexation with genetic materials.^{359, 360, 361, 10} Evidence suggests that STXM is advantageous to overcome complications for characterizing CNTs due to its small size and complex chemistry.³⁶² Unlike STXM, other X-ray absorption techniques can only analyze large sample size, which often presents interferences due to the signals of impurities (graphitic soot, reaction catalyst etc).³⁶² STXM can avoid these complications effectively by allowing microspectroscopy of selected clear zones having identified isolated CNT. Moreover, it is also efficient to provide better spatial resolution and less radiation damage as compared to other techniques like scanning photoemission microscopy or transmission electron spectromicroscopy.^{363, 364} Transmission electron microscopy (TEM) combined with STXM has been applied to provide detailed understanding of structural features of CNTs.³⁶² TEM was used to pick meaningful regions for analyzing individual CNT devoid of impurities and aggregated carbon nanomaterials. Stack microspectroscopy was done through STXM to obtain sequence imaging over a range of photon energies. The results were capable of providing complete quantitative chemical mapping of CNTs in the region of interest. Furthermore, the analysis was also successful in differentiating between an isolated CNT (rectangle), mixture of carbon impurities and CNTs (trapezoid) and the substrate (pentagon) by unique NEFAXS spectrums (Figure A1.1A). Comparison between the spectra from different regions in the image highlights similarities and differences which elaborate further details of the structures and morphologies (Figure A1.1B).³⁶²

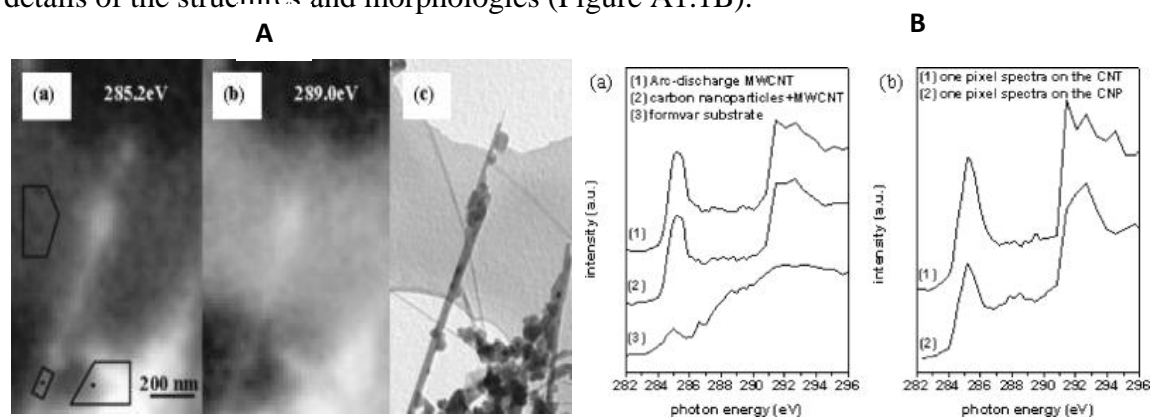


Figure A2. 1 (A) STXM images at 285.2eV (MWCNT signal enhanced) and 289.0eV (Formvar substrate signal enhanced), and corresponding TEM picture (B) (a) Spectra of arc-discharge MWCNT, MWCNT+CNP powder, and Formvar substrate (b) One pixel spectra taken on the MWCNT and on MWCNT and on the CNP. Reprinted with permission from³⁶² Copyright © 2006 American Institute of Physics

STXM is also applied to study the surface functionalization of CNTs in combination with other techniques (Infrared, Thermogravimetry and Raman Spectroscopy).³⁶⁵ Key advantage of using STXM over other characterization techniques is the possibility to visualize specific regions of functionalization, which can interpret dependence of the process upon factors like orientation and exposed environments. Figure A1.2 highlights specific regions of functionalization and spectral fingerprints before and after dodecyl derivatization of CNTs.³⁶⁵ Similar concept can also be applied to determine cellular uptake of carbon nanomaterials.³⁶⁶ Since STXM can differentiate differently bonded carbon atoms, members of carbon nano family can be mapped and distinguished with other carbon containing biomolecules in the cell (e.g. proteins, lipids etc).

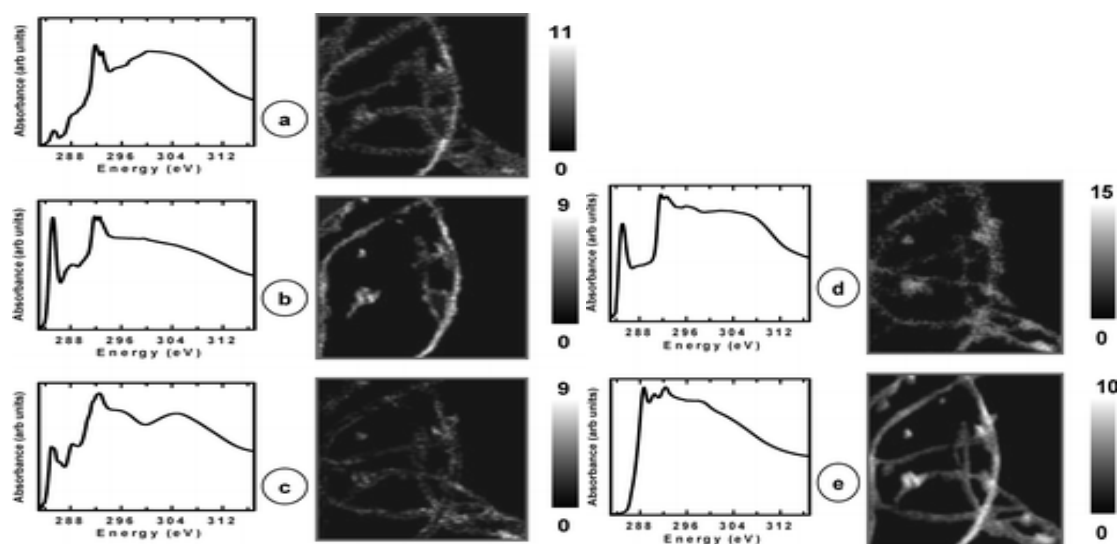


Figure A2. 2 STXM of the dodecyl-functionalized WCPP (wet chemical purification procedure- SWCNT (single-walled CNT): (left panels) C 1s reference spectra used to fit the C 1s image sequence in order to derive the associated component maps (right panels). Component maps of (a) horizontal SWCNT (π^* -weak); (b) vertical SWCNT (π^* -strong); (c) oxidized SWCNT; (d) carbon onions and other carbon contaminations (CNP); (e) dodecyl. Reprinted with permission from³⁶⁵ Copyright © 2010 American Chemical Society.

Quality of CNTs can also be analysed through STXM by investigating spectral differences due to vertical and horizontal orientations (dichroic effect). The samples having strong dichroic effect indicate optimum quality and low impurities.³⁶⁵

Fullerenes, also known as buckyballs are another class of carbon nanomaterials widely researched for its potential application as delivery vectors.^{367, 368, 369} Metallofullerene is a novel modification which comprise of a metallic molecule trapped inside a fullerene cage. They are recently investigated to overcome resistance of cancer cells towards platinum based anti-cancer drugs.³⁷⁰ Metallofullerenes have unique electron transfer properties from the encaged metal ions to surrounding carbons,³⁷¹ which protect the metallic therapeutic moiety against leakage and dissociation.³⁷² Additional to drug delivery applications, metallofullerenes are also investigated for immunomodulatory responses. Though immune active responses can propagate fullerene induced inflammation,^{373, 374} but this activity is also researched as targeted immune therapy for tumour-bearing patients.³⁷⁵ Poly-hydroxylated metallofullerenol ($Gd@C_{82}(OH)_{22}$) have been shown to polarize the release of cytokines, stimulate T-helper cells and macrophages and induce tumor cell apoptosis.³⁷⁵ Recently, STXM was applied to study the cellular uptake of poly-hydroxy metallofullerenes and its ability to activate macrophages to release pro-inflammatory cytokines.³⁷² NEFAXS spectrum of Gadolinium (Gd) was first generated at M-edge to obtain an estimation of its absorption energy. Mouse macrophages were then scanned at specified photon energies after *in vitro* and *in vivo* peritoneal delivery to obtain Gd distribution map, which correlates with the cellular distribution of metallofullerenols (Figure A1.3).³⁷²

For gene delivery applications, quantum dots (QDs) are also widely researched.^{376, 377, 378} STXM was employed in analyzing sub cellular localization of cadmium based QDs having telluride element as one of its component. Chemical mapping of telluride element at its specified absorption energies are indicative of the cellular distribution of QDs.³⁷⁹ These studies suggest that STXM is suitable to be applied for element-specific analysis.

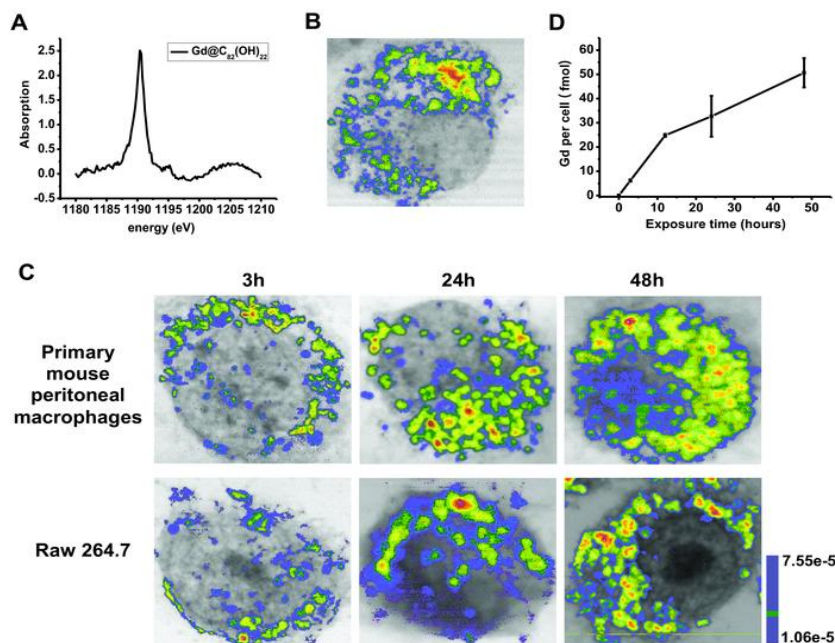


Figure A2.3 Internalization of metallofullerenol by macrophages (in vivo and in vitro). (A) A Gd M-edge NEXAFS spectrum obtained from Gd@C₈₂(OH)₂₂ nanoparticles. (B) Soft X-ray STXM dual energy contrast images of Gd@C₈₂(OH)₂₂ internalized by a primary mouse peritoneal macrophage *in vivo*. (C) Soft X-ray STXM dual energy contrast images of time-dependent uptake of Gd@C₈₂(OH)₂₂ by primary mouse peritoneal macrophages and RAW 264.7 cell line *in vitro*. (D) ICP-MS quantification of time-dependent uptake in macrophages of primary mouse peritoneal macrophages. Reprinted with permission from ³⁷² Copyright © 2014 WILEY-VCH Verlag GmbH & Co. KGaA Weinheim.

STXM is also applied to characterize NP mediated ionic therapy for malignant cancers. ³⁸⁰ Adsorption of sodium ions on nanodiamond (ND) surface was investigated at photon energies above and below K-edge of sodium. Intracellular delivery of sodium ions was also analysed using STXM images of the cells taken at sodium specific photon energies. The amount of intracellular sodium was compared as a function of presence and absence of serum proteins in the cell culture medium. ³⁸⁰

STXM served as an impressive tool to evaluate tissue penetration and distribution of hard NPs applied for topical treatment approaches. ²⁴⁰ Analysis of membrane interaction at individual particle level is possible. Variable sized gold and silica core NPs having silica and gold shell respectively were analyzed for penetration in human skin using STXM in combination with other

conventional microscopic imaging. Scanning of images at photon energies specific to gold and silicon revealed degree of penetration and distribution of NPs in different layer of the skin.

Conclusively, synchrotron dependent x-ray microscopy serves as a convenient tool to evaluate hard nanomaterials employed in different therapies as carriers. The technique provides ease of performing microscopic imaging in combination with detailed spectral analysis to build meaningful interpretations regarding novel treatment approaches.

11 Bibliography

1. Gerber D, Targeted therapies: a new generation of cancer treatments. *Am Fam Physician* **2008**, 77 (3), 311-9.
2. Brannon-Peppas L, Blanchette J, Nanoparticle and targeted systems for cancer therapy. *Adv Drug Deliv Rev* **2004**, 56 (11), 1649-59.
3. Pinto-Alphandary H, Andreumont A, Couvreur P, Targeted delivery of antibiotics using liposomes and nanoparticles: research and applications. *Int J Antimicrob Agents* **2000**, 13 (3), 155-68.
4. Toti U, Guru B, Hali M, McPharlin C, Wykes S, Panyam J, Whittum-Hudson J, Targeted delivery of antibiotics to intracellular chlamydial infections using PLGA nanoparticles. *Biomaterials* **2011**, 32 (27), 6606-13.
5. Kresina T, Branch A, Chapter 1 Molecular medicine and gene therapy: an introduction. In *An Introduction to Molecular Medicine and Gene Therapy*, Kresina, T., Ed. John Wiley & Sons: 2004; pp 1-24.
6. Tidd D, Warenus H, Partial protection of oncogene, anti-sense oligodeoxynucleotides against serum nuclease degradation using terminal methylphosphonate groups. *Br J Cancer* **1989**, 60 (3), 343-50.
7. Waehler R, Russell S, Curiel D, Engineering targeted viral vectors for gene therapy. *Nat Rev Genet* **2007**, 8 (8), 573-87.
8. Thomas C, Ehrhardt A, Kay M, Progress and problems with the use of viral vectors for gene therapy. *Nat Rev Genet* **2003**, 4 (5), 346-58.
9. Bianco A, Kostarelos K, Prato M, Applications of carbon nanotubes in drug delivery. *Curr Opin Chem Biol* **2005**, 9 (6), 674-9.
10. Kam N, Liu Z, Dai H, Functionalization of carbon nanotubes via cleavable disulfide bonds for efficient intracellular delivery of siRNA and potent gene silencing. *J Am Chem Soc* **2005**, 127 (36), 12492-3.

11. Chang I, Hwang K, Ho J, Lin C, Hwu R, Horng J, Facile surface functionalization of nanodiamonds. *Langmuir* **2010**, *26* (5), 3685-3869.
12. Huang L, Chang H, Adsorption and immobilization of cytochrome c on nanodiamonds. *Langmuir* **2004**, *20* (14), 5879-5884.
13. Vial S, Mansuy C, Sagan S, Irinopoulou T, Burlina F, Boudou J, Chassaing G, Lavielle S, Peptide-grafted nanodiamonds: preparation, cytotoxicity and uptake in cells. *Chembiochem* **2008**, *9* (13), 2113-2119.
14. Krueger A, Stegk J, Liang Y, Lu L, Jarre G, Biotinylated nanodiamond: simple and efficient functionalization of detonation diamond. *Langmuir* **2008**, *24* (8), 4200-4204.
15. Liu Y, Gu Z, Margrave JL, Khabashesku VN, Functionalization of Nanoscale Diamond Powder: Fluoro-, Alkyl-, Amino-, and Amino Acid-Nanodiamond Derivatives. *Chem Mater* **2004**, *16* (20), 3924-3930.
16. .
17. Suarez-Martinez I, Grobert N, Ewels CP, Encyclopedia of carbon nanoforms. In *Advances in Carbon Nanomaterials: Science and Applications*, CRC Press: 2010; p 9.
18. Lin T, Bajpai V, Ji T, Dai L, Chemistry of carbon nanotubes. *Aust J Chem* **2003**, *56*, 635-651.
19. Mittal V, Carbon Nanotubes Surface Modifications: An Overview. In *Surface Modification of Nanotube (First Edition)*, Wiley-VCH Verlag GmbH & Co. KGaA: 2011; pp 1-2.
20. yadav B, Kumar R, Structure, properties and applications of fullerenes. *Int J Nanotech App* *2* (1), 15-24.
21. Zhang Y, Bai Y, Yan B, Functionalized carbon nanotubes for potential medicinal applications. *Drug Discov Today* **2010**, *15* (11-12), 428 - 435.
22. Barnard AS, Sternberg M, Crystallinity and surface electrostatics of diamond nanocrystals. *J Mater Chem* **2007**, *17*, 4811-4819.
23. Astefanei A, Núñez O, Galceran MT, Characterization and determination of fullerenes: A critical review. *Analytica Chimica Acta* **2015**, *882*, 1-21.

24. Kulakova II, Modification of Surface and the Physicochemical Properties of Nanodiamonds "Surface Chemistry of Nanodiamonds. *J Phys Part C Solid* **2004**, 46 (4), 636-643.
25. Spitsyn BV, *Problems and Achievements of Physicochemical and Engineering Science in the Field of Nanomaterials*; Moscow, 2002; p 102.
26. Kratochvílová I, Kovalenko A, Fendrych F, Petráková V, Záliš S, Nesládek M, Tuning of nanodiamond particles' optical properties by structural defects and surface modifications: DFT modelling. *J Mater Chem* **2011**, 21 (45), 18248-18255.
27. Chao JI, Perevedentseva E, Chang CC, Cheng CY, Liu KK, Chung PH, Tu JS, Chu CD, Cai SJ, Cheng CL, Chapter 9: Protein-Nanodiamond COMplexes for Cellular Surgery. In *Nanodiamonds: Applications in Biology and Nanoscale Medicine*, Ho D, Ed. Springer Science & Business Media: Evanston, IL, 2009; pp 206-208.
28. Rummeli MH, Ayala P, Pichler T, Carbon nanotubes and related structure: production and formation. In *Carbon nanotubes and related structures: synthesis, characterization, functionalization and applications*, Martin N, Guldi DM, Eds. John Wiley & Sons: 2010; p 1.
29. Georgakilas V, Tagmatarchis N, Pantarotto D, Bianco A, Briand J, Prato M, Amino acid functionalisation of water soluble carbon nanotubes. *Chem Commun (Camb)* **2002**, 24, 3050-1.
30. Ivanova M, Lamprecht C, Loureiro M, Huzil T, Foldvari M, Pharmaceutical characterization of solid and dispersed carbon nanotubes as nanoexcipients. *Int J Nanomedicine* **2012**, 7, 403-415.
31. Arsawang U, Saengsawang O, Rungrotmongkol T, Sornmee P, Wittayanarakul K, Remsungnen T, Hannongbua S, How do carbon nanotubes serve as carriers for gemcitabine transport in a drug delivery system? *J Mol Graph Model.* **2011**, 29 (5), 591-6.
32. Liu Z, Sun X, Nakayama-Ratchford N, Dai H, Supramolecular Chemistry on Water-Soluble Carbon Nanotubes for Drug Loading and Delivery. *ACS Nano* **2007**, 1 (1), 50-56.
33. Liu Z, Chen K, Davis C, Sherlock S, Cao Q, Chen X, Dai H, Drug delivery with carbon nanotubes for in vivo cancer treatment. *Cancer Res* **2008**, 68 (16), 6652-60.

34. Liu K, Zheng W, Wang C, Chiu Y, Cheng C, Lo Y, Chen C, Chao J, Covalent linkage of nanodiamond-paclitaxel for drug delivery and cancer therapy. *Nanotechnology* **2010**, *21* (31), 315106.
35. Ali-Boucetta H, Al-Jamal K, McCarthy D, Prato M, Bianco A, Kostarelos K, Multiwalled carbon nanotube-doxorubicin supramolecular complexes for cancer therapeutics. *Chem Commun (Camb)* **2008**, *4*, 459-61.
36. Salaam A, Hwang P, Poonawalla A, Green H, Jun H, Dean D, Nanodiamonds enhance therapeutic efficacy of doxorubicin in treating metastatic hormone-refractory prostate cancer. *Nanotechnology* **2014**, *25* (42), 425103.
37. Huang H, Pierstorff E, Osawa E, Ho D, Active nanodiamond hydrogels for chemotherapeutic delivery. *Nano lett* **2007**, *7* (11), 3305-3314.
38. Adnan A, Lam R, Chen H, Lee J, Schaffer D, Barnard A, Schatz G, Ho D, Liu W, Atomistic simulation and measurement of pH dependent cancer therapeutic interactions with nanodiamond carrier. *Mol Pharm* **2011**, *8* (2), 368-74.
39. Tannock I, Rotin D, Acid pH in tumors and its potential for therapeutic exploitation. *Cancer Res* **1989**, *49* (16), 4373-84.
40. Hampel S, Kunze D, Haase D, Krämer K, Rauschenbach M, Ritschel M, Leonhardt A, Thomas J, Oswald S, Hoffmann V, Büchner B, Carbon nanotubes filled with a chemotherapeutic agent: a nanocarrier mediates inhibition of tumor cell growth. *Nanomedicine (Lond)* **2008**, *3* (2), 175-82.
41. O'Connell M, Boul P, Ericson L, Huffman C, Wang Y, Haroz E, Kuper C, Tour J, Ausman K Smalley R, Reversible water-solubilization of single-walled carbon nanotubes by polymer wrapping. *Chem Phys Lett* **2001**, *342* (3-4), 265-271.
42. Partha R, Mitchell L, Lyon J, Joshi P, Conyers J, Buckysomes: fullerene-based nanocarriers for hydrophobic molecule delivery. *ACS Nano* **2008**, *2* (9), 1950-8.
43. Partha R, Lackey M, Hirsch A, Casscells SW, Conyers JL, Self assembly of amphiphilic C60 fullerene derivatives into nanoscale supramolecular structures. *J Nanobiotechnology* **2007**, *5*, 6.

44. Tóth E, Bolskar R, Borel A, González G, Helm L, Merbach A, Sitharaman B, Wilson L, Water-soluble gadofullerenes: toward high-relaxivity, pH-responsive MRI contrast agents. *J Am Chem Soc* **2005**, *127* (2), 799-805.
45. Bolskar R, Benedetto A, Husebo L, Price R, Jackson E, Wallace S, Wilson L, Alford J, First soluble M@C₆₀ derivatives provide enhanced access to metallofullerenes and permit in vivo evaluation of Gd@C₆₀[C(COOH)₂]₁₀ as a MRI contrast agent. *J Am Chem Soc* **2003**, *125* (18), 5471-8.
46. Sitharaman B, Tran L, Pham Q, Bolskar R, Muthupillai R, Flamm S, Mikos A, Wilson L, Gadofullerenes as nanoscale magnetic labels for cellular MRI. *Contrast Media Mol Imaging* **2007**, *2* (3), 139-146.
47. Komatsu K, Murata M, Murata Y, Encapsulation of molecular hydrogen in fullerene C₆₀ by organic synthesis. *Science* **2005**, *307* (5707), 238-240.
48. Lopez A, Mateo-Alonso A, Prato M, Materials chemistry of fullerene C₆₀ derivatives. *J Mater Chem* **2011**, *21*, 1305-1318.
49. Yang H, Lu C, Liu Z, Jin H, Che Y, Olmstead M, Balch A, Detection of a family of gadolinium-containing endohedral fullerenes and the isolation and crystallographic characterization of one member as a metal-carbide encapsulated inside a large fullerene cage. *J Am Chem Soc* **2008**, *130* (51), 17296-300.
50. Ouyang D, Shah N, Zhang H, Smith S, Parekh H, Reducible disulfide-based non-viral gene delivery systems. *Mini Rev Med Chem* **2009**, *9* (10), 1242-50.
51. Kawakami S, Hashida M, In vivo gene transfer by ligand-modified gene carriers. In *Non-viral Gene Therapy: Gene Design and Delivery*, Taira K, Kataoka K, Niidome T, Eds. Springer Science & Business Media: 2006; pp 228-229.
52. Ruponen M, Honkakoski P, Rönkkö S, Pelkonen J, Tammi M, Urtti A, Extracellular and intracellular barriers in non-viral gene delivery. *J Control Release* **2003**, *93* (2), 213-7.
53. Lee C, Liu Y, Reineke T, General structure-activity relationship for poly(glycoamidoamine)s: the effect of amine density on cytotoxicity and DNA delivery efficiency. *Bioconjug Chem* **2008**, *19* (2), 428-40.

54. Dominska M, Dykxhoorn D, Breaking down the barriers: siRNA delivery and endosome escape. *J Cell Sci.* **2010**, *123* (8), 1183-9.
55. Liang W, Lam JKW, Endosomal Escape Pathways for Non-Viral Nucleic Acid Delivery Systems. In *Biochemistry, Genetics and Molecular Biology- Molecular Regulation of Endocytosis*, INTECH Open Access Publisher: 2012.
56. Xu Y, Szoka FC, Mechanism of DNA release from cationic liposome/DNA complexes used in cell transfection. *Biochemistry* **1996**, *35* (18), 5616–5623.
57. Kyriakides T, Cheung C, Murthy N, Bornstein P, Stayton P, Hoffman A, pH-sensitive polymers that enhance intracellular drug delivery in vivo. *J Control Release* **2002**, *78* (1-3), 295-303.
58. Nishimura Y, Takeda K, Ezawa R, Ishii J, Ogino C, Kondo A, A display of pH-sensitive fusogenic GALA peptide facilitates endosomal escape from a Bio-nanocapsule via an endocytic uptake pathway. *J Nanobiotechnology* **2014**, *12*, 11.
59. Erazo-Oliveras A, Muthukrishnan N, Baker R, Wang TY, Pellois JP, Improving the Endosomal Escape of Cell-Penetrating Peptides and Their Cargos: Strategies and Challenges. *Pharmaceuticals (Basel)* **2012**, *5* (11), 1177–1209.
60. Liu Z, Zhang Z, Zhou C, Jiao Y, Hydrophobic modifications of cationic polymers for gene delivery. *Adv Polym Sci* **2010**, *35* (9), 1144–1162.
61. Shim M, Kwon Y, Dual mode polyspermine with tunable degradability for plasmid DNA and siRNA delivery. *Biomaterials* **2011**, *32* (16), 4009-20.
62. Zabner J, Fasbender A, Moninger T, Poellinger K, Welsh M, Cellular and molecular barriers to gene transfer by a cationic lipid. *J Biol Chem.* **1995**, *270* (32), 18997-9007.
63. Schaffer D, Fidelman N, Dan N, Lauffenburger D, Vector unpacking as a potential barrier for receptor-mediated polyplex gene delivery. *Biotechnol Bioeng* **2000**, *67* (5), 598-606.
64. Pollard H, Remy J, Loussouarn G, Demolombe S, Behr J, Escande D, Polyethylenimine but not cationic lipids promotes transgene delivery to the nucleus in mammalian cells. *J Biol Chem* **1998**, *273* (13), 7507-11.

65. Lechardeur D, Lukacs G, Intracellular barriers to non-viral gene transfer. *Curr Gene Ther* **2002**, 2 (2), 183-94.
66. Yin H, Kanasty R, Eltoukhy A, Vegas A, Dorkin J, Anderson D, Non-viral vectors for gene-based therapy. *Nat Rev Genet* **2014**, 15 (8), 541-55.
67. Zhang Y, Li J, Shen Y, Wang M, Li J, Poly-l-lysine Functionalization of Single-Walled Carbon Nanotubes. *J. Phys. Chem. B* **2004**, 108 (39), 15343–15346.
68. Martín R, Alvaro M, Herance J, García H, Fenton-treated functionalized diamond nanoparticles as gene delivery system. *ACS Nano* **2010**, 4 (1), 65-74.
69. Zhang X, Chen M, Lam R, Xu X, Osawa E, Ho D, Polymer-functionalized nanodiamond platforms as vehicles for gene delivery. *ACS Nano* **2009**, 3 (9), 2609-16.
70. Liu Z, Tabakman SM, Chen Z, Dai H, Preparation of carbon nanotube bioconjugates for biomedical applications. *Nat Protoc* **2009**, 4, 1372 - 1381.
71. Schrand A, Dai L, Schlager J, Hussain S, Osawa E, Differential biocompatibility of carbon nanotubes and nanodiamonds. *Diam Relat Mater* **2007**, 16 (12), 2118–2123.
72. Liu KK, Cheng CL, Chang CC, Chao JI, Biocompatible and detectable carboxylated nanodiamond on human cell. *Nanotechnology* **2007**, 18 (32), 325102.
73. Bianco A, Kostarelos K, Prato M, Making carbon nanotubes biocompatible and biodegradable. *Chem Commun (Camb)* **2011**, 47 (37), 10182-8.
74. Luo M, Deng X, Shen X, Dong L, Liu Y, Comparison of cytotoxicity of pristine and covalently functionalized multi-walled carbon nanotubes in RAW 264.7 macrophages. *J Nanosci Nanotechnol* **2012**, 12 (1), 274-83.
75. Bottini M, Rosato N, Bottini N, EG-modified carbon nanotubes in biomedicine: current status and challenges ahead. *Biomacromolecules* **2011**, 12, 3381-93.
76. Narayan RJ, Boehm, R. D.; Sumant, A. V., Medical Applications of Diamond Particle and surfaces. *Mater Today* **2011**, 14 (4), 154-163.
77. Dolmatov VY, Detonation synthesis ultradispersed diamonds: properties and applications. *Russ Chem Rev* **2001**, 70 (7), 607 - 626.

78. Manus L, Mastarone D, Waters E, Zhang X, Schultz-Sikma E, Macrenaris K, Ho D, Meade T, Gd(III)-nanodiamond conjugates for MRI contrast enhancement. *Nano Lett* **2010**, *10* (2), 484-489.
79. Wu CC, Han CC, Chang HC, Applications of surface-functionalized diamond nanoparticles for mass-spectrometry-based proteomics. *J Chin Chem Soc-Taip* **2010**, *57*, 583-594.
80. Saini G, Jensen D, Wiest L, Vail M, Dadson A, Lee M, Shutthanandan V, Linford M, Core-shell diamond as a support for solid-phase extraction and high-performance liquid chromatography. *Anal Chem* **2010**, *82* (11), 4448-56.
81. Fedyanina ON, Nesterenko PN, Regularities of chromatographic retention of phenols on microdispersed sintered detonation nanodiamond in aqueous—organic solvents. *Russ J Phys Chem A* **2010**, *84* (3), 476-480.
82. Paci JT, Man HB, Saha B, Ho D, Schatz GC, Understanding the Surfaces of Nanodiamonds. *J Phys Chem C* **2013**, *117* (33), 17256–17267.
83. Szabo T, Berkesi O, Forgo P, Josepovits K, Sanakis Y, Petridis D, Dekany I, Evolution of Surface Functional Groups in a Series of Progressively Oxidized Graphite Oxides. *Chem Mater* **2006**, *18* (11), 2740-2749.
84. Kaur R, Badea I, Nanodiamonds as novel nanomaterials for biomedical applications: drug delivery and imaging systems. *Int J Nanomed* **2013**, *8*, 203-220.
85. Kruger A, Kataoka F, Ozawa M, Fujino T, Suzuki Y, Aleksenskii AE, Vul AY, Osawa E, Unusually tight aggregation in detonation nanodiamond: Identification and disintegration. *Carbon* **2005**, *43* (8), 1722-1730.
86. Ōsawa E, Recent progress and perspectives in single-digit nanodiamond. *Diam Relat Mater* **2007**, *16* (12), 2018-2022.
87. Iakoubovskii K, Mitsuishi K, Furuya K, High-resolution electron microscopy of detonation nanodiamond. *Nanotechnology* **2008**, *19*, 155705.

88. Shiryaev AA, Iakoubovskii K, Grambole D, Dubrovinskaia N, Spectroscopic study of defects and inclusions in bulk poly- and nanocrystalline diamond aggregates. *J Phys-Condens Mat* **2006**, *18* (40), L493.
89. Vereschagin AL, Sakovich GV, Komarov VF, Petrov EA, Properties of ultrafine diamond clusters from detonation synthesis. *Diam Relat Mater* **1994**, *3* (1-2), 160-162.
90. Galli G, Structure, Stability and Electronic Properties of Nanodiamonds. In *Computer-Based Modeling of Novel Carbon Systems and Their Properties, Carbon Materials: Chemistry and Physics 3*, Colombo L, Fasolino A, Eds. Springer: 2010; pp 37-56.
91. Yan CS, Vohra YK, Multiple twinning and nitrogen defect center in chemical vapor deposited homoepitaxial diamond. *Diam Relat Mater* **1999**, *8* (11), 2022–2031.
92. Zhou G, Lelkes PI, Gogotsi Y, Mochalin V, Functionalized Nanodiamond Reinforced Biopolymers. US 13/498,436, October 25, 2012.
93. Mochalin V, Shenderova O, Ho D, Gogotsi Y, The properties and applications of nanodiamonds. *Nat Nanotechnol* **2011**, *7* (1), 11-23.
94. Grausova L, Bacakova L, Kromka A, Potocky S, Vanecek M, Nesladek M, Lisa V, Nanodiamond as promising material for bone tissue engineering. *J Nanosci Nanotechnol* **2009**, *9* (6), 3524-3534.
95. Ho D, Lam R, Nano diamonds as vehicles for systemic and localized drug delivery. *Informa Healthcare* **2009**, *6* (9), 883-895.
96. Zhang Q, Mochalin V, Neitzel I, Knoke I, Han J, Klug C, Zhou J, Lelkes P, Gogotsi Y, Fluorescent PLLA-nanodiamond composites for bone tissue engineering. *Biomaterials* **2011**, *32* (1), 87-94.
97. Dvorak-Ewell M, Chen T, Liang N, Garvey C, Liu B, Tu C, Chang W, Bikle D, Shoback D, Osteoblast extracellular Ca²⁺ -sensing receptor regulates bone development, mineralization, and turnover. *J Bone Miner Res* **2011**, *26* (12), 2935-2947.
98. Rodan G, Martin T, Role of osteoblasts in hormonal control of bone resorption - a hypothesis. *Calcified Tissue Int* **1982**, *34* (3), 311.

99. Yuan Y, Chen Y, Liu JH, Wang H, Liu Y, Biodistribution and Fate of Nanodiamond in vivo. *Diam Relat Mater* **2009**, *18* (1), 95-100.
100. Chen M, Pierstorff ED, Lam R, Li SY, Huang H, Osawa E, Ho D, Nanodiamond-mediated delivery of water-insoluble therapeutics. *ACS nano* **2009**, *3* (7), 2016-2022.
101. Shimkunas R, Robinson E, Lam R, Lu S, Xu X, Zhang X, Huang H, Osawa E, Ho D, Nanodiamond-insulin complexes as pH-dependent protein delivery vehicles. *Biomaterials* **2009**, *30* (29), 5720-5728.
102. Chen M, Zhang XQ, Man HB, Lam R, Chow EK, Ho D, Nanodiamond Vectors Functionalized with Polyethylenimine for siRNA Delivery. *J Phys Chem Lett-US* **2010**, *1* (21), 3167-3171.
103. Gibson N, Luo T, Brenner D, Shenderova O, Immobilization of mycotoxins on modified nanodiamond substrates. *Biointerphases* **2011**, *6* (4), 210-217.
104. Puzyr AP, Baron AV, Purtov KV, Bortnikov EV, Skobelev NN, Mogilnaya OA, Bondar VS, Nanodiamonds with novel properties: A biological study. *Diam Relat Mater* **2007**, *16* (12), 2124–2128.
105. Fu CC, Lee HY, Chen K, Lim TS, Wu HY, Lin PK, Wei PK, Tsao PH, Chang HC, Fann W, Characterization and application of single fluorescent nano diamonds as cellular biomarkers. *PNAS* **2007**, *104* (3), 727–732.
106. Smestad GP, Chapter 2: Absorbing Solar Energy. In *Optoelectronics of Solar Cells*, SPIE Press: 2002; p 32.
107. Chao JI, Perevedentseva E, Chang CC, Cheng CY, Liu KK, Chung PH, Tu JS, Chu CD, Cai SJ, Cheng CL, Chapter 9: Protein-Nanodiamond COMplexes for Cellular Surgery. In *Nanodiamonds: Applications in Biology and Nanoscale Medicine*, Ho D, Ed. Springer Science & Business Media: Evanaton, 2009; pp 205-207.
108. Faklarisa O, Botsoa J, Sauvage T, Roch JF, Treussart F, Photoluminescent nanodiamonds: Comparison of the photoluminescence saturation properties of the NV color center and a cyanine dye at the single emitter level, and study of the color center concentration under different preparation conditions. *Diam Relat Mater* **2010**, *19* (7-9), 988–995.

109. Zhang X, *Biological effects of three kinds of carbon nanomaterials*; Shanghai, 2010; pp 61-64.
110. Trono J, Mizuno K, Yusa N, Matsukawa T, Yokoyama K, Uesaka M, Size, concentration and incubation time dependence of gold nanoparticle uptake into pancreas cancer cells and its future application to X-Ray Drug Delivery System. *J Radiat Res* **2011**, 52 (1), 103-109.
111. Alkilany AM, Murphy CJ, Toxicity and cellular uptake of gold nano particles: What we have learned so far? *J Nanopart Res* **2010**, 12 (7), 2313-2333.
112. Xing Y, Xiong W, Zhu L, Osawa E, Hussin S, Dai L, DNA damage in embryonic stem cells caused by nanodiamonds. *ACS Nano* **2011**, 5 (3), 2376-2384.
113. El-Say KM, Nanodiamonds as drug delivery system: Applications and Prospective. *J Appl Pharm Sci* **2011**, 1 (6), 29-39.
114. Ho D, *Nanodiamonds: Applications in Biology and Nanoscale Medicine*. Springer; 2010 edition: 2010.
115. Chao JI, Perevedentseva E, Chang CC, Cheng CY, Liu KK, Chung PH, Tu JS, Chu CD, Cai SJ, Cheng CL, Chapter 9: Protein-Nanodiamond complexes for Cellular Surgery. In *Nanodiamonds: Applications in Biology and Nanoscale Medicine*, Ho D, Ed. Springer Science & Business Media: 2009; p 197.
116. Kruger A, Liang Y, Jarre G, Stegk J, Surface functionalisation of detonation diamond suitable for biological application. *J Mater Chem* **2006**, 16, 2322–2328.
117. Barnard AS, Self-assembly in nanodiamond agglutinates. *Journal of Material Chemistry* **2008**, 18, 4038-4041.
118. Chang LY, Ōsawa E, Barnard AS, Confirmation of the electrostatic self-assembly of nanodiamonds. *Nanoscale* **2011**, 3, 958-962.
119. Huang H, Dai L, Wang DH, Tanc LS, Osawa E, Large-scale self-assembly of dispersed nanodiamonds. *J Mater Chem* **2008**, 18, 1347–1352.

120. Kuznetsov V, Chivilin A, Moroz E, Kolomiichuk V, Shikhutdinov S, Butenko Y, et al., Effect of explosion conditions on the structure of detonation soots: Ultradisperse diamond and onion carbon. *Carbon* **1994**, *32* (5), 873–882.
121. Raty J, Galli G, Bostedt C, Van Buuren T, Terminello L, Quantum confinement and fullerenelike surface reconstructions in nanodiamonds. *Phys Rev Lett* **2003**, *90* (3), 037401.
122. Ozawa M, Goto H, Kusunoki M, Osawa E, Continuously Growing Spiral Carbon Nanoparticles as the Intermediates in the Formation of Fullerenes and Nanoonions. *J Phys Chem B* **2002**, *106* (29), 7135–7138.
123. Eidelman ED, Siklitsky VI, Sharonova, LV, Yagovkina, MA, Vul', AY, Takahashi M, Inakuma M, Ozawa M, Ōsawa E, A stable suspension of single ultrananocrystalline diamond particles. *Diam Relat Mater* **2005**, *14* (11-12), 1765-1769.
124. Liang Y, Ozawa M, Krueger A, General Procedure to Functionalize Agglomerating Nanoparticles Demonstrated on Nanodiamond. *ACS nano* **2009**, *3* (8), 2288–2296.
125. Osawa E, Disintegration and purification of Crude Aggregates of Detonation Nanodiamonds. In *Synthesis, Properties and Applications of Ultrananocrystalline Diamond: Proceedings of the NATO ARW on Synthesis, Properties and Applications of Ultrananocrystalline Diamond*, Gruen DM, Shenderova OA, Vul AY, Eds. Springer Science & Business Media: 2005; Vol. 192, pp 231-240.
126. Knieke C, Steinborn C, Romeis S, Peukert W, Faes SB, Kwade A, Nanoparticle production in stirred media mills: Opportunities and limitations. *C Chem Eng Technol Special Issue: Grinding and Milling* **2010**, *33* (9), 1401–1411.
127. Pentecost A, Gour S, Mochalin V, Knoke I, Gogotsi Y, Deaggregation of Nanodiamond powders using Salt and Sugar assisted milling. *ACS Apl Mater Ins* **2010**, *2* (11), 3289-3294.
128. Zhang P, Yang J, Li W, Wang W, Liu C, Griffith M, Liu W, Cationic polymer brush grafted-nanodiamond via atom transfer radical polymerization for enhanced gene delivery and bioimaging. *J Mater Chem* **2011**, *21*, 7755-7764.

129. Zhang B, Li Y, Fang C, Chang C, Chen C, Chen Y, Chang H, Receptor-mediated cellular uptake of folate-conjugated fluorescent nanodiamonds: a combined ensemble and single-particle study. *Small* **2009**, *5* (23), 2716-21.
130. Zhang X, Fu C, Feng L, Ji Y, Tao L, Huang Q, Li S, Wei Y, PEGylation and polyPEGylation of nanodiamond. *Polymer* **2012**, *53* (15), 3178.
131. Petrova I, Shenderova O, Grishko V, Tyler T, Cunningham G, McGuire G, Detonation nanodiamonds simultaneously purified and modified by gas treatment. *Diam Relat Mater* **2007**, *16* (12), 2098–2103.
132. Pichota V, Comet M, Fousson E, Baras C, Senger A, Le Normand F, Spitzer D, An efficient purification method for detonation nanodiamonds. *Diam Relat Mater* **2008**, *17* (1), 13-22.
133. Shenderova O, Petrov I, Walsh J, Grichko V, Tyler T, Cunningham G, Modification of detonation nanodiamonds by heat treatment in air. *Diam Relat Mater* **2006**, *15* (11-12), 1799–1803.
134. Kaur R, Chitanda JM, Michel D, Maley J, Borondics F, Yang P, Verrall RE, Badea I, Lysine functionalized nano diamonds: synthesis, physiochemical characterization and nucleic acid binding studies. *Int J Nanomed* **2012**, *7*, 3851–3866.
135. Shenderova O, Hens S, Vlasov I, Turner S, Lu YG, Tendeloo GV, Schrand A, Burikov SA, Dolenko TA, Carbon-Dot-Decorated Nanodiamonds. *Part Part Syst Char* **2014**, *31* (5), 580–590.
136. Jee AY, Lee M, Surface Functionalization and Physicochemical Characterization of Diamond Nanoparticles. *J Curr Appl Phys* **2009**, *9* (2), e144-e147.
137. Krueger A, The structure and reactivity of nanoscale diamond. *J Mater Chem* **2008**, *18*, 1485–1492.
138. Gaebel T, Bradac C, Chen J, Rabeau JR, Size Reduction of Nanodiamonds via air oxidation. *Diam Relat Mater* **2012**, *2*, 28-32.

139. Osswald S, Yushin G, Mochalin V, Kucheyev S, Gogotsi Y, Control of sp²/sp³ carbon ratio and surface chemistry of nanodiamond powders by selective oxidation in air. *J Am Chem Soc* **2006**, *128* (35), 11635-11642.
140. Xu K, Xue Q, A new method for Deaggregation of Nanodiamonds from Explosive Detonation: Graphitization – Oxidation Method. *J Phys Part C Solid* **2004**, *46* (4), 649-650.
141. Liu K, Chen M, Chen P, Lee T, Cheng C, Chang C, Ho Y, Chao J, Alpha-bungarotoxin binding to target cell in a developing visual system by carboxylated nanodiamond. *Nanotechnology* **2008**, *19* (20), 205102.
142. Krueger A, Stegk J, Liang Y, Lu L, Jarre G, Biotinylated nanodiamond: simple and efficient functionalization of detonation diamond. *Langmuir* **2008**, *24* (8), 4200-4.
143. Datta A, Kirca M, Fu Y, To AC, Surface structure and properties of functionalized nanodiamonds: a first-principles study. *Nanotechnology* **2011**, *22* (6), 065706.
144. Lia L, Davidson JL, Lukehart CM, Surface functionalization of nanodiamond particles via atom transfer radical polymerization. *Carbon* **2006**, *44* (11), 2308–2315.
145. Spitsyn BV, Gradoboev MN, Galushko TB, Karpukhina TA, Serebryakova NV, Kulakova II, Melnik NN, Purification and Functionalization of Nanodiamond. *Synthesis, Properties and Applications of Ultrananocrystalline Diamond NATO Science Series* **2005**, *192*, 241-252.
146. Clark J. Introducing Acyl Chloride (acid chlorides) 2004. <http://www.chemguide.co.uk/organicprops/acylchlorides/background.html>.
147. Kong X, Lora Huang LC, Vivian Liao SC, Han CC, Chang HC, Polylysine-Coated Diamond Nanocrystals for MALDI-TOF Mass Analysis of DNA Oligonucleotides. *Anal Chem* **2005**, *77* (13), 4273–4277.
148. Vaijayanthimala V, Tzeng YK, Chang HC, Li CL, The biocompatibility of fluorescent nanodiamonds and their mechanism of cellular uptake. *Nanotechnology* **2009**, *20* (42), 425103.

149. Zhao L, Nakae Y, Qin H, Ito T, Kimura T, Kojima H, Chan L, Komatsu N, Polyglycerol-functionalized nanodiamond as a platform for gene delivery: Derivatization, characterization, and hybridization with DNA. *Beilstein J Org Chem* **2014**, *10*, 707-713.
150. Perevedentseva E, Cheng CY, Chung PH, Tu JS, Hsieh YH, Cheng CL, The interaction of the protein lysozyme with bacteria *E. coli* observed using nanodiamond labelling. *Nanotechnology* **2007**, *18* (31), 315102.
151. Perevedentseva E, Cai P, Chiu Y, Cheng C, Characterizing protein activities on the lysozyme and nanodiamond complex prepared for bio applications. *Langmuir* **2011**, *27* (3), 1085-1091.
152. Wang H, Niu C, Yang Q, Badea I, Study on protein conformation and adsorption behaviors in nanodiamond particle-protein complexes. *Nanotechnology* **2011**, *22* (14), 145703.
153. Youngson RM, *Collins- Dictionary of Human Biology*. HarperCollins: Glasgow, 2006.
154. Cox M, Nelson DR, Lehninger AL, *Lehninger Principles of Biochemistry*. W.H. Freeman: San Francisco, 2005.
155. Klyszejko-Stefanowicz L, Krajewska WM, Lipinska A, Chapter 2: Histone occurrence, isolation, characterization and biosynthesis. In *Histones and other basic nuclear proteins*, Stein GS, Stein JL, Eds. CRC Press: 1989; pp 18-55.
156. Taverna S, Li H, Ruthenburg A, Allis C, Patel D, How chromatin-binding modules interpret histone modifications: lessons from professional pocket pickers. *Nat Struct Mol Bio* **2007**, *14* (11), 1025-40.
157. Ghosh P, Kim C, Han G, Forbes N, Rotello V, Efficient gene delivery vectors by tuning the surface charge density of amino acid-functionalized gold nanoparticles. *ACS Nano* **2008**, *2* (11), 2213-8.
158. Petros R, DeSimone J, Strategies in the design of nanoparticles for therapeutic applications. *Nat Rev Drug Discov* **2010**, *9* (8), 615-627.
159. Owens D, Peppas N, Opsonization, biodistribution, and pharmacokinetics of polymeric nanoparticles. *Int J Pharm* **2006**, *307* (1), 93-102.

160. Wong J, Brugger A, Khare A, Chaubal M, Papadopoulos P, Rabinow B, Kipp J, Ning J, Suspensions for intravenous (IV) injection: a review of development, preclinical and clinical aspects. *Adv Drug Deliv Rev* **2008**, 60 (8), 939-954.
161. Alexis F, Pridgen E, Molnar L, Farokhzad O, Factors affecting the clearance and biodistribution of polymeric nanoparticles. *Mol Pharm* **2008**, 5 (4), 505-515.
162. Ilium L, et al., Blood clearance and organ deposition of intravenously administered colloidal particles. The effects of particle size, nature and shape. *Int J Pharm* **1982**, 12 (2-3), 135-146.
163. Wei Q, Zhan L, Juanjuan B, Jing W, Jianjun W, Taoli S, Yi'an G, Wangsuo W, Biodistribution of co-exposure to multi-walled carbon nanotubes and nanodiamonds in mice. *Nanoscale Res Lett* **2012**, 7 (1), 473.
164. Nie S, Understanding and overcoming major barriers in cancer nanomedicine. *Nanomedicine (Lond)*. **2010**, 5 (4), 5230528.
165. Zhang X, Wang S, Fu C, Feng L, Ji Y, Tao L, Li S, Wei Y, PolyPEGylated nanodiamond for intracellular delivery of a chemotherapeutic drug. *Polym Chem* **2012**, 3 (10), 2716-2719.
166. Yuan Y, Chen Y, Liu JH, Wang H, Liu Y, Biodistribution and fate of nanodiamonds in vivo. *Diam Relat Mater* **2009**, 18 (1), 95-100.
167. Hillaireau H, Couvreur P, Nanocarriers' entry into the cell: relevance to drug delivery. *Cell Mol Life Sci* **2009**, 66 (17), 2873-2896.
168. Rothen-Rutishauser B, Schurch S, Gehr P, Chapter 7: Interaction of particles with membranes. In *Particle Toxicology*, Donaldson K, Borm P, Eds. CRC Press: 2006; p 140.
169. Kuhn D, Vanhecke D, Michen B, Blank F, Gehr P, Petri-Fink A, Rothen-Rutishauser B, Different endocytotic uptake mechanisms for nanoparticles in epithelial cells and macrophages. *Beilstein J Nanotechnol* **2014**, 5, 1625-1636.
170. Douglas K, Piccirillo C, Tabrizian M, Cell line-dependent internalization pathways and intracellular trafficking determine transfection efficiency of nanoparticle vectors. *Eur J Pharm Biopharm* **2008**, 68 (3), 676-687.

171. Li W, Chen C, Ye C, Wei T, Zhao Y, Lao F, Chen Z, Meng H, Gao Y, Yuan H, Xing G, Zhao F, Chai Z, Zhang X, Yang F, Han D, Tang X, Zhang Y, The translocation of fullerene nanoparticles into lysosome via the pathway of clathrin-mediated endocytosis. *Nanotechnology* **2008**, *19* (14), 145102.
172. Kam N, Dai H, Carbon nanotubes as intracellular protein transporters: generality and biological functionality. *J Am Chem Soc* **2005**, *127* (16), 6021-6026.
173. Faklaris O, Joshi V, Irinopoulou T, Tauc P, Sennour M, Girard H, Gesset Cl, Arnault C, Thorel A, Boudou JP, Curmi PA, Photoluminescent Diamond Nanoparticles for cell Labelling: Study of the uptake mechanism in mammalian cells. *ACS Nano* **2009**, *3* (12), 3955–3962.
174. Schmid S, Clathrin-coated vesicle formation and protein sorting: an integrated process. *Ann Rev Biochem* **1997**, *66*, 511-548.
175. Conner SD, Schmid SL, Regulated portals of entry into the cell. *Nature* **2003**, *422*, 37-44.
176. Liu K, Wang C, Cheng C, Chao J, Endocytic carboxylated nanodiamond for the labeling and tracking of cell division and differentiation in cancer and stem cells. *Biomaterials* **2009**, *30* (26), 4249-4259.
177. Alhaddad A, Durieu C, Dantelle G, Le CE, Malvy C, Treussart F, Bertrand J, Influence of the internalization pathway on the efficacy of siRNA delivery by cationic fluorescent nanodiamonds in the Ewing sarcoma cell model. *PLoS One* **2012**, *7* (12), e52207.
178. Perevedentseva E, Hong SF, Huang KJ, Chiang IT, Lee CY, Tseng YT, Cheng CL, Nanodiamond internalization in cells and the cell uptake mechanism. *J Nanopart Res* **2013**, *15*, 1834.
179. Chithrani BD, Chan WCW, Elucidating the Mechanism of Cellular Uptake and Removal of Protein-Coated Gold Nanoparticles of Different Sizes and Shapes. *Nano Lett* **2007**, *7* (6), 1542–1550.
180. Gao H, Shi W, Freund LB, Mechanics of receptor-mediated endocytosis. *Proc Natl Acad Sci USA* **2005**, *102* (27), 9469–9474.

181. Razani B, Woodman S, Lisanti M, Caveolae: from cell biology to animal physiology. *Pharmacol Rev* **2002**, *54* (3), 431-467.
182. Wang Z, Tiruppathi C, Minshall R, Malik A, Size and dynamics of caveolae studied using nanoparticles in living endothelial cells. *ACS Nano* **2009**, *3* (12), 4110-4116.
183. Lesniak A, Fenaroli F, Monopoli M, Åberg C, Dawson K, Salvati A, Effects of the presence or absence of a protein corona on silica nanoparticle uptake and impact on cells. *ACS Nano* **2012**, *6* (7), 5845-57.
184. Gunawan C, Lim M, Marquisb CP, Amal R, Nanoparticle–protein corona complexes govern the biological fates and functions of nanoparticles. *J Mater Chem B* **2014**, *2*, 2060-2083.
185. Cedervall T, Lynch I, Foy M, Berggard T, Donnelly S, Cagney G, Linse S, Dawson K, Detailed identification of plasma proteins adsorbed on copolymer nanoparticles. *Angew Chem Int Ed Engl* **2007**, *46* (30), 5754-6.
186. Tenzer S, et al., Rapid formation of plasma protein corona critically affects nanoparticle pathophysiology. *Nat Nanotechnol* **2013**, *8*, 772–781.
187. Alkilany A, Nagaria P, Hexel C, Shaw T, Murphy C, Wyatt M, Cellular uptake and cytotoxicity of gold nanorods: molecular origin of cytotoxicity and surface effects. *Small* **2009**, *5* (6), 701-8.
188. Rahman M, Laurent S, Tawil N, Yahia LH, Mahmoudi M, Nanoparticle and Protein Corona. In *Protein-Nanoparticle Interactions*, Springer: 2013; Vol. 15, pp 21-44.
189. Lu N, Li J, Tian R, Peng Y, Binding of human serum albumin to single-walled carbon nanotubes activated neutrophils to increase production of hypochlorous acid, the oxidant capable of degrading nanotubes. *Chem Res Toxicol* **2014**, *27* (6), 1070-7.
190. Solarska-Ściuk K, Gajewska A, Glińska S, Studzian M, Michlewska S, Balcerzak Ł, Skolimowski J, Kolago B, Bartosz G, Intracellular transport of nanodiamond particles in human endothelial and epithelial cells. *Chem-Biol Interact* **2014**, *219*, 90-100.
191. Khalil I, Kogure K, Akita H, Harashima H, Uptake pathways and subsequent intracellular trafficking in nonviral gene delivery. *Pharmacol Rev* **2006**, *58* (1), 32-45.

192. Kumar V, Pichon C, Refregiers M, Guerin B, Midoux P, Chaudhuri A, Single histidine residue in head-group region is sufficient to impart remarkable gene transfection properties to cationic lipids: evidence for histidine-mediated membrane fusion at acidic pH. *Gene Ther* **2003**, *10* (15), 1206-15.
193. Petit T, Girard H, Trouvé A, Batonneau-Gener I, Bergonzo P, Arnault J, Surface transfer doping can mediate both colloidal stability and self-assembly of nanodiamonds. *Nanoscale* **2013**, *5* (19), 8958-8962.
194. Varkouhi A, Scholte M, Storm G, Haisma H, Endosomal escape pathways for delivery of biologicals. *J Control Release* **2011**, *151* (3), 220-228.
195. Badea I, Verrall R, Chitanda JM, Kaur R, Alwani S, Functionalized nanodiamonds as delivery platforms for nucleic acids. 20140314850, 2014.
196. Li J, Zhu Y, Li W, Zhang X, Peng Y, Huang Q, Nanodiamonds as intracellular transporters of chemotherapeutic drug. *Biomaterials* **2010**, *31* (32), 8410-8418.
197. Yuan Y, Wang X, Liu GJH, Wang T, Gu Y, Yang ST, Zhen S, Wang H, Liu Y, Pulmonary toxicity and translocation of nanodiamonds in mice. *Diam Relat Mater* **2010**, *19* (4), 291-299.
198. Schrand AM, Suzanne A, Hens C, Shenderova OA, Nanodiamond particles: properties and perspectives for bioapplications. *Crc Cr Rev Sol States* **2009**, *34* (1-2), 18-74.
199. Chang YR, Lee HY, Chen K, Chang CC, Tsai DS, Fu CC, Lim TS, Tzeng YK, Fang CY, Han CC, Mass production and dynamic imaging of fluorescent nanodiamonds. *Nat Nanotechnol* **2008**, *3* (5), 284-288.
200. Ho D, Beyond the sparkle: the impact of nanodiamonds as biolabeling and therapeutic agents. *ACS Nano* **2009**, *3* (12), 3825-3829.
201. Wen CJ, Liu X, Li X, Guan J, Sun D, Lin Y, Tang S, Zhou G, Lin J, Studies on nanodiamond prepared by explosive detonation by Raman and infrared spectroscopy. *Guang Pu Xue Yu Guang Pu Fen Xi* **2005**, *25* (5), 681-4.

202. Butenkoa YV, Kuznetsova VL, Paukshtisa EA, Stadnichenkoa AI, Mazova IN, Moseenkova SI, Boronina AI, Kosheeva SV, The Thermal Stability of Nanodiamond Surface Groups and Onset of Nanodiamond Graphitization. *Fuller Nanotub Car N* **2006**, *14* (2-3), 557-564.
203. Dandekar A, Baker RTK, Vannice MA, Characterization of activated carbon, graphitized carbon fibers and synthetic diamond powder using TPD and DRIFTS. *Carbon* **1998**, *36* (12), 1821–1831.
204. Verma A, Stellacci F, Effect of surface properties on nanoparticle-cell interactions. *Small*. **2010**, *6* (1), 12-21.
205. Nel AE, Mädler L, Velegol D, Xia T, Hoek EMV, Somasundaran P, Klaessig F, Castranova V, Thompson M, Understanding biophysicochemical interactions at the nano–bio interface. *Nat Mater* **2009**, *8*, 543 - 557.
206. Datta S, Brunet A, Greenberg M, Cellular survival: a play in three Akts. *Genes Dev* **1999**, *13* (22), 2905-27.
207. Alberts B, Johnson A, Lewis J, Raff M, Roberts K, Walter P, *Molecular Biology of the Cell*. Garland Science: Newyork, 2002.
208. Zhu Y, Li J, Li W, Zhang Y, Yang X, Chen N, Sun Y, Zhao Y, Fan C, Huang Q, The Biocompatibility of Nanodiamonds and their Applications in Drug Delivery Systems. *Theranostics* **2012**, *2* (3), 302-312.
209. Kruger A, Kataoka F, Ozawa M, Fujino T, Suzuki Y, Aleksenskii AE, Vul AY, Osawa E, Unusually tight aggregation in Detonation Nanodiamonds: Identification and Disintegration. *Carbon* **2005**, *43* (8), 1722-1730.
210. El-Say, K. M., Nanodiamond as a drug delivery system: Applications and prospective. *J App Pharm Sci* **2011**, *01* (06), 29-39.
211. Ho D, *Nanodiamonds: Applications in Biology and Nanoscale Medicine*. 2010 ed.; Springer: 2010.

212. Liu Y, Gu Z, Margrave JL, Khabashesku VN, Functionalization of Nanoscale Diamond Powder: Fluoro-, Alkyl-, Amino-, and Amino Acid-Nanodiamond Derivatives. *Chem Mater* **2004**, *16* (20), 3924–3930.
213. Chow E, Zhang X, Chen M, Lam R, Robinson E, Huang H, Schaffer D, Osawa E, Goga A, Ho D, Nanodiamond therapeutic delivery agents mediate enhanced chemoresistant tumor treatment. *Sci Transl Med* **2011**, *3* (73), 73ra21.
214. Pati IS, Rhodes D, Burgess D, DNA-based therapeutics and DNA delivery systems: a comprehensive review. *AAPS J* **2005**, *7* (1), E61-77.
215. Castanotto D, Rossi JJ, The promises and pitfalls of RNA-interference-based therapeutics. *Nature* **2009**, *457* (7228), 426-433.
216. Opalinska J, Gewirtz A, Nucleic-acid therapeutics: basic principles and recent applications. *Nat Rev Drug Discov* **2002**, *1* (7), 503-514.
217. Alhaddad A, Adam M, Botsoa J, Dantelle G, Perruchas S, Gacoin T, Mansuy C, Lavielle S, Malvy C, Treussart F, Bertrand J, Nanodiamond as a vector for siRNA delivery to Ewing sarcoma cells. *Small* **2011**, *7* (21), 3087-95.
218. Li J, Chin K, Chapter 10: Methods to nanoparticle conjugation to monoclonal antibodies. In *Antibody-Mediated Drug Delivery Systems: Concepts, Technology, and Applications*, Pathak Y, Benita S, Eds. John Wiley & Sons: 2012; pp 192-193.
219. Izak-Nau E, Voetz M, Eiden S, Duschl A, Puentes V, Altered characteristics of silica nanoparticles in bovine and human serum: the importance of nanomaterial characterization prior to its toxicological evaluation. *Part Fibre Toxicol* **2013**, *10* (1), 56.
220. Lundqvist M, Stigler J, Cedervall T, Berggård T, Flanagan M, Lynch I, Elia G, Dawson K, The evolution of the protein corona around nanoparticles: a test study. *ACS Nano* **2011**, *5* (9), 7503-9.
221. Monopoli M, Walczyk D, Campbell A, Elia G, Lynch I, Bombelli F, Dawson K, Physical-chemical aspects of protein corona: relevance to in vitro and in vivo biological impacts of nanoparticles. *J Am Chem Soc* **2011**, *133* (8), 2525-34.

222. Yan Y, Gause K, Kamphuis M, Ang C, O'Brien-Simpson N, Lenzo J, Reynolds E, Nice E, Caruso F, Differential roles of the protein corona in the cellular uptake of nanoporous polymer particles by monocyte and macrophage cell lines. *ACS Nano* **2013**, 7 (12), 10960-70.
223. Treuel L, Brandholt S, Maffre P, Wiegele S, Shang L, Nienhaus G, Impact of protein modification on the protein corona on nanoparticles and nanoparticle-cell interactions. *ACS Nano* **2014**, 8 (1), 503-13.
224. Holt B, Dahl K, Islam M, Quantification of uptake and localization of bovine serum albumin-stabilized single-wall carbon nanotubes in different human cell types. *Small* **2011**, 7 (16), 2348-55.
225. Du S Kendall K, Toloueinia P, Mehrabadi Y, Gupta G, Newton J, Aggregation and adhesion of gold nanoparticles. *J Nanopart Res* **2012**, 14, 758.
226. Neugart F, Zappe A, Jelezko F, Tietz C, Boudou J, Krueger A, Wrachtrup J, Dynamics of diamond nanoparticles in solution and cells. *Nano Lett* **2007**, 7 (12), 3588-91.
227. Xin X, Xu G, Li H, Dispersion and Property Manipulation of Carbon Nanotubes by Self-Assembles of Amphiphilic Molecules. In *Physical and Chemical Properties of Carbon Nanotubes*, INTECH: 2013; pp 255-273.
228. Carmona-Ribeiro, Vieira DB, Ana M, Cationic nanoparticles for delivery of amphotericin B: preparation, characterization and activity in vitro. *J Nanobiotechnology* **2008**, 6.
229. Cherng J, van de Wetering P, Talsma H, Crommelin D, Hennink W, Effect of size and serum proteins on transfection efficiency of poly ((2-dimethylamino)ethyl methacrylate)-plasmid nanoparticles. *Pharm Res* **1996**, 13 (7), 1038-42.
230. Audouy S, Molema G, de Leij L, Hoekstra D, Serum as a modulator of lipoplex-mediated gene transfection: dependence of amphiphile, cell type and complex stability. *J Gene Med* **2000**, 2 (6), 465-476.
231. Vesaratchanon S, Nikolov A, Wasan D, Sedimentation in nano-colloidal dispersions: effects of collective interactions and particle charge. *Adv Colloid Interfac* **2007**, (134-135), 268-78.

232. Allouni Z, Cimpan M, Høl P, Skodvin T, Gjerdet N, Agglomeration and sedimentation of TiO₂ nanoparticles in cell culture medium. *Colloid Surface B* **2009**, *68* (1), 83-87.
233. Dobrovolskaia M, Patri A, Zheng J, Clogston J, Ayub N, Aggarwal P, Neun B, Hall J, McNeil S, Interaction of colloidal gold nanoparticles with human blood: effects on particle size and analysis of plasma protein binding profiles. *Nanomedicine* **2009**, *5* (2), 106-17.
234. Lacerda S, Park J, Meuse C, Pristiniski D, Becker M, Karim A, Douglas J, Interaction of gold nanoparticles with common human blood proteins. *ACS Nano* **2010**, *4* (1), 365-79.
235. Aggarwal P, Hall J, McLeland C, Dobrovolskaia M, McNeil S, Nanoparticle interaction with plasma proteins as it relates to particle biodistribution, biocompatibility and therapeutic efficacy. *Adv Drug Deliver Rev* **2009**, *61* (6), 428-37.
236. Akinc A, Querbes W, De S, et al., Targeted delivery of RNAi therapeutics with endogenous and exogenous ligand-based mechanisms. *Mol Ther* **2010**, *10* (7), 1357-64.
237. Pino Pd, Pelaz B, Zhang Q, Maffre P, Nienhausbc GU, Parak WJ, Protein corona formation around nanoparticles – from the past to the future. *Mater Horiz* **2014**, *1*, 301.
238. Honary S, Zahir F, Effect of Zeta Potential on the Properties of Nano-Drug Delivery Systems - A Review (Part 2). *Trop J Pharm Res* **2013**, *12* (2), 265-273.
239. Ade H, Stoll H, Near-edge X-ray absorption fine-structure microscopy of organic and magnetic materials. *Nat Mater* **2009**, *8*, 281-290.
240. Graf C, Meinke M, Gao Q, Hadam S, Raabe J, Sterry W, Blume-Peytavi U, Lademann J, Rühl E, Vogt A, Qualitative detection of single submicron and nanoparticles in human skin by scanning transmission x-ray microscopy. *J Biomed Opt* **2009**, *14* (2).
241. Goode A, Hine N, Chen S, Bergin S, Shaffer M, Ryan M, Haynes P, Porter A, McComb D, Mapping functional groups on oxidised multi-walled carbon nanotubes at the nanometre scale. *Chem Commun* **2014**, *50* (51), 6744-7.
242. Behrens S, Kappler A, Obst M, Linking environmental processes to the in situ functioning of microorganisms by high-resolution secondary ion mass spectrometry (NanoSIMS) and scanning transmission X-ray microscopy (STXM). *Environ Microbiol* **2012**, *14* (11), 2851-69.

243. Hitchcock A, Dynes J, Johansson G, Wang J, Botton G, Comparison of NEXAFS microscopy and TEM-EELS for studies of soft matter. *Micron* **2008**, *39* (6), 741-8.
244. Koprinarov I, Hitchcock AP, X-ray Spectromicroscopy of Polymers: An introduction for the non-specialist. In *Unicorn McMaster (BIMR)*.
245. Lawrence J, Swerhone G, Leppard G, Araki T, Zhang X, West M, Hitchcock A, Scanning transmission X-ray, laser scanning, and transmission electron microscopy mapping of the exopolymeric matrix of microbial biofilms. *Appl Environ Microb* **2003**, *69* (9), 5543-54.
246. Suzuki H, Toyooka T, Ibuki Y, Simple and easy method to evaluate uptake potential of nanoparticles in mammalian cells using a flow cytometric light scatter analysis. *Envir Sci Tech* **2007**, *41* (8), 3018-3024.
247. Smith BR, Niebert M, Plakhotnik T, Zvyagin AV, Transfection and imaging of diamond nanocrystals as scattering optical labels. *J Lumin* **2007**, *127* (1), 260-263.
248. Hui YY, Cheng CL, Chang HC, Nanodiamonds for optical bioimaging. *J Phys D: Appl Phys* **2010**, *43*, 374021.
249. Halamoda Kenzaoui B, Chapuis Bernasconi C, Guney-Ayra S, Juillerat-Jeanerret L, Induction of oxidative stress, lysosome activation and autophagy by nanoparticles in human brain-derived endothelial cells. *Biochem J* **2012**, *441* (3), 813-821.
250. Marina O, Sanders C, Mourant J, Correlating light scattering with internal cellular structures. *Biomed Opt Express* **2012**, *3* (2), 296-312.
251. Biosciences, BD
252. Zuhorn I, Visser W, Bakowsky U, Engberts J, Hoekstra D, Interference of serum with lipoplex-cell interaction: modulation of intracellular processing. *Biochim Biophys Acta* **2002**, *1560* (1-2), 25-36.
253. Tandia B, Vandenbranden M, Wattiez R, Lakhdar Z, Ruyschaert J, Elouahabi A, Identification of human plasma proteins that bind to cationic lipid/DNA complex and analysis of their effects on transfection efficiency: implications for intravenous gene transfer. *Mol Ther* **2003**, *8* (2), 264-273.

254. Lesniak A, Campbell A, Monopoli M, Lynch I, Salvati A, Dawson K, Serum heat inactivation affects protein corona composition and nanoparticle uptake. *Biomaterials* **2010**, *31* (36), 9511-8.
255. Rejman J, Conese M, Hoekstra D, Gene transfer by means of lipo- and polyplexes: role of clathrin and caveolae-mediated endocytosis. *J Lipos Res* **2006**, *16* (3), 237-247.
256. Rejman J, Oberle V, Zuhorn I, Hoekstra D, Size-dependent internalization of particles via the pathways of clathrin- and caveolae-mediated endocytosis. *Biochem J* **2004**, *377* (Pt 1), 159-169.
257. dos Santos T, Varela J, Lynch I, Salvati A, Dawson K, Effects of transport inhibitors on the cellular uptake of carboxylated polystyrene nanoparticles in different cell lines. *PLoS One* **2011**, *6* (9), e24438.
258. Kummitha CM, Malamas AS, Lu ZR, Albumin pre-coating enhances intracellular siRNA delivery of multifunctional amphiphile/siRNA nanoparticles. *Int J Nanomed* **2012**, *7*, 5205–5214.
259. Piao L, Li H, Teng L, Yung B, Sugimoto Y, Brueggemeier R, Lee R, Human serum albumin-coated lipid nanoparticles for delivery of siRNA to breast cancer. *Nanomedicine* **2013**, *9* (1), 122-129.
260. Pelkmans L, Helenius A, Endocytosis Via Caveolae. *Traffic* **2002**, *3* (5), 311-320.
261. Caracciolo G, Callipo L, De Sanctis S, Cavaliere C, Pozzi D, Laganà A, Surface adsorption of protein corona controls the cell internalization mechanism of DC-Chol-DOPE/DNA lipoplexes in serum. *Biochim Biophys Acta* **2010**, *1798* (3), 536-543.
262. Saptarshi SR, Duschl A, Lopata AL, Interaction of nanoparticles with proteins: relation to bio-reactivity of the nanoparticle. *J Nanobiotechnology* **2013**, *11*, 26.
263. Dutta D, Sundaram S, Teegarden J, Riley B, Fifield L, Jacobs J, Addleman S, Kaysen G, Moudgil B, Weber T, Adsorbed proteins influence the biological activity and molecular targeting of nanomaterials. *Toxicol Sci.* **2007**, *100* (1), 303-15.

264. Kim E, Ehrmann K, Uhlhorn S, Borja D, Arrieta-Quintero E, Parel J, Semiautomated analysis of optical coherence tomography crystalline lens images under simulated accommodation. *J Biomed Opt* **2011**, *16* (5), 056003.
265. Assessment of adenoviral vector safety and toxicity: report of the National Institutes of Health Recombinant DNA Advisory Committee. 2002.
266. Marshall E, Gene therapy death prompts review of adenovirus vector. *Science* **1999**, *286* (5448), 2244-5.
267. Schnell M, Zhang Y, Tazelaar J, Gao G, Yu Q, Qian R, Chen S, Varnavski A, LeClair C, Raper S, Wilson J, Activation of innate immunity in nonhuman primates following intraportal administration of adenoviral vectors. *Mol Ther* **2001**, *3* (5 (Pt 1)), 708-22.
268. Nair V, Retrovirus-induced oncogenesis and safety of retroviral vectors. *Curr Opin Mol Ther* **2008**, *10* (5), 431-8.
269. Pack D, Hoffman A, Pun S, Stayton P, Design and development of polymers for gene delivery. *Nat Rev Drug Discov* **2005**, *4* (7), 581-93.
270. Martin B, Sainlos M, Aissaoui A, Oudrhiri N, Hauchecorne M, Vigneron J, Lehn J, Lehn P, The design of cationic lipids for gene delivery. *Curr Pharm Des* **2005**, *11* (3), 375-94.
271. Lee S, Bae K, Kim S, Lee K, Park T, Amine-functionalized gold nanoparticles as non-cytotoxic and efficient intracellular siRNA delivery carriers. *Int J Pharm.* **2008**, *364* (1), 94-101.
272. Hartono SB, Gu W, Kleitz F, Liu J, He L, Middelberg APJ, Yu C, Lu GQM, Qiao SZ, Poly-l-lysine Functionalized Large Pore Cubic Mesostructured Silica Nanoparticles as Biocompatible Carriers for Gene Delivery. *ACS Nano* **2012**, *6* (3), 2104-2117.
273. Schiffelers RM, Ansari A, Xu J, Zhou Q, Tang Q, Storm G, Molema G, Lu PY, Scaria PV, Woodle MC, Cancer siRNA therapy by tumor selective delivery with ligand-targeted sterically stabilized nanoparticle. *Nucleic Acids Res* **2004**, *32* (19), e149.
274. Santel A, Aleku M, Keil O, Endruschat J, Esche V, Durieux B, Löffler K, Fechtner M, Röhl T, Fisch G, Dames S, Arnold W, Giese K, Klippel A, Kaufmann J, RNA interference in the

mouse vascular endothelium by systemic administration of siRNA-lipoplexes for cancer therapy. *Gene Ther* **2006**, *13* (18), 1360-70.

275. Nykänen A, Haley B, Zamore P, ATP requirements and small interfering RNA structure in the RNA interference pathway. *Cell* **2001**, *107* (3), 309-21.

276. Martinez J, Patkaniowska A, Urlaub H, Lührmann R, Tuschl T, Single-stranded antisense siRNAs guide target RNA cleavage in RNAi. *Cell* **2002**, *110* (5), 563-74.

277. Bumcrot D, Manoharan M, Koteliansky V, Sah D, RNAi therapeutics: a potential new class of pharmaceutical drugs. *Nat Chem Biol* **2006**, *2* (12), 711-9.

278. Hughes MD, Hussain M, Nawaz Q, Sayyed P, Akhtar S, The cellular delivery of antisense oligonucleotides and ribozymes. *Drug Discov. Today* **2001**, *6* (6), 303-315.

279. Morachis J, Mahmoud E, Sankaranarayanan J, Almutairi A, Triggered rapid degradation of nanoparticles for gene delivery. *J Drug Deliv* **2012**, *2012*, 291219.

280. Khodthong C, Ismaili I, Juckem, L, *The Impact of Transfection Mediated Toxicity - Gene Expression and Cytotoxicity Analysis of Transfection Reagents*; Madison. Wisconsin, 2012.

281. van Engeland M, Nieland L, Ramaekers F, Schutte B, Reutelingsperger C, Annexin V-affinity assay: a review on an apoptosis detection system based on phosphatidylserine exposure. *Cytometry* **1998**, *31* (1), 1-9.

282. Caldas H, Altura RA, Apoptosis-inducing genes for treating cancer. US 8017747 B2, 2011.

283. Piazza G, Rahm A, Krutzsch M, Sperl G, Paranka N, Gross P, Brendel K, Burt R, Alberts D, Pamukcu R, Antineoplastic drugs sulindac sulfide and sulfone inhibit cell growth by inducing apoptosis. *Cancer Res* **1995**, *55* (14), 3110-3116.

284. Hasbold J, Klaus GG, Anti-immunoglobulin antibodies induce apoptosis in immature B cell lymphomas. *Eur J Immunol* **1990**, *20* (8), 1685-1690.

285. Treatment of stage III melanoma *Canadian Cancer Society* [Online], 2015. <http://www.cancer.ca/en/cancer-information/cancer-type/skin-melanoma/treatment/stage-iii/?region=on>.

286. Krueger A, Boedeker T, Deagglomeration and functionalization of detonation nanodiamond with long alkyl chains. *Diam Relat Mater* **2008**, *17* (7-10), 1367–1370.
287. Mogil'naya O, Bondar V, Comparative Study of Antibacterial Properties of Lysozyme upon Its Adsorption and Covalent Binding to Nanodiamonds. *Nanotechnol Russ* **2012**, *7* (11-12), 658-665.
288. Singh J, Yang P, Michel D, Verrall R, Foldvari M, Badea I, Amino acid-substituted gemini surfactant-based nanoparticles as safe and versatile gene delivery agents. *Curr Drug Deliv* **2011**, *8* (3), 299-306.
289. Singh J, Michel D, Getson H, Chitanda J, Verrall R, Badea I, Development of amino acid substituted gemini surfactant-based mucoadhesive gene delivery systems for potential use as noninvasive vaginal genetic vaccination. *Nanomedicine (Lond)* **2015**, *10* (3), 405-417.
290. Labille J, Brant J, Stability of nanoparticles in water. *Nanomedicine (Lond)* **2010**, *5* (6), 985-998.
291. Alpatova A, Shan W, Babica P, Upham B, Rogensues A, Masten S, Drown E, Mohanty A, Alocilja E, Tarabara V, Single-walled carbon nanotubes dispersed in aqueous media via non-covalent functionalization: effect of dispersant on the stability, cytotoxicity, and epigenetic toxicity of nanotube suspensions. *Water Res* **2010**, *44* (2), 505-520.
292. Claudia G, Guohui W, Benjamin J, Joseph A, Precise Quantification of Nanoparticle Internalization. *ACS Nano* **2013**, *7* (6), 4933-4955.
293. Kumar A, Pandey A, Singh S, Shanker R, Dhawan A, A flow cytometric method to assess nanoparticle uptake in bacteria. *Cytometry A* **2011**, *79* (9), 707-712.
294. Wang X, Guo J, Chen T, Nie H, Wang H, Zang J, Cui X, Jia G, Multi-walled carbon nanotubes induce apoptosis via mitochondrial pathway and scavenger receptor. *Toxicol In Vitro* **2012**, *26* (6), 799-806.
295. Conel M.O'D. Alexander, Chondrite *Encyclopedia Britannica* [Online], 2013. <http://www.britannica.com/EBchecked/topic/114270/chondrite>.

296. Shenderova O, McGuire G, Types of nanocrystalline diamond. In *Ultrananocrystalline Diamond: Synthesis Properties and Applications*, Shenderova, O.; Gruen, D., Eds. William Andrew: New York, 2006; pp 79-114.
297. Dolmatov VY, Veretennikova MV, Marchukov VA, Sushchev VG, Currently Available Methods of Industrial Nanodiamond Synthesis. *J Phys Part C Solid* **2004**, *46* (4), 611-615.
298. Baidakova M, Vul A, New prospects and frontiers of nanodiamond clusters. *J Phys D: Appl Phys* **2007**, *40* (20), 6300-6311.
299. Fang L, Ohfuji H, Irifune T, A Novel Technique for the Synthesis of Nanodiamond Powder. *J Nanomater* **2013**, *2013* (2013).
300. Khachatryan AK, Aloyan SG, May PW, Sargsyan R, Khachatryan VA, Baghdasaryan VS, Graphite-to-diamond transformation induced by ultrasound cavitation. *Diam Relat Mater* **2008**, *17*, 931-936.
301. Sun J, Lei Y, Zhai Q, Yang X, Yang J, Du X, Preparation of nanodiamonds by laser irradiation of graphite. *Chin Opt Lett* **2005**, *3* (5), 287-288.
302. Fang L, Ohfuji H, Toru S, Tetsuo I, Experimental study on the stability of graphitic C₃N₄ under high pressure and high temperature. *Diam Relat Mater* **2011**, *20* (5-6), 819-825.
303. Hu S, Sun J, Tian F, Jiang L, The formation of multiply twinning structure and photoluminescence of well-dispersed nanodiamonds produced by pulsed-laser irradiation. *Diam Relat Mater* **2008**, *17* (2), 142-146.
304. Johnson LD, Chapter 17: Practicle Considerations in Selection and Applications of Fluorescent Probes. In *Handbook of Biological Confocal Microscopy*, Pawley J, Ed. Springer Science & Business Media: 2010; p 362.
305. Ko HC, Yuan CT, Tang J, Probing and controlling fluorescence blinking of single semiconductor nanoparticles. *Nano rev* **2011**, *2*.
306. Davis RW, Timlin JA, Kaiser JN, Sinclair MB, Jones HDT, Lane TW, Accurate Detection of Low Levels of Fluorescence Emission in Autofluorescent Background: Francisella-Infected Macrophage Cells. *Micro Microanal* **2010**, *16* (4), 478-487.

307. Wee TL, Mau YW, Fang CY, Hsu HL, Han CC, Chang HC, Preparation and characterization of green fluorescent nanodiamonds for biological applications. *Diam Relat Mater* **2009**, *18* (2-3), 567-573.
308. Meijer J, Burchard B, Domhan M, Wittmann C, Gaebel T, Popa I, Jelezko F, Wrachtrup J, Generation of single colour centers by focussed nitrogen implantation. *Appl Phys Lett* **2005**, *87*, Art. No. 261909.
309. Rabeau JR, Reichart P, Tamanyan G, Jamieson DN, Prawer S, Jelezko F, Gaebel T, Popa I Domhan M, Wrachtrup J, Implantation of labelled single nitrogen vacancy centers in diamond using N¹⁵. *Appl Phys Lett* **2006**, *88*, 023113.
310. Spinicelli P, Dreau A, Rondin L, Silva F, Achard J, Xavier S, Bansropun S, Debuisschert T, Pezzanga S, Meijer J, Jacques V, Roch JF, Engineered arrays of nitrogen-vacancy color centers in diamond based on implantation of CN⁻ molecules through nanoapertures. *New J Phys* **2011**, *13*, 025014.
311. Bray K, Previdi R, Gibson B, Shimoni O, Aharonovich I, Enhanced photoluminescence from single nitrogen-vacancy defects in nanodiamonds coated with phenol-ionic complexes. *Nanoscale* **2015**.
312. Mochalin V, Gogotsi Y, Wet chemistry route to hydrophobic blue fluorescent nanodiamond. *J Am Chem Soc* **2009**, *131* (13), 4594-4595.
313. Wu T, Tzeng Y, Chang W, Cheng C, Kuo Y, Chien C, Chang H, Yu J, Tracking the engraftment and regenerative capabilities of transplanted lung stem cells using fluorescent nanodiamonds. *Nat Nanotechnol* **2013**, *8* (9), 682-689.
314. Hsu TC, Liu KK, Chang HC, Hwang E, Chao JI, Labeling of neuronal differentiation and neuron cells with biocompatible fluorescent nanodiamonds. *Sci Rep* **2014**, *4*, 5004.
315. Weng MF, Chiang SY, Wang NS, Niu H, Fluorescent nanodiamonds for specifically targeted bioimaging: Application to the interaction of transferrin with transferrin receptor. *Diam Relat Mater* **2009**, *18* (2), 587-591.
316. Chang HC, In *Fluorescent nano diamonds for super – resolution Bioimaging and long term cell tracking*, 76th meeting of Israel Chemical Society, 2011.

317. Zhang X, Lam R, Xu X, Chow E, Kim H, Ho D, Multimodal nanodiamond drug delivery carriers for selective targeting, imaging, and enhanced chemotherapeutic efficacy. *Adv Mater* **2011**, *23* (41), 4770-4775.
318. Huynh VT, Pearson S, Noy JM, Abboud A, Utama RH, Lu H, Stenzel MH, Nanodiamonds with Surface Grafted Polymer Chains as Vehicles for Cell Imaging and Cisplatin Delivery: Enhancement of Cell Toxicity by POEGMEMA Coating. *ACS Macro Lett* **2013**, *2* (3), 246-250.
319. Chang IP, Hwang KC, Chiang CS, Preparation of fluorescent magnetic nanodiamonds and cellular imaging. *J Am Chem Soc* **2008**, *130* (46), 15476.
320. Grobner T, Gadolinium—a specific trigger for the development of nephrogenic fibrosing dermopathy and nephrogenic systemic fibrosis? *Nephrol Dial Transpl* **2006**, *21* (4), 1104-1108.
321. Chen E, Gaathon O, Trusheim M, Englund D, Wide-field multispectral super-resolution imaging using spin-dependent fluorescence in nanodiamonds. *Nano Lett* **2013**, *13* (5), 2073-2077.
322. Colpin Y, Swan A, Zvyagin A, Plakhotnik T, Imaging and sizing of diamond nanoparticles. *Opt Lett* **2006**, *31* (5), 625-627.
323. Michealson S, Hoffman A, Chapter 8: Bonding and Concentration of Hydrogen. In *Ultrananocrystalline Diamond: Synthesis, Properties and Applications*, Shenderova OA, Gruen DM, Eds. William Andrew: 2012; p 254.
324. Pope I, Payne L, Zorinants G, Thomas E, Williams O, Watson P, Langbein W, Borri P, Coherent anti-Stokes Raman scattering microscopy of single nanodiamonds. *Nat Nanotechnol* **2014**, *9* (11), 940-946.
325. Li Y, Tong Y, Cao R, Tian Z, Yang B, Yang P, In vivo enhancement of anticancer therapy using bare or chemotherapeutic drug-bearing nanodiamond particles. *Int J Nanomed* **2014**, *9*, 1065-1082.
326. Xiao J, Duan X, Yin Q, Zhang Z, Yu H, Li Y, Nanodiamonds-mediated doxorubicin nuclear delivery to inhibit lung metastasis of breast cancer. *Biomaterials* **2013**, *34* (37), 9648-9656.

327. Broz P, Driamov S, Ziegler J, Ben-Haim N, Marsch S, Meie W, Huziker P, Toward intelligent Nanosize Bioreactors: A pH- Switchable, Channel equipped, functional polymer nanocontainer. *Nano Lett* **2006**, 6 (10), 2349–2353.
328. Savjani KT, Gajjar AK, Savjani JK, Drug Solubility: Importance and Enhancement Techniques. *ISRN Pharm* **2012**, 2012, 195727.
329. Huang H, Pierstorff E, Osawa E, Ho D, Protein-mediated assembly of nanodiamond hydrogels into a biocompatible and biofunctional multilayer nanofilm. *Acs Nano* **2008**, 2 (2), 203-212.
330. Lam R, Chen M, Pierstorff E, Huang H, Osawa E, Ho D, Nanodiamond-Embedded Microfilm Devices for Localized Chemotherapeutic Elution. *ACS Nano* **2008**, 2 (10), 2095–2102.
331. Kamatari YO, Konno T, Kataoka M, Akasaka K, The methanol-induced globular and expanded denatured states of cytochrome c: a study by CD fluorescence, NMR and small-angle X-ray scattering. *J Mol Biol* **1996**, 259 (3), 512-523.
332. Cheng YY, Lin SH, Chang HC, Su MC, Probing Adsorption, Orientation and Conformational Changes of Cytochrome c on Fused Silica Surfaces with the Soret Band. *J Phys Chem A* **2003**, 107 (49), 10687-10694.
333. Yeap W, Tan Y, Loh K, Using detonation nanodiamond for the specific capture of glycoproteins. *Anal Chem* **2008**, 80 (12), 4659-4665.
334. Roy I, Ohulchanskyy TY, Bharali DJ, Pudavar HE, Mistretta RA, Kaur N, Prasad PN, Optical tracking of organically modified silica nanoparticles as DNA carriers: A nonviral, nanomedicine approach for gene delivery. *PNAS* **2005**, 102 (2), 279-284.
335. Yezhelyev MV, Xiaohu G, Xing Y, Al-Hajj A, Nie S, MO'Regan R, Emerging use of nanoparticles in diagnosis and treatment of breast cancer. *Lancet Oncol* **2006**, 7 (8), 657-667.
336. Soppimath K, Aminabhavi T, Kulkarni A, Rudzinski W, Biodegradable polymeric nanoparticles as drug delivery devices. *J Control Release* **2001**, 70 (1-2), 1-20.

337. Baruchel J, Bleuet P, Bravin A, Coan P, Lima E, Madsen A, Ludwig W, Pernot P, Jean S, Advances in synchrotron hard X-ray based imaging. *CR Phys (Synchrotron x-rays and condensed matter)* **2008**, 9 (5-6), 624-641.
338. Gao Y, Liu N, Chen C, Luo Y, Li Y, Zhang Z, Zhao Y, Zhao B, Iidad A, Chai Z, Mapping technique for biodistribution of elements in a model organism, *Caenorhabditis elegans*, after exposure to copper nanoparticles with microbeam synchrotron radiation X-ray fluorescence. *J Anall Atom Spectrom* **2008**, 23 (8), 1121-1124.
339. Hitchcock AP, Morin C, Tyliszczak T, Koprinarov IN, Ikeura-Sekiguchi H, Lawrence JR, Leppard GG, Soft X-ray Microscopy of Soft matter-Hard information from two softs. *Surf Rev Lett* **2002**, 09 (01).
340. Hitchcock AP, Stöver HDH, Croll LM, Childs FR, Chemical Mapping of Polymer Microstructure Using Soft X-ray Spectromicroscopy. *Aust J Chem* **2005**, 58, 423-432.
341. Ade H, X-Ray Spectromicroscopy. *Experimental Methods in the Physical Sciences (Vacuum Ultraviolet Spectroscopy II)* **1998**, 32, 225-262.
342. Gordon ML, Cooper G, Morin C, Araki T, Turci CC, Kaznatcheev K, Hitchcock AP, Inner-Shell Excitation Spectroscopy of the Peptide Bond: Comparison of the C 1s, N 1s, and O 1s Spectra of Glycine, Glycyl-Glycine, and Glycyl-Glycyl-Glycine. *J Phys Chem* **2003**, 107 (32), 6144–6159.
343. Lytle FW, Wei PSP, Greigor RB, Via GH, Sinfelt JH, Effect of chemical environment on magnitude of xray absorption resonance at L I I I edges. Studies on metallic elements, compounds, and catalysts. *J Chem Phys* **1979**, 70, 4849.
344. Stöhr J, *NEXAFS Spectroscopy*. Springer: 1992; Vol. Vol. 25.
345. In *X-Ray Optics*.
346. Magowan C, Meyer-Ilse W, Brown J, Biological Imaging. In *The center of X-ray Optics*, 2010.

347. Loo BJ, Sauerwald I, Hitchcock A, Rothman S, A new sample preparation method for biological soft X-ray microscopy: nitrogen-based contrast and radiation tolerance properties of glycol methacrylate-embedded and sectioned tissue. *J Microsc* **2001**, 204 (Pt 1), 69-86.
348. Auernhammer GK, Fauth K, Ullrich B, Zhao J, Weigand M, Vollmer D, Time-resolved X-ray microscopy of nanoparticle aggregates under oscillatory shear. *J Synchrotron Radiat* **2009**, 16, 307-309.
349. Debbage P, Targeted drugs and nanomedicine: present and future. *Curr Pharm Design* **2009**, 15 (2), 153-72.
350. Guthi J, Yang S, Huang G, Li S, Khemtong C, Kessinger C, Peyton M, Minna J, Brown K, Gao J, MRI-visible micellar nanomedicine for targeted drug delivery to lung cancer cells. *Mol Pharm* **2010**, 7 (1), 32-40.
351. Jiang Z, Sun C, Yin Z, Zhou F, Ge L, Liu X, Kong F, Comparison of two kinds of nanomedicine for targeted gene therapy: premodified or postmodified gene delivery systems. *Int J Nanomed* **2012**, 7, 2019-31.
352. Düzgüneş N, de Ilarduya C, Genetic nanomedicine: gene delivery by targeted lipoplexes. *Method Enzymol* **2012**, 509, 355-67.
353. Kong F, Zhou F, Ge L, Liu X, Wang Y, Mannosylated liposomes for targeted gene delivery. *Int J Nanomed* **2012**, 7, 1079-89.
354. Rungta RL, Choi HB, Lin PJ, Ko RW, Ashby D, Nair J, Manoharan M, Cullis PR, MacVicar BA, Lipid Nanoparticle Delivery of siRNA to Silence Neuronal Gene Expression in the Brain. *Mol Ther Nucleic Acids* **2013**, 2.
355. Tam YYC, Chen S, Cullis PR, Advances in Lipid Nanoparticles for siRNA Delivery. *Pharmaceutics* **2013**, 5 (3), 498–507.
356. Ballarín-González B, Ebbesen M, Howard K, Polycation-based nanoparticles for RNAi-mediated cancer treatment. *Cancer Lett* **2013**, 352 (1), 66-80.
357. Lin Q, Chen J, Zhang Z, Zheng G, Lipid-based Nanoparticles in the Systemic Delivery of siRNA. *Nanomedicine* **2014**, 9 (1), 105-120.

358. Watts B, Thomsen L, Dastoor P, Methods in carbon K-edge NEXAFS: Experiment and analysis. *Journal Electron spectrosc* **2006**, *151* (2), 105-120.
359. Ahmed M, Jiang X, Deng Z, Narain R, Cationic glyco-functionalized single-walled carbon nanotubes as efficient gene delivery vehicles. *Bioconjugate Chem* **2009**, *20* (11), 2017-22.
360. Singh R, Pantarotto D, McCarthy D, Chaloin O, Hoebeke J, Partidos C, Briand J, Prato M, Bianco A, Kostarelos K, Binding and condensation of plasmid DNA onto functionalized carbon nanotubes: toward the construction of nanotube-based gene delivery vectors. *J Am Chem Soc* **2005**, *127* (12), 4388-96.
361. Klumpp C, Kostarelos K, Prato M, Bianco A, Functionalized carbon nanotubes as emerging nanovectors for the delivery of therapeutics. *Biochim Biophys Acta* **2006**, *1758* (3), 404-12.
362. Felten A, Hody H, Bittencourt C, Pireaux JJ, Scanning transmission x-ray microscopy of isolated multiwall carbon nanotubes. *Appl Phys Lett* **2006**, *89*, 093123.
363. Goldoni A, Larciprete R, Gregoratti L, Kaulich B, Kiskinova M, Zhang Y, Dai H, Sangaletti L, Parmigiani F, X-ray photoelectron microscopy of the C1s core level of free-standing single-wall carbon nanotube bundles. *Appl Phys Lett* **2002**, *80*, 2165.
364. Rightor EG, Hitchcock AP, Ade H, Leapman RD, Urquhart SG, Smith AP, Mitchell G, Fischer D, Shin HJ, Warwick T, Spectromicroscopy of Poly(ethylene terephthalate): Comparison of Spectra and Radiation Damage Rates in X-ray Absorption and Electron Energy Loss. *J Phys Chem B* **1997**, *101* (11), 1950-1960.
365. Najafi E, Wang J, Hitchcock A, Guan J, Dénomée S, Simard B, Characterization of single-walled carbon nanotubes by scanning transmission X-ray spectromicroscopy: purification, order and dodecyl functionalization. *J Am Chem Soc* **2010**, *132* (26), 9020-9.
366. Nerl H, Cheng C, Goode A, Bergin S, Lich B, Gass M, Porter A, Imaging methods for determining uptake and toxicity of carbon nanotubes in vitro and in vivo. *Nanomedicine (London)* **2011**, *6* (5), 849-65.

367. Maeda-Mamiya R, Noiri E, Isobe H, Nakanishi W, Okamoto K, Doi K, Sugaya T, Izumi T, Homma T, Nakamura E, In vivo gene delivery by cationic tetraamino fullerene. *PNAS* **2010**, *107* (12), 5339-5344.
368. Sitharaman B, Zakharian T, Saraf A, Misra P, Ashcroft J, Pan S, Pham Q, Mikos A, Wilson L, Engler D, Water-soluble fullerene (C60) derivatives as nonviral gene-delivery vectors. *Mol Pharm* **2008**, *5* (4), 567-78.
369. Isobe H, Nakanishi W, Tomita N, Jinno S, Okayama H, Nakamura E, Gene delivery by aminofullerenes: structural requirements for efficient transfection. *Chemistry, Asian J* **2006**, *1* (1-2), 167-75.
370. Liang XJ, Meng H, Wang Y, He H, Meng J, Lu J, Wang PC, Zhao Y, Gao X, Sun B, Chen C, Xing G, Shen D, Gottesman MM, Wu Y, Yin Jj, Jia L, Metallofullerene nanoparticles circumvent tumor resistance to cisplatin by reactivating endocytosis. *PNAS* **2010**, *107* (16), 7449-7454.
371. Shinohara H, Endohedral metallofullerenes. *Rep Prog Phys* **2000**, *63* (6), 843-892.
372. Chen Z, Liu Y, Sun B, Li H, Dong J, Zhang L, Wang L, Wang P, Zhao Y, Chen C, Polyhydroxylated Metallofullerenols Stimulate IL-1 β Secretion of Macrophage through TLRs/MyD88/NF- κ B Pathway and NLRP3 Inflammasome Activation. *Small* **2014**, *10* (12), 2362-72.
373. Sayes CM, Marchione AA, Reed KL, Warheit DB, Comparative Pulmonary Toxicity Assessments of C60 Water Suspensions in Rats: Few Differences in Fullerene Toxicity in Vivo in Contrast to in Vitro Profiles. *Nano Lett* **2007**, *7* (8), 2399–2406.
374. Park E, Kim H, Kim Y, Yi J, Choi K, Park K, Carbon fullerenes (C60s) can induce inflammatory responses in the lung of mice. *Toxicol Appl Pharm* **2010**, *244* (2), 226-33.
375. Liu Y, Jiao F, Qiu Y, Li W, Lao F, Zhou G, Sun B, Xing G, Dong J, Zhao Y, Chai Z, Chen C, The effect of Gd@C82(OH)22 nanoparticles on the release of Th1/Th2 cytokines and induction of TNF-alpha mediated cellular immunity. *Biomaterials* **2009**, *30* (23-24), 3934-45.
376. Tan W, Jiang S, Zhang Y, Quantum-dot based nanoparticles for targeted silencing of HER2/neu gene via RNA interference. *Biomaterials* **2007**, *28* (8), 1565-71.

377. Chen AA, Derfus AM, Khetani SR, Bhatia SN, Quantum dots to monitor RNAi delivery and improve gene silencing. *Oxford J: Nucliec Acid Res* **2005**, 33 (22), e190.
378. Jia N, Lian Q, Shen H, Wang C, Li X, Yang Z, Intracellular delivery of quantum dots tagged antisense oligodeoxynucleotides by functionalized multiwalled carbon nanotubes. *Nano Lett* **2007**, 7 (10), 2976-80.
379. Chen N, He Y, Su Y, Li X, Huang Q, Wang H, Zhang X, Tai R, Fan C, The cytotoxicity of cadmium-based quantum dots. *Biomaterials* **2012**, 33 (5), 1238-44.
380. Zhu Y, Li W, Zhang Y, Li J, Liang L, Zhang X, Chen N, Sun Y, Chen W, Tai R, Fan C, Huang Q, Excessive sodium ions delivered into cells by nanodiamonds: implications for tumor therapy. *Small* **2012**, 8 (11), 1771-9.

12 Permissions to Reproduce Figures

Figure 1.1

The screenshot displays the Copyright Clearance Center RightsLink interface. At the top left is the Copyright Clearance Center logo. To its right is the RightsLink logo. Further right are navigation buttons for Home, Account Info, and Help, along with a Live Chat icon. Below the navigation is a Taylor & Francis logo and a dark blue box containing the text "Solid State and Materials Sciences". The main content area lists the following details:

- Title:** Carbon Nanostructures
- Author:** O. A. Shenderova, V. V. Zhimov, D. W. Brenner
- Publication:** Critical Reviews in Solid State and Materials Sciences
- Publisher:** Taylor & Francis
- Date:** Jul 1, 2002

Below these details is the copyright notice: "Copyright © 2002 Taylor & Francis". On the right side, a grey box shows the user is logged in as "Saniya Alwani" with account number "3000882226" and a "LOGOUT" button.

Thesis/Dissertation Reuse Request

Taylor & Francis is pleased to offer reuses of its content for a thesis or dissertation free of charge contingent on resubmission of permission request if work is published.

BACK

CLOSE WINDOW

Copyright © 2015 Copyright Clearance Center, Inc. All Rights Reserved. [Privacy statement](#), [Terms and Conditions](#). Comments? We would like to hear from you. E-mail us at customercare@copyright.com

Figure 1.2 (A)



RightsLink®

[Home](#)
[Account Info](#)
[Help](#)



Live Chat



Title: Functionalized carbon nanotubes for potential medicinal applications

Author: Yi Zhang, Yuhong Bai, Bing Yan

Publication: Drug Discovery Today

Publisher: Elsevier

Date: June 2010

Copyright © 2010 Elsevier Ltd. All rights reserved.

Logged in as:
Saniya Alwani
Account #: 3000882226

LOGOUT

Review Order

Please review the order details and the associated [terms and conditions](#). To edit billing or contact information please click on 'account info' at the top of this page.

Licensed content publisher	Elsevier
Licensed content publication	Drug Discovery Today
Licensed content title	Functionalized carbon nanotubes for potential medicinal applications
Licensed content author	Yi Zhang, Yuhong Bai, Bing Yan
Licensed content date	June 2010
Licensed content volume number	15
Licensed content issue number	11-12
Number of pages	8
Type of Use	reuse in a thesis/dissertation
Portion	figures/tables/illustrations
Number of figures/tables/illustrations	1
Format	both print and electronic
Are you the author of this Elsevier article?	No
Will you be translating?	No
Original figure numbers	1
Title of your thesis/dissertation	Amino acid Functionalized Nanodiamonds as Gene Delivery Vectors: Synthesis, Physicochemical Characterization and Cellular Interaction Studies
Expected completion date	Sep 2015
Estimated size (number of pages)	185
Elsevier VAT number	GB 494 6272 12
Permissions price	0.00 CAD
VAT/Local Sales Tax	0.00 CAD / 0.00 GBP
Total	0.00 CAD

Figure 1.2 (B)

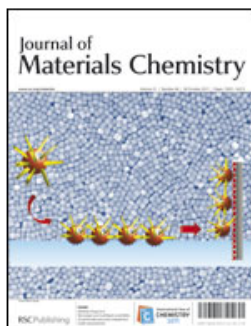


RightsLink®

Home

Account Info

Help



Title: Crystallinity and surface electrostatics of diamond nanocrystals
Author: Amanda S. Barnard, Michael Sternberg
Publication: Journal of Materials Chemistry
Publisher: Royal Society of Chemistry
Date: Oct 2, 2007
Copyright © 2007, Royal Society of Chemistry

Logged in as:
Saniya Alwani
Account #:
3000882226

LOGOUT

Order Completed

Thank you very much for your order.

This is a License Agreement between Saniya S Alwani ("You") and Royal Society of Chemistry. The license consists of your order details, the terms and conditions provided by Royal Society of Chemistry, and the [payment terms and conditions](#).

[Get the printable license.](#)

License Number	3664370522403
License date	Jul 08, 2015
Licensed content publisher	Royal Society of Chemistry
Licensed content publication	Journal of Materials Chemistry
Licensed content title	Crystallinity and surface electrostatics of diamond nanocrystals
Licensed content author	Amanda S. Barnard, Michael Sternberg
Licensed content date	Oct 2, 2007
Volume number	17
Issue number	45
Type of Use	Thesis/Dissertation
Requestor type	academic/educational
Portion	figures/tables/images
Number of figures/tables/images	1
Distribution quantity	1
Format	print and electronic
Will you be translating?	no
Order reference number	None
Title of the thesis/dissertation	Amino acid Functionalized Nanodiamonds as Gene Delivery Vectors: Synthesis, Physicochemical Characterization and Cellular Interaction Studies
Expected completion date	Sep 2015
Estimated size	185

Figure 1.2 (C)



RightsLink®

Home

Account Info

Help



Title: Characterisation and determination of fullerenes: A critical review
Author: Alina Astefanei, Oscar Núñez, Maria Teresa Galceran
Publication: Analytica Chimica Acta
Publisher: Elsevier
Date: 2 July 2015

Logged in as:
 Saniya Alwani
 Account #:
 3000882226

LOGOUT

Copyright © 2015 Elsevier B.V. All rights reserved.

Order Completed

Thank you very much for your order.

This is a License Agreement between Saniya S Alwani ("You") and Elsevier ("Elsevier"). The license consists of your order details, the terms and conditions provided by Elsevier, and the [payment terms and conditions](#).

[Get the printable license.](#)

License Number	3664351248944
License date	Jul 08, 2015
Licensed content publisher	Elsevier
Licensed content publication	Analytica Chimica Acta
Licensed content title	Characterisation and determination of fullerenes: A critical review
Licensed content author	Alina Astefanei, Oscar Núñez, Maria Teresa Galceran
Licensed content date	2 July 2015
Licensed content volume number	882
Licensed content issue number	n/a
Number of pages	21
Type of Use	reuse in a thesis/dissertation
Portion	figures/tables/illustrations
Number of figures/tables/illustrations	1
Format	both print and electronic
Are you the author of this Elsevier article?	No
Will you be translating?	No
Original figure numbers	1
Title of your thesis/dissertation	Amino acid Functionalized Nanodiamonds as Gene Delivery Vectors: Synthesis, Physicochemical Characterization and Cellular Interaction Studies
Expected completion date	Sep 2015
Estimated size (number of pages)	185
Elsevier VAT number	GB 494 6272 12
Permissions price	0.00 CAD

Figure 1.3 (A)

ELSEVIER LICENSE TERMS AND CONDITIONS

Jul 08, 2015

This is a License Agreement between Saniya S Alwani ("You") and Elsevier ("Elsevier") provided by Copyright Clearance Center ("CCC"). The license consists of your order details, the terms and conditions provided by Elsevier, and the payment terms and conditions.

All payments must be made in full to CCC. For payment instructions, please see information listed at the bottom of this form.

Supplier	Elsevier Limited The Boulevard,Langford Lane Kidlington,Oxford,OX5 1GB,UK
Registered Company Number	1982084
Customer name	Saniya S Alwani
Customer address	B 329, Health Sciences building
Saskatoon, SK S7N 1K3	
License number	3664400069536
License date	Jul 08, 2015
Licensed content publisher	Elsevier
Licensed content publication	Chemical Physics Letters
Licensed content title	Reversible water-solubilization of single-walled carbon nanotubes by polymer wrapping
Licensed content author	Michael J. O'Connell,Peter Boul,Lars M. Ericson,Chad Huffman,Yuhuang Wang,Erik Haroz,Cynthia Kuper,Jim Tour,Kevin D. Ausman,Richard E. Smalley
Licensed content date	13 July 2001
Licensed content volume number	342
Licensed content issue number	3-4
Number of pages	7
Start Page	265
End Page	271
Type of Use	reuse in a thesis/dissertation
Intended publisher of new work	other
Portion	figures/tables/illustrations
Number of figures/tables/illustrations	1
Format	both print and electronic
Are you the author of this Elsevier article?	No
Will you be translating?	No
Original figure numbers	4

Title of your thesis/dissertation	Amino acid Functionalized Nanodiamonds as Gene Delivery Vectors: Synthesis, Physicochemical Characterization and Cellular Interaction Studies
Expected completion date	Sep 2015
Estimated size (number of pages)	185
Elsevier VAT number	GB 494 6272 12
Permissions price	0.00 CAD
VAT/Local Sales Tax	0.00 CAD / 0.00 GBP
Total	0.00 CAD

Figure 1.3 (B)

ELSEVIER LICENSE TERMS AND CONDITIONS

Jul 08, 2015

This is a License Agreement between Saniya S Alwani ("You") and Elsevier ("Elsevier") provided by Copyright Clearance Center ("CCC"). The license consists of your order details, the terms and conditions provided by Elsevier, and the payment terms and conditions.

All payments must be made in full to CCC. For payment instructions, please see information listed at the bottom of this form.

Supplier	Elsevier Limited The Boulevard,Langford Lane Kidlington,Oxford,OX5 1GB,UK
Registered Company Number	1982084
Customer name	Saniya S Alwani
Customer address	B 329, Health Sciences building
Saskatoon, SK S7N 1K3	
License number	3664400439926
License date	Jul 08, 2015
Licensed content publisher	Elsevier
Licensed content publication	Journal of Molecular Graphics and Modelling
Licensed content title	How do carbon nanotubes serve as carriers for gemcitabine transport in a drug delivery system?
Licensed content author	Uthumporn Arsawang,Oraphan Saengsawang,Thanyada Rungrotmongkol,Purinchaya Sornmee,Kitiyaporn Wittayanarakul,Tawun Remsungnen,Supot Hannongbua
Licensed content date	February 2011
Licensed content volume number	29
Licensed content issue number	5
Number of pages	6
Start Page	591
End Page	596
Type of Use	reuse in a thesis/dissertation
Intended publisher of new work	other
Portion	figures/tables/illustrations
Number of figures/tables/illustrations	1
Format	both print and electronic
Are you the author of this Elsevier article?	No
Will you be translating?	No

Original figure numbers	1 a
Title of your thesis/dissertation	Amino acid Functionalized Nanodiamonds as Gene Delivery Vectors: Synthesis, Physicochemical Characterization and Cellular Interaction Studies
Expected completion date	Sep 2015
Estimated size (number of pages)	185
Elsevier VAT number	GB 494 6272 12
Permissions price	0.00 CAD
VAT/Local Sales Tax	0.00 CAD / 0.00 GBP
Total	0.00 CAD

Figure 1.4 (A)



RightsLink®

Home

Account Info

Help



ACS Publications
Most Trusted. Most Cited. Most Read.

Title: Detection of a Family of Gadolinium-Containing Endohedral Fullerenes and the Isolation and Crystallographic Characterization of One Member as a Metal–Carbide Encapsulated inside a Large Fullerene Cage

Author: Hua Yang, Chunxin Lu, Ziyang Liu, et al

Publication: Journal of the American Chemical Society

Publisher: American Chemical Society

Date: Dec 1, 2008

Copyright © 2008, American Chemical Society

Logged in as:

Saniya Alwani

Account #:
3000882226

LOGOUT

PERMISSION/LICENSE IS GRANTED FOR YOUR ORDER AT NO CHARGE

This type of permission/license, instead of the standard Terms & Conditions, is sent to you because no fee is being charged for your order. Please note the following:

- Permission is granted for your request in both print and electronic formats, and translations.
- If figures and/or tables were requested, they may be adapted or used in part.
- Please print this page for your records and send a copy of it to your publisher/graduate school.
- Appropriate credit for the requested material should be given as follows: "Reprinted (adapted) with permission from (COMPLETE REFERENCE CITATION). Copyright (YEAR) American Chemical Society." Insert appropriate information in place of the capitalized words.
- One-time permission is granted only for the use specified in your request. No additional uses are granted (such as derivative works or other editions). For any other uses, please submit a new request.

If credit is given to another source for the material you requested, permission must be obtained from that source.

BACK

CLOSE WINDOW

Copyright © 2015 Copyright Clearance Center, Inc. All Rights Reserved. [Privacy statement](#). [Terms and Conditions](#).
Comments? We would like to hear from you. E-mail us at customercare@copyright.com

Figure 1.4 (B)

ROYAL SOCIETY OF CHEMISTRY LICENSE TERMS AND CONDITIONS

Jul 08, 2015

This is a License Agreement between Saniya S Alwani ("You") and Royal Society of Chemistry ("Royal Society of Chemistry") provided by Copyright Clearance Center ("CCC"). The license consists of your order details, the terms and conditions provided by Royal Society of Chemistry, and the payment terms and conditions.

All payments must be made in full to CCC. For payment instructions, please see information listed at the bottom of this form.

License Number	3664410353990
License date	Jul 08, 2015
Licensed content publisher	Royal Society of Chemistry
Licensed content publication	Journal of Materials Chemistry
Licensed content title	Materials chemistry of fullerene C60 derivatives
Licensed content author	Alejandro Montellano López,Aurelio Mateo-Alonso,Maurizio Prato
Licensed content date	Oct 29, 2010
Volume number	21
Issue number	5
Type of Use	Thesis/Dissertation
Requestor type	academic/educational
Portion	figures/tables/images
Number of figures/tables/images	1
Format	print and electronic
Distribution quantity	1
Will you be translating?	no
Order reference number	None
Title of the thesis/dissertation	Amino acid Functionalized Nanodiamonds as Gene Delivery Vectors: Synthesis, Physicochemical Characterization and Cellular Interaction Studies
Expected completion date	Sep 2015
Estimated size	185
Total	0.00 CAD

Figure 1.5



RightsLink®

Home

Account Info

Help



Title: Non-viral vectors for gene-based therapy
Author: Hao Yin, Rosemary L. Kanasty, Ahmed A. Eltoukhy, Arturo J. Vegas, J. Robert Dorkin, Daniel G. Anderson
Publication: Nature Reviews Genetics
Publisher: Nature Publishing Group
Date: Jul 15, 2014
 Copyright © 2014, Rights Managed by Nature Publishing Group

Logged in as:
 Saniya Alwani
 Account #:
 3000882226

LOGOUT

Order Completed


Thank you very much for your order.

This is a License Agreement between Saniya S Alwani ("You") and Nature Publishing Group ("Nature Publishing Group"). The license consists of your order details, the terms and conditions provided by Nature Publishing Group, and the [payment terms and conditions](#).



[Get the printable license.](#)

License Number	3664430915297
License date	Jul 08, 2015
Licensed content publisher	Nature Publishing Group
Licensed content publication	Nature Reviews Genetics
Licensed content title	Non-viral vectors for gene-based therapy
Licensed content author	Hao Yin, Rosemary L. Kanasty, Ahmed A. Eltoukhy, Arturo J. Vegas, J. Robert Dorkin, Daniel G. Anderson
Licensed content date	Jul 15, 2014
Type of Use	reuse in a dissertation / thesis
Volume number	15
Issue number	8
Requestor type	academic/educational
Format	print and electronic
Portion	figures/tables/illustrations
Number of figures/tables/illustrations	1
High-res required	no
Figures	1
Author of this NPG article	no
Your reference number	None
Title of your thesis / dissertation	Amino acid Functionalized Nanodiamonds as Gene Delivery Vectors: Synthesis, Physicochemical Characterization and Cellular Interaction Studies
Expected completion date	Sep 2015
Estimated size (number of pages)	185
Total	0.00 CAD

Figure 2.1 (B)




Welcome, **Saniya**
Not you?

Log out |  Cart (0) | Manage Account | Feedback | Help |  Live Help

Get Permission / Find Title
Publication Title or ISBN/ISSN
[Advanced Search Options](#)

[Back to view orders](#)

Confirmation Number: 11404824
Order Date: 07/20/2015

 [Print this page](#)
[Print terms & conditions](#)
[Print citation information \(What's this?\)](#)

Customer Information

Customer: Saniya Alwani
Account Number: 3000882226
Organization: Saniya Alwani
Email: ssa930@mail.usask.ca
Phone: +1 (306) 251-2125


Search order details by:

This is not an invoice

Order Details

International Journal of Nanomedicine

Order detail ID: 67758014
ISSN: 1178-2013
Publication Type: e-Journal
Volume:
Issue:
Start page:
Publisher: DOVE Medical Press

Permission Status:  **Granted**
Permission type: Republish or display content
Type of use: Republish in a thesis/dissertation
Order License Id: 3673231058102

Billing Status:
N/A

Note: This item was invoiced separately through our **RightsLink service**. [More info](#) **\$ 0.00**

Total order items: 1 **Order Total: \$0.00**

Figure 2.3

Re: Book-Chapter permission to reproduce the figure

Lucy Evans [Lucy.Evans@iop.org] on behalf of Permissions [permissions@iop.org]

To:

Alwani, Saniya

Attachments:

IOP Publishing Figure 3 pe~

Dear Saniya Shiraz Alwani,
Thank you for your request to reproduce IOP Publishing material.

Figure 5 - Nanotechnology 19 (2008) 155705 to be reused in 'Carbon Nanomaterial Sourcebook', Taylor and Francis.

We are happy to grant permission for the use you request on the terms set out below.

Conditions

Non-exclusive, non-transferrable, revocable, worldwide, permission to use the material in print and electronic form will be granted **subject to the following conditions:**

- Permission will be cancelled without notice if you fail to fulfil any of the conditions of this letter.
 - You will make reasonable efforts to contact the author(s) to seek consent for your intended use. Contacting one author acting expressly as authorised agent for their co-authors is acceptable.
 - You will reproduce the following prominently alongside the material:
 - the source of the material, including author, article title, title of journal, volume number, issue number (if relevant), page range (or first page if this is the only information available) and date of first publication. This information can be contained in a footnote or reference note; or
 - a link back to the article (via DOI); and
 - if practical and IN ALL CASES for works published under any of the Creative Commons licences the words "© IOP Publishing. Reproduced by permission of IOP Publishing. All rights reserved"
 - The material will not, without the express permission of the author(s), be used in any way which, in the opinion of IOP Publishing, could distort or alter the author(s)' original intention(s) and meaning, be prejudicial to the honour or reputation of the author(s) and/or imply endorsement by the author(s) and/or IOP Publishing.
 - Payment of £0 is received in full by IOP Publishing prior to use.
- If you have any questions, please feel free to contact our Permissions team at permissions@iop.org.
I should be grateful if you would acknowledge receipt of this email.

Kind regards,

Lucy Evans

Publishing Assistant

IOP Publishing

Please note: We do not usually provide signed permission forms as a separate attachment. Please print this email and provide it to your publisher as proof of permission.

From: "Alwani, Saniya" <ssa930@mail.usask.ca>
To: "permissions@iop.org" <permissions@iop.org>,
Date: 28/01/2015 17:41
Subject: Book-Chapter permission to reproduce the figure

To Whom It May Concern

I am preparing a book chapter for Taylor and Francis Books, Inc. I would appreciate permission to reproduce the following item in both print and electronic editions. The publisher requires to obtain "permission for non-exclusive world rights in this and all subsequent editions, revisions, and derivative works in English and in foreign translations, in all formats, including electronic media"

Following are the details :

Figure 5 (page 4 of the article)

DOI: 10.1088/0957-4484/19/15/155705

Title: High Resolution Electron Microscopy of Detonation Nanodiamonds

Authors: K Iakoubovskii, KMitsuishi and K Furuya

Journal: Nanotechnology 19

Published on: 12 March 2008

Pages 155705 (5pp)

Publisher: IOP Publishing

Online at: stacks.iop.org/Nano/19/155705

Title of the book in which the material will appear: Carbon Nanomaterial Sourcebook

Author of the work: Saniya Alwani & Ildiko Badea

Affiliation of authors: Drug Design and Discovery group, College of Pharmacy and Nutrition, University of Saskatchewan

Publisher of the work: Taylor and Francis Books, Inc.

Unless you indicate otherwise, I will use complete reference given below as the credit line in the reference list:

Iakoubovskii, K., Mitsuishi, K. & Furuya, K., 2008. High-resolution electron microscopy of detonation nanodiamond. *Nanotechnology*, Volume 19, p. 155705


Please also find attached official permission request form provided by the publisher. I would greatly appreciate your prompt attention to this request.

Thank you

Sincerely,

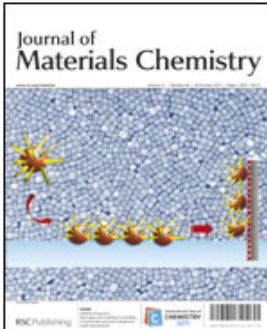
Saniya Shiraz Alwani
M.Sc. Candidate
College of Pharmacy and Nutrition
University of Saskatchewan

Figure 2.4



RightsLink®

[Home](#)
[Account Info](#)
[Help](#)



Title: Surface functionalisation of detonation diamond suitable for biological applications

Author: Anke KrÄ¼ger, Yuejiang Liang, Gerald Jarre, Jochen Stegk

Publication: Journal of Materials Chemistry

Publisher: Royal Society of Chemistry

Date: May 18, 2006

Copyright © 2006, Royal Society of Chemistry

Logged in as:
Saniya Alwani
Account #:
3000882226

LOGOUT

Order Completed

Thank you very much for your order.

This is a License Agreement between Saniya S Alwani ("You") and Royal Society of Chemistry. The license consists of your order details, the terms and conditions provided by Royal Society of Chemistry, and the [payment terms and conditions](#).

[Get the printable license.](#)

License Number	3557740142321
License date	Jan 28, 2015
Licensed content publisher	Royal Society of Chemistry
Licensed content publication	Journal of Materials Chemistry
Licensed content title	Surface functionalisation of detonation diamond suitable for biological applications
Licensed content author	Anke KrÄ¼ger, Yuejiang Liang, Gerald Jarre, Jochen Stegk
Licensed content date	May 18, 2006
Volume number	16
Issue number	24
Type of Use	Book/Textbook
Requestor type	academic/educational
Portion	figures/tables/images
Number of figures/tables/images	1
Distribution quantity	1
Format	print and electronic
Will you be translating?	no
Order reference number	None
Title of the book	Carbon Nanomaterial Sourcebook
Author of the book	Klaus D. Sattler (Editor)
Publisher of the book	Taylor and Francis Inc.
Expected publication date	Sep 2015
Estimated size of the book (number of pages)	500
Total	0.00 CAD

Figure 2.5

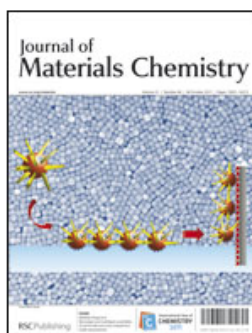


RightsLink®

Home

Account Info

Help



Title: Self-assembly in nanodiamond agglutinates
Author: Amanda S. Barnard
Publication: Journal of Materials Chemistry
Publisher: Royal Society of Chemistry
Date: Jul 30, 2008
 Copyright © 2008, Royal Society of Chemistry

Logged in as:
 Saniya Alwani
 Account #:
 3000882226

LOGOUT

Order Completed

Thank you very much for your order.

This is a License Agreement between Saniya S Alwani ("You") and Royal Society of Chemistry. The license consists of your order details, the terms and conditions provided by Royal Society of Chemistry, and the [payment terms and conditions](#).

[Get the printable license.](#)

License Number	3557751133476
License date	Jan 28, 2015
Licensed content publisher	Royal Society of Chemistry
Licensed content publication	Journal of Materials Chemistry
Licensed content title	Self-assembly in nanodiamond agglutinates
Licensed content author	Amanda S. Barnard
Licensed content date	Jul 30, 2008
Volume number	18
Issue number	34
Type of Use	Book/Textbook
Requestor type	academic/educational
Portion	figures/tables/images
Number of figures/tables/images	1
Distribution quantity	1
Format	print and electronic
Will you be translating?	yes
Number of languages	3
Languages	English and all foreign languages
Order reference number	None
Title of the book	Carbon Nanomaterial Sourcebook
Author of the book	Klaus D. Sattler (Editor)
Publisher of the book	Taylor and Francis Inc.
Expected publication date	Sep 2015
Estimated size of the book (number of pages)	500
Total	0.00 CAD

Figure 2.6



Home

Account Info

Help



Title: Unusually tight aggregation in detonation nanodiamond: Identification and disintegration
Author: A. Krüger, F. Kataoka, M. Ozawa, T. Fujino, Y. Suzuki, A.E. Aleksenskii, A. Ya. Vul', E. Ōsawa
Publication: Carbon
Publisher: Elsevier
Date: July 2005

Logged in as:
 Saniya Alwani
 Account #:
 3000882226
[LOGOUT](#)

Copyright © 2005 Elsevier Ltd. All rights reserved.

Order Completed

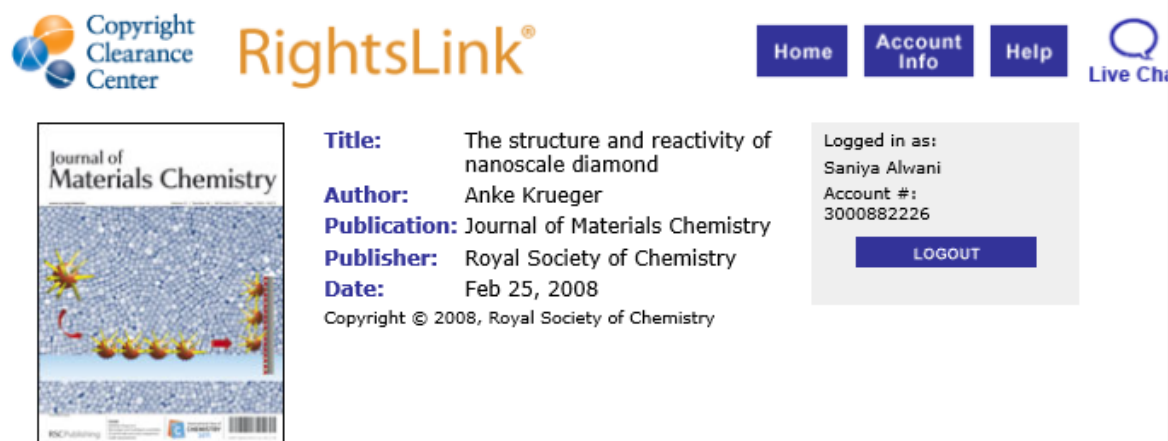
Thank you very much for your order.

This is a License Agreement between Saniya S Alwani ("You") and Elsevier ("Elsevier"). The license consists of your order details, the terms and conditions provided by Elsevier, and the [payment terms and conditions](#).

[Get the printable license.](#)

License Number	3557761089878
License date	Jan 28, 2015
Licensed content publisher	Elsevier
Licensed content publication	Carbon
Licensed content title	Unusually tight aggregation in detonation nanodiamond: Identification and disintegration
Licensed content author	A. Krüger, F. Kataoka, M. Ozawa, T. Fujino, Y. Suzuki, A.E. Aleksenskii, A. Ya. Vul', E. Ōsawa
Licensed content date	July 2005
Licensed content volume number	43
Licensed content issue number	8
Number of pages	9
Type of Use	reuse in a book/textbook
Requestor type	author of new work
Intended publisher of new work	Taylor & Francis
Portion	figures/tables/illustrations
Number of figures/tables/illustrations	1
Format	both print and electronic
Are you the author of this Elsevier article?	No
Will you be translating?	Yes
Number of languages	3
Languages	English and all other languages
Original figure numbers	figure 8
Title of the book	Carbon Nanomaterial Sourcebook
Publisher of the book	Taylor and Francis Inc.
Author of the book	Klaus D. Sattler (Editor)
Expected publication date	Sep 2015
Estimated size of the book (number of pages)	500
Elsevier VAT number	GB 494 6272 12
Permissions price	0.00 CAD
VAT/Local Sales Tax	0.00 CAD / 0.00 GBP
Total	0.00 CAD

Figure 2.9



The screenshot shows the RightsLink website interface. At the top left is the Copyright Clearance Center logo. To its right is the RightsLink logo. Further right are navigation buttons for Home, Account Info, and Help, and a Live Chat icon. The main content area is divided into three sections:

- Journal Cover:** A thumbnail image of the Journal of Materials Chemistry cover, featuring a molecular structure.
- Article Details:**
 - Title:** The structure and reactivity of nanoscale diamond
 - Author:** Anke Krueger
 - Publication:** Journal of Materials Chemistry
 - Publisher:** Royal Society of Chemistry
 - Date:** Feb 25, 2008
 - Copyright © 2008, Royal Society of Chemistry
- User Information:**
 - Logged in as: Saniya Alwani
 - Account #: 3000882226
 - A blue LOGOUT button is present below the account information.

Order Completed

Thank you very much for your order.

This is a License Agreement between Saniya S Alwani ("You") and Royal Society of Chemistry. The license consists of your order details, the terms and conditions provided by Royal Society of Chemistry, and the [payment terms and conditions](#).

[Get the printable license.](#)

License Number	3557840427016
License date	Jan 28, 2015
Licensed content publisher	Royal Society of Chemistry
Licensed content publication	Journal of Materials Chemistry
Licensed content title	The structure and reactivity of nanoscale diamond
Licensed content author	Anke Krueger
Licensed content date	Feb 25, 2008
Volume number	18
Issue number	13
Type of Use	Book/Textbook
Requestor type	academic/educational
Portion	figures/tables/images
Number of figures/tables/images	1
Distribution quantity	1
Format	print and electronic
Will you be translating?	yes
Number of languages	3
Languages	English and all foreign languages
Order reference number	None
Title of the book	Carbon Nanomaterial Sourcebook
Author of the book	Klaus D. Sattler (Editor)
Publisher of the book	Taylor and Francis Inc.
Expected publication date	Sep 2015
Estimated size of the book (number of pages)	500
Total	0.00 CAD

Figure 2.10



Copyright
Clearance
Center

RightsLink®

Home

Account Info

Help


 Live Chat



Title: The properties and applications of nanodiamonds

Author: Vadym N. Mochalin, Olga Shenderova, Dean Ho, Yury Gogotsi

Publication: Nature Nanotechnology

Publisher: Nature Publishing Group

Date: Dec 18, 2011

Copyright © 2011, Rights Managed by Nature Publishing Group

Logged in as:
Saniya Alwani
Account #:
3000882226

LOGOUT

Order Completed

Thank you very much for your order.

This is a License Agreement between Saniya S Alwani ("You") and Nature Publishing Group ("Nature Publishing Group"). The license consists of your order details, the terms and conditions provided by Nature Publishing Group, and the [payment terms and conditions](#).

[Get the printable license.](#)

License Number	3557840981811
License date	Jan 28, 2015
Licensed content publisher	Nature Publishing Group
Licensed content publication	Nature Nanotechnology
Licensed content title	The properties and applications of nanodiamonds
Licensed content author	Vadym N. Mochalin, Olga Shenderova, Dean Ho, Yury Gogotsi
Licensed content date	Dec 18, 2011
Type of Use	reuse in a book / textbook
Volume number	7
Issue number	1
Requestor type	academic/university or research institute
Format	print and electronic
Portion	figures/tables/illustrations
Number of figures/tables/illustrations	1
High-res required	no
Figures	Figure 5 :Surface modification
Author of this NPG article	no
Your reference number	None
Title of the book	Carbon Nanomaterial Sourcebook
Publisher of your Book	Taylor and Francis Inc.
Author of the book	Klaus D. Sattler (Editor)
Expected publication date	Sep 2015
Estimated size of your book (number of pages)	500
Total	0.00 CAD

Figure 2.12



The screenshot shows the RightsLink interface. At the top left is the Copyright Clearance Center logo. In the center is the RightsLink logo. On the right are navigation buttons for Home, Account Info, and Help, along with a Live Chat icon. Below the logos is the Nature Publishing Group (NPG) logo. The main content area displays the following information:

- Title:** Strategies in the design of nanoparticles for therapeutic applications
- Author:** Robby A. Petros and Joseph M. DeSimone
- Publication:** Nature Reviews Drug Discovery
- Publisher:** Nature Publishing Group
- Date:** Aug 1, 2010

Below this information is a copyright notice: "Copyright © 2010, Rights Managed by Nature Publishing Group". To the right of this information is a user login box showing the user is logged in as Saniya Alwani with account number 3000882226, and a LOGOUT button.

Order Completed

Thank you very much for your order.

This is a License Agreement between Saniya S Alwani ("You") and Nature Publishing Group ("Nature Publishing Group"). The license consists of your order details, the terms and conditions provided by Nature Publishing Group, and the [payment terms and conditions](#).

[Get the printable license.](#)

License Number	3557850018660
License date	Jan 28, 2015
Licensed content publisher	Nature Publishing Group
Licensed content publication	Nature Reviews Drug Discovery
Licensed content title	Strategies in the design of nanoparticles for therapeutic applications
Licensed content author	Robby A. Petros and Joseph M. DeSimone
Licensed content date	Aug 1, 2010
Type of Use	reuse in a book / textbook
Volume number	9
Issue number	8
Requestor type	academic/university or research institute
Format	print and electronic
Portion	figures/tables/illustrations
Number of figures/tables/illustrations	1
High-res required	no
Figures	Figure 2: Modes of cellular internalization of nanoparticles and respective size limitations.
Author of this NPG article	no
Your reference number	None
Title of the book	Carbon Nanomaterial Sourcebook
Publisher of your Book	Taylor and Francis Inc.
Author of the book	Klaus D. Sattler (Editor)
Expected publication date	Sep 2015
Estimated size of your book (number of pages)	500
Total	0.00 CAD

Figure 2.13

RE: Book-Chapter permission to reproduce the figure

PNAS Permissions [PNASPermissions@nas.edu]

Permission is granted for your use of the figure as described in your message. Please cite the PNAS article in full, and include "Copyright (2007) National Academy of Sciences, U.S.A." as a copyright note. Because this material published between 1993 and 2008, a copyright note is needed. Let us know if you have any questions.

Best regards,
Kay McLaughlin for
Diane Sullenberger
Executive Editor
PNAS

From: Alwani, Saniya [mailto:ssa930@mail.usask.ca]
Sent: Wednesday, January 28, 2015 12:12 PM
To: PNAS Permissions
Subject: Book-Chapter permission to reproduce the figure

To Whom It May Concern

I am preparing a book chapter for Taylor and Francis Books, Inc. I would appreciate permission to reproduce the following item in both print and electronic editions. The publisher requires to obtain **"permission for non-exclusive world rights in this and all subsequent editions, revisions, and derivative works in English and in foreign translations, in all formats, including electronic media"**

Following are the details :

Figure 4A and B

(The purpose underlying the text require figures preferably without the graph given in Figure 4C, if permission for use is granted. Explanation of the figure 4A and B will be retained in its entirety as provided by the author)

DOI: 10.1073/pnas.0605409104

Title: Characterization and application of single fluorescent nanodiamonds as cellular biomarkers

Authors: Chi-Cheng Fu, Hsu-Yang Lee, Kowa Chen, Tsong-Shin Lim, Hsiao-Yun Wu, Po-Keng Lin, Pei-Kuen Wei, Pei-Hsi Tsao, Huan-Cheng Chang, and Wunshain Fann

Journal: Proceedings of the National Academy of Sciences of the United States of America (PNAS) Volume 104, Number 3

Published on: 16 January 2007

Pages: 727-732

Publisher: PNAS

Online at: <http://web.thu.edu.tw/tslim/www/07-PNAS-104-727.pdf>

Title of the book in which the material will appear: Carbon Nanomaterial Sourcebook

Author of the work: Saniya Alwani & Ildiko Badea

Affiliation of authors: Drug Design and Discovery group, College of Pharmacy and Nutrition, University of Saskatchewan

Publisher of the work: Taylor and Francis Books, Inc.

Unless you indicate otherwise, I will use complete reference given below as the credit line in the reference list:

Fu, C.-C.et al., 2007. Characterization and application of single fluorescent nano diamonds as cellular biomarkers. *PNAS*, 104(3), p. 727–732


Please also find attached official permission request form provided by the publisher. I would greatly appreciate your prompt attention to this request.

Thank you

Sincerely,

Saniya Shiraz Alwani
M.Sc. Candidate
College of Pharmacy and Nutrition
University of Saskatchewan

Figure 2.14

 **Welcome, Saniya** | [Log out](#) | [Cart \(0\)](#) | [Manage Account](#) | [Feedback](#) | [Help](#) | [Live Help](#)

Get Permission / Find Title
 [Go](#)
[Advanced Search Options](#)

Note: Copyright.com supplies permissions but not the copyrighted content itself.

1 PAYMENT 2 REVIEW 3 CONFIRMATION

Step 3: Order Confirmation

[Start new search >](#) [View your Order History >](#)

[Print order information:](#) includes order confirmation, terms and conditions, and citation information [\(What's this?\)](#)

Thank you for your order! A confirmation for your order will be sent to your account email address. If you have questions about your order, you can call us at +1.855.239.3415 Toll Free, M-F between 3:00 AM and 6:00 PM (Eastern), or write to us at info@copyright.com. This is not an invoice.

Confirmation Number: 11404902
Order Date: 07/20/2015

If you paid by credit card, your order will be finalized and your card will be charged within 24 hours. If you choose to be invoiced, you can change or cancel your order until the invoice is generated.

Payment Information

Saniya Alwani
ssa930@mail.usask.ca
+1 (306) 251-2125
Payment Method: n/a

International Journal of Nanomedicine

Order detail ID: 67759369	Permission Status: ✔ Granted
Order License Id: 3673260533938	Permission type: Republish or display content
ISSN: 1178-2013	Type of use: Republish in a thesis/dissertation
Publication Type: e-Journal	View details
Volume:	
Issue:	
Start page:	
Publisher: DOVE Medical Press	

Note: This item will be invoiced or charged separately through CCC's **RightsLink** service. [More info](#) **\$ 0.00**

This is not an invoice.

Total order items: 1 **Order Total: 0.00 USD**

Figure A1.1

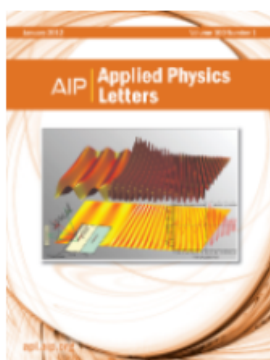


RightsLink®

Home

Account Info

Help



Title: Scanning transmission x-ray microscopy of isolated multiwall carbon nanotubes
Author: A. Felten, H. Hody, C. Bittencourt, et al.
Publication: Applied Physics Letters
Volume/Issue: 89/9
Publisher: AIP Publishing LLC
Date: Sep 1, 2006
Page Count: 3
 Rights managed by AIP Publishing LLC.

Logged in as:
 Saniya Alwani
 Account #:
 3000882226

LOGOUT

Order Completed

Thank you very much for your order.

Click [here](#) for Payment Terms and Conditions.

[Get a printable version for your records.](#)

License Number	3673260890118
Order Date	Jul 20, 2015
Publisher	AIP Publishing LLC
Publication	Applied Physics Letters
Article Title	Scanning transmission x-ray microscopy of isolated multiwall carbon nanotubes
Author	A. Felten, H. Hody, C. Bittencourt, et al.
Online Publication Date	Sep 1, 2006
Volume number	89
Issue number	9
Type of Use	Thesis/Dissertation
Requestor type	Author (original article)
Format	Print and electronic
Portion	Figure/Table
Number of figures/tables	1
Title of your thesis / dissertation	Amino acid Functionalized Nanodiamonds as Gene Delivery Vectors: Synthesis, Physicochemical Characterization and Cellular Interaction Studies
Expected completion date	Sep 2015
Estimated size (number of pages)	185
Total	0.00 CAD

Figure A1.2



RightsLink®

Home

Account
Info

Help



Most Trusted. Most Cited. Most Read.

Title:

Characterization of Single-Walled Carbon Nanotubes by Scanning Transmission X-ray Spectromicroscopy: Purification, Order and Dodecyl Functionalization

Author:

Ebrahim Najafi, Jian Wang, Adam P. Hitchcock, et al

Publication:

Journal of the American Chemical Society

Publisher:

American Chemical Society

Date:

Jul 1, 2010

Copyright © 2010, American Chemical Society

Logged in as:

Saniya Alwani

Account #:

3000882226

LOGOUT

PERMISSION/LICENSE IS GRANTED FOR YOUR ORDER AT NO CHARGE

This type of permission/license, instead of the standard Terms & Conditions, is sent to you because no fee is being charged for your order. Please note the following:

- Permission is granted for your request in both print and electronic formats, and translations.
- If figures and/or tables were requested, they may be adapted or used in part.
- Please print this page for your records and send a copy of it to your publisher/graduate school.
- Appropriate credit for the requested material should be given as follows: "Reprinted (adapted) with permission from (COMPLETE REFERENCE CITATION). Copyright (YEAR) American Chemical Society." Insert appropriate information in place of the capitalized words.
- One-time permission is granted only for the use specified in your request. No additional uses are granted (such as derivative works or other editions). For any other uses, please submit a new request.

If credit is given to another source for the material you requested, permission must be obtained from that source.

Figure A1.3



RightsLink®

[Home](#)
[Account Info](#)
[Help](#)




Title: Polyhydroxylated Metallofullerenols Stimulate IL-1 β Secretion of Macrophage through TLRs/MyD88/NF- κ B Pathway and NLRP3 Inflammasome Activation

Author: Zhiyun Chen, Ying Liu, Baoyun Sun, Han Li, Jinqun Dong, Lijuan Zhang, Liming Wang, Peng Wang, Yuliang Zhao, Chunying Chen

Publication: Small

Publisher: John Wiley and Sons

Date: Mar 11, 2014

© 2014 WILEY-VCH Verlag GmbH & Co. KGaA, Weinheim

Logged in as:
Saniya Alwani
Account #: 3000882226

LOGOUT

Order Completed

Thank you for your order.

This Agreement between Saniya S Alwani ("You") and John Wiley and Sons ("John Wiley and Sons") consists of your license details and the terms and conditions provided by John Wiley and Sons and Copyright Clearance Center.

Your confirmation email will contain your order number for future reference.

[Get the printable license.](#)

License Number	3673261412117
License date	Jul 20, 2015
Licensed Content Publisher	John Wiley and Sons
Licensed Content Publication	Small
Licensed Content Title	Polyhydroxylated Metallofullerenols Stimulate IL-1 β Secretion of Macrophage through TLRs/MyD88/NF- κ B Pathway and NLRP3 Inflammasome Activation
Licensed Content Author	Zhiyun Chen, Ying Liu, Baoyun Sun, Han Li, Jinqun Dong, Lijuan Zhang, Liming Wang, Peng Wang, Yuliang Zhao, Chunying Chen
Licensed Content Date	Mar 11, 2014
Licensed Content Pages	11
Type of use	Dissertation/Thesis
Requestor type	University/Academic
Format	Print and electronic
Portion	Figure/table
Number of figures/tables	1
Original Wiley figure/table number(s)	1
Will you be translating?	No
Title of your thesis / dissertation	Amino acid Functionalized Nanodiamonds as Gene Delivery Vectors: Synthesis, Physicochemical Characterization and Cellular Interaction Studies
Expected completion date	Sep 2015
Expected size (number of pages)	185
Requestor Location	Saniya S Alwani B 329, Health Sciences building Wiggins Ave, University of Saskatchewan Saskatoon, SK S7N 1K3 Canada Attn: Saniya S Alwani
Billing Type	Invoice
Billing address	Saniya S Alwani B 329, Health Sciences building Wiggins Ave, University of Saskatchewan Saskatoon, SK S7N 1K3 Canada Attn: Saniya S Alwani
Total	0.00 CAD